DRUG DELIVERY SYSTEMS FOR TREATMENT OF DIABETES MELLITUS

A Dissertation
Submitted to the Graduate Faculty
of the
North Dakota State University
of Agriculture and Applied Science

By

Divya Sharma

In Partial Fulfillment of the Requirements
for the Degree of
DOCTOR OF PHILOSOPHY

Major Department:
Pharmaceutical Sciences

December 2019

Fargo, North Dakota

North Dakota State University
Graduate School

Title

DRUG DELIVERY SYSTEMS FOR TREATMENT OF DIABETES MELLITUS

By

Divya Sharma

The Supervisory Committee certifies that this ***disquisition*** complies with North Dakota State University's regulations and meets the accepted standards for the degree of

DOCTOR OF PHILOSOPHY

SUPERVISORY COMMITTEE:

Jagdish Singh, Ph.D.
Chair

Chengwen Sun, Ph.D.

Yagna PR Jarajapu, Ph.D.

Amrita Banerjee, Ph.D.

Rhonda Magel, Ph.D.

John Ballantyne, Ph.D.

Approved:

December 13, 2019
Date

Dr. Jagdish Singh
Department Chair

ABSTRACT

Daily injections for basal insulin therapy are far from ideal resulting in hypo/hyperglycemic episodes associated with fatal complications in type-1 diabetes patients. The purpose of this study was to develop a thermosensitive copolymer-based *in situ* depot forming delivery system to provide controlled release of insulin for extended duration following a single subcutaneous injection, closely mimicking physiological basal insulin requirement. Size and nature of the incorporated therapeutic were observed to affect the release profile of insulin. Modification with zinc and chitosan preserved thermal, conformational, and chemical stability of insulin during the entire duration of storage (up to 9 months at 4 °C) and release (up to 3 months at 37 °C). *In vivo*, daily administration of long-acting insulin, glargine, resulted in fluctuating blood glucose levels between 91 – 443 mg/dL in type 1 diabetic rats. However, single administration of oleic acid-grafted-chitosan-zinc-insulin complexes incorporated in copolymer formulation demonstrated slow diffusion of insulin complexes maintaining peak-free basal insulin level of 21 mU/L for 91 days. Sustained release of basal insulin also correlated with efficient glycemic control (blood glucose <120 mg/dL), prevention of diabetic ketoacidosis and absence of cataract development, unlike other treatment groups. The suggested controlled basal insulin delivery system has the potential to significantly improve patient compliance by improving glycemic control and eliminating life-threatening diabetes complications.

Furthermore, oleic acid-grafted-chitosan (CO) nanomicelles were investigated as a non-viral vector to deliver plasmid DNA encoding short hairpin RNA (shRNA) against pro-inflammatory cytokines to adipose tissue macrophages and adipocytes for the treatment of insulin resistance. Nanomicelles modified using mannose (COM) and adipose homing peptide (AHP) (COA) showed significantly higher uptake and transfection efficiency in inflamed macrophages-

adipocytes co culture owing to glucose transporter-1 and prohibitin receptor mediated internalization, respectively. Ligand modified nanomicelles loaded with shRNA against tumor necrosis factor alpha (COM-TNFα) and monocyte chemoattractant protein-1 (COA-MCP1) demonstrated significant attenuation of pro-inflammatory cytokines and improved insulin sensitivity and glucose tolerance in obese-diabetic mice for six weeks post treatment with single dose of optimized formulation. Overall, chitosan nanomicelles mediated targeted gene therapy can help attenuate inflammation, the chief underlying cause of insulin resistance, thereby helping reverse the progression of diabetes.

ACKNOWLEDGEMENTS

I would like to express my sincere gratitude to my advisor, Dr. Jagdish Singh, whose research perspective, expertise, constructive criticism, and attention to detail considerably added to my graduate experience.

I genuinely thank my graduate advisory committee members, Dr. Chengwen Sun, Dr. Yagna Jarajapu, Dr. Amrita Banerjee, Dr. John Ballantyne, and Dr. Rhonda Magel for their expertise which significantly contributed to different stages of my research. I specially thank Dr. Amrita Banerjee for being a co-mentor on "treatment of insulin resistance" project.

I convey my sincere thanks to my seniors, lab colleagues and fellow graduate students, Dr. Sushant Lakkadwala, Dr. Bruna Rodriguez, Sanjay Arora, Riddhi Trivedi, Bivek Chaulagain, and Richard Nii Lante Lamptey for creating a supportive environment at work.

I acknowledge all the current and previous faculty members, staff and students of the department of Pharmaceutical Sciences for helping me directly or indirectly during my research.

My warm and sincere thanks to Janet Krom, Diana Kowalski, Tiffany Olson, and Jean Trautmann, for their assistance with administrative work, Dr. Jodie Haring and Megan Ruch for help with animal work, Jordan Flaten for his help with histology, and Dana Davis & CHP Ambassadors for contributing to my overall personal and professional development.

I gratefully acknowledge financial supports from the NIH (grant# R15GM114701), ND EPSCoR for its seed award (FAR0030636), and the Department of Pharmaceutical Sciences, NDSU, for making my research possible.

Finally, I am immensely thankful of my family members, Sanjay Arora, Hari Krishan Sharma, Rama Sharma, Raghav Sharma, Bhavya Sharma, Pinky Arora, and Ramnik Arora for their constant support, love, and understanding.

DEDICATION

Dedicated to my mother,

Mrs. Rama Sharma

and my father,

Mr. Hari Krishan Sharma.

TABLE OF CONTENTS

LIST OF TABLES

LIST OF FIGURES

LIST OF ABBREVIATIONS

AFM……..... Atomic force microscope

AHP…….....Adipose homing peptide

ANOVA……..... Analysis of variance

APC…….....Antigen presenting cell

ATMs……..... Adipose tissue macrophages

BAT…….....Brown adipose tissue

BCA……..... Bicinchoninic acid

^{13}C……..... Carbon nuclear magnetic resonance

CD……..... Circular dichroism

CMC…….....Critical micelle concentration

CS…….....Chitosan

CSO…….....Chitosan oligosaccharide

DA%……..... Degree of acetylation

DAPI……..... 4',6-diamidino-2-phenylindole

DLS……..... Dynamic light scattering

DM……..... Diabetes mellitus

DMEM……..... Dulbecco's Modified Eagle’s Medium

DMSO……..... Dimethyl sulfoxide

DNA…….....Deoxyribonucleic acid

DNase……..... Deoxyribonuclease

DSC…….....Differential scanning calorimetry

EDC……..... 1-Ethyl-3-(3-dimethylaminopropyl) carbodiimide

ELISA……..... Enzyme linked immunosorbent assay

EtBr……..... Ethidium bromide

EVAT……..... Epididymal visceral adipose tissue

FACS……..... Fluorescence activated cell sorting

FBS……..... Fetal bovine serum

FITC……..... Fluorescein isothiocyanate

FTIR……..... Fourier transform infrared

GFP……..... Green fluorescent protein

GLUT-1……..... Glucose transporter-1

GPC……..... Gel permeation chromatography

GR%……..... Grafting ratio

GT……..... Glucose tolerance

H&E……..... Hematoxylin & eosin

^{1}H NMR……..... Proton nuclear magnetic resonance

HEK-293……..... Human embryonic kidney 293

IgG……..... Immunoglobulin G

IL……..... Interleukin

IST……..... Insulin sensitivity test

ITC……..... Isothermal calorimetry

kb……..... Kilobase

kDa……..... Kilodalton

LPS……..... Lipopolysaccharide

MAN……..... α-D-mannopyranosylphenyl isothiocyanate

MCP-1……..... Monocyte chemoattractant protein-1

mIU……..... Mili international unit

MTT……..... 3-(4,5-dimethylthiazol-2-yl)-2,5-diphenyltetrazolium bromide

Mw……..... Molecular weight

MWCO……..... Molecular weight cut-off

N/P ratio……..... Ratio of free amino groups on the polymer to phosphate groups in DNA

NHS……..... N-hydroxysuccinimide

OA……..... Oleic acid

PBS……..... Phosphate buffered saline

PDI……..... Polydispersity index

pDNA……..... Plasmid DNA

PEG……..... Polyethylene glycol

PEI……..... Polyethylenimine

pGFP……..... Plasmid DNA encoding green fluorescent protein

PLA……..... Poly(D,L-lactide)

PGA……..... Polyglycolide

PLGA……..... Polylactide-coglycolide

PVAT……..... Perirenal visceral adipose tissue

pβ-gal……..... Plasmid DNA encoding β-galactosidase

RAW 264.7……..... Murine macrophage cells

RNA……..... Ribonucleic acid

RNAi……..... Ribonucleic acid interference

RP-HPLC……..... Reversed phase high performance liquid chromatography

rpm……..... Revolutions per minute

RT……..... Room temperature

SAT……..... Subcutaneous adipose tissue

SD……..... Standard deviation

SEC……..... Size exclusion chromatography

shRNA……..... Short hairpin ribonucleic acid

STZ……..... Streptozotocin (2-deoxy-2-(3-(methyl-3-nitrosoureido)-D-glucopyranose)

TBE……..... Tris-borate-ethylenediaminetetraacetic acid

TFA……..... Trifluoroacetic acid

THF……..... Tetrahydrofuran

Tm……..... Midpoint transition temperature

TNBSA……..... 2,4,6-trinitrobenzene sulfonic acid

TNFα……..... Tumor necrosis factor-alpha

UV……..... Ultraviolet

WAT……..... White adipose tissue

ΔH……..... Transition enthalpy

LIST OF APPENDIX FIGURES

1. INTRODUCTION

1.1. Background and significance

1.1.1. Diabetes mellitus

Diabetes mellitus (DM) is an expanding global health problem.[1,2] It is currently estimated to affect more than 8.5% of global adult population (422 million) and about 12.2% of the U.S. adult population (30.2 million). DM rising rapidly with an estimated 1.5 million cases diagnosed each year in U.S. alone. It is also the seventh leading cause of death worldwide. DM is classified as a chronic progressive metabolic syndrome characterized by relative or absolute deficiency of insulin. Insulin is peptide hormone secreted by β-cells of pancreas to control blood sugar levels. Type 1 DM occurs due to selective autoimmune destruction of pancreatic β-cells, leading to absolute deficiency of insulin production (5—10% of total DM cases). According to current knowledge it cannot be prevented, however, tight glycemic control with efficient exogenous insulin therapy can delay the onset and progression of associated complications.[3] Type 2 DM results from reduced action of insulin on insulin-responsive cells (insulin resistance), and/or inadequate insulin secretion owing to progressive β-cell dysfunction or loss (> 90% of total DM cases). Obesity, a state of chronic low-level inflammation, is strongly associated in the development of insulin resistance and progression of type-2 diabetes. Underlying mechanisms of insulin resistance are strongly associated with an inflammatory state of macrophages and adipocytes, triggering pro-inflammatory cytokines and adipokines secretion. These pro-inflammatory factors and cytokines interferes with insulin signaling in insulin-sensitive tissues particularly the liver, adipose tissues and skeletal muscles leading to insulin resistance.

1.1.2. Cost of diabetes

Diabetic individuals with higher-than-optimal blood glucose are at higher risks of development of cardiovascular diseases, hypertension, stroke, kidney failure, nerve damage, limb amputations and overall reduced quality of life.[4,5] Alongside being a major health concern, diabetes presents a huge financial burden on national economies. The total estimated expenditure due to diagnosed diabetes in the U.S. was $327 billion in 2017.[6] Additionally, people with diabetes incur average medical expenditures of approximately $16,750 per year which is about 2.3 times higher than expenditures in its absence. Economic cost of diabetes increased by 26% between 2012 and 2017 which is majorly attributed to its rising prevalence, increased frequency of chronic complications, poor insurance coverage, and higher cost of new treatments.[6,7] Over the last decade, price of insulin has skyrocketed with as much as 585% increase between 2001 and 2015 for major brands (Humalog®). This in turn forces people to reduce amount of insulin they take thereby risking serious complications.[8,9] Subsequently, 60% of people with type-1 DM and 45% of people with type-2 DM fail to achieve their target blood glucose levels.[8,10,11] Accordingly, there is a huge unmet need for cheaper, effective and patient compliant diabetes treatment strategies.

1.1.3. Basal insulin

Exogenous insulin delivery is a necessity for type 1 diabetics and eventually for type 2 diabetics, upon failure of oral antidiabetic therapy. In a healthy human, there are two types of insulin secretions: stimulated and basal. Stimulated insulin is secreted in response to high blood glucose following food intake. Basal insulin is secreted continuously at a rate of 0.5 – 1 U/h between meals and throughout the night (**Figure 1**).[11] This slow and constant release of insulin ensures a controlled glucose output from liver *via* gluconeogenesis thereby allowing sufficient glucose levels for cerebral energy production long with other housekeeping functions during

periods of fasting.[12] Basal insulin requirement in type-1 DM is currently approached using insulin pump therapy or once/twice daily disposable devices which are accompanied by injection-associated pain, discomfort, increased risk of infection as well as psychological and economical stress for patients and their families.[13] Moreover, none of these devices are able to deliver basal level insulin at a controlled rate for more than a day.[14] Recently, researchers working on developing daily or weekly insulin delivery systems have had some success, but the translation to clinical practice is burdened with challenges such as cost, patient compliance, reproducibility and most importantly stability of the system and insulin.[15–17]

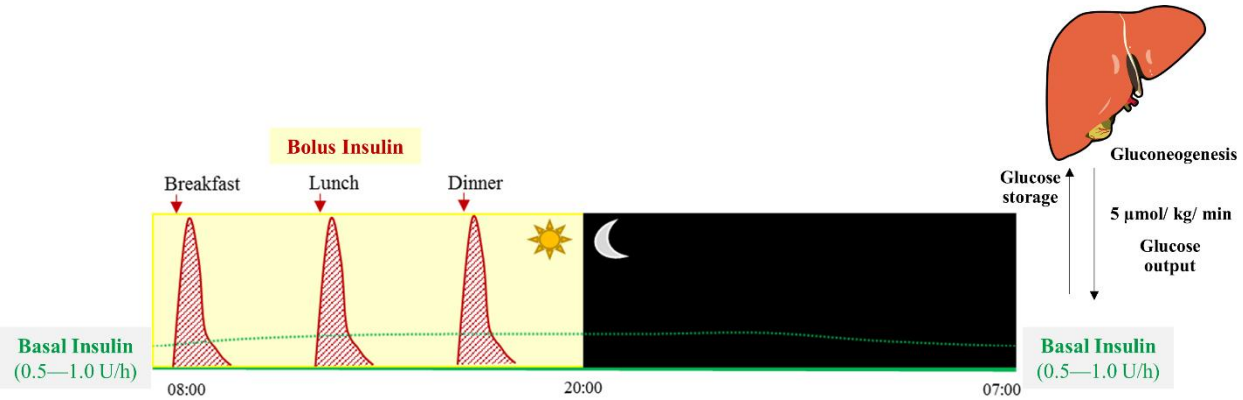

Figure 1. Schematic showing basal insulin release in a healthy body.

1.1.4. Inflammation and type-2 diabetes

Type-2 DM is the common form of diabetes (90—95% of diabetes cases) characterized by insulin resistance and abnormalities in insulin production. Chronic inflammation in obesity is a key factor associating obesity, insulin resistance and type-2 DM in a vicious loop.[18] Nearly one-third of world population and two-thirds of U.S. population is obese or overweight.[18,19] Obesity induces a complex remodeling of adipose tissue, which undergoes hyperplasia and hypertrophy to accommodate the excess caloric intake (**Figure 2**).[20] Furthermore, there is excessive infiltration and accumulation of monocytes into adipose tissue during obesity owing to increased expression

of monocyte chemoattractant protein-1 (MCP-1) on white adipose tissue. These monocytes in adipose tissue differentiate into macrophages (adipose tissue macrophages, ATMs) that undergo polarization transition from anti-inflammatory M2 phenotype to pro-inflammatory M1 phenotype.[21] Henceforth, obesity-development correlates with elevated levels of pro-inflammatory cytokines such as tumor necrotic factor alpha (TNF-α) and interleukins (IL-1β, IL-6) secreted by both adipocytes and ATMs.[21] Additionally, in obesity serum levels of insulin-sensitizing adipokines such as adiponectin and leptin are decreased, while insulin desensitizing adipokines such as resistin and retinol binding protein-4 (RBP-4) are found to be increased.[22,23]

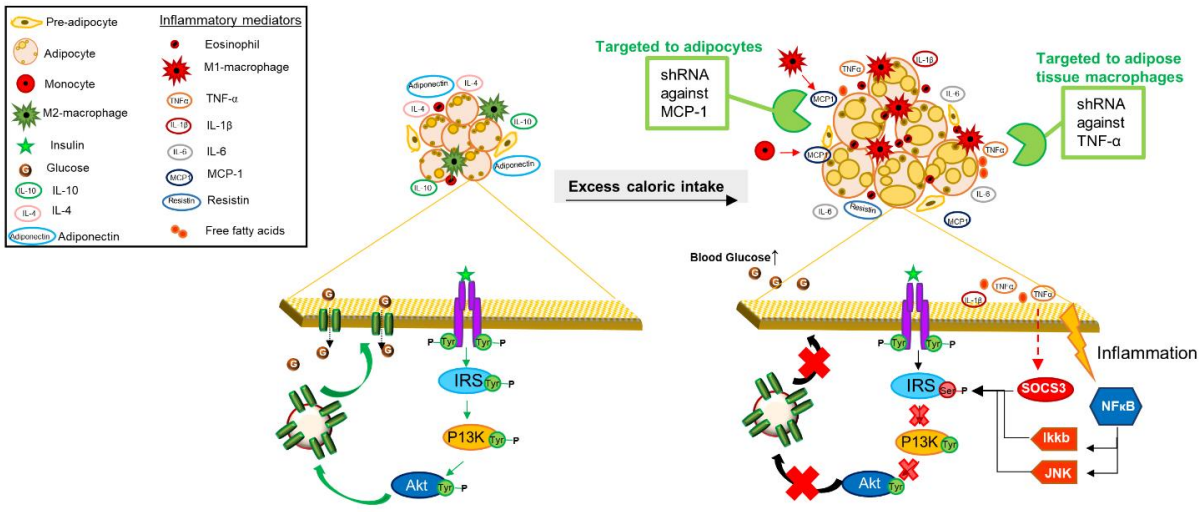

Figure 2. Schematic showing changes in obese adipose tissue leading to insulin resistance.

1.2. Treatment strategies used in this research

1.2.1. Resorbable thermosensitive polymers

Temperature sensitive or thermoresponsive polymers are the most widely studied type of stimuli-sensitive smart polymers for drug delivery owing to the ease and benefit of exploiting change in their state in response to physiological temperature. Broadly, a mixture of the

biodegradable/biocompatible copolymer and drugs/protein/peptide can be prepared by simple mixing in aqueous copolymer solution below gelation temperature to form a partially dissolved (colloidal state dispersion such as suspension, or emulsion) or completely dissolved drug delivery system which could be injected parenterally, or administered topically/transdermally, and/or inserted into a cavity (ocular, vaginal, transurethral, rectal, nasal, oral, or aural).

Following administration, the formulation would undergo thermal gelation at physiological temperature (typically body temperature being above the transition temperature) forming a depot entrapping the drug in the polymer matrix.[24] The release from these copolymeric delivery system follows two mechanisms acting simultaneously: diffusion of incorporated drug, and degradation of polymer matrix. Mostly, the initial release is diffusion-controlled and the later stage is a combination of both with degradation being dominant.[25] Thermosensitive copolymers made of polylactide (PLA) and polyglycolide (PGA), polyethylene glycol (PEG), polylactide co-glycolide (PLGA) have the advantages of being easy to manufacture, soluble in water, avoidance of toxic organic solvents, simple formulation, ease of administration, controlled release of the incorporated drug, and ability to adjust copolymer composition for controlling the release period by modifying the degradation rate, permeability of the matrix and hence the drug release profile.

Additionally, the drug release profile can also be altered by varying the copolymer concentration while carefully modulating injectability.[26] Optimization is required to reach a balance between a strong gel network and desired release rate.[27]

1.2.1.1. Thermosensitive polymer-based drug delivery systems

The use of amphiphilic block copolymers for drug delivery was first proposed in early 1980s.[28] The innovation of using PLA/PGA/PLGA/PEG copolymers for drug delivery applications lies in the simplicity of using these copolymers to deliver a wide variety of drugs,

hormones, as well as sensitive proteins and peptides with efficacy. Sustained delivery of various such therapeutics is highly desired as the conventional drug delivery methods are far from ideal. Frequent subcutaneous, intramuscular, or intravenous injections at short intervals, daily application of patches which adhere poorly and/or cause irritation, poor oral bioavailability, and short half-life after parenteral administration confronts the need for a better controlled delivery system without toxicity.[29] Simultaneously, an additional advantage observed with these block copolymers is the protection of the incorporated drugs from chemical degradation which is extremely helpful for easily chemically degraded drugs as well as sensitive protein and peptide based drugs. Chen et al. (2005) studied the release profile of model protein lysozyme using PLGA-PEG-PLGA thermosensitive copolymer of varying block lengths and aqueous copolymer concentrations. Controlled delivery of lysozyme was reported in a biologically active form, with significant lowering of burst release with increasing copolymer concentration.[30] Similar studies were done with mPEG-PLGA-mPEG copolymer and the effect of extending the PLGA block resulting in decreased degradation and controlled release of the protein for a longer duration was reported.[31]

Controlled delivery of salmon calcitonin, a polypeptide hormone for the prevention and management of osteoporosis, was also investigated using mPEG-PLGA-mPEG triblock copolymer *in vitro* and in female rat model. Calcitonin suspended in 40% w/v aqueous copolymer solution administered subcutaneously was seen to protect the rat from methylprednisolone acetate induced osteoporosis for up to 40 days.[32] Representative examples of sustained release depot-based drug delivery systems of PLA/PEG/PGA/PLGA diblock and triblock copolymers are summarized in **Table 1.**

Table 1. Representative examples of depot-based drug delivery systems of polylactide and polyglycolide diblock and triblock copolymers.

Copolymer	Drug or active ingredients	Major effects	Ref.
PLGA–PEG–PLGA	Lysozyme	Increasing the PLGA block lengths of copolymers decreased initial burst release. Increasing copolymer concentration reduced the rate of drug release	30
mPEG-PLA	7-Ethyl-10-hydroxy camptothecin	Passive accumulation of polymeric micelles in solid tumors *via* enhanced penetration and retention effect was observed *in vitro* and *in vivo*.	33
PLGA-PEG-PLGA	Cyclosporin, paclitaxel	Improved solubilization of poorly water soluble drugs. Increased chemical stability.	27
PLGA-PEG-PLGA	Dexamethasone acetate	Enhanced corneal permeability and prolonged precorneal retention. Increased Cmax and AUC. Improved bioavailability, and higher drug efficacy.	34
PLGA-PEG-PLGA	Exendin-4	Increased stability. Possible addition of excipients reduced burst release.	35
PLGA-PEG-PLGA	Recombinant human insulin	Controlled basal insulin release observed up to 15 days *in vitro* and *in vivo* after single subcutaneous injection.	36
PLGA–PEG–PLGA (Regel®)	Paclitaxel, pGH, G-CSF, insulin, rHbsAg	Reduced clearance of paclitaxel after direct intratumoral injection with minimal distribution into any organ. Controlled release of equivalent amount of pGH, insulin, and G-CSF after single subcutaneous administration compared to daily intravenous conventional therapy.	37
PLGA–PEG–PLGA	Levonorgestrel, Testosterone, Growth hormone	Increasing the hydrophobic PLGA block length of copolymers significantly decreased the release rate. Controlled zero-order *in vitro* release was observed. Enhanced absolute bioavailability of pGH compared to s.c. aqueous pGH solution.	38
PLGA-PEG-PLGA	PLK1shRNA/PEI-Lys complexes and doxorubicin	Synergistic anti-tumor efficacy of co-incorporated drugs. Reduced systemic toxicity owing to localized tumor delivery.	39
mPEG-PLGA-mPEG	Lysozyme, Salmon calcitonin	Controlled release of the protein for a longer duration by extending the PLGA block resulting from decreased degradation rate of the copolymer matrix.	32,40

1.2.1.2. Thermosensitive copolymer for controlled delivery of insulin

Controlled delivery of proteins and peptides is a highly challenging effort owing to low half-life, implicit instability and structural constraints. These are also some of the preeminent reasons that render basal level insulin delivery to type I diabetes patients a daunting task. Multiple frequent injections or round the clock insulin pump are conventionally used nowadays in order to maintain normoglycemia. Delivery of sensitive proteins and peptides has been extensively studied using PLA/PLGA based triblock thermosensitive copolymers. PLGA-PEG-PLGA thermosensitive triblock copolymers showed a controlled release of different proteins for ~2 weeks.[36,41] This copolymer system demonstrated high burst release of hydrophilic drugs like insulin owing to the higher hydrophilic GA content in the copolymer backbone. PLA being more hydrophobic than PLGA was hypothesized to undergo a slower degradation owing to retarded hydration, swelling and hydrolysis, and was further investigated for the controlled basal delivery of insulin. PLA-PEG-PLA triblock copolymers showed significantly lower burst release with desirable zero-order release profile over a period of 2-3 months.[42] Later, by incorporation of chitosan-zinc-insulin complexes in PLA-PEG-PLA copolymer, a controlled basal insulin delivery of ~63 days was obtained *in vitro*.[43] In an additional study, biocompatibility of the delivery system and efficacy of the released insulin was successfully confirmed *in vivo* using streptozotocin-induced diabetic rat model.[44] Release of drug incorporated in thermosensitive copolymer matrix is effected by a combination of diffusion through copolymer matrix and slow hydrolytic degradation of the copolymer. Several parameters such as copolymer concentration, drug loading, size of drug molecule, and hydrophobicity of drug/copolymer may affect release rate from such controlled drug delivery systems.

1.2.2. Chitosan for gene delivery

Chitin, a structural component in crustacean exoskeleton, is second most abundant biomolecule in nature.[45,46] It is very similar in structure to cellulose and has a significant role in biochemical cycling of nitrogen and carbon in aquatic ecosystem.[47,48] Chitosan (CS), which is deacetylated chitin, gathered interest around the globe for application as a gene delivery vector. CS consists of unprecedented qualities like cationic charge, high biocompatibility, ease of chemical modification and low immunogenicity.[49,50] It is virtually harmless to animals and humans.[51,52] The first scientific report of CS dates back to 1859.[53] Currently, it is widely researched in many fields due to its unique properties like easy modification of amine groups, availability of different chain lengths, biocompatibility, stability, wound healing properties, and effectiveness in cellular adhesion and proliferation.[54,55] Chemical and biological properties of CS can differ among CS polymers which can be attributed to different processes used for its extraction from chitin thereby affecting their chain length and degree of deacetylation. Although, CS has some unique properties, its shortcomings are related to its solubility issues at physiological pH and relatively low transfection ability.[56,57] However, ease of chemical alteration of CS structure helps obtain the desired properties.

1.2.2.1. Physico-chemical properties of Chitosan

CS are part of polymer family of randomly distributed d-glucosamine (deacetylated units) and N-acetyl-d-glucosamine (acetylated units) linked by β (1,4) glycosidic bonds.[58] CS polymer consist of a polysaccharide backbone which degrades before melting and therefore lacks thermoplastic properties which is typical of polymers with extensive hydrogen bonding.[59] CS molecules in solid state are generally organized in an ordered crystalline manner. It has two polymorphs: hydrous and anhydrous crystal form.[60,61]

CS is cationic in nature at acidic pH (pH < 6) owing to the protonation of its basic amino groups in polymer chain (pKa = 6 - 6.5).[62] This property allows it to easily solubilize in dilute acidic solutions but insoluble in most of organic solvents as well as in aqueous solutions at basic and neutral pH.[63] Solubility of this polymer not only depends on the degree of deacetylation but also on the chain length. Low molecular weight CS is easily soluble as compared to high molecular weight polymer chain.[64] CS is also a very good viscosity enhancer under acidic conditions.[65] The viscosity of CS solution is affected by pH, molecular weight, concentration, temperature, degree of deacetylation and ionic strength. The viscosity of solution decreases with increase in temperature.[66] It also depends on the acid used to solubilize CS. Additionally, gel formation property of CS with anionic hydrocolloids is used for controlled drug delivery. Furthermore, high charge density on CS makes it antimicrobial in nature.[67,68]

The reactivity of CS is mainly based on the presence of free amino and hydroxyl groups on its polymer backbone. The primary amine groups majorly undergo formation of Schiff base or N-acylation reactions. Presence of positive charge on CS backbone allows it to form polyelectrolyte complexes with negatively charged phosphate groups in nucleic acids to form polyplexes. Also the positive nature of CS as micelles helps in its interaction with negatively charged cell membrane resulting in its easier internalization *via* endocytosis. Additionally, at neutral or basic pH, it has been reported to bind with nucleic acids *via* hydrogen bonding and hydrophobic interactions.[69] Degree of deacetylation, molecular weight, charge ratio of nucleic acid to polymer, and pH are some of the factors which can influence the efficiency of transfection using CS-based delivery systems.[70–72] It was seen that intracellularly low molecular weight CS releases DNA easily whereas large molecular weight CS protects DNA more efficiently. Hence, a reasonable balance should be achieved to obtain high transfection efficiency.[73]

Also it was noted that a smaller chain length CS require higher nitrogen to phosphate ratio (N:P) for stable polyplex formation. At low N:P, smaller chain length CS form unstable complexes with nucleic acids yielding low transfection efficacy.[73]

1.2.2.2. Modifications of chitosan

Ease of chemical modification of CS lead to its wide spread suitability in various fields. The major purpose of modification is to improve specific functional properties and solubility at physiological pH, basic pH or in organic solvents. The presence of primary amine and hydroxyl groups makes it possible to achieve desired properties for the polymer like solubility, viscosity, charge density, hydrophobicity, and targeting ability. Amino groups of CS are more reactive to chemical modification, therefore, they require protection if hydroxyl groups are intended to be modified.[59] Across the globe, scientists have achieved vast array of modifications to achieve CS polymer with unique properties. Functional groups of CS can undergo reactions like acetylation, etherification, quarternization, esterification, phosphorylation, carboxymethyaltion, amongst others. Carboxymethylation is one of the most common modification on CS which helps in the formation of its water soluble derivatives.[74] Carboxymethylated derivatives of CS attracted great interest from fields like gene delivery, biosensors, biological imaging, and food science. Increased solubility of CS with carboxymethyl modification is largely due to the presence of either excess positive or negative charges. Moreover, quaternization of more than 25% amine groups on a CS polymer chain allows it to be soluble at all pH.[74]

Furthermore, scientists have modified CS to attach various ligands to achieve targeting ability to specific cellular locations *in vivo*. CS derivatives having functional molecules on its surface can potentially enhance its ability to target a specific organ.[75] Ligands including but not limited to galactose, transferrin, mannose, and folate have been studied to target CS-based delivery

systems to their respective receptors.[76–81] It was reported that introduction of thiol groups helps in increasing the stability of CS-based polyplexes.[82,83] Additionally, thiol modification also helps in release of nucleic acid inside the cell. Modification of CS with thioglycolic acid or 2-iminothiolate has also been reported to improve the transfection efficiency as well as for efficient intracellular release.[84,85] Several peptides and amino acids have also been studied to aid in targeted delivery and cell penetration.[86,87] Conjugation of CS with arginine and with non-polar amino acids has also been investigated to improve the overall hydrophilicity or hydrophobicity of the complex, respectively. Such conjugation also facilitates higher level of penetration inside cells alongside improved transfection.[88,89] Thus, fine tuning CS with chemical modifications can lead to new and biocompatible non-viral gene delivery systems with promising wide array of therapeutic benefits.

1.2.2.3. Mechanism of chitosan-based gene delivery systems

The transfer of genetic material from extracellular environment to an intracellular organelle (nucleus for pDNA and shRNA or cytoplasm for siRNA and miRNA) is the major goal of gene delivery. The mechanism of gene delivery is divided into five stages as follows: extracellular protection, biological membrane, endosomal system, nucleus, and transcription & translational processes.[90] Presence of DNase in the extracellular environment is additionally one of the major barriers to gene delivery. Due to the presence of DNase, DNA gets degraded spontaneously upon intravenous, intramuscular or mucosal administration.[91–93] Moreover, the negative charge of both DNA and cell membrane results in very low uptake of DNA by the cell owing to poor association between them. Therefore, DNA is generally complexed with a molecule like CS to enhance internalization, to protect it from enzymatic degradation, and to keep it stable during internalization process. It was shown that cellular uptake did not appear to be rate limiting step for CS particles having positive charge and size less than 200 nm in diameter.[94,95] Many groups around the globe

conjugated ligands to CS nanoparticles to target receptors/transporters specific to cells in order to increase cellular uptake *via* endocytosis. [96] The endocytosis pathways include phagocytosis, clathrin-mediated endocytosis, caveolae-mediated endocytosis, and micropinocytosis.[97] CS-DNA polyplex after internalization into endosomes needs to release the gene into the cytoplasm for transfection process. The transfection efficiency of CS is believed to be dependent on its release from endosome into cytoplasm *via* proton sponge effect.[98] Poor endo-lysosomalytic proton sponge effect, long duration for uncoupling CS-gene complex, and limited membrane perturbing ability explains low transfection ability of CS.[70]

Additionally, membrane perturbation ability of CS-based systems is believed to be associated with its degree of protonation.[99] It was seen that incorporation of poly(propyl acrylic acid) (PPAA), a pH sensitive polymer, with CS-DNA complex enhances its transfection efficiency due to improved membrane disruption ability.[100] Similar results were observed when uronic acid and PEI were combined with CS in separate studies showing improved transfection efficiency.[101,102] Increasing osmolarity and rupturing of endosome by CS degradation products is another method of endosomal escape.[103] Endosomal escape is believed to be the major rate-limiting step in CS related transfection.[94,104] Once the pDNA reaches cytoplasm, various types of DNA-binding proteins make a large complex with the plasmid.[105] The transcription factors complexed with plasmids interact with importin β and various other proteins that connects the complex with kinesin and dynein for their movement beside microtubules towards nucleus.[106] The pDNA then enters the nucleus *via* nuclear pore complex.[107,108]

1.2.2.4. Biocompatibility, biodegradability and stability of chitosan-based systems

CS is considered to be biocompatible with approval for dietary applications in Italy, Japan and Finland.[109] It has LD_{50} of 16 g/kg in mice (oral test) which is equivalent of salt and sugars.[110,111]

CS has been approved for its use in wound dressings by FDA.[112] A group in Sweden compared the toxicity profile of CS and polyethylenimine (PEI) at genetic level.[103] Cyclooxygenase 1 and 2 (COX-1 and COX-2) are enzymes involved in inflammatory processes. The Chung group found that the expression of both cyclooxygenases was increased with transfection process through PEI whereas it was downregulated in case of CS.[74] Moreover, Heme-oxygenase-1 (HO-1) gene, induced by oxidative stress and inflammatory cytokines, is up-regulated by PEI but not CS.[113] CS degradation product, N-acetylglucosamine, has shown anti-inflammatory properties and can be responsible for this effect. CS cyto-compatibility has been tested and proven numerous times with various types of cells.[114] It was shown that degree of deacetylation (DDA) affects cell attachment.[74] It was reported that higher the DDA, more will be cellular attachment in case of keratinocytes and Schwann cells.[114–116] Inside the body, CS can be broken down by enzymes which can cleave glucosamine to N-acetyl-glucosamine, glucosamine to glucosamine, and N-acetyl-glucosamine to N-acetyl-glucosamine bonds. Earlier CS was thought to be degraded *via* lysozymes and bacterial enzymes in colon but recently eight chitinases have been found in humans with some suggested to attain enzymatic activities.[117,118] The magnitude and degree of biodegradation of CS *in vivo* depends on its DDA.[119,120] Interestingly, various proteases were found to be capable of degrading CS with leucine amino-peptidase being most efficient.[51] CS degradation after intravenous administration has been hardly reported in literature. In one of the few studies published, CS oligosaccharides resulted in up-regulation of lysozyme activity in rabbit's blood.[121]

Stability of formulation is also one of the major parameters for efficient therapeutic effects. Although CS-based systems gained much attention over the last few decades, very few studies have looked into the long term stability of these systems.[122–125] Lyophilized CS-DNA complexes were able to maintain their transfection efficacy in excess of 4 weeks.[126,127] However, CS-DNA

complex stored in PBS remained stable for only couple of hours.[128] There are various factors which affect the stability of a formulation. These factors can be divided in two broad categories: (A) Internal factors (such as purity level, moisture content, DDA), and (B) External factors (such as humidity and temperature). Molecular weight of CS polymer was also found to affect its thermal stability.[129] Heat generated during compression in table processing can affect the molecular weight distribution of CS in tablet.[130] Several studies have shown that DDA of CS can affect its hydrolytic degradation and thermal behavior.[129,131,132] It was found that DDA and rate of acidic hydrolysis of CS polymer are inversely correlated.[133] In addition environmental temperature also have an effect on CS degradation. Studies shows that CS solution stored at room temperature or higher leads to increased rate of degradation of CS chains whereas no significant chain loss was observed at 5 °C.[133,134] For long term storage of CS nanoparticles, lyophilization is a well-established method. Lyophilized CS-lecithin nanoparticles after seven months of storage did not show any alteration in their physicochemical properties and were able to re-disperse easily without any aggregates.[135] Nevertheless, lyophilization can damage unmodified, and in some cases, modified CS polymer chains.[136] Despite great potential, long term stability of CS can pose a substantial drawback in its pharmaceutical applications and requires keen investigation. A summary of CS-based gene delivery systems is given in **table 2**.

Table 2. Studies using chitosan-based gene delivery in animal models.

Formulation	Chitosan Mw (kDa)	Gene	Disease	Route of administration	Key outcomes	Ref.
TAT-g-CS nanoparticles	11.3	siRNA	Breast cancer	Intratumoral	Good biocompatibility, Downregulate the expression of target genes, inhibit proliferation and metastasis of 4T1-Luc tumor cells.	[137]
Man-CS-Phe/DNA polyplexes	50	pHBsAg	Hepatitis B	Intradermal	Multi-fold increase in anti-HBsAg titers observed up to six weeks; Increased lymphocyte proliferation as well as increased interferon (IFN)-γ and interleukin (IL)-4 production.	[139]
CS-pDNA microparticles	1400	pnlacF	Ampicillin resistance	Oral	Chitosan DNA microparticles protected encapsulated pDNA from nuclease degradation, Transport of pDNA to Peyer's patches through M cells, demonstrated higher level of gene expression in stomach and small intestine of mice.	[140]
pDNA/ N-acyl LMWC Polyplexes	50	pUMVC 3-mIL4 and IL10	Type 1A diabetes	Intramuscular	Demonstrated significantly high expression of interleukin (IL)-4 and interleukin (IL)-10 production in mice, reduced levels of blood glucose, TNF-α and IFN-γ.	[142]
CS-pDNA nanoparticles	71.3	pCAGG S	Influenza	Intramuscular	Demonstrated high antibody titer in mice serum increased HI antibody titer in mice serum, stimulated specific B lymphocytes increased humoral immunity and antibody titers.	[143]
CS-pDNA chitoplexes	Low viscous	pCAGG S-MCS	Influenza	Intranasal	High levels of ion channel protein (M2) and nucleoprotein (NP) specific serum IgG and IgA antibodies in mice serum.	[144]

1.2.2.5. Limitations of chitosan-based gene delivery systems

Several extracellular and intracellular barriers limit the efficiency of gene transfer by non-viral methods. Depending on the route of administration, the delivery system faces diverse anatomical barriers starting from epithelial and endothelial cells to extracellular matrix to access the target site.[147,148] Simultaneously, the gene delivery vector needs to be capable of escaping the phagocytes and extracellular nucleases present at systemic circulation. Overpassing these, another critical step is to cross the cell membrane which commonly involves multiple mechanisms such as endocytosis, pinocytosis or phagocytosis or even passive transport.[149] Intracellularly, upon been taken up by endosomes, the delivery system can be subjected to enzymatic degradation. CS-based delivery systems have demonstrated ability to escape endosomes, the mechanisms involved were discussed in previous sections. Upon their release from endosomes, the presence of enzymes and proteins in cytoplasm make the traffic to nucleus very critical. The nuclear envelope represents an additional barrier. Finally, the last limitations comprise the release of nucleic acid from the complex and cellular transfection.[150–152]

CS without structural chemical modification has limited applications as gene delivery systems.[153,154] The low charge density under physiological pH leads to low solubility, aggregation and poor stability of unmodified CS-based form. Consequently, it leads to a compromised buffering capacity, and the weak proton sponge effect does not contribute to endosomal escape mechanism resulting in a low endosomolytic effect.[155–157] Several strategies have been implemented to overcome these limitations that CS imposes, such as modification of CS structure, conjugation, grafting, copolymerization or encapsulation into nanoparticles.[158] This process includes a careful choice of a specific CS considering its molecular weight, degree of deacetylation, chemical modifications and the nature of the eventual substituents to suit the

physicochemical properties. Thus, it enables extensive possibilities for CS derivatives and the management of product properties for the desired function. Targeted CS-based gene delivery has been designed to address a very important obstacle in the development of these type of formulations, the lack of cell-specificity.[80,159–163]

1.2.2.6. Targeting adipose tissue macrophages

Previous work from our lab has focused on targeting inflammation in type-1 DM with positive outcomes.[142] Moreover, previous studies from our lab have shown significantly improved transfection and uptake of mannose conjugated CS nanomicelles by RAW 264.7 macrophages.[139] Additionally, superior biocompatibility, targeting efficiency and transfection efficacy was achieved *in vitro* and *in vivo* using mannose conjugated CS-based nanomicelles for enhanced intradermal delivery of hepatitis B DNA vaccine.[139] M1 polarized macrophages specifically and abundantly express glucose transporter-1 (GLUT-1) for which mannose is a substrate (Km ~6mM).[164,165] A comprehensive analysis of human tissue samples reported that GLUT-1 is absent or undetectable in many normal tissues including liver, lungs, breast, ovary, pancreas, uterus, thyroid, stomach and skeletal muscles.[166] Therefore, local administration of mannose modified CS nanomicelles to regions of high macrophage density (e.g. peripheral tissues) is a promising strategy for a targeted approach.

1.2.2.7. Targeting adipocytes

Ligand-directed peptidomimetic CKGGRAKDC-GG-$_D$(KLAKAK)$_2$ called adipotide was created as an anti-obesity peptide for targeted ablation of white adipose tissue (WAT) leading to weight reduction in obese individuals.[167,168] CKGGRAKDC was found to selectively home in fat cells by targeting prohibitin receptor present in white fat vasculature *via* receptor-mediated cell internalization. The homing sequence was linked to a pro-apoptotic and lipolytic sequence

$(KLAKAK)_2$ which following cellular internalization, was designed to disrupt mitochondrial membranes and lead to programmed cell death. These two functional domains were linked together by a glycinyl-glycine bridge.[167] Treatment with adipotide resulted in targeted apoptosis in WAT, rapid weight loss and improved insulin resistance in obese monkeys.[167] Due to its remarkable efficacy in causing weight reduction in obesity it was briefly introduced in the market, however, the treatment was associated with serious adverse effects such as dehydration, severe pain, lumps at injection site, kidney lesions, and significant kidney damage that lead to its discontinuation. Nevertheless, adipose homing peptide (AHP, "CKGGRAKDC") efficiently targets adipose tissue allowing preferential uptake and internalization by prohibitin receptor in adipose vasculature.[169] Therefore, conjugation of this peptide on to CS may facilitate effective targeting and accumulation of silencing RNA loaded CS nanomicelles to adipose tissues.[169–171]

1.3. Statement of problem and research objectives

1.3.1. Basal insulin delivery in diabetes mellitus

Daily injections of insulin are a necessary requirement for all patients with type-1 DM and many patients with type-2 DM. Basal insulin requirement in type 1 diabetes is currently approached using insulin pump therapy or once daily disposable devices. Frequent injections are associated with pain, discomfort, increased risk of infection, and risk of life-threatening hypoglycemia.[14,172,173] Moreover, multiple administrations corresponding to variable basal insulin profiles are associated with damage to nerves, blood vessels and organ resulting in an increased frequency of diabetic complications.[174] Controlled delivery of proteins such as insulin is challenging owing to its short half-life and low thermal stability. Distinctive properties of insulin to self-associate in the presence of zinc and to form polyelectrolyte complexes with cationic polymer CS can be explored (**Figure 3**). Modification of insulin with CS and zinc is expected to

minimize burst release as well as preserve its stability over a prolonged duration of release and storage.

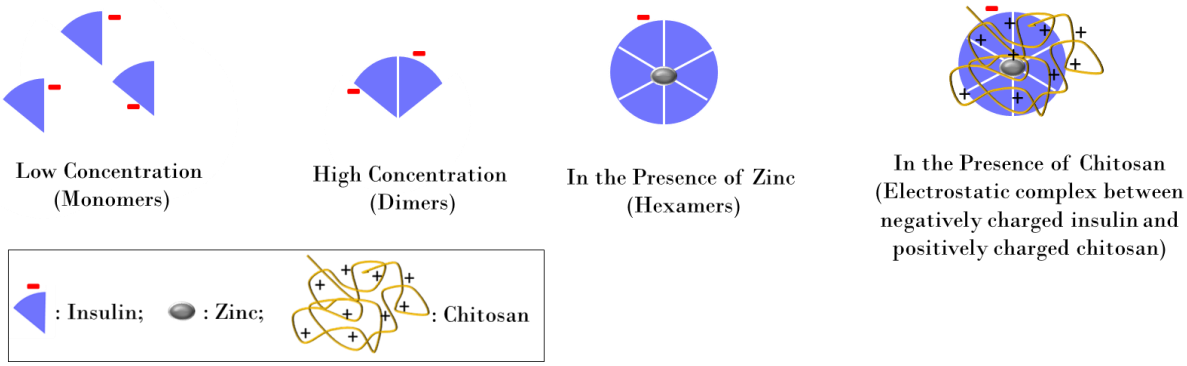

Figure 3. Schematic representation of modification of insulin using zinc and chitosan.

The aim of this study is to formulate and optimize a thermosensitive copolymer-based controlled delivery system incorporating CS-zinc-insulin complexes capable of delivering insulin at basal level for an extended period. Previously, it has been reported that CS-zinc-insulin complexes incorporated in thermosensitive copolymer released insulin at a controlled rate in a biologically stable form.[43,44] Additionally, it has been well established that size and hydrophobicity of the incorporated molecule plays a major role in the degradation profile of copolymer and consequently, release profile of the incorporated molecule.[175,176] In this research, we explore a dual approach and test the effect of chain length and hydrophobic modification of CS on *in vitro* release profile and stability of CS-zinc-insulin complexes. We **hypothesize** that copolymeric depot incorporating CS-zinc insulin complexes prepared using hydrophobically modified smaller chain length CS will deliver insulin at a basal rate for an extended period in a conformationally and chemically stable, biologically active form. Reducing size of CS-zinc-insulin complexes using smaller chain length of CS will help in reducing rate of copolymer degradation. Secondly, complex formation between fatty acid-grafted-CS and zinc-insulin hexamers will reduce the overall

hydrophilicity of insulin leading to low initial burst release and prolonged release duration owing to slow diffusion of the complex through the copolymer matrix. A schematic of depot-in-depot approach is illustrated in **figure 4**. Although the concept of making insulin more hydrophobic has been explored in numerous ways, but chemical modification of insulin largely reduces its binding affinity to insulin receptor resulting in a decreased biological potency.[177–179] Electrostatic complex formation between insulin and hydrophobically modified CS is expected to increase the overall hydrophobicity of insulin without affecting its stability or potency.

Overall, controlled release of insulin at basal level will result in a better management of blood glucose levels and prevent formation of ketone bodies in type-1 DM animal model, in comparison to daily injections of long-acting insulin (conventional treatment strategy).

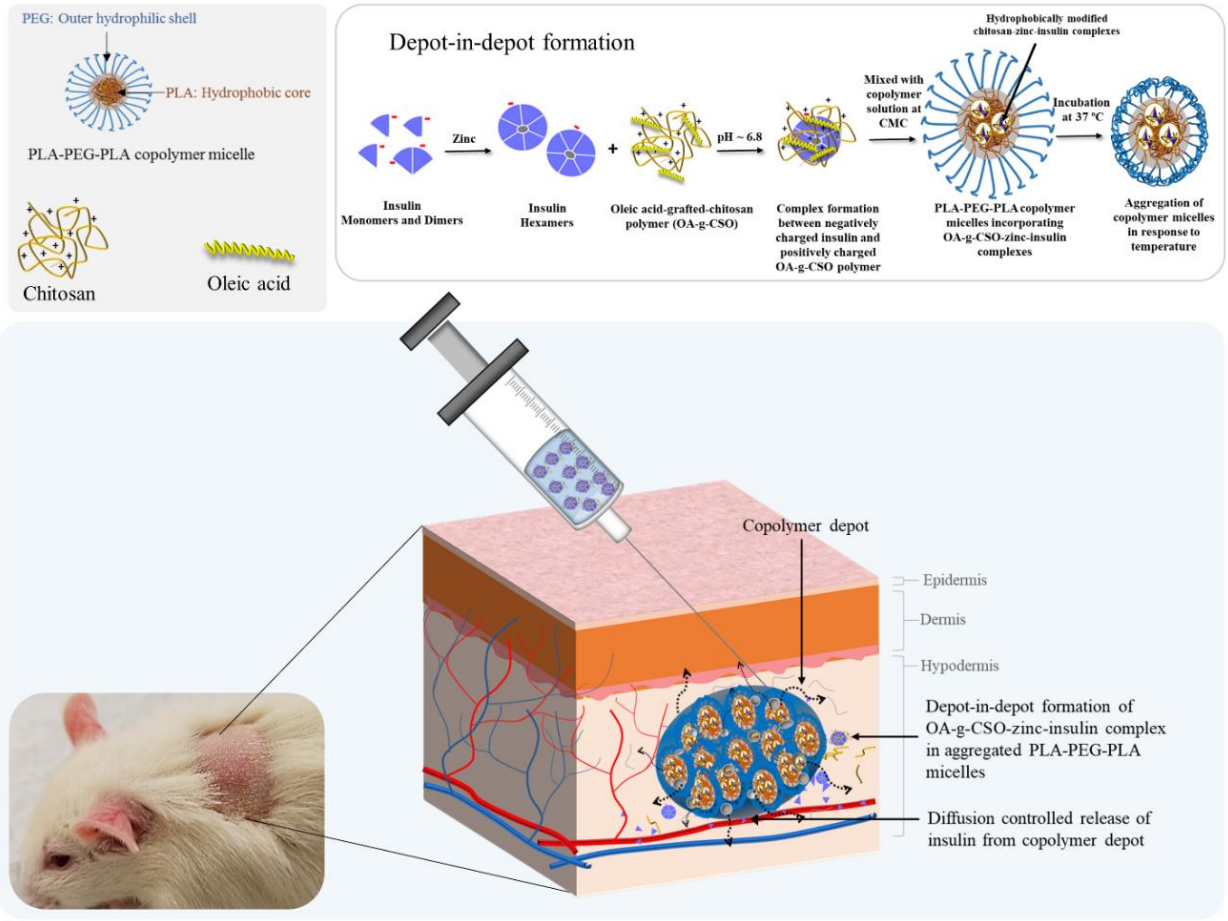

Figure 4. Schematic for depot in depot formulation, administration and release of hydrophobically modified chitosan-zinc-insulin complexes incorporated in triblock poly(D,L-lactide)-poly(ethylene glycol)-poly(D,L-lactide) (PLA-PEG-PLA) thermosensitive smart copolymer solution for controlled delivery of basal insulin.

1.3.2. Anti-inflammatory therapy for treatment of insulin resistance

Recent preclinical and clinical investigations aimed at downregulating pro-inflammatory cytokines have shown significant potential in improving insulin sensitivity. Non-steroidal anti-inflammatory drugs like salicylates have been found to improve glycemic control by decreasing inflammatory mediators.[180–182] However, high doses of these drugs are required for extended periods of time to obtain efficacy which often results in development of adverse effects resulting in cardiac, hepatic and renal impairment along with serious gastrointestinal disorders.[183] In another study, TNF-α neutralization in obese rats significantly improved insulin induced peripheral

glucose uptake.[184] Also, clinical trials using small molecule anti-inflammatory drugs such as TNF-α and IL-1 receptor antagonists showed improvement in insulin sensitivity.[185,186,187,188] However, need for systemic administration of these drugs is a major limitation to their application. Serious off-target adverse effects such as infection, interstitial pneumonia, and liver failure were observed owing to generalized suppression of the immune system.[189] Additionally, researchers trying to block distinct pro-inflammatory cytokine pathways have achieved limited success.[180,184,185,188] Studies performed using TNF-α inhibitor did not achieve required efficacy in ~70% of the patients with rheumatoid arthritis.[190,191] Cross-talk between adipocytes and immune system prevents long-term benefits and inflammation recurrence.[192] A combinational approach for treatment targeting both adipocytes and ATMs may result in a better response. This can be further supported by the fact that different cytokines mediate insulin resistance by somewhat different pathways.[189] Moreover, many pro-inflammatory cytokines such as TNF-α, IL-1β and IL-6 are paracrine in nature with low circulating levels and much higher tissue concentrations, further illustrating the necessity to target such therapies specifically to adipocytes and ATMs.[193]

Gene therapy has emerged as a promising strategy for treatment of wide range of pathological conditions. Genes are the essential blueprints that contain information required to make functional proteins. Conventional therapies often provide symptomatic relief or lead to treatment outcomes that are only effective temporarily. Gene therapy has the potential to target the root cause of various diseases by cell-specific modulation of the genetic code. Therefore, to control the progression of DM and its complications we propose targeted delivery of silencing RNA against pro-inflammatory cytokines to ATMs and adipocytes to specifically attenuate inflammatory pathways at their origin that will in turn improve insulin sensitivity.

1.3.3. Chitosan-mediated RNA interference for treatment of insulin resistance

High therapeutic efficacy following gene therapy necessitates delivering genetic load to target cells with high specificity. In this study, we propose oleic acid-grafted-CS polymer modified with mannose or AHP to target ATMs or adipocytes, respectively. Targeted delivery of silencing RNA against TNF-α and MCP-1 would specifically attenuate inflammatory pathways that will in turn improve insulin bioactivity. This study aims to leverage the intimate relationship between adipocytes, ATMs and the immune system that leads to obesity-induced insulin resistance by specifically targeting macrophages and adipocytes using local administration of CS-based nanomicelles to modulate inflammation while reducing off-target interactions and potentiating overall therapeutic efficacy. Furthermore, amphiphilic fatty acid-grafted-CS polymers self-assemble in an aqueous environment to form micelles capable of forming nanoscale complexes with negatively charged nucleic acids (RNA, DNA). These nanoscale complexes allow superior gene transfection owing to enhanced adsorption on to the lipophilic cellular membranes and effective intracellular dissociation releasing free nucleic acid.[194–196] Surface of these nanomicelles can be further modified with ligands allowing selective targeting, enhanced cell binding and internalization.[139] Moreover CS polymeric nanomicelles have been widely studied to be biocompatible, biodegradable, safe and efficient delivery vectors for gene therapy for a chronic disease like diabetes. We **hypothesize** that downregulating inflammation *via* adipose tissue targeted RNA interference (RNAi) using CS nanomicelles as a non-viral vector will help alleviate insulin resistance in a safe and effective manner. Mannose and AHP conjugated CS nanomicelles will result in targeted accumulation and superior transfection of incorporated nucleic acids in target cells. Additionally, combinational therapy of multiple RNAi strategies will potentially exert a synergistic outcome in modulating inflammation.

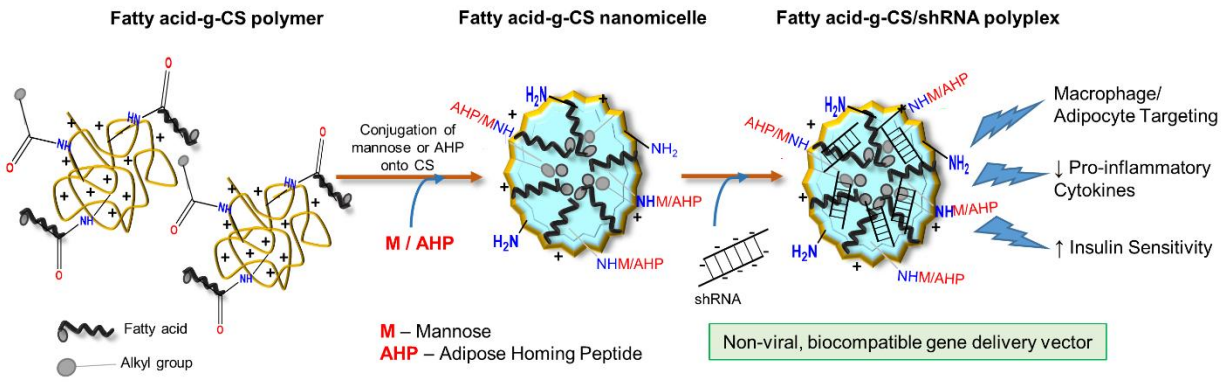

Figure 5. Schematic illustration of macrophage and adipocytes targeted chitosan nanomicelles for RNA interference mediated downregulation of pro-inflammatory cytokines.

We tested our hypotheses through the following specific aims:

1.3.4. Specific Aim 1: To optimize formulation parameters *in vitro* for controlled release of basal level insulin

- To synthesize triblock poly(D, L-lactide)-poly-(ethylene glycol)-poly(D, L-lactide) (PLA–PEG–PLA, 1500–1500–1500, 4500 Da) thermosensitive copolymer using ring opening polymerization method. Determine structural composition of the synthesized copolymer using proton (^{1}H) and carbon (^{13}C) nuclear magnetic resonance spectroscopy (NMR) and gel permeation chromatography (GPC), and phase transition temperature using tube inversion method.
- To synthesize oleic acid grafted CS polymers by carbodiimide-mediated coupling reaction. Determine structural composition of synthesized oleic acid-grafted-CS polymers using ^{1}H NMR and fourier transform infrared spectroscopy (FT-IR), and grafting percentage using trinitrobenzenesulfonic acid reagent assay (TNBSA).

- To modify stability of insulin by forming zinc-insulin hexamers and further stabilization of the hexameric form by electrostatic complex formation between negatively charged zinc-insulin hexamers and positively charged CS polymer at physiological pH.
- To study the effect of different chain length of CS and oleic acid modification of CS on the thermal stability of insulin using Nano differential scanning calorimetry (Nano DSC).
- To study binding constant, enthalpy of complex formation, and the stoichiometry of interaction between zinc-insulin hexamers and CS polymers using isothermal calorimetry (ITC).
- To study the effect of different chain length of CS on the degradation profile of PLA-PEG-PLA copolymer using size exclusion chromatography (SEC).
- To study effect of zinc and different CS polymers on *in vitro* release profile of insulin using *in vitro* release model.
- To study the stability of insulin released from thermosensitive triblock copolymer depot *in vitro* and in formulation upon storage at 4°C, using nano-DSC, circular dichroism spectroscopy, and reversed phase high performance liquid chromatography (RP-HPLC).

1.3.5. Specific Aim 2: To study *in vivo* release profile, bioactivity of insulin released, and biocompatibility of the delivery systems

- To study the *in vivo* release profile, absorption and bioactivity of insulin released from thermosensitive copolymeric depot in streptozotocin (STZ) induced diabetic rat model.
- To compare the efficacy of optimized controlled release formulation with daily administration of marketed long-acting insulin glargine (Lantus® U-100) by studying glycemic control, blood ketone levels, cataract formation, and body weight over a prolonged period.

- To assess *in vitro* biocompatibility using MTT (3-(4,5-dimethylthiazol-2-yl)-2,5-diphenyltetrazolium bromide) cell viability assay.
- To assess *in vivo* biocompatibility using histological analysis of the depot site using bright field microscopy.
- To study the immunogenic potential of insulin released *in vivo* using an indirect enzyme linked immunosorbent assay (ELISA) technique.

1.3.6. Specific Aim 3: To optimize and evaluate *in vitro* biocompatibility, uptake, transfection and efficacy of RNA interference using chitosan nanomicelles

- To design mannose and adipose homing peptide (AHP) conjugated CS polymeric nanomicelles to specifically target glucose transporter-1 (GLUT-1) present on adipose-tissue macrophages (ATMs) and prohibitin receptor on adipocytes, respectively.
- To synthesize and characterize fatty acid, mannose and AHP conjugated CS polymer.
- To prepare and characterize CS nanomicelles and pDNA polyplexes.
- To study the ability of synthesized CS polymers in obtaining pDNA condensation, protection from nucleases, and endosomal buffering.
- To prepare *in vitro* inflammatory cell culture model using M1 polarized RAW 264.7 macrophages and differentiated 3T3-L1 adipocytes.
- To study *in vitro* biocompatibility, cellular uptake, mechanism of uptake and transfection efficiency using model pDNA.
- To assess *in vitro* RNA interference efficacy of plasmid encoding shRNA against TNFα and MCP-1

1.3.7. Specific Aim 4: To assess *in vivo* biodistribution, safety and efficacy of optimized formulations in the treatment of insulin resistance

- To develop high fat diet fed obese and diabetic preclinical mouse model.
- To study *in vivo* biodistribution of FITC conjugated CS nanomicelles and pDNA polyplexes following subcutaneous administration in obese diabetic mouse model.
- To study *in vivo* biocompatibility following formulation administration using histological analysis of various organs and injection site tissue.
- To study *in vivo* RNA interference efficiency of plasmid encoding shRNA against TNFα and MCP-1, determined using specific cytokine ELISA kits in serum, and subcutaneous and visceral adipose tissues.
- To determine *in vivo* efficacy of targeted downregulation of pro-inflammatory cytokines by assessing insulin sensitivity and glucose tolerance before and after treatment with optimized formulation.

Together, our proposed studies aim to introduce better treatment strategies to reduce diabetes burden and diabetic complications in the long run. A cheaper and biologically relevant basal insulin therapy will improve patient compliance and outcomes. Moreover, insulin resistance, a major issue in diabetes, if reduced by downregulating inflammation, will reverse the progression of disease and lower risk of associated-complications concomitant to the disease.

2. MATERIALS AND METHODS

2.1. Materials

The list of materials used in this study is presented in table 2.

Table 3. Materials used and their source.

Materials	Source and location
10% Neutral buffered formalin	Richard-Allan Scientific (Kalamazoo, MI, USA)
1-Ethyl-3-(3-dimethylaminopropyl) carbodiimide hydrochloride (EDC.HCl)	Creosalus Inc. (KY, USA)
2,4,6-Trinitrobenzenesulfonic acid solution (TNBSA)	Sigma–Aldrich (MO, USA)
3-(4,5-Dimethylthiazol-2-yl)-2,5-diphenyl-tetrazolium bromide (MTT)	Sigma–Aldrich (MO, USA)
3T3-L1 cells (ATCC® Cl-173™)	American Type Culture Collection (ATCC, Rockville, MD, USA)
Acetonitrile	Sigma Aldrich Co. (St. Louis, MO, USA)
Anhydrous zinc acetate	Alfa Aesar, (MA, USA)
Beta-galactosidase enzyme assay kit	Promega (Madison, WI, USA)
Chitosan (average molecular weight 5, 20, 30, 50, and 200 kDa, ~85-90% degree of deacetylation)	Glentham Life Sciences (Corsham, WT, UK)
D,L-lactide	Alfa Aesar, (MA, USA)
Dimethyl sufoxide	Calbiochem USA

Table 3. Materials used and their source (continued).

Materials	Source and location
Dulbecco's modified eagle's medium (DMEM)	American Type Culture Collection (ATCC, Rockville, MD, USA)
Fluorescein isothiocyanate (FITC)	Thermo Fisher Scientific (Waltham, IL, USA)
Glucometer	Bayer Contour® Glucometer, Mishawaka, IN, USA
Human embryonic kidney (HEK-293) cell line	American Type Culture Collection (ATCC, Rockville, MD, USA)
Human recombinant insulin (Cell Prime™ R-Insulin)	EMD Millipore Corporation (MA, USA)
Lipopolysaccharides	Sigma Aldrich (St. Louis, MO, USA)
Micro BCA protein assay kit	Pierce Biotechnology Inc. (Rockford, IL, USA)
Mouse Picokine™ Elisa Kit TNFα (Ek0527) , MCP-1 (Ek0568), IL-1β (Ek0394), IL-6 (Ek0411) and Adiponectin (Ek0596)	Boster Biological Technology (Pleasanton, CA, USA)
Murine macrophage (RAW 264.7) Cells	American Type Culture Collection (ATCC, Rockville, MD, USA)
N-Hydroxysuccinimide (NHS)	Alfa Aesar (MA, U.S.A.)
Oleic acid	Spectrum Chemical (NJ, USA)
Phosphate buffered saline (PBS)	American Type Culture Collection (ATCC, Rockville, MD, USA)
Plasmid DNA encoding beta-galactosidase (Gwiz-βgal)	Aldevron LLC (Fargo, ND, USA)
Plasmid DNA encoding green fluorescent protein (Gwiz-GFP)	Aldevron LLC (Fargo, ND, USA)

Table 3. Materials used and their source (continued).

Materials	Source and location
Plasmid encoding shRNA against MCP-1 (TL501987A lot#0116)	Origene Technologies Inc. (Rockville, MD, USA)
Plasmid encoding shRNA against TNFα (TL515379C lot#1215**)**	Origene Technologies Inc. (Rockville, MD, USA)
Plasmid scrambled control (TR30021)	Origene Technologies Inc. (Rockville, MD, USA)
Polyelthylene glycol (1500 Da)	Sigma Aldrich Co. (St. Louis, MO, USA)
Polystyrene standards	Sigma–Aldrich (MO, USA)
Rat immunoglobulin G (Igg)	Alpha Diagnostic International (TX, USA)
Stannous octoate	Pfaltz and Bauer Inc., (Waterbury, CT, USA)
Streptozotocin	Enzo Life Sciences (NY, USA)
α-D-Mannopyranosylphenyl isothiocyanate	Toronto Research Chemicals (Toronto, ON, Canada)

All other reagents were of analytical grade and were used without further modification.

2.2. Animals

Animal study protocol and experiments were reviewed and approved by the North Dakota State University Animal Care Use Committee (IACUC, Protocol #A18028 and #A19022). Male Sprague-Dawley rats were purchased from Charles River Laboratories Inc., USA. Male 4 weeks old C57BL/6 mice were purchased from The Jackson laboratory USA.

2.3. Experimental methods

2.3.1. Synthesis and characterization of thermosensitive triblock copolymer

Thermosensitive triblock copolymer poly(D,L-lactide)-poly(ethylene glycol)-poly(D,L-lactide) (PLA-PEG-PLA, 1500-1500-1500, 4500 Da) was synthesized using ring opening polymerization of D,L-lactide catalyzed by stannous octoate using PEG (1500 Da) as an initiator, in anhydrous atmosphere (**Figure 6**).[42] Briefly, PEG (9.99 g) was dissolved in anhydrous toluene (40 mL) in a three-necked round bottom flask at 90 ˚C in nitrogen atmosphere for 0.5 h. D,L-lactide (19.98 g) was added to the solution and temperature was increased to 120 ˚C. Reactants were allowed to dissolve completely to form a homogenous mixture followed by addition of stannous octoate (0.03% w/w, ~9 µL). Reaction was carried out under continuous stirring at 120 ˚C for 12 h. Reactant mixture was then dried in a vacuum oven to evaporate toluene completely. Crude copolymer was then purified by dissolving it in ice cold water followed by heating to 80 ˚C to precipitate out the copolymer. Purification step was repeated 2 – 3 times to separate out unreacted monomers and catalyst. Finally, precipitated copolymer was lyophilized to get rid of residual water.

Structural composition of synthesized copolymer was determined using proton (^{1}H) and carbon (^{13}C) nuclear magnetic resonance (NMR) spectroscopy using deuterated chloroform ($CDCl_3$) as a solvent (10 mg/0.6 mL). Tetramethylsilane (TMS) signal was used for calibration and its signal was taken as zero chemical shift. Bruker spectrometer operated at 400 MHz and 25 °C was used for measurements. ^{13}C NMR spectra was also obtained to confirm the presence of PLA and PEG blocks. Analysis was performed using Bruker TopSpin 3.2.b.69 software.

Number average molecular weight (M_n), weight average molecular weight (M_w), and molecular weight distribution (polydispersity index, PDI) of synthesized copolymer (0.2% w/v in tetrahydrofuran (THF)) was determined using gel permeation chromatography (GPC) (Eco SEC HLC-8320-GPC system, Tosoh Bioscience, Japan) with a differential refractometer (DRI) detector. Separations were performed using 2 TSK gel SuperH3000 6.0 mm ID × 15 cm columns with an eluent flow rate of 0.35 ml min^{-1}. Columns and detectors were thermostated at 40 ˚C, with eluent THF and injection volume 10 µL. Calibration was conducted using polystyrene standards (Agilent EasiVial PS-H 4ml).

Injectability of different aqueous copolymer concentrations was determined by injecting 0.5 mL copolymer into a glass tube using 25 G needle. Sol-gel transition temperature was noted by tube inversion method by immersing the tubes containing copolymer solution in a water bath at 8 °C, followed by raising the temperature 2 °C/step and observing phase transition of copolymer by inverting the tube horizontally.

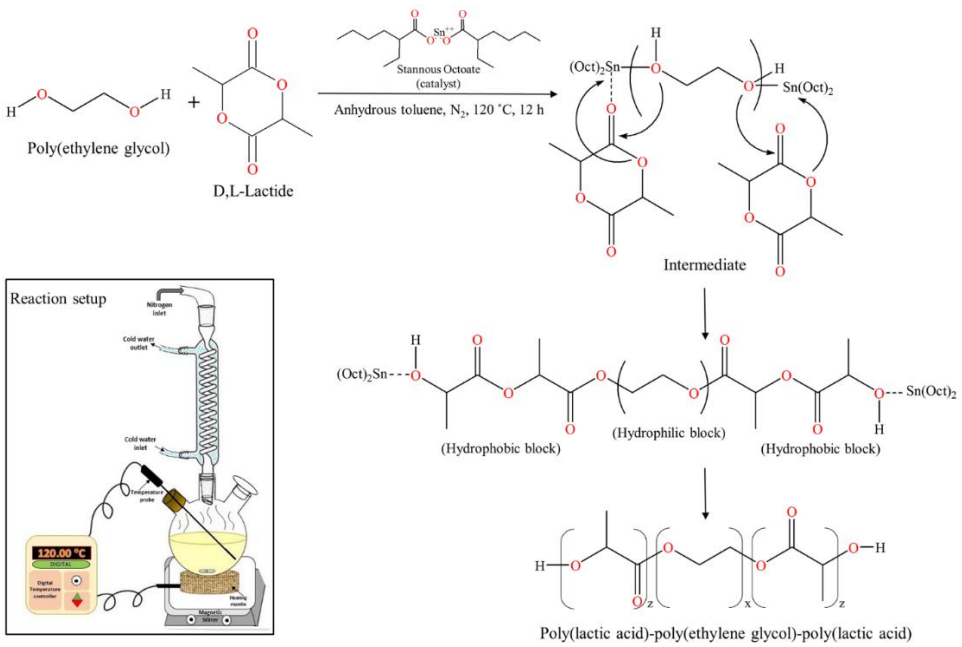

Figure 6. Synthesis of triblock copolymer poly(D, L-lactide)-poly(ethylene glycol)-poly(D, L-lactide) (PLA-PEG-PLA) *via* ring opening polymerization of D,L-lactide with poly(ethylene glycol) catalyzed by stannous octoate. (Inset: Reaction setup)

2.3.2. Synthesis and characterization of oleic acid grafted chitosan polymer

Oleic acid grafted CS oligosaccharide polymer (OA-g-CSO) was synthesized using carbodiimide mediated coupling reaction as described in our previous work with slight modifications.[196] Briefly, CSO (500 mg) was dissolved in 10 mL deionized water acidified to pH 5.0 using glacial acetic acid. OA (0.3 or 0.6 mol/mol of monomer unit of CSO) was dissolved in 1 mL of ethanol followed by the addition of EDC.HCl (5 mol/mol of OA) and NHS (5 mol/mol of OA) followed by stirring on a magnetic stirrer to allow complete mixing. After 20 min, the mixture of activated OA in ethanol was added dropwise to CSO solution under constant stirring. The reaction was proceeded at room temperature (~ 25 ˚C) for 12 h. The resultant product was dialyzed using 1 kDa molecular weight cut off dialysis membrane (Thermo Scientific, IL, U.S.A.) against deionized water for 24 h to remove water soluble by-products, followed by lyophilization to remove water. The lyophilized product was washed thrice by mixing it with ethanol and filtration

through 0.2 µm nylon filter paper (Cole-Parmer, IL, U.S.A.). The precipitate was vacuum dried to obtain the OA-g-CSO polymer. OA conjugation on CSO was confirmed using ^{1}H NMR and Fourier-transform infrared spectroscopy (FT-IR) techniques. Grafting efficiency of OA onto CSO backbone was determined using 2,4,6-trinitrobenzene sulfonic acid (TNBSA) reagent.

For ^{1}H NMR experiments, CSO and OA-g-CSO polymers were dissolved in deuterium oxide containing 1% deuterated acetic acid as a solvent at a concentration of 10 mg/0.6 mL. ^{1}H NMR spectra were recorded using a Bruker 400 MHz spectrometer at 25 ˚C (32 scans and 1.5 s delay) and analyzed using Bruker TopSpin 3.2.b.69 software. FT-IR spectra was recorded using a Thermo Scientific Nicolet iS-10 FT-IR spectrometer equipped with a diamond crystal Smart iTX accessory. Background was taken before each sample and the scan parameters were set to % transmittance mode, 64 scans, 4.0 resolution, and 0.482 cm^{-1} data spacing. All spectra were analyzed using the OMNIC 9.3.30 software by Thermo Scientific.

The degree of fatty acid substitution was determined using TNBSA, a sensitive and rapid bio-reagent for quantitative determination of free amine groups. Briefly, 0.2 mg/mL sample solution was prepared in sodium bicarbonate buffer (0.1 M, pH 8.5) in a glass vial. TNBSA reagent (0.02% w/v, 0.25 mL) was added to 0.5 mL of each sample and mixed well. The solution was incubated at 37 °C for 2 hours followed by addition of 0.125 mL of 1N HCl to each sample. Absorbance was measured at 335 nm using a spectrophotometer. Six replicates were performed for each sample. CSO polymer without any grafting was taken as control. Percentage grafting (GR%) was determined using **equation 1**.

$$GR\ \% = (1 - A_{test}/A_{control}) \times 100\ \% \quad (1)$$

Where, A_{test} is average absorbance of OA-g-CSO polymer and $A_{control}$ is the average absorbance of the CSO polymer without any grafting.

2.3.3. Calorimetric investigation of insulin modified using zinc and chitosan

2.3.3.1. Characterization of thermal stability using nano differential scanning calorimetry

Calorimetric determination of thermal stability and association of insulin upon addition of zinc, different chain lengths of CS, and OA-g-CSO polymers was determined using nano DSC (TA Instruments, DE, USA). Formation of zinc-insulin hexamers was facilitated by adding homogenous solution of zinc ions (zinc acetate dissolved in 10 mM HCl) to insulin solution in PBS (10 mM, pH 7.4) at 1:5 molar ratio of insulin hexamer to zinc ions, at room temperature (25 ˚C) with mild intermittent mixing for 10 min. Electrostatic complex formation between negatively charged zinc-insulin hexamers and positively charged CS polymer was facilitated by adding CS polymer (5 moles of CS monomer unit per mole of protein) to zinc-insulin hexamers followed by 15 min of incubation at room temperature (25 ˚C) with mild intermittent mixing. CS-zinc-insulin complexes containing CS of different chain lengths (5, 30, 50, 200 kDa) and OA-g-CSO polymer with different degree of OA grafting (25%, 45%) were prepared in identical manner. Degassed samples were loaded into nano DSC cells. Data was collected by scanning the samples from 10 to 110 °C at a scan rate of 1 °C/min. Reference scan was performed using PBS (10 mM, pH 7.4) in both the reference and sample cell and was subtracted from sample scan during data analysis. Analysis was performed using Nanoanalyze® software provided with the instrument. Transition curve were fitted using two-state scaled model following the “pseudo” V’ant Hoff method.

2.3.3.2. Characterization of binding interaction using isothermal calorimetry

Isothermal calorimetry technique was used to investigate the effect of the effect of CS chain length and hydrophobic modification of CSO on binding constant, enthalpy of complex formation, and the stoichiometry of interaction between zinc-insulin hexamers and CS polymers. Interaction was studied using nano ITC (TA instruments, USA) with a cell volume of 1 mL at 25 °C

temperature. All samples were degassed for 10 min under vacuum prior to use. The sample cell was filled with zinc-insulin hexamers dissolved in PBS, 10mM, pH 7.4 (2 mg/mL ~ 0.057 mM negatively charged hexameric units). Reference cell was filled with buffer solution only. CS polymer solution (1.2 mg/mL ~ 6 mM of free amino groups) was titrated into the thermostated cell by means of a syringe while continuous stirring at 250 rpm to allow homogenous mixing of reactants. Each titration integrated 25 subsequent 10 µL injections programmed to proceed at 400 s intervals. The heat of dilution of polymer solution titrated into PBS alone was subtracted from each experiment to obtain the net binding heat changes. Data was analyzed using Nanoanalyze® software (version 3.7.5).

2.3.4. Preparation of delivery systems

A simple and robust method for formulation of a delivery system is highly desired for achieving good reproducibility between batches as well as obtaining a cost-effective method for preparation of final product. Aqueous copolymeric delivery systems containing either free insulin, zinc-insulin hexamers, or CS-zinc-insulin complexes were prepared using zinc acetate as the zinc donor followed by electrostatic complex formation with CS polymer. Effect of successive chain lengths of CS (5, 30, 50, and 200 kDa) was studied first. Consequently, based on initial *in vitro* insulin release and degradation profile of PLA-PEG-PLA triblock copolymer, smaller chain length CS oligosaccharide (CSO, 5 kDa) hydrophobically modified using OA, was used to prepare OA-g-CSO-zinc-insulin complexes. Thermosensitive triblock copolymer PLA-PEG-PLA (1500-1500-1500, 4500 Da) was selected based on previous studies.[44] Formulations were prepared by suspending either free insulin, zinc-insulin hexamers, CS-zinc-insulin complexes or $OA_{(45\%)}$-g-CSO-zinc-insulin complexes, in aqueous copolymeric solution (35% w/v) followed by mild mixing on a vortex (Thermo Scientific, USA) at 1800 rpm for 5 min as described earlier.[197]

Briefly, zinc ions were added to insulin solution in PBS at 1:5 molar ratio of insulin hexamer to zinc ions, followed by mild mixing at room temperature for 10 min. CS or $OA_{(45\%)}$-g-CSO-zinc-insulin complexes were prepared by adding CS monomer in five times molar excess per unit mole of zinc-insulin hexamers followed by intermittent mixing at room temperature for 15 min. Zinc-insulin hexamers, CS or OA-g-CSO-zinc-insulin complexes were collected following centrifugation at 4 °C at 3,000 rpm for 10 min. The precipitates were homogenously suspended in aqueous copolymer solution to obtain the final formulation. Free/non-complexed insulin was quantified in the supernatant using micro BCA protein assay kit.

2.3.5. *In vitro* release profile of insulin

In vitro release profile of delivery systems in presence of insulin, zinc-insulin hexamers, CS-zinc-insulin complexes prepared using CS of successive chain lengths: 5, 30, 50, and 200 kDa, and OA-g-CSO polymer was performed. *In vitro* release profile was studied by injecting the respective formulation into borosilicate glass tubes and incubating them at 37 °C water bath to allow phase transition to a gel depot (**Figure 7**). Pre-warmed PBS (10 mM, pH 7.4) was added as release medium. Aliquots were taken at regular intervals and replaced with fresh pre-warmed PBS. Amount of insulin released was quantified using micro BCA protein assay kit. Cumulative amount of insulin released was calculated following concentration correction method described by Chen *et al.* [198]

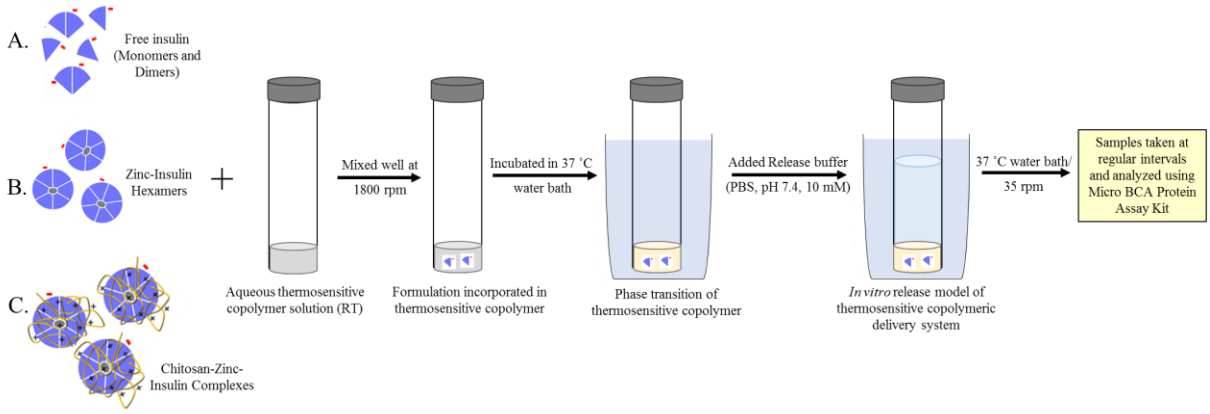

Figure 7. Schematic representation of formulation and *in vitro* release study model for thermosensitive copolymeric-depot based delivery system incorporating either (A) Free insulin, (B) Zinc-insulin hexamers, or (C) CS-zinc-insulin complexes.

2.3.6. Mass loss of copolymer during *in vitro* release

Amount of copolymer lost during *in vitro* release was determined by removing release medium of delivery systems at fixed intervals (15, 30, and 45 days) followed by lyophilization of the remaining copolymer. Weight remaining of the delivery system was then calculated by weighing the copolymer and comparing it to the initial amount.

2.3.7. Reduction in copolymer molecular weight during *in vitro* release

Molecular weight of the copolymer remaining was determined at fixed intervals (15, 30, and 45 days) using SEC-HPLC. Lyophilized copolymer residues were dissolved in THF and analyzed using Agilent Technologies' (Santa Clara, CA, USA) 1120 series compact LC system coupled with Agilent 1200 series refractive index detector, thermostated at 35 ˚C. Polystyrene standards of different molecular weights were used for calibration. Analysis was performed using Waters styragel column (HR4E, 5 µm, 7.8 mm x 300 mm; Milford, MA, USA), THF as the carrier solvent, 1 mL/min flow rate, and 50 µL injection volume.

2.3.8. Stability studies

2.3.8.1. Stability of insulin released from delivery system

Thermal, chemical and conformational stability of insulin released *in vitro* from optimized formulation was investigated using nano DSC, RP-HPLC, and CD spectroscopy, respectively. Aliquots containing released insulin were centrifuged, filtered and degassed prior to analysis. Thermal transition of released insulin was recorded using nano DSC as specified earlier. Chemical stability was determined by RP-HPLC using Agilent 1120 compact LC system using chromatographic conditions presented in **table 4**. Data acquisition and analysis was performed using EZChrom Elite™ 3.3.2 software (Agilent, CA, USA).

Conformational stability using CD spectrophotometer was determined by scanning the samples in near-UV region (250-300 nm) and far-UV region (200-250 nm) to investigate the changes in tertiary and secondary structure, respectively. Spectra were recorded at a scan rate of 5 nm/min at 25 °C with a quartz cuvette (0.1 cm path length). Background interference obtained by scanning fresh PBS (10 mM, pH 7.4) in the same range was subtracted from all samples before analysis. Spectra manager®2 software (Jasco, Tokyo, Japan) was used for spectrum and secondary structure analysis.

Table 4. Chromatographic conditions for studying chemical stability of insulin using RP-HPLC.

Column	Thermo Scientific™ Hypersil GOLD™ C18 column (250 x 4.6 mm, 5 μm)
Mobile phase A	0.1% v/v TFA in deionized water
Mobile phase B	0.1% v/v TFA in acetonitrile
Elution	Gradient
Mobile phase composition	75:25 (A:B) to 50:50 (A:B)
Flow rate	0.8 ml/min
Injection volume	25 μl
Run time	25 min
Detector, Detection wavelength	UV, 280 nm

2.3.8.2. Storage stability of insulin in formulation

Long-term storage stability of insulin in optimized formulation was also determined after 1, 3, 6 and 9 months of storage at 4 ˚C. PBS and acetonitrile mixture (1:1 v/v) was used to extract insulin from stored copolymer formulations followed by analysis using nano DSC, RP-HPLC and CD spectroscopy as discussed earlier.

2.3.9. Biocompatibility of delivery system

2.3.9.1. In vitro Biocompatibility

Biocompatibility of the copolymer with and without OA-g-CSO polymer was tested *in vitro* in fibroblast cells (3T3-L1) and human embryonic kidney cells (HEK-293). Copolymer solution (35% w/v, 0.5 mL) with and without OA-g-CSO was extracted into PBS (10 mM, pH 7.4, 5 mL) following 10-day incubation at 37 ˚C to mimic accumulation of copolymer degradation

products at physiological temperature. Extraction was also performed at 70 ˚C to mimic long-term accumulation of copolymer degradation products since the degradation rate of PLA/PEG based copolymers is higher at increased temperature. Cells were plated in 96-well plates and allowed to attach. Dilutions of the copolymeric extracts were prepared in serum-free DMEM and added to the cells followed by incubation for 24, 48, or 72 hours. Post-incubation 3-(4,5-Dimethylthiazol-2-yl)-2,5-diphenyltetrazolium bromide (MTT) assay was used to determine cell viability. Untreated cells and cells treated with formalin buffer were taken as negative and positive control, respectively. Relative cell viability was calculated using following **equation 2**.

$$\text{Cell viability (\%)} = (A_{treated} / A_{untreated}) \times 100 \quad (2)$$

Where, $A_{treated}$ is average absorbance of wells incubated with polymer extract dilutions and $A_{untreated}$ is the average absorbance of the control wells incubated with serum-free DMEM.

2.3.9.2. In vivo biocompatibility

In vivo biocompatibility of the formulation was evaluated by injecting 0.5 mL of the delivery system or saline subcutaneously in the dorsal neck region of rats. The depot-site was monitored regularly by visual examination. The rats were sacrificed at 1, 7, 30, 90 days' post administration, followed by excision of the subcutaneous tissue surrounding the injection site and fixing them in 10% neutrally buffered formalin. Histological analysis was performed on 5µm thick sections stained with hematoxylin eosin (H&E) and Gomori's trichome stains for visualization of inflammatory cells and presence of collagen deposition, respectively. Subcutaneous tissue collected from rats without any injection and post-injection with 5% (v/v) neutral buffered formalin were taken as negative and positive controls, respectively.

2.3.10. *In vivo* insulin release and bioactivity

Male Sprague-Dawley rats weighing 180 – 200 g were used in this study. Rats were housed in a temperature-controlled facility maintained at 12 h light-dark cycle with *ad libitum* access to food and water. At the end of the study rats were euthanized using CO_2 asphyxiation.

2.3.10.1. Type-1 diabetes induction

Male Sprague-Dawley rats weighing 180 – 200 g were selected for this study. Female rats are more susceptible to streptozotocin (STZ) treatment. They show lower insulin, higher glucose levels, and high mortality rate as compared with male rats, and were therefore not selected for this study.[199] After acclimatization to the housing conditions, single dose of freshly prepared STZ (55 mg/kg body weight) dissolved in ice cold citrate buffer (0.1 M, pH 4.5) was injected intraperitoneally to induce diabetes. Post-injection rats were housed in groups of two per cage, and provided with 5% (w/v) sucrose solution in drinking water to counteract the potential risk of hypoglycemia expected by massive insulin release under the influence of STZ. One-week post STZ injection blood glucose levels were measured following 12 h overnight fast. A lancet was used to obtain a drop of blood (< 20 µL) tested using Contour®Next blood glucose meter and glucose testing strips (Ascensia Diabetes Care, NJ, USA). Animals with fasting blood glucose levels > 200 mg/dL were considered diabetic and randomly assigned to the treatment groups (Groups II – VII) as described in **table 5**.

2.3.10.2. Formulation administration

Assuming basal insulin requirement of 0.5 IU/kg/day, a total dose of 45 IU/kg body weight for 90 days was selected for controlled basal insulin release. Rats without any treatment were used as healthy control (Group I). STZ treated diabetic rats without any insulin treatment were taken as negative control (Group II). Group III was subcutaneously injected with a single dose of insulin

solution (0.5 IU/kg) dissolved in PBS (10mM, pH 7.4). Group IV was subcutaneously injected with once-daily glargine (Lantus® U-100) at a dose of 0.5 IU/kg/day for 90 days. Group V – VII were subcutaneously injected with a single dose of copolymeric formulation incorporating either free insulin, CSO-zinc-insulin complexes or OA-g-CSO-zinc-insulin complexes, injected subcutaneously at the dorsal neck region using a 25 G needle (**Figure 4**).

Table 5. Treatment groups for studying *in vivo* release profile of insulin.

Group number	Treatment	Insulin dose (IU/kg)	Frequency of administration
I	Healthy control	-	-
II	Diabetic control	-	-
III	Free insulin solution	0.5 IU/kg	Single
IV	Glargine	0.5 IU/kg/day	Repeated every 24 h
V	Free insulin in thermosensitive copolymer solution	45 IU/kg	Single
VI	CSO-Zinc insulin complexes in thermosensitive copolymer solution	45 IU/kg	Single
VII	Oleic acid-g-CSO zinc insulin complexes in thermosensitive copolymer solution	45 IU/kg	Single

2.3.10.3. Blood sampling and quantification of serum insulin level

Blood sampling was performed on overnight fasted rats using tail vein puncture. Blood samples were allowed to coagulate for 30 min at room temperature and serum was collected following centrifugation at 2000 g for 10 min at 4 °C. Insulin was quantified using human insulin enzyme linked immunosorbent assay (Mercodia Human Insulin ELISA (Uppsala, Sweden) Catalog# 10-1113-01) using manufacturer's protocol.

2.3.10.4. Determination of blood glucose and ketone levels

Blood glucose levels were measured 12 h overnight fasting using Contour®Next blood glucose meter and glucose testing strips. Blood ketone levels were measured similarly at 1, 2, and 3-month interval analyzed using Precision Xtra® blood ketone meter and ketone testing strips (Abott Diabetes care, CA, USA).

2.3.10.5. Determination of cataract formation

Cataract formation in rats was determined visually and considered partial for strong nuclear cataract formation with perinuclear area opacity and complete for total opacity of lens.[200,201]

2.3.10.6. Determination of body weight

Body weight of the animals before and after STZ-treatment and following insulin treatment was noted regularly over the entire study duration.

2.3.10.7. Detection of anti-insulin antibodies

Rat serum samples collected after 1, 2 and 3 months after treatment were analyzed for rat anti-insulin IgG antibodies using indirect ELISA (Alpha Diagnostic International (TX, USA), Catalog# 3750-RIG) using manufacturer's protocol.

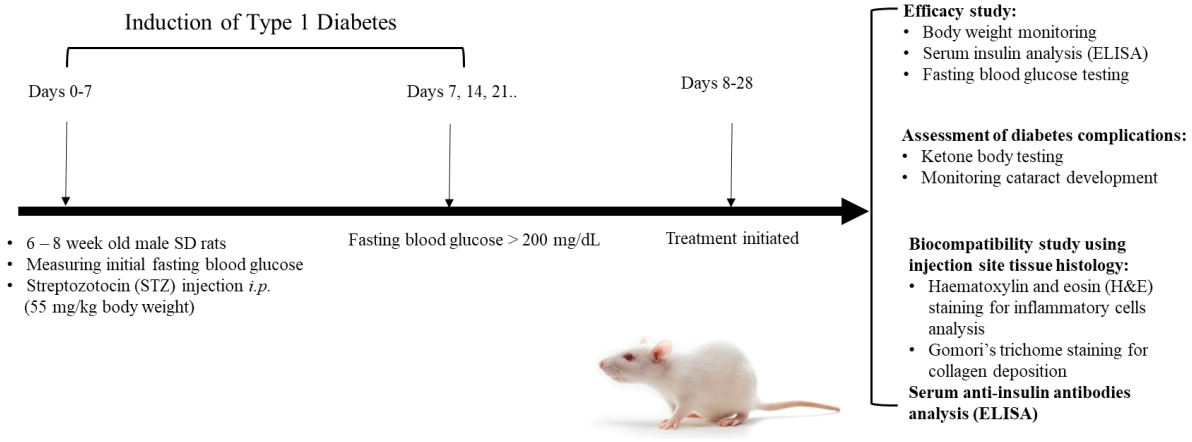

Figure 8. Experimental plan for determining *in vivo* release profile, bioactivity of insulin released, and biocompatibility of the delivery systems.

2.3.11. Synthesis and characterization of oleic acid, mannose and adipose homing peptide grafted chitosan polymer

OA was grafted onto CS backbone using carbodiimide mediated coupling of amine group of CS with carboxyl group of OA. Conjugation of α-D-mannopyranosylphenyl isothiocyanate (MAN) onto CS backbone was facilitated by thiourea reaction between amine group of CS and isothiocyanate group of MAN. The detailed procedures have been discussed earlier.[139] Briefly, CS (200 mg, molecular weight 20 kDa) was dissolved in 5 mL of deionized water acidified to pH 5.0 using glacial acetic acid. OA (0.06 mol/mol of glucosamine unit of CS) was dissolved in 2 mL of ethanol followed by the addition of EDC.HCl (5 mol/mol of OA) and NHS (5 mol/mol of OA). This activated mixture was then added dropwise to CS solution under constant stirring. The reaction was allowed to take place at room temperature (25 ˚C, RT) for 6 h. Dialysis was performed using 3.5 kDa molecular weight cut off dialysis membrane (Thermo Scientific, IL, U.S.A.) against deionized water for 48 h to remove unreacted EDC.HCl and NHS. Dialyzed product was then frozen at −80 °C and lyophilized (temperature −49 °C and vacuum, 0.02 mBar) until a stable weight polymer was obtained. The lyophilized product was washed thrice using ethanol to remove

unreacted OA, and final precipitate dried to obtain CS-OA polymer. Furthermore, MAN and AHP conjugation was done by mixing CS or CS-OA polymer solution in deionized water (pH 4.5 using glacial acetic acid) with MAN or AHP (0.06 mol/mol of glucosamine unit of CS). The reaction was continued for 24 h at RT, dialyzed against deionized water for 48 h, and lyophilized to obtain the final product. Ligand conjugation on CS was confirmed using ^{1}H NMR and FT-IR as described earlier using Bruker 400 MHz spectrometer and Thermo Scientific Nicolet iS-10 FT-IR spectrometer, respectively.[196] Degree of substitution was determined using trinitrobenzene sulfonic acid (TNBSA) reagent for conjugation of OA or MAN, and BCA kit for conjugation of AHP, using manufacturer's protocols.

2.3.11.1. Fluorescence Labeling of Polymers

FITC was covalently labeled to sample polymers by dropwise adding FITC (2 mg/mL in anhydrous methanol) solution to sample polymer solution (20 mg/mL in 1% v/v glacial acetic acid in DI water) under continuous magnetic stirring at RT. The reaction was continued for 2 h in dark followed by freeze drying protected from light. FITC conjugated product was washed thrice with anhydrous methanol to remove unconjugated dye followed by vacuum drying to obtain FITC-labeled sample polymers. FITC conjugation per sample polymer was determined using manufacturer's protocol, by measuring extinction coefficient at 495 nm (73,000 cm^{-1} M^{-1}).[202] FITC labelled polymers were used in *in vitro* uptake and *in vivo* biodistribution studies.

2.3.12. Preparation and characterization of chitosan nanomicelles and pDNA polyplexes

Sample polymers were dissolved in sodium acetate buffer (20 mM, pH 6.5, 1 mg/mL) and extruded through 0.2 µm polycarbonate membrane (GE Healthcare, PA, U.S.A.) to obtain uniform sized nanomicelles. Critical micelle concentration (CMC) was determined using pyrene as a hydrophobic fluorescence probe.[196] Pyrene dissolved in acetone was added to sample tubes (0.6

μM) followed by drying to remove acetone. CS-OA, CS-OA-MAN and CS-OA-AHP polymers were dissolved in sodium acetate buffer (20 mM, pH 6.5) and dilutions were prepared from 0.001 to 2 mg/mL were added to pyrene containing sample tubes followed by sonication treatment for 15 min using a bath sonicator. After equilibration in dark for 3 h, fluorescence spectra were recorded for each sample using SpectraMax M5 microplate reader (Molecular Devices, CA, USA) at emission wavelength range 360 – 450 nm and excitation wavelength 336 nm. CMC value was determined using the ratio of emission intensity of first peak to third (I_1, 373 nm/ I_3, 393 nm) plotted against the decadic logarithm (log_{10}) of concentration.

Polyplexes were prepared by adding CS polymer solution dropwise to pDNA solution (N to P ratio of 20) followed by vortexing for 5 min. Association of pDNA to sample polymers was simultaneously confirmed by indirect centrifugation method. Polyplex solutions were centrifuged at 30,000 × g for 30 min at 4 ˚C and the supernatant was analyzed for free pDNA using Hoechst dye. Average hydrodynamic diameter and zeta potential measurements were performed using Zetasizer Nano-ZR (Malvern Instruments, Malvern, U.K.).

2.3.13. Determination of pDNA condensation, protection from nucleases and endosomal buffering capacity

Ability of CS polymeric nanomicelles to form complex with pDNA to condense it as well as protect it from nuclease degradation was determined using agarose gel retardation assay.[139] Polyplexes were prepared using each CS polymer sample as described earlier using 1 μg of pDNA. Each sample was mixed with loading buffer (0.25 g bromophenol blue, 6 mL 50% (v/v) glycerol, q.s. to 10 mL using deionized water) at 5:1 ratio before loading into the wells. Electrophoresis was performed on 0.8% (w/v) agarose gel containing 0.5 μg/mL of ethidium bromide (EtBr) at 80 V for 90 min in Tris-borate-ethylenediaminetetraacetic acid (TBE, 1X, Thermo Fisher Scientific)

buffer. The bands were visualized using Applegen Omega Lum™ G Imaging system using EtBr (UV 302) filter.

The ability of CS polymer to protect the complexed pDNA was investigated using DNase I protection assay as reported earlier.[139] Briefly the polyplexes were incubated with DNase I enzyme (2 µg pDNA per unit of DNase I enzyme) at 37 °C. Naked pDNA incubated with enzyme was used as positive control. Variation in pDNA absorbance at 260 nm wavelength was recorded at 10 min intervals for 1 h.[139] The reaction was stopped by adding 5 µL of 100 mM EDTA solution and the complexes were dissociated by incubating with 20 µL heparin solution (5 mg/mL) for 2 h. The samples with released pDNA were then analyzed using agarose gel electrophoresis as mentioned earlier.

Endosomal buffering capacity of CS and ligand-conjugated CS polymers was studied using acid-base titration assay.[202] Polymer samples were dissolved in 150 mM NaCl solution and adjusted to pH 10 using 0.1N NaOH. Titration was performed using 0.1 N HCl (20 µL increments) at 25 °C and simultaneously recording the pH value.

2.3.14. Preparation of *in vitro* cell culture model

M1 polarized RAW 264.7 macrophages (ATCC, Rockville, MD, USA), differentiated 3T3-L1 adipocytes and their contact co-culture were used in this study. All experiments were performed at 37 ˚C in 5% CO_2 environment. RAW 264.7 (ATCC, Rockville, MD, USA) cells were cultured in DMEM containing 10% fetal bovine serum (FBS). Polarization to M1 phenotype was stimulated by adding of lipopolysaccharides (LPS) (100 ng/mL final concentration in cell culture medium, DMEM only) and incubating for 24 h.[196]

3T3-L1 pre-adipocyte (ATCC, Rockville, MD, USA) were cultured in pre-adipocyte expansion medium (DMEM with 10% bovine calf serum). Differentiation to mature adipocytes

was effected in three steps. First the cells were allowed to reach 100% confluence and cultured for additional 48 h in pre-adipocyte expansion medium. The growth medium was then replaced by differentiation medium (DMEM with 10% FBS, 1 µM dexamethasone, 500 µM isobutylmethylxanthine, and 1 µg/mL insulin) and cells incubated for 48 h.[196] Finally, the differentiation medium was replaced by adipocyte maintenance medium (DMEM with 10% FBS and 1 µg/mL insulin) and cells were cultured for 14 days with maintenance medium replenished every 48 – 72 h. Differentiation was confirmed using oil red O staining using the method described by Dhal *et al*.[203]

Contact co-culture mimicking physiological adipose tissue environment in obesity was prepared by adding 4×10^4 M1 polarized RAW 264.7 cells per 1×10^5 differentiated 3T3-L1 adipocytes.[204,205] Differentiated 3T3-L1 adipocytes were cultured as discussed above. M1 polarized RAW 264.7 macrophages were added to differentiated adipocytes and allowed to attach overnight for 12 h, in the presence of LPS (DMEM with 10% FBS, 1 µg/mL insulin, and 100 ng/mL LPS).

Cyto-compatibility, transfection and RNAi studies were carried out by incubating the formulation with cells in cell culture medium with physiological diabetic concentration of glucose and mannose (DMEM only with 8 mM glucose, 50 µM mannose) for 4 h, followed by addition of complete growth medium (DMEM, 10% FBS) for the remaining incubation period.

Cellular uptake experiments were performed as specified, with different concentration of physiological sugars in PBS medium.

2.3.15. *In vitro* cytocompatibility assay

MTT colorimetric assay was used to assess cellular compatibility of CS polymers synthesized in this study using M1 polarized RAW 264.7 macrophages, differentiated 3T3-L1

adipocytes and their contact co-culture as an *in vitro* inflammatory cell culture model. Cells were seeded in 96-well plates and M1 polarization, 3T3-L1 differentiation, co-culture preparation was performed as described earlier. Cells were treated with increasing concentration (0.1, 0.2, 0.5, 1 mg/mL) of sample polymers in serum free DMEM containing 50 µM mannose and 8 mM glucose for 4 h. Cells without any treatment were taken as control. Subsequently, media was carefully removed and cells were incubated with complete growth medium (DMEM with 10% FBS, 100 ng/mL LPS) for 48 h. Following incubation media was carefully aspirated and MTT solution (100 µL, 1 mg/mL in serum-free DMEM) was added to each well and allowed to react for 3 h. Unreacted MTT was removed carefully, cells rinsed with cold PBS, and formazan crystals dissolved by adding 150 µL of dimethyl sulfoxide. Absorbance was recorded at 570 nm using SpectraMax M5 microplate reader (Molecular Devices, CA, USA). Relative cell viability was calculated using **equation 3**.

$$\text{Cell viability (\%)} = (A_{sample} / A_{control}) \times 100 \quad (3)$$

Where, A_{sample} is average absorbance of wells incubated with CS polymer samples and $A_{control}$ is the average absorbance of the untreated control wells.

2.3.16. Determination of cellular uptake

Cellular uptake of respective formations was tested using FITC-labeled polymer/pDNA polyplexes in M1 polarized RAW 264.7 macrophages, differentiated 3T3-L1 adipocytes and their contact co-culture. Cells were seeded in 24-well plate at a density of 1×10^5 cells/well and M1 polarization, 3T3-L1 differentiation, co-culture preparation was performed as described earlier. FITC-labeled polymer/pDNA polyplexes containing 1 µg of pDNA at N to P ratio of 20 were added to each well and incubated at 37 °C in DPBS medium. Uptake process was terminated at 0.5, 1, 2 and 4 h by discarding the polyplex containing medium and washing the cells three times

with DPBS. Qualitative assessment of cellular uptake process was performed by further incubation with 2.5 µg/mL DAPI for 20 min for nuclei staining followed by imaging at 20X magnification using Leica DFC 3000G fluorescence microscope (IL, U.S.A). The percentage uptake per mg of protein was calculated by taking the fluorescence of cell lysate obtained by treatment with Triton X-100 solution (1% v/v) analyzed using SpectraMax M5 microplate reader (Molecular Devices, CA, USA). The excitation and emission wavelength were set as 495 and 519 nm, respectively. Normalization was performed by assessing total protein content of cell lysate quantified using Pierce BCA protein assay kit (Waltham, MA, U.S.A.) as per the manufacturer's protocol.

2.3.17. Competition assay and mechanism of cellular uptake

An *in vitro* competition assay was performed to confirm GLUT-1 mediated uptake of OA and MAN grafted CS polymeric nanomicelles at non-diabetic and diabetic physiological concentrations of glucose and mannose. LPS activated RAW 264.7 cells were pre-incubated with 40 µM of mannose + 5 mM glucose (non-diabetic physiological blood sugar concentration) and 50 µM of mannose + 8 mM glucose (diabetic physiological blood sugar concentration) in DPBS medium for 20 min prior to uptake study. Individual concentrations of non-diabetic and diabetic glucose and mannose concentrations were also tested. PBS only (0 mM sugar concentration) and 25 mM glucose concentration were tested as negative and positive control, respectively. Activated macrophages were incubated with FITC-labeled polyplexes at 37 °C for 2 h (optimized time point of cellular uptake study). Subsequently, medium was carefully aspirated and cells were rinsed thrice using DPBS. Cells were lysed using Triton X-100 solution (1% v/v) and percentage uptake per mg of protein was calculated by analyzing fluorescence of cell lysate as described earlier.

CS polymeric vectors undergo cellular uptake mainly by endocytic pathways. These pathways include micropinocytosis, claveolae-mediated endocytosis and clathrin-mediated

endocytosis. To investigate cellular uptake pathway in M1 polarized RAW 264.7 macrophages and differentiated 3T3-L1 adipocytes, cells were pre-incubated for 30 min with either sodium azide (10 mM) or at 4 °C to inhibit all energy-dependent endocytosis, amiloride (50 µg/mL) to prevent micropinocytosis, colchicine (100 µg/mL) to inhibit claveolae formation, and chlorpromazine (10 µg/mL) to prevent formation of clathrin vesicles. The uptake process was studied as mentioned earlier using FITC-labeled polymer/pDNA polyplexes incubated for 2 h, followed by analysis of percentage uptake per mg of protein calculated by analyzing fluorescence of cell lysate as described earlier.

2.3.18. *In vitro* gene transfection

One critical limitation of non-viral gene delivery vectors is low gene transfection ability. Effect of CS chain length on transfection efficiency was determined using CS chain length 5, 20 or 50 kDa complexed with plasmid encoding for enzyme β-galactosidase. Transfection efficiency was determined 48 h post transfection in inflammatory contact co-culture model of M1 polarized RAW 264.7 macrophages and differentiated 3T3-L1 adipocytes. The transfection efficiency of CS and ligand conjugated CS polymers was evaluated using plasmid encoding for enzyme β-galactosidase and green fluorescent protein (GFP) in M1 polarized RAW 264.7 macrophages, differentiated 3T3-L1 adipocytes and their contact co-culture. For all transfection experiments, cells were seeded in 24-well plates at density of 1 x 10^5 cells/well in DMEM containing 10% FBS. RAW 264.7 macrophages were cultured to achieve ~60 – 70% confluence and polarized to M1 phenotype using LPS (LPS final concentration ~100 ng/mL in DMEM only, incubated with cells for 24 h). Differentiated 3T3-L1 cell culture and co-culture were prepared as mentioned earlier. Sample polymer and pDNA stock solution were prepared in sodium acetate buffer (20 mM, pH 6.5). Polyplexes were prepared by dropwise addition of sample polymer solution into pDNA

solution at N to P ratio of 20 followed by vortex mixing at 1800 rpm for 10 s and sonication treatment for 15 min using Aquasonic bath sonicator (VWR scientific products, GA, U.S.A.). Final polymer concentration was maintained above its CMC. Culture medium was replaced with serum free DMEM containing 50 µM mannose and 8 mM glucose prior to transfection. Following equilibration at RT for 30 min, formulations were added to the wells and incubated for 4 h. Following incubation, the transfection medium was replaced with serum and LPS containing DMEM (10% FBS, 100 ng/mL LPS) and further cultured for 48 h. Cells without any treatment and treatment with naked pDNA were used as negative and passive control, respectively. Cells treatment with FuGENE® HD transfection reagent (Promega Corporation, Madison, WI, USA) were used as positive control. β-galactosidase expression per mg of total protein content was determined by analyzing cell lysate using β-galactosidase enzyme assay system (Promega Corporation, Madison, WI, USA) and BCA protein assay kit (Pierce, Waltham, MA, USA), respectively, as per respective manufacturer's protocols. Fluorescence activated cell sorting (FACS) analysis was used to determine percentages of successfully transfected GFP positive cells using a flow cytometer. Qualitative analysis of GFP expression was performed by taking images at 20X magnification using Leica DFC 3000G fluorescence microscope (IL, U.S.A).

2.3.19. *In vitro* RNA interference efficacy of plasmid encoding shRNA against TNF-α and MCP-1.

Plasmids encoding shRNA against TNF-α (shTNFα) and MCP-1(shMCP1) were investigated for RNA interference in an *in vitro* inflammatory co-culture model of M1 polarized RAW 264.7 macrophages and differentiated 3T3-L1 adipocytes. Dual modified nanomicelles prepared using COM or COA polymer, which showed superior transfection using model plasmids, were used to prepare polyplexes with pDNA encoding shRNA against TNF-α (shTNFα – COM)

or MCP-1 (shMCP1 – COA), respectively. Cells without any treatment were used to assess basal level of cytokines. Cells treated with naked pDNA were used as passive control. pDNA encoding for scrambled shRNA were used as negative control both with (scram-shRNA – COM or scram-shRNA – COA) and without (scram-shRNA in PBS) the formulation. Cytokine analysis was performed 72 h post transfection in both culture supernatant and cell lysate using mouse PicoKine™ ELISA kit (Boster Biological Technology) for quantifying TNF-α, MCP-1, IL-1β, IL-6 and adiponectin levels. Total cytokine concentrations were plotted for different formulation groups after normalization for supernatant volume and total protein content.

2.3.20. Development of obese diabetic mice model

Male 4 weeks old C57BL/6 mice were used in this study. Female mice have a lower propensity of weight gain, and development of obesity compared to male mice, therefore were not selected for this study.[206] Animals were housed in a temperature-controlled facility maintained at 12 h light-dark cycle with *ad libitum* access to food and water. Post-acclimatization, initial blood glucose level, insulin sensitivity (IST) and glucose tolerance (GT) was performed in fasted mice.

2.3.20.1. Insulin sensitivity assay

Mice were fasted for 6 h (starting in the morning with free access to water) and their initial fasting blood glucose was noted.[207] Insulin sensitivity was measured by injecting 0.5 U/kg insulin solution (i.p.) in sterile saline (working stock: 0.1 U/mL) using 27 G needle and measuring blood glucose 15, 30, 60, 90, and 120 min post injection. A significant change in blood glucose level (~40% drop compared to initial levels) was defined as normal insulin sensitivity. At the end of this study animals were provided with food and water.

2.3.20.2. Glucose tolerance assay

Mice were fasted for 6 h (starting in the morning with free access to water) and their initial fasting blood glucose was noted.[207] Glucose tolerance was measured by injecting 20% w/v D-glucose (i.p.) at a dose of 2 g per kg body weight using a 27 G needle. Blood glucose was recorded 15, 30, 60, 90, and 120 min post injection. Animals were considered to have normal glucose tolerance if blood glucose levels were ≤ 140 mg/dL 2 h post glucose administration. At the end of this study animals were provided with food and water.

All mice showed fasting blood glucose level < 120 mg/dL, were insulin sensitive and glucose tolerant. Thereafter, mice in control diet group were fed with standard mice chow (Lab Diets). Remaining mice were fed with high-fat diet (Envigo TD.88137, 42% Kcal fat, 34% sucrose by weight). Body weight, fasting blood glucose, IST, and GT were determined at regular intervals. Mice that showed low insulin sensitivity and glucose tolerance were added to different treatment groups. Age-matched control-diet fed mice were used as healthy non-diabetic control. At the end of the study mice were euthanized using CO_2 asphyxiation.

2.3.21. Determination of *in vivo* biodistribution and biocompatibility in obese diabetic mice model

Biodistribution of CS polymer/pDNA polyplexes was performed in high-fat diet fed obese diabetic mice following subcutaneous administration. Each group was injected with nanomicelles prepared using CS-FITC, CS-OA-FITC, CS-MAN-FITC, CS-AHP-FITC, CS-OA-MAN-FITC or CS-OA-AHP-FITC at a dose of 0.5 mg pDNA/kg body weight. Control groups were injected with either PBS or free dye (FITC, dose: 0.01 mg/kg). Animals were sacrificed 24 h post administration, their blood was withdrawn using cardiac puncture, and organs harvested including heart, lungs, liver, spleen, kidneys, subcutaneous injection site (left ventral abdominal region), and

subcutaneous remote site (dorsal neck region). Blood samples were allowed to clot at room temperature following centrifugation at 2000 g for 10 min to collect the serum. Organs were washed twice with DPBS, and weighed and stored at – 80 °C until assayed. Samples were homogenized using Biospec Products tissue tearer (Bartlesville, OK, USA) and the dye was extracted in solvent A. Samples were centrifuged at 10,000 rpm for 15 min and supernatant with extracted dye was analyzed using HPLC-FLD. HPLC-FLD analysis conditions were maintained according to the method reported by Assi *et al* with slight modifications.[208] Isocratic elution was used with 58 % solvent A (methanol: glacial acetic acid: water, 60:5:515 v/v/v) and 42 % solvent B (acetonitrile). All data were normalized and represented as percentage of injected dose per gram of tissue (% ID/g of tissue). For biocompatibility analysis, all major organs were harvested and fixed in 10% neutral buffered formalin. Paraffin embedded samples were sectioned for 5 µm thickness and stained using hematoxylin and eosin (H&E) dye. Sections were carefully observed under bright field microscope at 20X and 40X magnification for histopathological changes and any sign of toxicity.

2.3.22. Determination of *in vivo* tissue and serum cytokine estimation, and efficacy in obese diabetic mice model

Concentration of TNF-α, MCP-1, IL-1β, IL-6 and adiponectin was evaluated at tissue and systemic level using cytokine specific mouse PicoKine™ ELISA kit (Boster Biological Technology, CA, USA). Inflammation at tissue level was determined by analyzing subcutaneous adipose tissue (SAT), epididymal visceral adipose tissue (EVAT) and perirenal visceral adipose tissue (PVAT). Systemic level of inflammatory mediators was evaluated by assessing cytokine concentration in mouse serum.

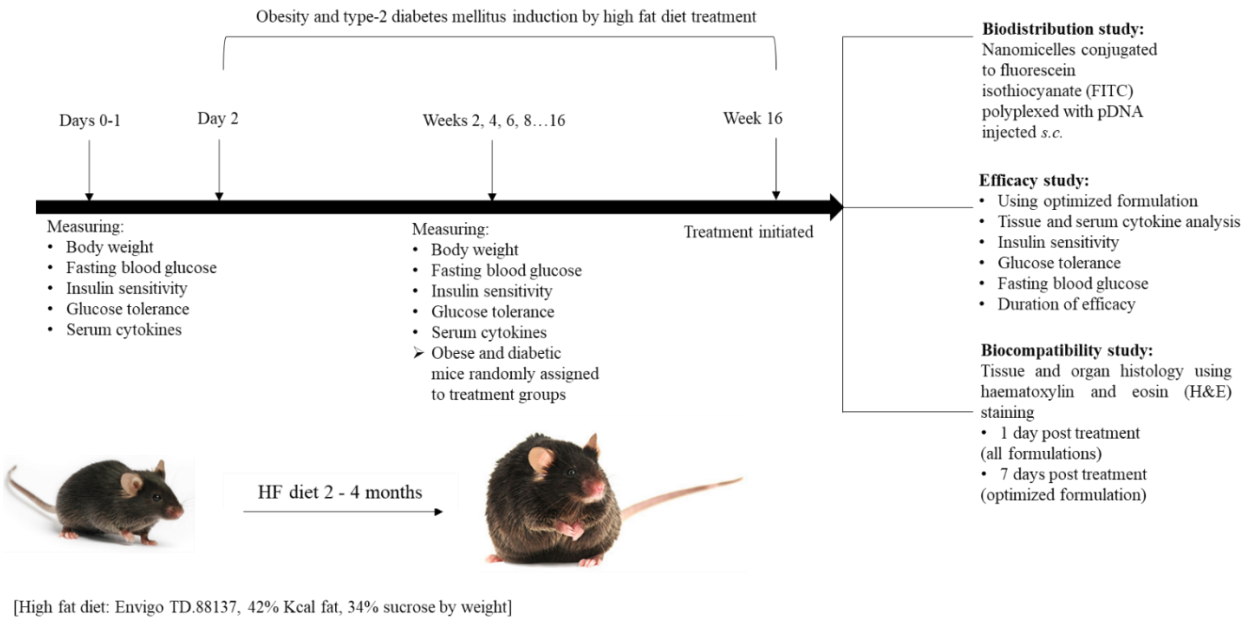

Figure 9. Experimental plan for assessing *in vivo* biodistribution, safety and efficacy of optimized formulations in the treatment of insulin resistance.

2.3.23. Statistical analysis

Data are expressed as mean ± standard deviation (SD). Statistical analyses were performed using two tailed student's t-test and one-way ANOVA (analysis of variance) coupled with post-hoc Tukey test using GraphPad Prism software (version 5.01). A p value of less than 0.05 was considered to be significant. For sound statistical analysis of the results, six animals will be used for each group. G*Power 3.1.9.2 calculation was performed considering small effect size, 0.05 α error, and 0.8 test power. Preliminary results from similar research in our lab was used for power analysis.[26,209]

3. RESULTS AND DISCUSSION

3.1. Synthesis and characterization of thermosensitive copolymer[1]

Ring opening polymerization is a widely used method for the synthesis of triblock copolymers of PLA, PLGA and PEG where the hydrophobic block is covalently linked to the hydrophilic block by an ester linkage.[210] PLA_{1500}-PEG_{1500}-PLA_{1500} triblock copolymer was selected based on previous research.[43] Copolymer was synthesized with ≥85% yield. Purified copolymer was characterized using ^{1}H and ^{13}C NMR (**Figure 10**). Signals corresponding to –CH of LA at 5.20, -CH_3 of LA at 1.55, -CH_2 of PEG at 3.66, and –CH_2 of EG's connecting unit to LA at 4.31 ppm were observed (**Figure 10A**). The signals corresponding to chemical groups -CH and -CH_3 of LA and -CH_2 of ethylene glycol in ^{1}H NMR were integrated and used to calculate the number average molecular weight (M_n) of the polymer.[211] ^{13}C NMR spectrum showed the presence of the groups, -C=O, -CH and -CH_3 in the PLA block at 169.35, 77.23 and 16.67 ppm, respectively, while -CH_2 group in PEG block was found at 69.18 ppm (**Figure 10B**). NMR spectra confirmed structure of the synthesized copolymer.

GPC was used to determine M_n, M_w and molecular weight distribution (PDI) of the synthesized copolymer. Retention time and PDI were found to be 11.025 min and 1.157, respectively, with a unimodal GPC trace (**Figure 10C**). Characteristics of the copolymer determined by NMR and GPC are summarized in **table 6**.

[1]This research work of primary author Divya Sharma is an article published by Taylor & Francis in *International Journal of Polymeric Materials and Polymeric Biomaterials* on 26 Aug 2019, available online: https://doi.org/10.1080/00914037.2019.1655750. The material in this chapter was co-authored by Divya Sharma, Sanjay Arora and Jagdish Singh. Divya Sharma carried out all research experiments, data collection, and data analysis. Sanjay Arora provided assistance in animal studies. Jagdish Singh provided research guidance and served as a proofreader.

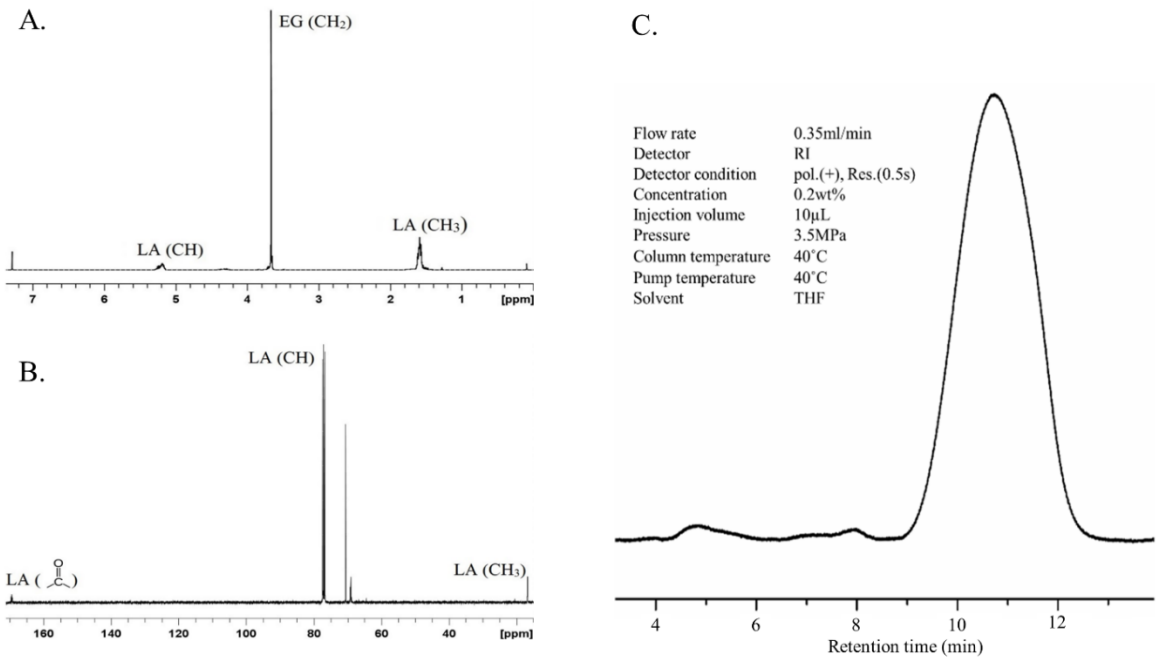

Figure 10. (A) Proton (^{1}H) nuclear magnetic resonance spectrum, (B) Carbon (^{13}C) nuclear magnetic resonance spectrum, and (C) Gel permeation chromatogram, of PLA-PEG-PLA triblock copolymer.[1]

Table 6. Characteristics of PLA-PEG-PLA copolymer determined using proton nuclear magnetic resonance spectroscopy and gel permeation chromatography.[1]

	NMR		**GPC**		
Copolymer	Mw[a]	Mn[b]	Mw[c]	Mn[d]	Polydispersity[e] (Mw[c]/Mn[d])
PLA-PEG-PLA	4500	4660	5022	4339	1.147

Mw[a]: Theoretical molecular weight of copolymer
Mn[b]: Number average molecular weight determined by NMR
Mw[c]: Weight average molecular weight determined by GPC
Mn[d]: Number average molecular weight determined by GPC
Polydispersity index[e]: Determined by GPC

Aqueous solubility and injectability are two additional characteristics that make this copolymer a versatile delivery system. It avoids the use of toxic organic solvents in the formulation while allowing easy subcutaneous administration of formulation without a need for surgery. The aqueous copolymer solution (0.5 mL) was found to be easily injectable through a 25 G needle in the concentration range 10 – 35% w/v (**Figure 11A**). Phase transition of thermosensitive copolymers from an injectable solution form to a gel state is effected by an interplay between hydrophobic PLA blocks and hydrophilic PEG blocks. PLA-PEG-PLA copolymer shows a lower critical solution temperature (LCST) due to the hydrogen bonding between hydrophilic PEG blocks which is dominant at lower temperature, making the copolymer soluble. As the temperature increases above LCST, the hydrogen bonding gets weaker and hydrophobic interactions in the PLA blocks get stronger driving the transition to a gel/depot state.[210] Phase transition of PLA-PEG-PLA copolymer is depicted in **figure 11B**. Sol-gel transition temperature of different aqueous copolymer concentrations (w/v) was in the range 18°C to 26°C, increasing with decreasing copolymer concentration (**Figure 11C**). Therefore, following subcutaneous injection, at physiological temperature the formulation would instantaneously transition into an *in situ* depot incorporating the therapeutic (insulin) in the copolymeric matrix, which is then released at a controlled rate owing to its slow diffusion through the copolymer matrix and gradual hydrolytic degradation of the copolymer.

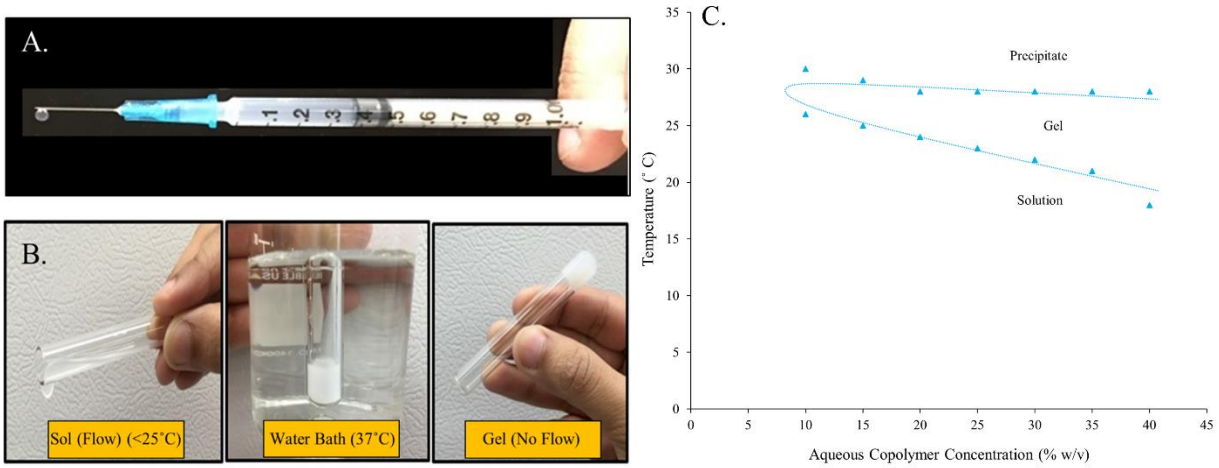

Figure 11. Picture images of aqueous PLA-PEG-PLA copolymer solution demonstrating (A) Injectability through a 25 G needle, (B) Phase transitioning ability in response to temperature, and (C) Graphical representation of sol-gel-precipitate transition of different aqueous copolymer concentrations in response to temperature determined by tube inversion method.[1]

3.2. Synthesis and characterization of oleic acid grafted chitosan polymer

OA-g-CSO polymer was successfully synthesized using carbodiimide mediated coupling reaction. In this reaction 1-ethyl-3-(-3-dimethylaminopropyl) carbodiimide hydrochloride (EDC.HCl) along with N-hydroxysuccinimide (NHS) acts as a zero-length cross-linker that creates a highly reactive upon interaction with a carboxyl group of fatty acid. The intermediate acylisourea ester then reacts with primary amine group of CSO to form peptidyl bond with the elimination of a water molecule. OA grafting on CSO backbone was characterized using ^{1}H NMR and FT-IR spectroscopy as shown in **figure 12 and 13**, respectively. ^{1}H NMR spectra of both CSO and OA-g-CSO polymers showed resonance corresponding to N-acetylglucosamine, glucosamine residue, ring protons at 1.9, 3.0, and 3.4 – 3.8 ppm, respectively. Additionally, OA-g-CSO polymer showed peaks corresponding to methyl and methylene groups of OA residue at 0.8 – 1.1 ppm, and amide bond associated methylene protons at 2.5 ppm.

FT-IR spectra of both CSO and OA-g-CSO polymers showed absorption peaks at 1655 cm-1, 1585 cm^{-1} and 1470 cm^{-1} which can be attributed to carbonyl stretching of secondary amides,

N-H bending vibrations of non-acylated primary amines of CSO, and N-H bending vibrations secondary amide band, respectively. OA-g-CSO polymers demonstrated absorption peaks at 2850 – 2950 cm^{-1} which can be attributed to methylene groups of OA. Moreover, with increased grafting percentage absorption intensity of peak at 1470 cm^{-1} decreased while at 1655 cm^{-1} and 1585 cm^{-1}, were found to be increased.

Grafting efficiency of OA onto CSO backbone was determine using TNBSA bio-reagent. TNBSA reacts with primary amine groups to form a highly chromogenic derivative (N-trinitrophenylamine) which can be quantified using absorption spectroscopy.[212,213] OA-g-CSO polymers with 25 ± 0.2 % and 45 ± 0.5 % grafting percentage were selected for further characterization in this study.

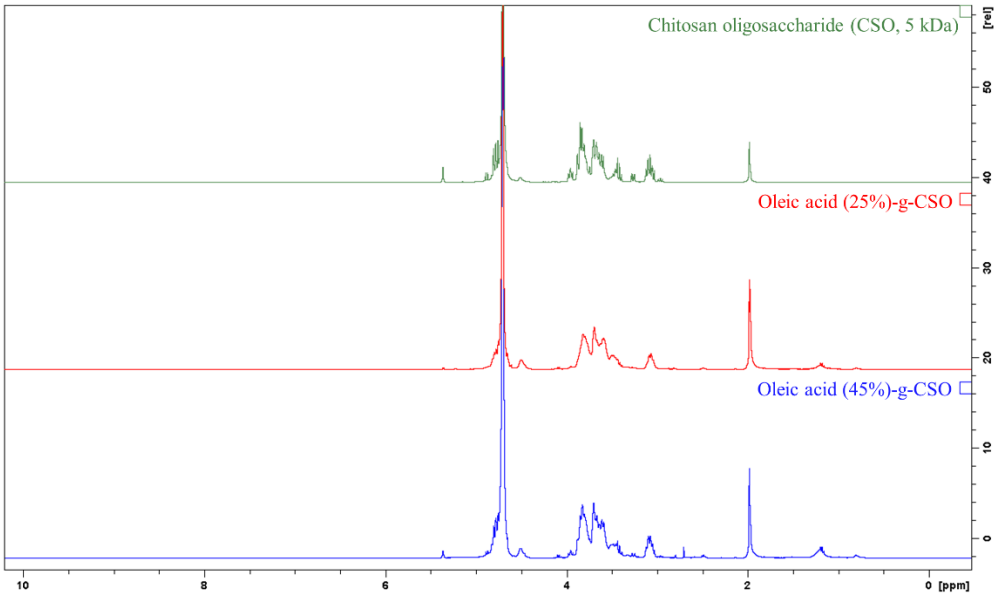

Figure 12. ^{1}H proton nuclear magnetic resonance (NMR) spectra of chitosan oligosaccharide (CSO, 5 kDa) and oleic acid grafted CSO polymers.

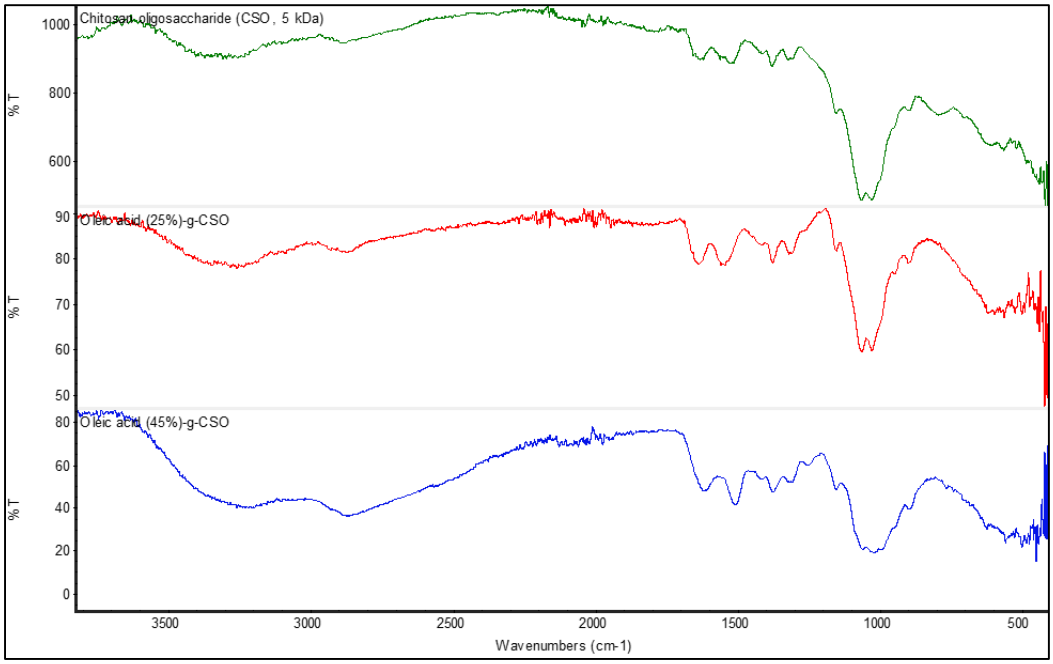

Figure 13. Fourier transform infrared (FT-IR) spectra of chitosan oligosaccharide (CSO, 5 kDa) and oleic acid grafted CSO polymers.

3.3. Calorimetric investigation of insulin modified with zinc and chitosan

Effect of addition of zinc, CS and OA-g-CSO polymers on the association state and thermal stability of insulin were investigated using nano DSC. Transition midpoint temperature (Tm) and transition enthalpy (ΔH) was determined for respective association state of insulin as summarized in **table 7**. The DSC thermogram obtained shows transition of free insulin monomers at Tm_1 51.87 ± 0.23 °C and insulin dimers at Tm_2 62.81 ± 0.29 °C (**Figure 14**). Addition of zinc ions allows association of three insulin dimers to form zinc-insulin hexamer with significantly improved thermal stability indicated by a higher Tm value of 72.57 ± 0.19 °C. Neutron crystallographic analysis suggests zinc-insulin hexamers have a net negative charge at physiological pH.[214] Furthermore, electrostatic complex formation between negatively charged zinc-insulin hexamers and positively charged CS resulted in a much higher Tm (86 – 89 °C) indicating increased thermostability of insulin when complexed with CS. CS polymer, which is positively charged at

physiological pH, stabilizes the hexameric form of insulin by forming electrostatic complex with negatively charged zinc-insulin hexamers resulting in significantly improved thermal stability of insulin as indicated by higher Tm value ~ 86 °C. Increasing chain length of CS demonstrated increasing Tm and transition enthalpy (ΔH) values indicating slightly higher thermal stability of insulin when complexed with longer chain length of CS. This effect may be explained by slight increase in protonation constant (pKa) of CS with increasing chain length.[215] Furthermore, interactions apart from electrostatic interactions between CS and zinc-insulin hexamers such as hydrophobic or non-specific interactions could be contributing to the binding between these molecules.[216] OA modification of CSO demonstrated lower Tm and ΔH values indicating slightly reduced thermal stability of insulin when complexed with OA-grafted-CSO (**Figure 15**). This could be attributed to reduced positive charge on CS backbone and weaker electrostatic complex formation between OA-g-CSO and zinc-insulin hexamers. The complex formation between OA modified CSO polymers and zinc-insulin hexamers was further studied using ITC.

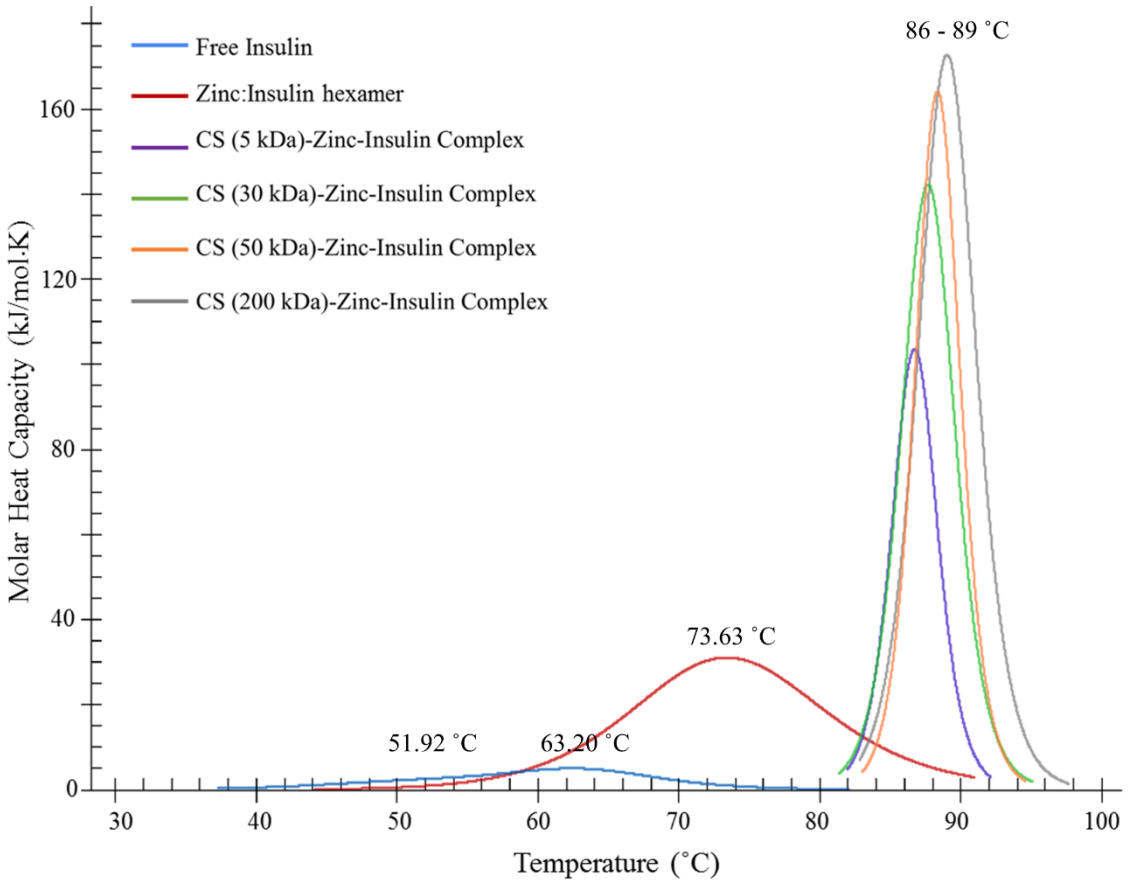

Figure 14. Differential scanning calorimetry thermogram of insulin, zinc-insulin hexamers and chitosan-zinc-insulin complexes prepared using different chain lengths of chitosan polymers. [Insulin: 1 mg/mL; Zinc acetate: 1:5 molar ratio of insulin hexamer to zinc ions; Chitosan: 5 moles of CS monomer unit per mole of insulin monomer; in phosphate buffered saline (10 mM, pH 7.4)][1]

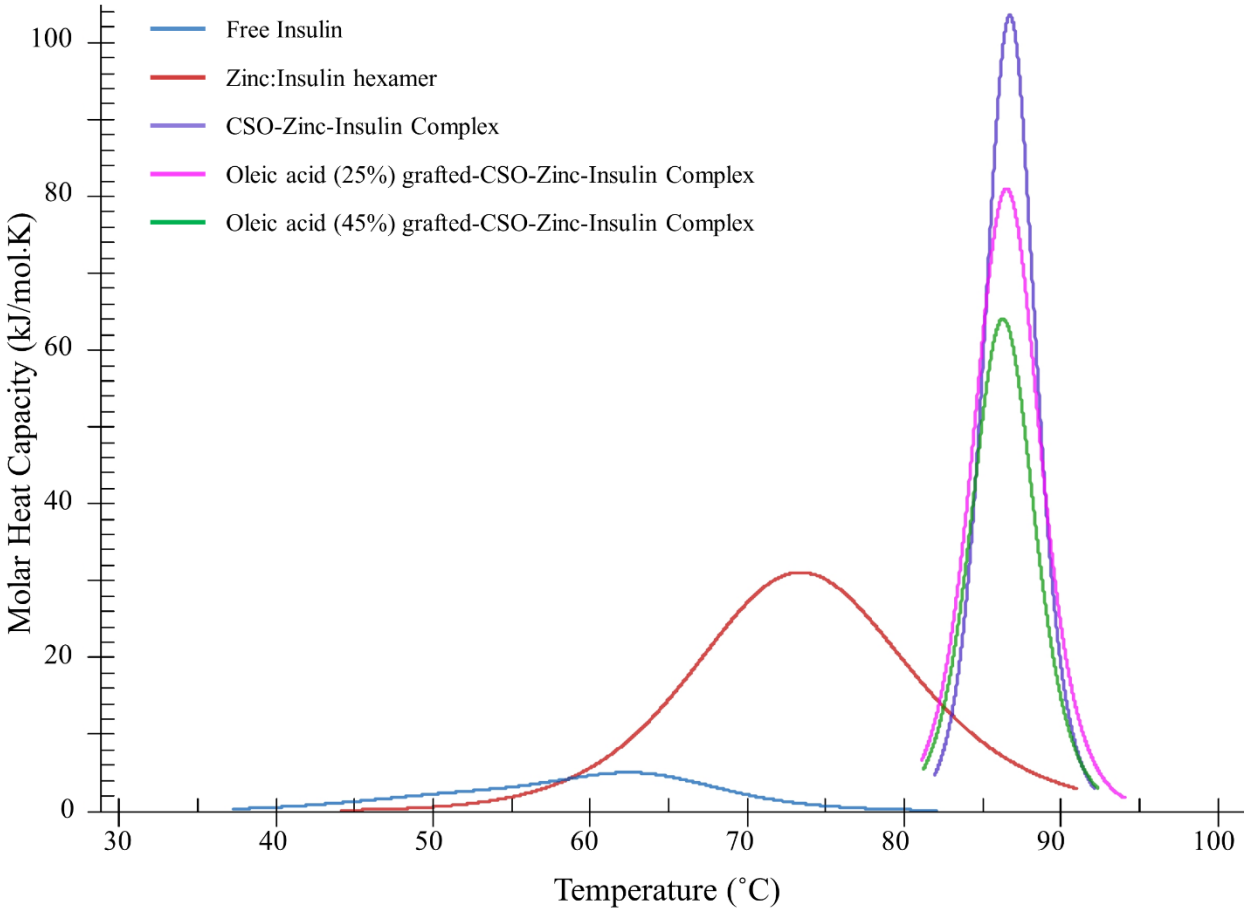

Figure 15. Differential scanning calorimetry thermogram of insulin, zinc-insulin hexamers and chitosan-zinc-insulin complexes prepared using oleic acid-grafted chitosan polymers. [Insulin: 1 mg/mL; Zinc ions: insulin hexamer (1:5); CSO monomer unit: insulin monomer (5:1); in phosphate buffered saline (10 mM, pH 7.4)]

Table 7. Midpoint transition temperature (Tm) and transition enthalpy (ΔH) of insulin, zinc-insulin hexamers and chitosan-zinc-insulin complexes prepared using different chain lengths of chitosan and oleic acid-grafted chitosan polymers, in phosphate buffered saline at pH 7.4. Data are expressed as mean ± S.D, n = 3.

Sample	Tm_1 (˚C)	Tm_2 (˚C)	ΔH (kJ/mol)
Insulin	51.87 ± 0.23	62.81 ± 0.29	97.27 ± 0.44
Zinc-Insulin hexamers	72.57 ± 0.19	-	344.15 ± 0.62
CSO (5 kDa) –Zinc-Insulin complex	86.73 ± 0.07	-	572.88 ± 4.33
CS (30 kDa) –Zinc-Insulin complex	87.69 ± 0.06	-	704.03 ± 1.12
CS (50 kDa) –Zinc-Insulin complex	88.36 ± 0.10	-	727.90 ± 0.97
CS (200 kDa) –Zinc-Insulin complex	89.04 ± 0.13	-	954.75 ± 3.69
Oleic acid (25%)-g-CSO-Zinc-Insulin complexes	86.53± 0.17	-	459.53 ± 5.29
Oleic acid (45%)-g-CSO-Zinc-Insulin complexes	86.30 ± 0.10	-	449.51 ± 3.21

Isothermal analysis was performed to quantitatively determine binding affinity between zinc-insulin hexamers and hydrophobically modified CSO. Integrated net binding heat changes for the interaction using different grafting ratio of OA onto CSO polymer is shown in **figure 16**. Electrostatic interaction between CSO polymer and zinc-insulin hexamer results in an exothermic reaction. Each subsequent injection of CSO polymer into the cell resulted in gradual neutralization of zinc-insulin hexamers indicated by decreased heat changes. Thermodynamic parameters of the respective interactions are summarized in **table 8.** The ITC thermogram for unmodified CSO titrated into zinc-insulin hexamers corresponded to higher binding constant (k) and more exothermic heat changes (ΔH) compared to OA-g-CSO polymers, indicating high binding affinity

and stronger electrostatic complex formation between CSO and zinc-insulin hexamers. This effect was well correlated to that observed using nano-DSC demonstrating higher transition enthalpy for CSO-zinc-insulin complexes (**Table 7**). This effect may be explained by reduced number of free amino groups upon OA grafting on CSO resulting in weaker ionic interaction between OA-g-CSO polymer and zinc-insulin hexamers. Free CSO polymer forms stronger electrostatic complex owing to higher positive charge density compared to OA-modified CSO polymer. Furthermore, increase in OA grafting ratio may lead to reduced binding constant and enthalpy of complex formation which may result in reduced thermal stability of insulin. Hence, OA modification of CSO can have detrimental effect on electrostatic interaction between CSO and zinc-insulin hexamers which may ultimately play a role in determining the overall stability and release of insulin from such complexes. However, OA grafting up to 45% showed comparable binding affinity to unmodified CSO indicating stable electrostatic interactions between OA-g-CSO polymer and zinc-insulin hexamers, which would play an essential role in maintaining insulin in a stable form throughout the duration of release and storage.

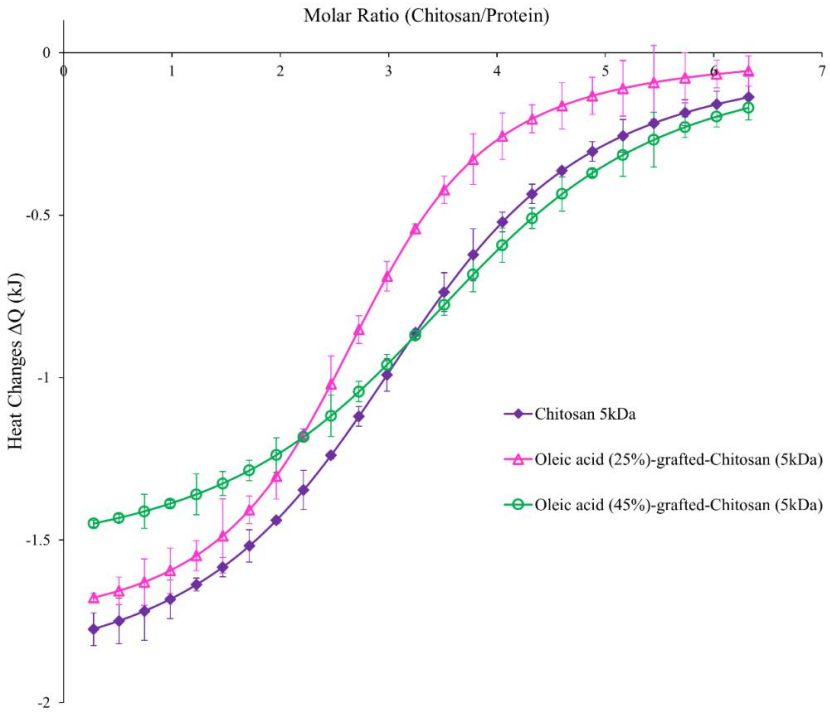

Figure 16. Integrated heats of interaction from calorimetric titrations of oleic acid grafted chitosan polymer (titrant) into zinc-insulin hexamers (titrand). [zinc-insulin hexamers, 2 mg/mL (~0.057 mM); CSO polymer solution, 1.2 mg/mL; in phosphate buffered saline (10 mM, pH 7.4)] Data are expressed as mean ± S.D, n = 3.

Table 8. Thermodynamic parameters of the binding interaction between oleic acid-grafted-chitosan polymers and zinc-insulin hexamers in phosphate buffered saline (10 mM, pH 7.4). Data are expressed as mean ± S.D, n = 3.

Polymer	**k × 10^7 (M^{-1})**	**n (mol)**	**ΔH (kJ mol^{-1})**
Chitosan 5 kDa	11.17 ± 0.09	3.04 ± 0.09	-25.75 ± 0.87
CS-g-Oleic acid (25%)	10.72 ± 0.27	3.26 ± 0.02	-23.96 ± 0.39
CS-g-Oleic acid (45%)	9.99 ± 0.18	3.76 ± 0.01	-21.13 ± 0.12

3.4. Effect of chitosan chain length on *in vitro* release profile of insulin[1]

Cumulative release profile of insulin, zinc-insulin hexamers and CS (50 kDa)-zinc-insulin complexes incorporated in thermosensitive copolymer solution is shown in **figure 17**. Release through PLA/PEG based hydrogels can be affected by size and nature of the copolymer as well as the incorporated therapeutic. Initial burst release is a major concern of such delivery systems owing to the rapid release of therapeutic present on the depot surface. The release is further effected by a combination of diffusion through copolymer matrix and slow hydrolytic degradation of the copolymer.[25] Addition of zinc and CS to free insulin significantly reduced initial burst release owing to the incorporation of less soluble zinc-insulin hexamers and CS-zinc-insulin complexes.[217] Initially, the release from the copolymer is dominated by the slow diffusion of the incorporated therapeutic from the copolymeric matrix. Free insulin monomers were released at a faster rate compared to zinc-insulin hexamers and CS-zinc-insulin complexes. This was observed probably due to the restricted diffusion of larger zinc-insulin hexamers and complexes through the copolymer matrix. Formulation incorporating free insulin monomers and zinc-insulin hexamers also showed a high secondary burst release at 21 and 28 days, respectively. At this stage degradation of the hydrophobic PLA chains of the copolymer become dominant leading to a faster release.[42] However, formulation containing CS showed low secondary burst release and released insulin at a controlled rate up to 60 days which is mainly due to the buffering action of CS. CS contains free NH_2 groups which act like a "proton-sponge" resisting pH change in its microenvironment.[196] This in turn lowers acid-catalyzed hydrolytic degradation of the copolymer further controlling the release of insulin for a longer duration. Promising improvement in stability and release profile of insulin upon formation of CS-zinc-insulin electrostatic complexes motivated us to investigate the effect of shorter and longer chain lengths of CS. CS chain length significantly

affected the rate of insulin release (**Figure 18**) with largest (200 kDa) and smallest chain length (5 kDa) releasing insulin at the fastest and slowest rate, respectively, with best fit for zero-order release kinetics (r^2 = 0.975 and 0.990, respectively). To further investigate the effect of different chain lengths of CS on the release profile of CS-zinc-insulin complexes through the copolymeric depot, hydrolytic degradation of the copolymer was studied by quantifying the percent mass loss and molecular weight of the copolymer remaining after regular intervals.

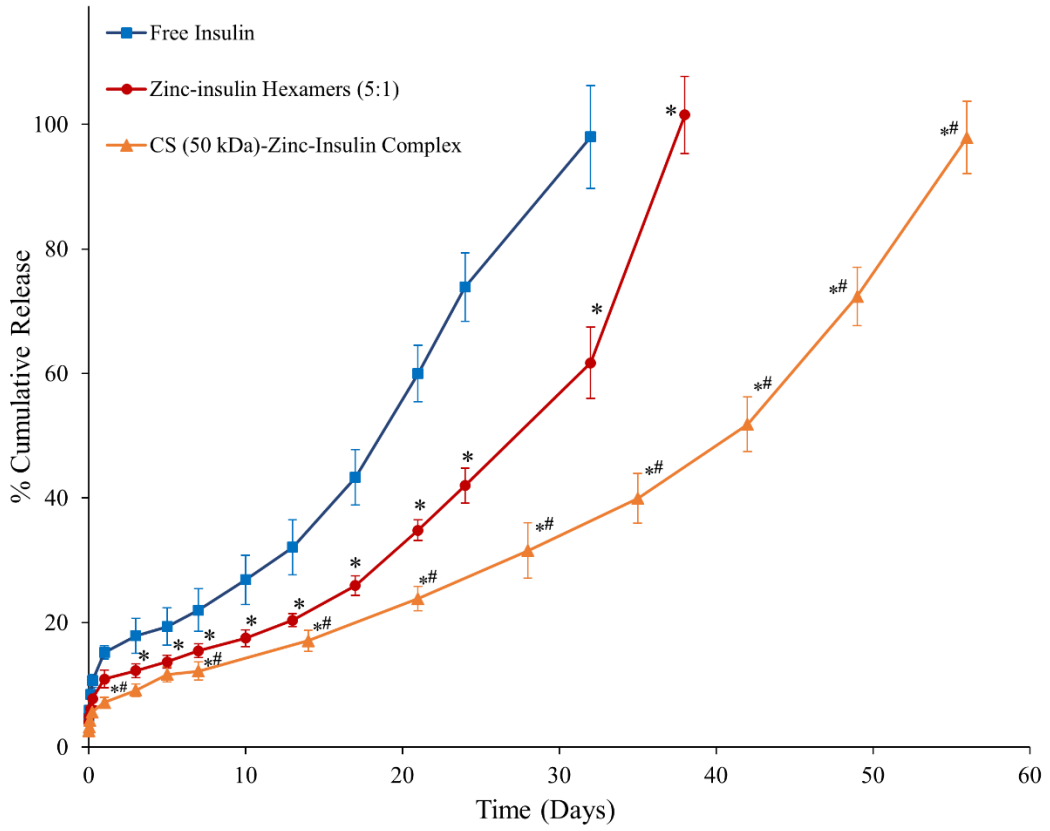

Figure 17. Effect of addition of zinc and chitosan on *in vitro* release of insulin from 35% (w/v) PLA_{1500}-PEG_{1500}-PLA_{1500} copolymer, drug loading: 0.01% (w/v). Data is expressed as mean ± SD, n = 4. [Key: (■) free insulin, (●) zinc-insulin hexamers, (▲) chitosan (50 kDa)-zinc-insulin complex; *: significantly lower compared to free insulin; #: significantly lower compared to zinc-insulin hexamers; at $p < 0.05$][1]

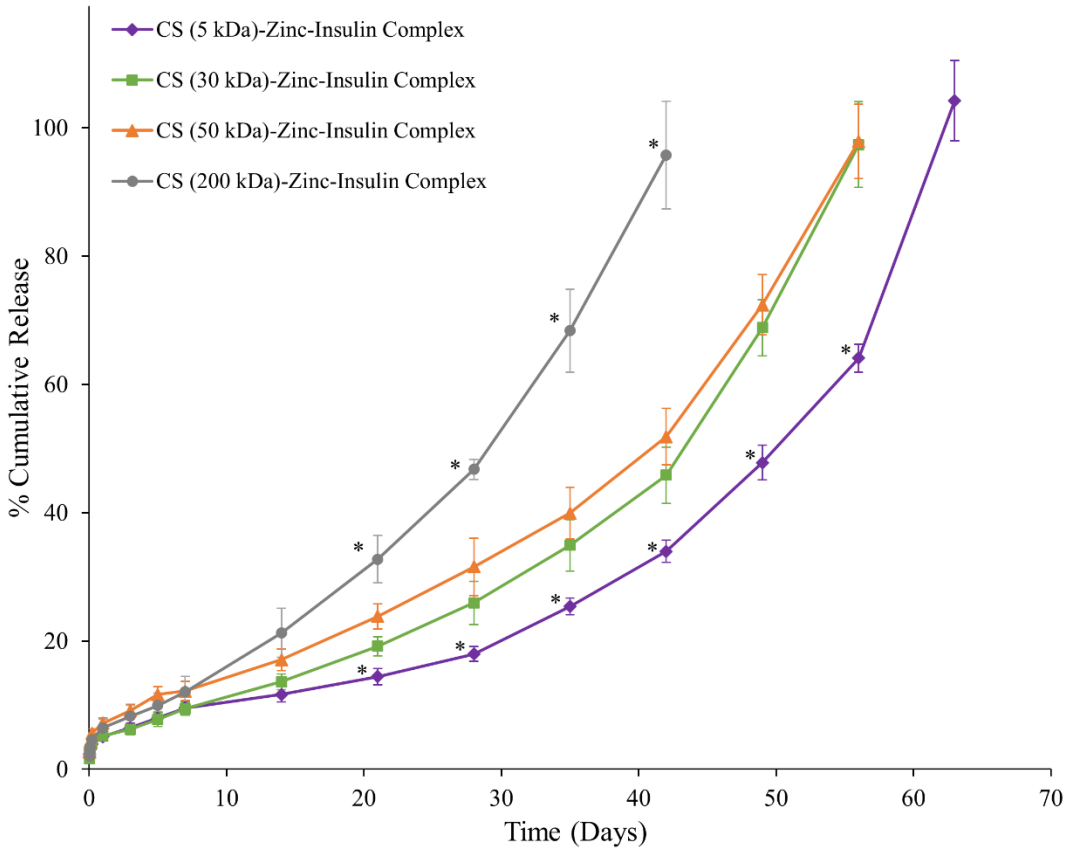

Figure 18. Effect of different chain lengths of chitosan on *in vitro* release of insulin from 35% (w/v) PLA_{1500}-PEG_{1500}-PLA_{1500} copolymer, drug loading: 0.01% (w/v). Data is expressed as mean ± SD, n = 4. [Key: (◆) chitosan (5 kDa)-zinc-insulin complex (■) chitosan (30 kDa)-zinc-insulin complex, (▲) chitosan (50 kDa)-zinc-insulin complex, , and (●) chitosan (200 kDa)-zinc-insulin complex; *: significantly different compared to chitosan (50 kDa)-zinc-insulin complex; at $p < 0.05$][1]

3.5. Hydrolytic degradation profile of triblock copolymer during *in vitro* release[1]

It has been well established that size and hydrophobicity of the incorporated molecule plays a major role in the degradation profile of PLA/PEG based copolymers consequently affecting release profile of the incorporated therapeutic.[175,176] Therefore, effect of increasing chain length of CS on release profile of insulin *via* CS-zinc-insulin complexes incorporated in PLA_{1500}-PEG_{1500}-PLA_{1500} triblock copolymer was determined by comparing the degradation profile of copolymer between the different formulations. Quantification of the percent mass loss after hydrolytic degradation showed that thermosensitive copolymer incorporating CS-zinc-insulin complexes of

higher chain length CS (200 kDa, large hydrophilic polymer) resulted in rapid mass loss of copolymer with time, implying that large sized complexes might have formed bigger pores and channels near the surface during initial release allowing rapid penetration of water molecules inside the gel, thus stimulating rapid degradation of copolymer (**Figure 19, 20**) and consequently, higher rate of insulin release (**Figure 18**).[176] However, thermosensitive copolymer incorporating CS-zinc-insulin complexes containing lower molecular weight CS (5 kDa) might have formed smaller CS-zinc-insulin complexes which resulted in comparatively smaller pore formation upon release and demonstrated slower degradation profile, evident from higher mass of copolymer remaining in the delivery system over time (**Figure 19A**). Simultaneously, copolymer molecular weight remaining after 30 days of *in vitro* release was significantly higher for copolymeric formulation containing smaller CS chain lengths (5 kDa) compared to longer chain lengths (**Figure 19B**). Furthermore, copolymer amount and molecular weight were found to decrease with increase in CS chain length indicating relationship between size of CS-zinc-insulin complexes formed and rate of hydrolytic degradation following initial release.

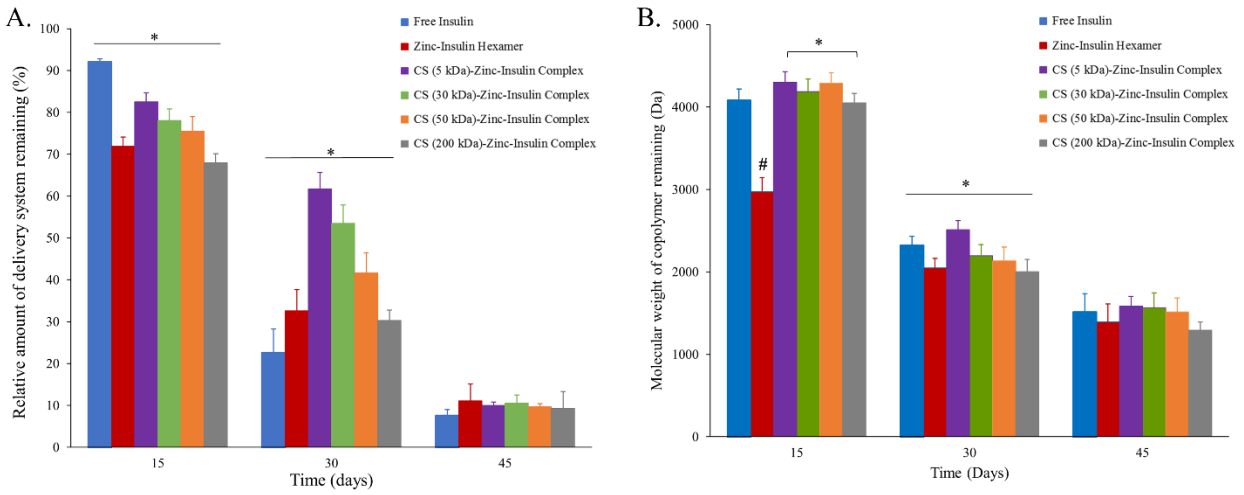

Figure 19. (A) Relative amount of delivery system remaining, and (B) Molecular weight of copolymer remaining, after hydrolytic degradation during *in vitro* release. Data expressed as mean ± SD, n = 4. [*: significantly different; #: significantly different from the rest; at $p < 0.05$][1]

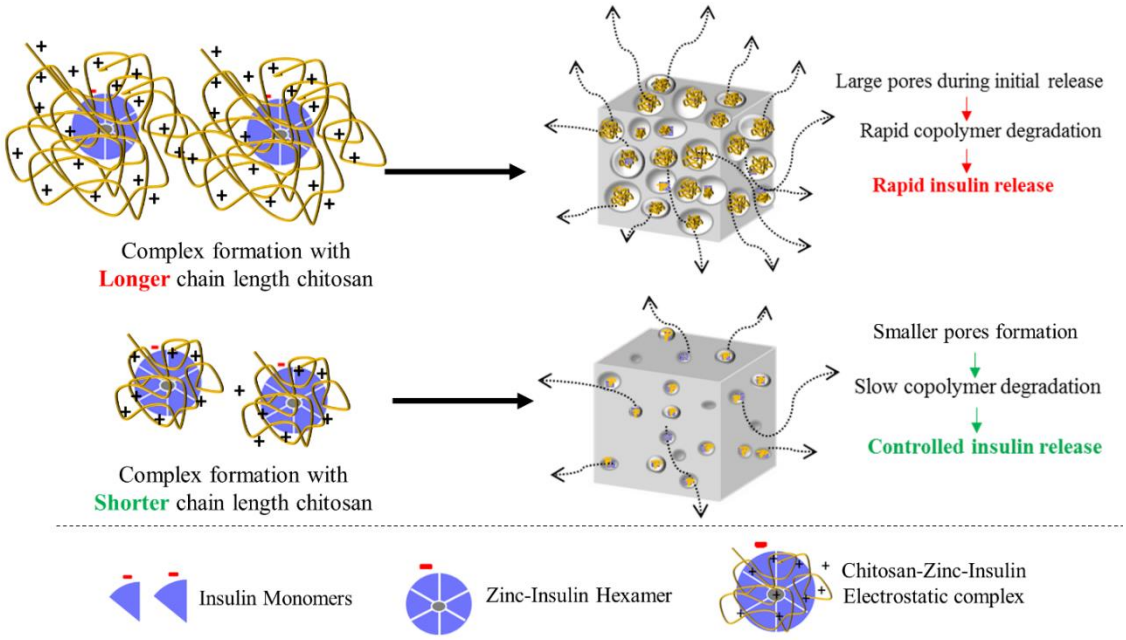

Figure 20. Schematic depicting effect of chitosan chain length used to prepare chitosan zinc-insulin complexes on rate of hydrolytic degradation of PLA-PEG-PLA thermosensitive triblock copolymer and *in vitro* release profile of incorporated insulin.[1]

3.6. Effect of hydrophobically modified chitosan on *in vitro* release profile of insulin

CSO-zinc-insulin complexes and $OA_{(45\%)}$-g-CSO-zinc-insulin complexes incorporated in thermosensitive copolymer solution is shown in **figure 21**. Free insulin monomers incorporated in thermosensitive copolymer demonstrated a high initial burst release (15.2 ± 2.2%) owing to the immediate release of hydrophilic insulin molecules present at the surface of the copolymeric depot. Addition of zinc and CSO to free insulin significantly reduced initial burst release to 10.1 ± 1.3% and 5.1 ± 0.7%, respectively, and further released insulin in a controlled manner. This was observed due to the restricted diffusion of larger zinc-insulin hexamers and CSO-zinc-insulin complexes through the copolymer matrix. Hexamer formation with zinc reduces overall hydrophilicity of the incorporated insulin reducing burst release, restricting diffusion and controlling the rate of release of insulin from the copolymeric depot for ~ 49 days in comparison to free insulin which shows release up to 28 days. Both free insulin and zinc-insulin hexamers containing formulation demonstrated a secondary burst release at 14 and 28 days, respectively. This is observed due to the faster release of incorporated insulin upon breakdown of the PLA chains. However, addition of CSO to the copolymeric depot minimizes secondary burst release and demonstrates constant release of insulin at a sustained rate for up to 70 days. This phenomenon is attributed to the buffering action of CSO polymer which resists pH change in its microenvironment helping in reducing degradation rate of the copolymer.[196] This in turn favors extended insulin release for a longer duration. OA-g-CSO-zinc-insulin complexes further reduced the burst release of insulin (3.8 ± 1.7%) and extended the rate of insulin release up to 80 days. PLA/PEG/PLGA based thermogels attain a domain structure (core-shell) with hydrophilic PEG chains forming the shell of the micelles and hydrophobic PLA chains forming the core of the micelles. Hydrophilic and hydrophobic molecules are assumed to partition between the

hydrophilic and hydrophobic domains, where initial release relates to a diffusion-controlled phenomenon from the hydrophilic domain followed by degradation-controlled release from the hydrophobic domain.[218] Hydrophobic modification of insulin by preparing OA-g-CSO-zinc-insulin complexes allows for its incorporation into the hydrophobic domain of PLA-PEG-PLA copolymer micelles. This results in slow diffusion of incorporated complexes throughout the degradation dominant stage resulting in sustained release profile of insulin for a prolonged period. Slow diffusion of insulin combined with buffering action of CSO polymer can together help achieve zero-order release profile of insulin relevant for providing physiological basal insulin needs.

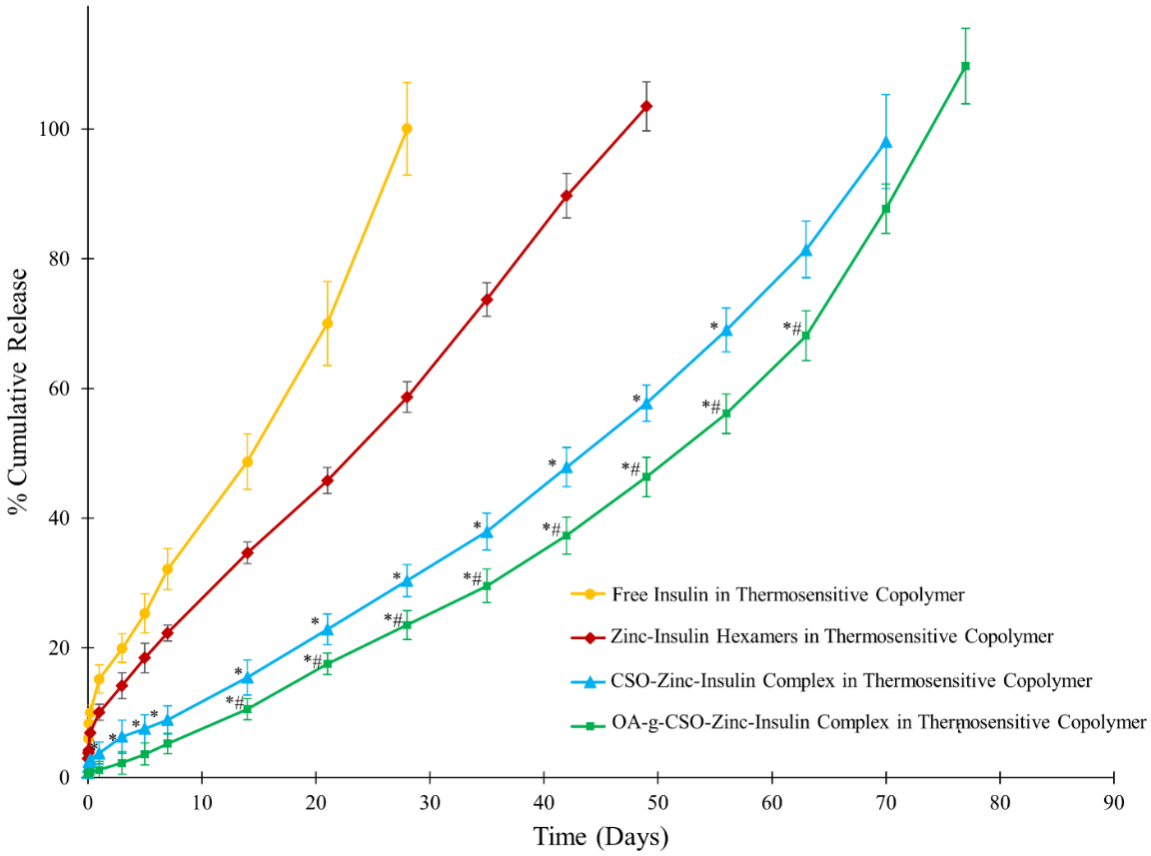

Figure 21. Effect of hydrophobic modification on chitosan oligosaccharide (CSO, 5 kDa) on *in vitro* release of insulin from 35% (w/v) PLA_{1500}-PEG_{1500}-PLA_{1500} copolymer, drug loading: 0.15% (w/v). Data is expressed as mean ± SD, n=4. [Key: (●) free insulin, (◆) zinc-insulin hexamers, (▲) CSO-zinc-insulin complex, (■) oleic $acid_{(45\%)}$-grafted-CSO-zinc-insulin complex; *: significantly lower compared to zinc-insulin hexamers; #: significantly lower compared to CSO-zinc-insulin complex; at $p < 0.05$]

3.7. Stability studies

3.7.1. Stability of insulin released from delivery system

Structural and conformational stability of insulin is pertinent to its biological activity. Insulin is a small globular protein that is present in nature in different oligomeric forms, mainly monomers, dimers, and hexamers. Insulin in its monomeric form is susceptible to denaturation and fibril formation while dimers and hexamers are more stable. Therefore, stabilization of insulin hexameric structure is an effective means of improving insulin stability and counteracting fibril

formation.[219] Conformationally, insulin comprises of higher order structures and alteration in its primary, secondary, tertiary or quaternary structure greatly influences its biological activity.[220,221] Therefore, controlled delivery systems intended for prolonged use of protein/peptide based therapeutics must ensure their structural and conformational stability as well as prevention of denaturation and aggregation.[221,222] Increasing the chain length of hydrophobic PLA block in PLA-PEG-PLA triblock copolymer allows for lower water content in the gel.[218] This further protects the incorporated insulin from degradation and/or aggregation inside the depot. CD spectrum in the near UV region (300 – 250 nm) relates to the differential absorption of left and right circularly polarized light by aromatic amino acid side chains (phenylalanine, tryptophan, tyrosine) and provides an estimate of tertiary structure of a protein.[223] Freshly prepared insulin solution showed a minima at ~ 273 nm depicting tertiary structure of insulin (**Figure 22A**). Spectrum obtained by scanning insulin samples released up to 90 days showed strong CD signal ~ 273 nm representing stable tertiary structure of insulin. Presence of secondary structural components (α helix, β sheets, and random coils) determined using CD spectroscopy can be used to evaluate conformational stability of insulin and other such proteins/peptide based.[31,32] CD spectrum in the far UV region (250 – 200 nm) provides an estimation of secondary structural features of insulin.[223] Scanning freshly prepared insulin solution in the far UV region demonstrates two minima at ~ 208 and 225 nm indicating presence of α helices (34.6 ± 1.7 %) and β sheets (4.8 ± 3.3 %) (**Table 9**). Insulin released from copolymeric depot demonstrated preservation of strong peaks at 208 and 225 nm confirming the ability of OA-g-CSO-zinc-insulin complexes in preserving conformational stability of insulin during the entire duration of release (**Figure 22B**). *In vitro* assessment of thermal stability of insulin can be performed using nano-DSC, such as determination of association state and folding/unfolding temperature. DSC thermogram of samples of insulin released *in vitro* from

OA-g-CSO-zinc-insulin complexes incorporated in thermosensitive copolymer depot demonstrated Tm values corresponding to the transition of OA-g-CSO-zinc-insulin complexes at initial time points, which later dissociated to zinc-insulin hexamers upon dilution (**Figure 22C**). High Tm values indicate prevention of aggregation of zinc-insulin hexamers in the depot when complexed with OA-g-CSO, allowing it to be released in a stable form for up to 90 days.[42,196,225,] Furthermore, detection of proteins and peptides and their degradation/aggregation products using RP-HPLC, is an effective tool for assessing their chemical stability. RP-HPLC is a versatile and reliable technique that enables detection of both covalent and non-covalent aggregates at low concentration based on their affinities towards a n-alkyl silica-based stationary phase, and an organic solvent mobile phase (e.g. acetonitrile) containing a strong ion-pairing agent (e.g. trifluoroacetic acid, TFA) to improve retention in the column. In this study, analysis of insulin released at 1, 30, 60 and 90 days using RP-HPLC showed retention of stable insulin ~ 11.6 min comparable to retention of freshly prepared insulin solution (standard) (**Figure 22D**). No additional peaks corresponding to degradation or aggregation of insulin were observed implying appreciable chemical stability of insulin inside the depot for the entire duration of release.

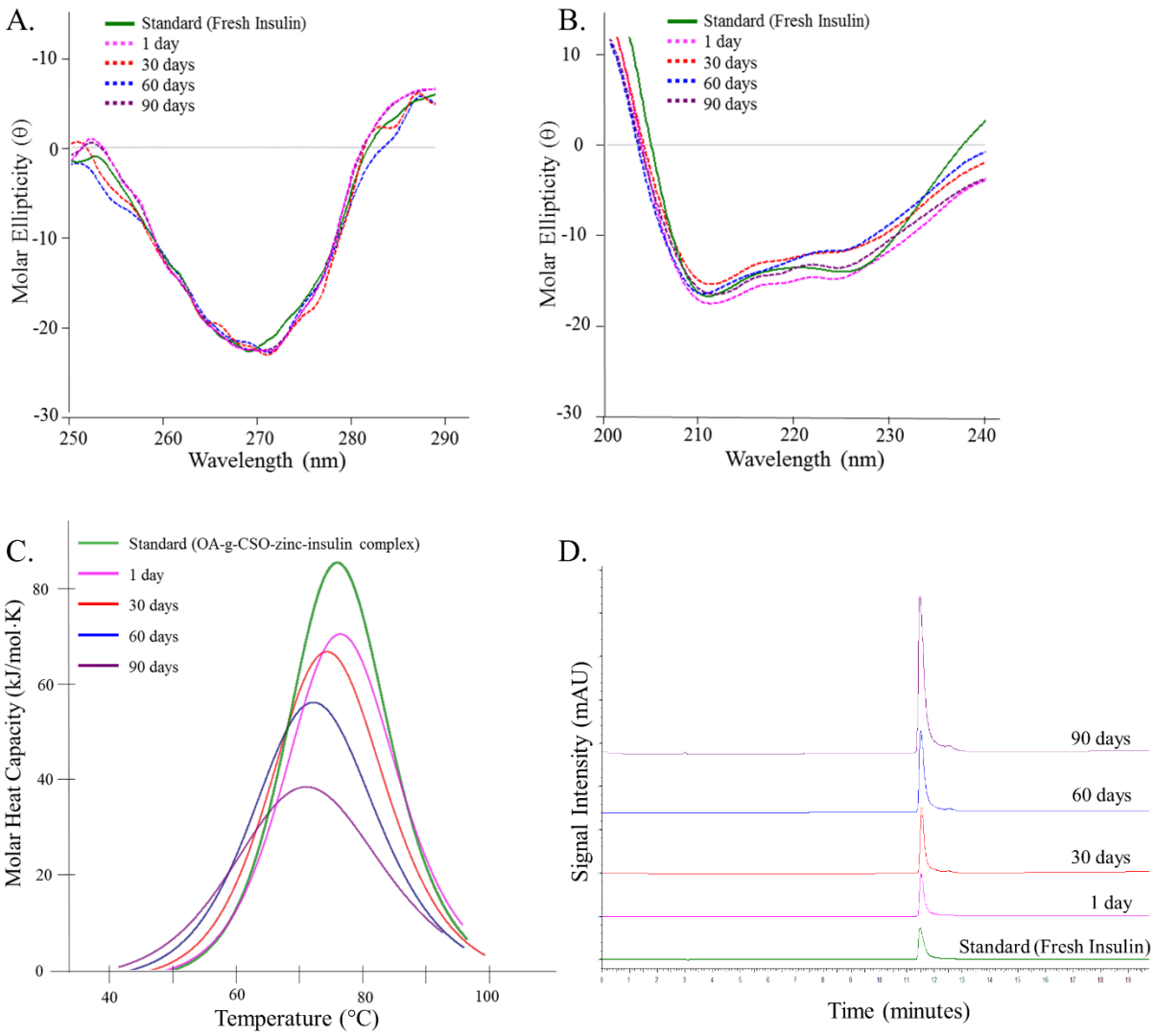

Figure 22. (A) Near-UV circular dichroism spectrum, (B) Far-UV circular dichroism spectrum, (C) Nano-differential scanning calorimetry fitted thermogram, and (D) Reversed phase high performance liquid chromatography, of insulin released *in vitro* at 1, 30, 60 and 90 days from Oleic acid$_{(45\%)}$-g-CSO-zinc-insulin complexes incorporated in thermosensitive copolymer formulation at 37 ˚C.

3.7.2. Storage stability of insulin in formulation

Depot-in-depot formation of OA-g-CSO-zinc-insulin complexes in PLA-PEG-PLA copolymer micelles reduces their interaction with the hydrophilic domain resulting in increased stability and shelf life of such formulation.[210,227] Additionally, positively charged OA-g-CSO polymer forms electrostatic complex with negatively charged zinc-insulin hexamers and stabilizes the insulin in hexameric form further improving its stability.[44] Insulin extracted from stored copolymer formulations showed stable tertiary and secondary structure in the far and near-UV region of CD spectrum after 1, 3, 6 and 9 months of storage at 4 °C (**Figure 23A and 23B**). Nano-DSC and RP-HPLC of the extracted insulin samples also demonstrated the presence of insulin in stable form as compared to freshly prepared standards up to 1, 3, 6, and 9 months' post storage at 4 °C (**Figure 23C and 23D**). These analyses demonstrate the exceptional ability of PLA-PEG-PLA copolymer and complex formation with CSO in preserving the structural and conformational stability of insulin in the prepared formulation for storage up to 9 months in refrigerated conditions.

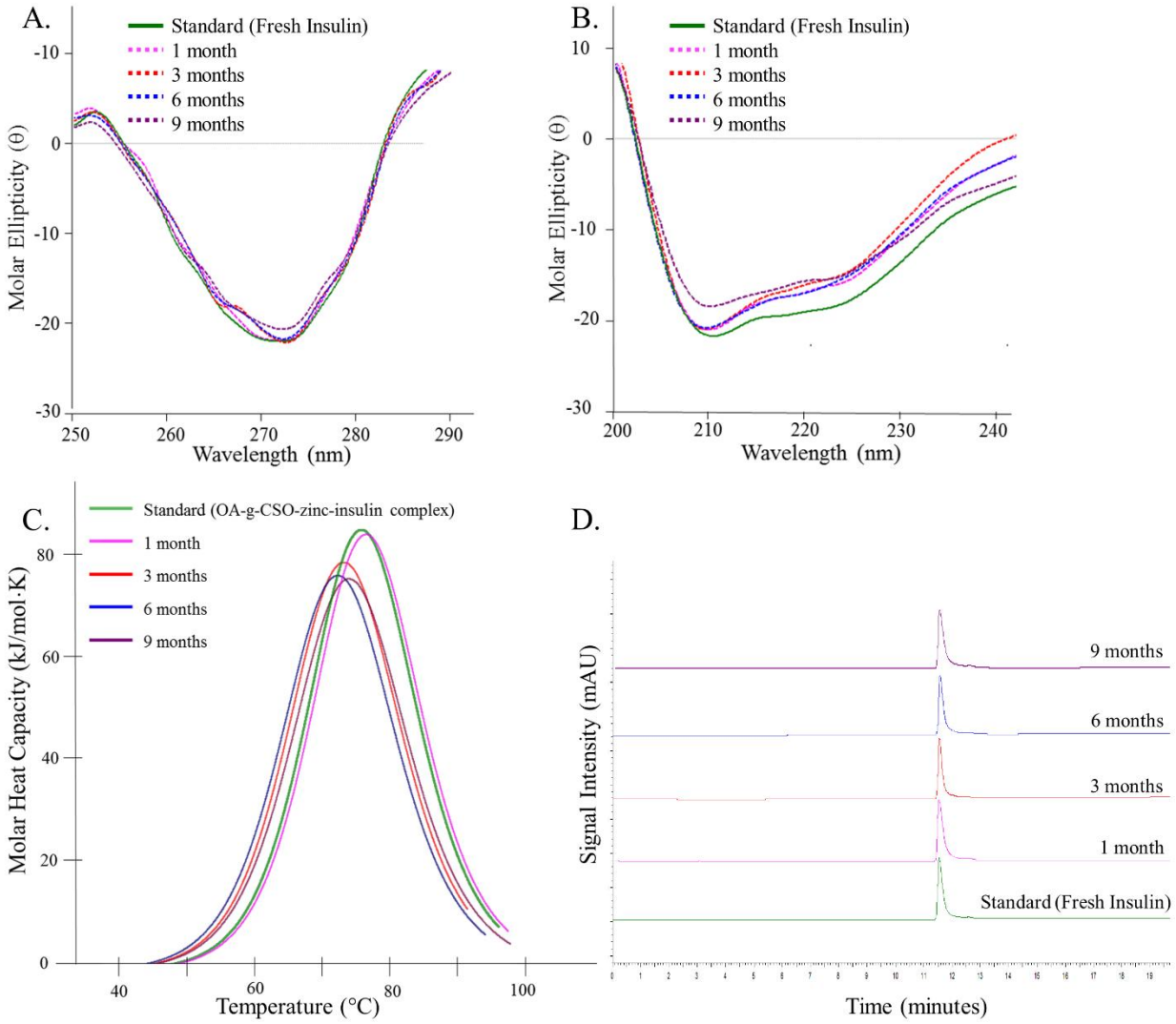

Figure 23. (A) Near-UV circular dichroism spectrum, (B) Far-UV circular dichroism spectrum, (C) Nano-differential scanning calorimetry fitted thermogram, and (D) Reversed phase high performance liquid chromatography, of insulin extracted from Oleic acid$_{(45\%)}$-g-CSO-zinc-insulin complexes incorporated in thermosensitive copolymer formulation after 1, 3, 6 and 9 months of storage at 4 ˚C.

Table 9. Secondary structure estimation of insulin. Data are expressed as mean ± SD, n = 4.

Sample	Days	α Helix	β Sheets	β Turns	Random Coils
Standard (Fresh Insulin in PBS)	-	34.6±1.7	4.8±3.3	29.3±1.9	31.3±3.1
Insulin released *in vitro* from Oleic acid-g-CSO-Zinc-Insulin complexes incorporated in thermosensitive copolymer formulation at 37˚C.	7	34.9±3.6	16.0±1.6	26.7±2.2	22.4±3.9
	30	26.7±1.1	31.5±8.2	20.4±4.4	21.4±1.9
	60	25.1±0.9	30.4±6.9	21.6±2.8	22.9±4.0
	90	23.9±3.8	39.6±1.5	17.6±4.9	18.9±5.1
Insulin extracted from Oleic acid-g-CSO-Zinc-Insulin complexes incorporated in thermosensitive copolymer formulation stored at 4˚C.	30	34.9±3.6	16.0±1.6	26.7±2.2	22.4±3.9
	90	34.8±2.5	17.3±1.0	25.5±4.6	22.4±4.1
	180	33.9±5.1	23.0±2.8	24.7±2.3	18.5±2.9
	270	35.1±1.7	26.4±3.0	22.2±3.6	16.3±8.2

3.8. *In vitro* and *in vivo* biocompatibility

This study was designed to evaluate the effect of short and long-term accumulation of PLA-PEG-PLA triblock copolymer with and without OA-g-CSO polymer by determining the effect of their degradation products on 3T3-L1 fibroblast cells and HEK 293 cells. Although copolymers constituting PLA and PEG are widely researched to be biodegradable and biocompatible, their long-term accumulation at the depot site needs to be investigated to demonstrate their safety for prolonged and/or repeated use.[228–230] OA-g-CSO polymer was also added to aqueous copolymer formulation while assessing the biocompatibility of the delivery system. Insulin and zinc were not included in this study owing to their effect on cellular properties such as cell proliferation which may interfere with distinctly assessing cytotoxic effects of the copolymeric delivery system.[231,232]

In this study, both 3T3-L1 and HEK-293 cells showed good cytocompatibility post incubation with copolymer extracts with and without OA-g-CSO polymer (**Figure 24**). It was noted that the presence of OA-g-CSO polymer improved cell viability, which can be attributed to the cell proliferative and wound healing properties of CSO [233]. Longer incubation period up to 48 and 72 h as well as extraction of copolymer at higher temperature (70 ˚C), both resulted in increased viability in both cell types indicating the positive contribution of copolymer degradation products in cell proliferation and viability. This is suspected to occur due to the consumption of copolymer degradation products *via* citric acid cycle leading to higher mitochondrial activity and cellular metabolism.[234] However, *in vivo* biocompatibility is a much more complex phenomenon. Various natural, synthetic and semisynthetic materials have been used for manufacture of implantable devices.[235] The major concern following such implantation is foreign body response resulting from the tissue injury resulting from the implantation along with the continued presence of the implant in the region.

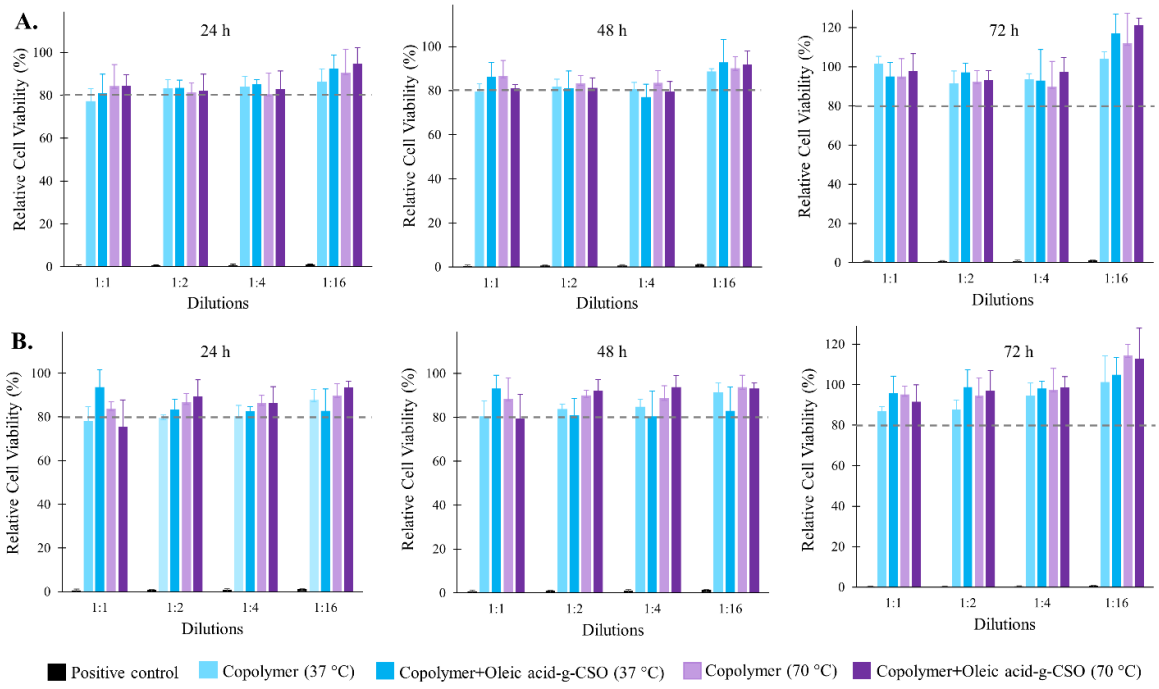

Figure 24. Graphical representation of percent relative cell viability at different dilutions of copolymer degradation products after 24, 48 and 72 h of incubated with (A) 3T3-L1 fibroblast cell line (B) HEK 293 cell line. Thermosensitive copolymer PLA-PEG-PLA incorporating oleic acid-g-CSO polymer was incubated with PBS for 10 days at 37 ˚C to extract the copolymer, CSO polymer and their degradation products. Biocompatibility was evaluated using MTT assay. Data expressed as mean ± SD, n = 4.

PLA-PEG-PLA based copolymers have an added advantage of being easily injectable, formation of *in situ* depot at injection site, and aqueous solubility avoiding the use of toxic organic solvents which can damage the incorporated therapeutic as well as cause pain/irritation upon administration. The presence of PEG chains forms an outer corona on these copolymeric micelles contributing to their low immunogenicity.[236] Additionally, PLA-PEG-PLA triblock copolymers show pliability and mucomimetic characteristics which helps in minimizing mechanical irritation from such controlled release depots.[237,238] Treatment of a chronic disease like type-1 DM requires all components of the delivery system intended for treatment to be biocompatible for long-term use.

To determine the biocompatibility of the PLA-PEG-PLA copolymer incorporating OA-g-CSO-zinc-insulin complexes *in vivo*, the depot was regularly observed and the subcutaneous tissue surrounding the injection site was excised and analyzed for inflammatory response. The chief stages of this process include short lived (few days) acute inflammation, which is mainly an attempt by the body to clear the foreign substance using hemodynamic forces like vascular dilation providing excess blood flow to the site, formation of a fibrin clot, permeation of salts, protein and water to cause edema, and infiltration and accumulation of numerous blood and tissue proteins including cytokines, growth factors and leukocytes. The tissue samples collected 1-day post administration show increased accumulation of inflammatory mediators (**Figure 25G**). This accumulation is similar to that observed in the control group injected with same volume of saline (0.5 mL) (**Figure 25C**). Positive control group injected with 5% (v/v) of formalin buffer shows much higher accumulation of inflammatory factors due to the relatively higher irritation and activation of foreign body response (**Figure 25B**). Continued inflammatory stimuli results in a chronic inflammatory response which proceeds by restructuring of the injection area by proliferation of blood vessels, connective tissue, fibroblasts and endothelial cells leading to conversion of initially formed fibrin clot to a highly vascularized granulation tissue, surrounding the implant. However, in the tissue excised 7-day post administration no such formation was observed in the tissue surrounding the implant (**Figure 25H**). Eventually active fibroblasts produce collagen and proteoglycans replacing the granulation tissue with extracellular matrix. Well defined collagen fibers form a fibrous wall around the implanted device and confines it from entering the surrounding tissue. Gomori's trichrome stain was used to determine the nature and presence of collagen deposition at the administration site. In our experiments, it was noted that the collagen deposition at the site of injection was increased initially (day 30), indicated by high intensity of

stained collagen fibers (**Figure 25L**). However, the collagen density at the end of the study was comparable to control, with no sign of residual scar tissue. The connective and muscular tissues surrounding the injection site appeared to be normal with no morphological changes compared to control, thus confirming the biodegradable and biocompatible nature of the delivery system.

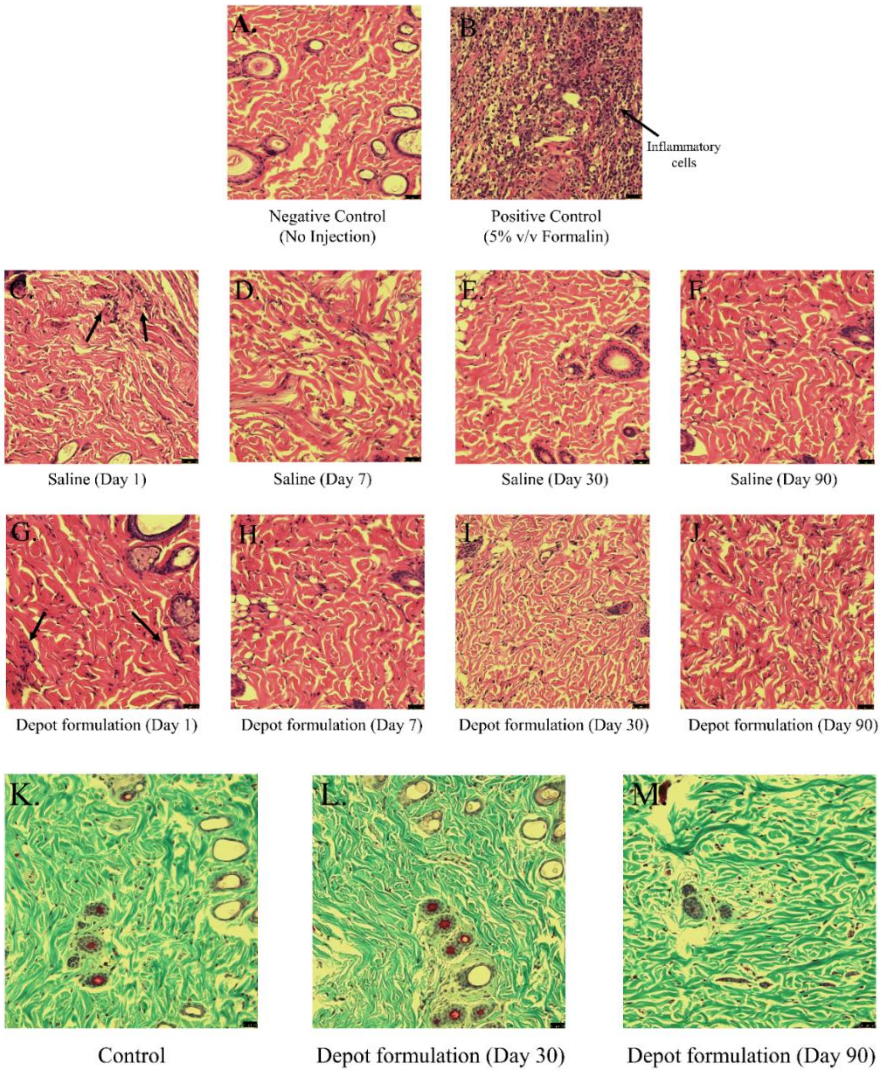

Figure 25. Bright field micrographs of H & E stained rat injection site skin tissue after (A) no injection (negative control), (B) 5% (v/v) Formalin (positive control), (C – F) 1, 7, 30 and 90 days' post administration of Saline, (G – J) 1, 7, 30 and 90 days' post administration of Oleic acid$_{(45\%)}$-g-CSO zinc insulin complexes incorporated in thermosensitive copolymer formulation. Bright field micrographs of Gomori's trichome stained rat injection site skin tissue after (K) no injection, and (L) 30 days, (M) 90 days, post administration of Oleic acid$_{(45\%)}$-g-CSO zinc insulin complexes incorporated in thermosensitive copolymer formulation.

3.9. *In vivo* insulin release and bioactivity

The overall aim for insulin therapy is to improve pharmacokinetic (PK) profile to obtain pharmacodynamic (PD) effects closely resembling insulin release and action in a healthy body [239,240]. Basal insulin release is estimated to be 0.1 - 0.2 U/kg/day in healthy individuals corresponding to fasting insulin concentration < 25 mU/L.[241] Ideal requirements of basal insulin therapy include flat PD profile, low hypoglycemic risk, and stable duration of action. Unfortunately, current insulin options do not fulfill these essential criteria. Insulin NPH (NPH: neutral protamine Hagedom) shows delayed absorption with an onset of 1 – 4 h and peak in 6 – 10 h, suggested as twice daily administration for basal insulin therapy, however high inter-individual variability, short duration of activity, and risk for severe hypoglycemia persuaded the need to develop longer-acting insulin analogues.[242] Insulin glargine is an bioengineered insulin analogue prescribed as once-daily administration to cover basal insulin for a 24 h period. Glargine forms precipitates in the surrounding subcutaneous tissue after injection which slowly re-dissolve delaying the absorption. However, it fails to mimic physiological insulin secretion and require high doses to provide 24 h coverage. High variability in the PK profile in current therapy directly influences PD effects, increasing hypoglycemic incidents due to unpredictability of insulin peaks, fluctuating blood glucose levels and increased occurrence of diabetes complications.[243–245] In an attempt to obtain a peak-less PK profile and reducing the frequency of administration for basal insulin therapy thermosensitive *in situ* gel forming systems have a competitive advantage. Insulin can easily be suspended in aqueous thermosensitive copolymer solution owing to their low critical solution temperature (LCST > 25 °C), which upon subcutaneous administration due to the physiological temperature (35 – 37 °C) being above their upper critical solution temperature (UCST) undergo phase transition to form a gel depot. As mentioned earlier, these copolymers are

biocompatible, biodegradable, and help preserve the stability of insulin inside the depot for the entire duration of release and storage. However, for modifying this system for basal insulin delivery three critical parameters *i.e.* burst release, release profile of insulin, and bioactivity of insulin released need to be considered. The initial burst release occurs due to the rapid release of therapeutic present on the surface of the depot. Burst release of insulin from such delivery systems needs to be addressed to avoid hypoglycemia. Thereafter, the release of therapeutic is dependent on diffusion through the copolymer matrix at an early stage followed by a combination of diffusion through the copolymer and degradation of copolymer at later stage.[246] Reduction in peaks and troughs throughout the duration of release is beneficial in mimicking physiological insulin release. In this study, we compared the PK profile of three thermosensitive copolymer-based formulations (Groups V, VI and VII) incorporating free insulin, zinc-insulin hexamers and OA-g-CSO zinc insulin complexes, respectively, with free insulin solution (single administration) and insulin glargine solution (Lantus® U-100, repeated administration at 24 h interval) (**Table 5**). Insulin solution resulted in C_{max} of 61.74 ± 6.47 mU/L with T_{max} 2 h followed by immediate absorption and drop in blood glucose with its glucose lowering effect lasting for 6 – 8 h (**Figure 26A**). Insulin glargine showed a relatively sustained profile of insulin release reaching peak serum concentration between 2 – 4 h and blood glucose lowering effect lasting between 18 – 20 h (**Figure 26B**). Thermosensitive copolymer formulation incorporating free insulin showed a burst release of 58.13 ± 5.01 mU/L in 24 h, followed by slow controlled release for 7 days and complete release by ~ 35 days (**Figure 27**). Both CSO-g-zinc-insulin complexes and OA-g-CSO zinc insulin complexes helped reduce the burst release by ~ 4.8 fold and showed gradual increase in serum insulin levels post administration with 19.95 ± 10.88 and 12.67 ± 4.07 mU/L in 24 h, respectively.

Formulation incorporating OA-g-CSO-zinc-insulin complexes demonstrated relatively stable serum insulin levels of 21.83 ± 3.29 mU/L for ~ 91 days. Formulations incorporating free insulin and CSO-zinc-insulin complexes released insulin at a faster rate demonstrating serum insulin levels of 19 – 65 mU/L over 28 days, and 42 – 15 mU/L over ~ 63 days, respectively. Since the release from such thermogels is significantly affected by the nature and size of the incorporated therapeutic, depot in depot formation by hydrophobic modification CSO polymer contributed significantly to a sustained release profile of insulin for an extended period.[197] Absorption of insulin is a complex phenomenon.[247,248] Association state of insulin has been regarded as the major determinant of rate of absorption. Monomeric form of insulin in biologically active. However, at micromolar concentration insulin monomers self-associate to form dimers. In the presence of zinc, three insulin dimers arrange to form a hexameric complex with reduced solubility. At physiological pH positively charged CSO polymer (CSO pKa 6.2 – 7) are capable of forming electrostatic complexes with negatively charged zinc-insulin hexamers (insulin pKa ~ 5.3) stabilizing the hexameric complex and preventing aggregation and degradation.[249,250] The complexes upon release undergo dissociation upon dilution to release zinc-insulin hexamers, that dissociate into dimers and finally release insulin monomers that are absorbed into systemic circulation. Slow dissociation of insulin from the complex helps in controlled availability of insulin as well as preserves the conformational and biological stability of insulin up till its release and absorption. Insulin mediates its PD effects through the insulin receptor. This effect was evaluated by monitoring blood glucose concentration in treated rats. High burst release of insulin in diabetic rats treated with insulin solution, and free insulin incorporated in thermosensitive copolymer solution rendered rapid lowering of blood glucose levels from ~ 400 to 72 and 68 mg/dL 2 h post administration, respectively (**Figures 26A and 27**). This is a serious concern and often requires

immediate medical attention as glucose concentrations lower than 60 mg/dL may lead to unconsciousness, seizures, diabetic coma and even death. The rats were duly monitored throughout the duration of blood glucose concentration lower than 75 mg/dL but no severe behavioral symptoms like shakiness, seizures, or abnormal activity were noted. This could be attributed to the coprophagic behavior of rats which may have prevented development of hypoglycemic shock state. CSO-zinc-insulin complexes and OA-g-CSO-zinc-insulin complexes incorporating formulations resulted in gradual lowering of blood glucose levels of 84 and 104 mg/dL 2 h post administration, respectively (**Figure 27**). Daily 24 h administration of glargine resulted in fluctuating blood glucose levels between 91 – 443 mg/dL. On the other hand, CSO-zinc-insulin complexes containing formulation resulted in blood glucose levels 97 ± 16 mg/dL for 77 days and OA-g-CSO-zinc-insulin complexes incorporating formulation resulted in blood glucose levels 102 ± 9 mg/dL for 91 days. There was no significant difference ($P < 0.05$) between the blood glucose levels of OA-g-CSO-zinc-insulin complexes formulation group between consecutive time intervals, and with healthy non-diabetic rats up to 63 days which can be attributed to the slow release of insulin diffusing from the depot inside the hydrophobic depot of the copolymer micelles. Such release profile is extremely beneficial for basal insulin therapy in diabetic individuals as it would prevent hyper- and hypo-glycemic episodes, night-time hypoglycemia, and steady glucose supply in fasting conditions for optimum physiological health and energy production. Moreover, hydrophobic modification of CSO-zinc-insulin complexes also helped achieve better *in vitro – in vivo* correlation which may be beneficial in tailoring the system to basal insulin range between 0.5 – 1 U/h/kg for patient-based therapy.

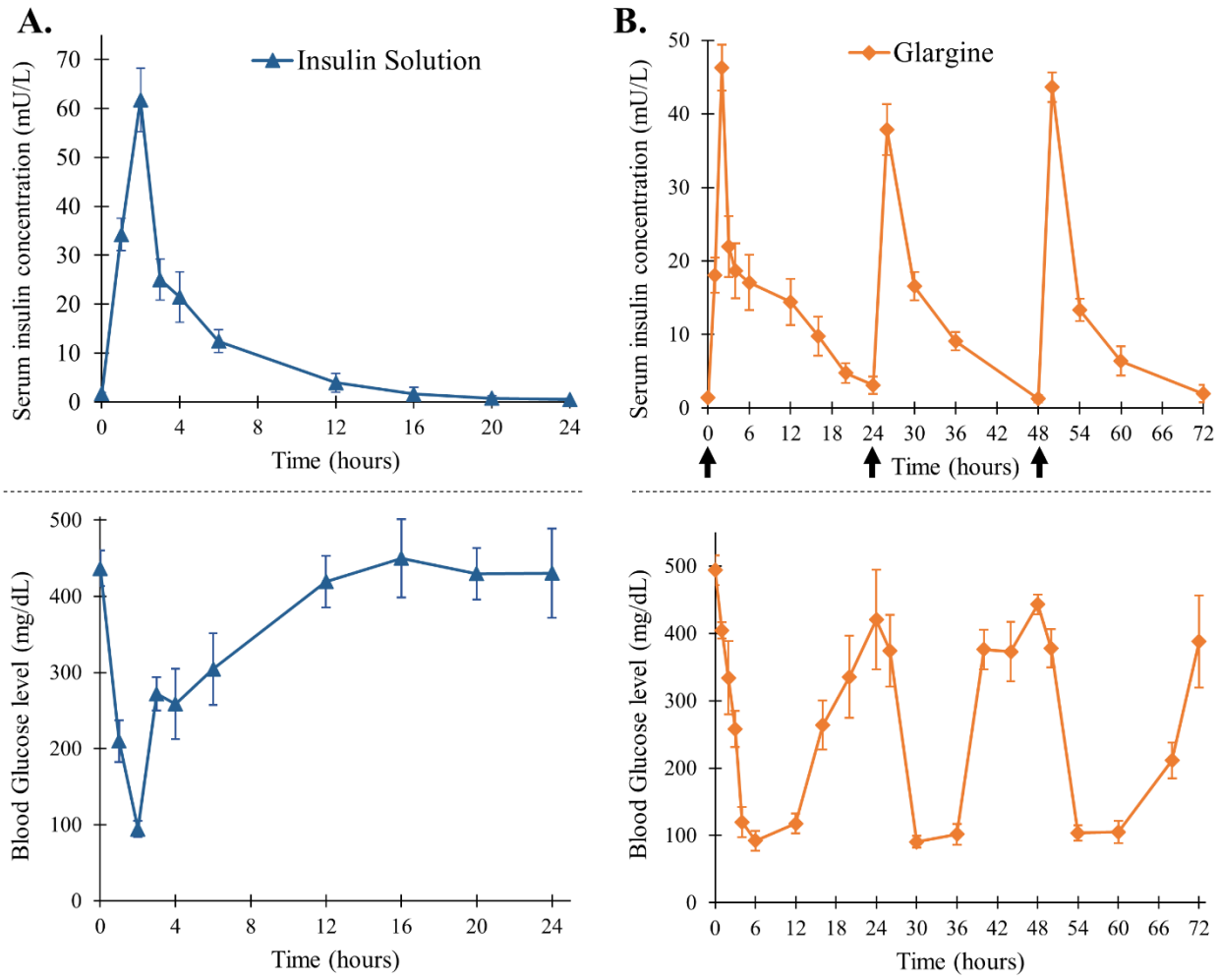

Figure 26. Serum insulin concentration and blood glucose level of STZ-induced diabetic rats upon treatment with (A) single administration of recombinant human insulin and (B) daily administration of insulin glargine (Lantus® U-100). [Data are expressed as mean ± S.D, n = 6; arrows mark administration of glargine; insulin dose: 0.5 IU/kg/day]

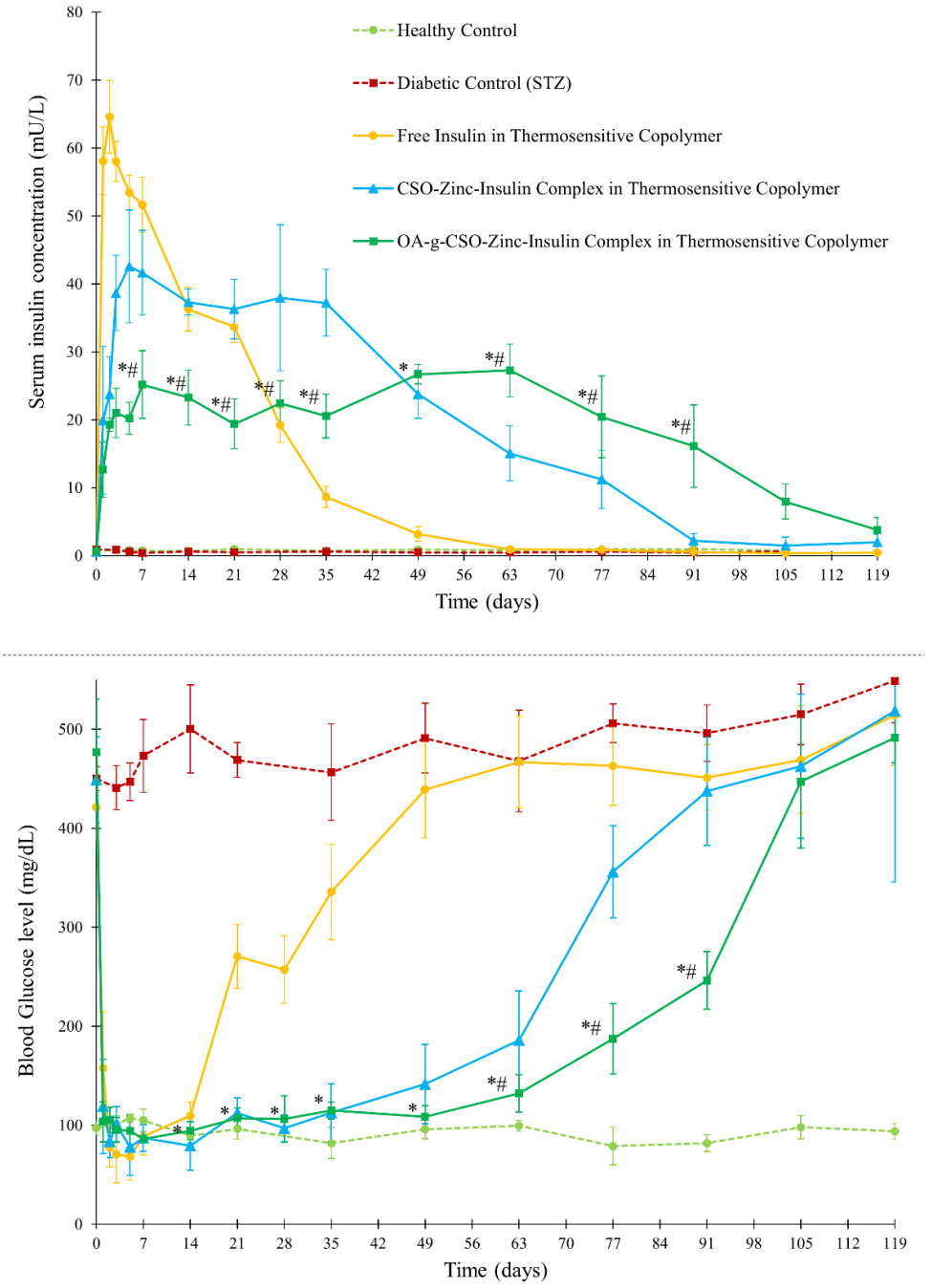

Figure 27. Serum insulin concentration and blood glucose level of STZ-induced diabetic rats upon insulin treatment. Key: Treatment with single administration of: (●) free insulin in thermosensitive copolymer, dose 45 IU/kg; (▲) CSO-zinc-insulin complex in thermosensitive copolymer, dose 45 IU/kg; or (■) oleic acid$_{(45\%)}$-grafted-CSO-zinc-insulin complex in thermosensitive copolymer, dose 45 IU/kg; (■) untreated STZ-induced diabetic control; (●) healthy non-diabetic control. [Data are expressed as mean ± S.D, n = 6; *: significantly different compared to glargine treated control; #: significantly different compared to CSO-zinc-insulin complex; at $p < 0.05$]

3.10. Determination of blood ketone levels and cataract formation

Persistent blood sugar spikes as expected from repeated insulin administration can cause severe complications like diabetic ketoacidocis (DKA), hyperglycemic hyperosmolar syndrome (HHS), damage to blood vessels, nerves, and organs leading to heart disease, stroke, nephropathy, neuropathy, retinopathy, nerve damage, limb amputations, skin infections, problems with teeth and gums, all leading to reduced quality of life and high medical cost. DKA is a life-threatening complication of diabetes which occurs due to build-up of ketones in the body as a result of fat breakdown during insulin-glucose imbalance. In the absence of sufficient insulin, DKA may develop in less than 24 h. In diabetes patients, DKA can be suspected with blood pH < 7.3 and plasma ketone concentration of > 3.0 mmol/L.[251] Inefficient insulin in the body may also cause HHS due to build-up of glucose resulting in high osmolarity, dehydration, and vision problems. This may lead to osmotic lens swelling and cataract development over time. Evaluation of efficient basal insulin therapy mandates prevention of both short and long-term complications of diabetes. Determination of blood ketone levels is an effective strategy of monitoring accumulation of ketones in the body and preventing DKA. STZ-treated diabetic rats (Group II) showed significant accumulation of blood ketones ($P < 0.05$) compared to healthy control with a concentration of 3.8 ± 0.2 and 4.1 ± 0.4 mmol/L within one- and three-months' post STZ-treatment, respectively (**Figure 28A**). Gradual rise in blood ketone levels was observed in the free insulin and CSO-zinc-insulin complexes incorporated in thermosensitive copolymer formulations group at two and three-month time-points, respectively. However, owing to the sustained maintenance of basal insulin levels in the OA-g-CSO-zinc-insulin complexes incorporated in thermosensitive copolymer formulation group there was insignificant build of ketones in the body, suggesting much lower risk of DKA associated complications (**Figure 28A**).

Daily treatments with insulin-glargine also helped preventing accumulation of ketone bodies, however required timely doses of insulin for 3 months accounting to 90 injections. Visual impairment and cataract development is also a common complication of diabetes. Reduction of glucose to sorbitol occurs through the polyol pathway catalyzed by the enzyme aldose reductase (AR). Hyperglycemia promotes AR-mediated accumulation of sorbitol in lens fibers and increase in osmotic, oxidative and ER stress, along with glycation of lens proteins that lead to degeneration, collapse, and liquefaction of lens fibers, resulting in formation of lens opacities and progression to cataract [251]. All the animals in the diabetic untreated group developed total opacity of lens (**Figure 28C**). Partial to complete cataract development was observed in insulin solution and free insulin incorporated in copolymer formulation within 60 – 90 days' post treatment (**Table 10**). However, no sign of cataract development (clear eye lens) was observed in the group treated with OA-g-CSO-zin-insulin complexes containing thermosensitive copolymeric depot-based formulation (**Figure 28B**). This study emphasizes the importance of steady basal insulin levels in maintenance of metabolic balance, normal physiological functions, and thereby prevention of complications in type-1 diabetes.

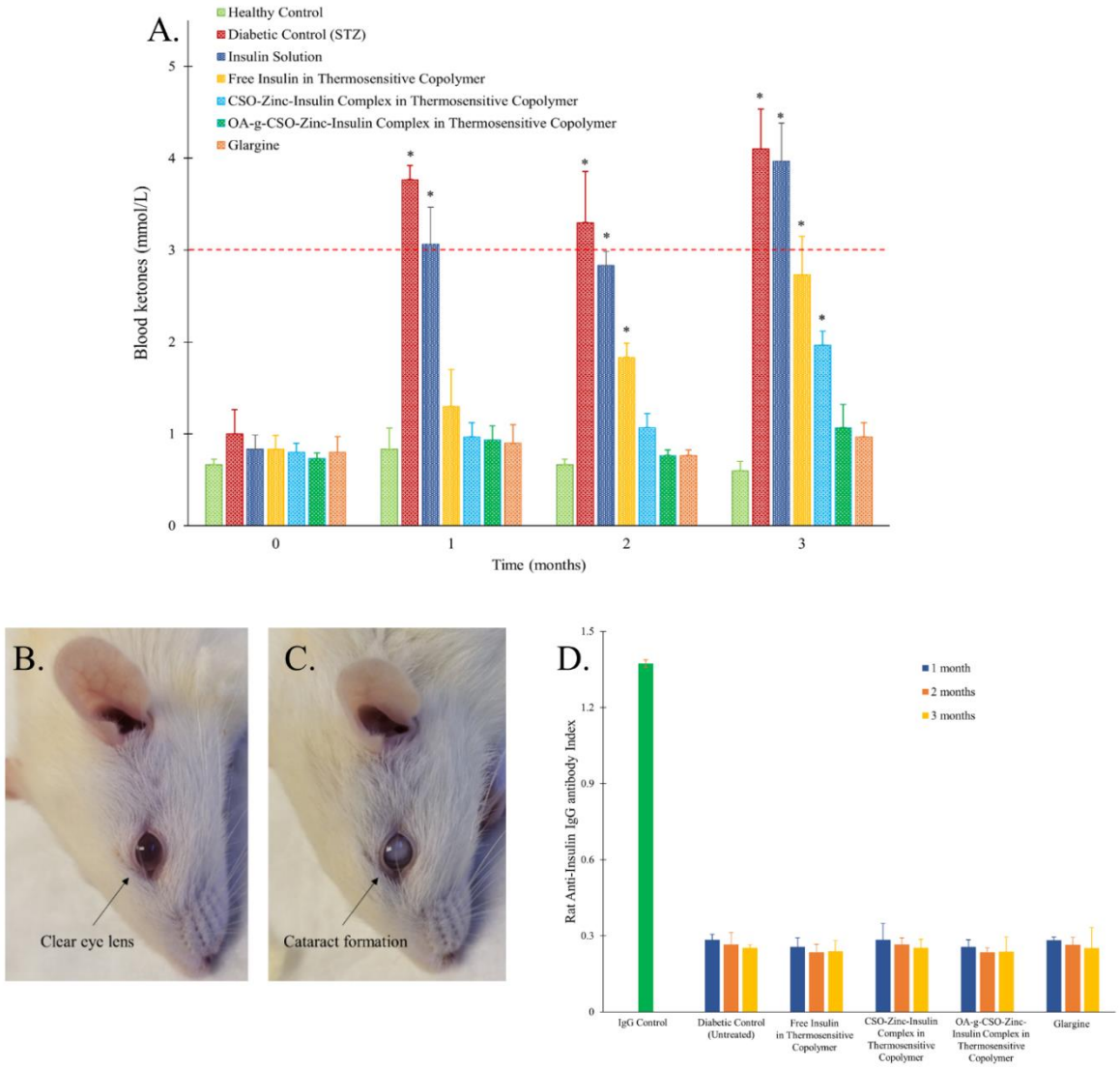

Figure 28. (A) Blood ketone level in rats following STZ and insulin treatment; (B) Clear eye lens following treatment with oleic acid$_{(45\%)}$-grafted-CSO-zinc-insulin complexes in thermosensitive copolymer; (C) Grade 4 cataract in untreated STZ-induced diabetic control; (D) Detection of anti-insulin antibodies following insulin treatment. Key: (●) healthy non-diabetic control; (■) untreated STZ-induced diabetic control; STZ-induced diabetic rats upon treatment with single administration of: (●) insulin solution, dose 0.5 IU/kg; (●) free insulin in thermosensitive copolymer, dose 45 IU/kg; (■) CSO-zinc-insulin complex in thermosensitive copolymer, dose 45 IU/kg; and (▲) oleic acid$_{(45\%)}$-grafted-CSO-zinc-insulin complex in thermosensitive copolymer, dose 45 IU/kg; or (◆) daily administration of glargine (Lantus® U-100), dose 0.5 IU/kg/day. [Data are expressed as mean ± S.D, n = 6; *: significantly higher compared to healthy non-diabetic control; at $p < 0.05$]

Table 10. Summary of cataract formation following STZ and insulin treatment in Sprague Dawley rats.

	CATARACT FORMATION			
	60 days		90 days	
Group	one eye	both eyes	one eye	both eyes
Healthy control	0	0	0	0
Diabetic control (STZ) (untreated)	1	4	-	**6**
Insulin solution	3	2	1	**5**
Free Insulin in copolymeric depot	4	1	2	4
CSO-Zinc-Insulin complex in copolymeric depot	1	0	2	0
Oleic acid-g-CSO-Zinc-Insulin complex in copolymeric depot	0	0	0	0
Glargine	0	0	1	0

3.11. Determination of body weight

Treatment of young adult rats with STZ produces a diabetic state characterized by reduced body weight, polyuria, polydipsia and hyperglycemia.[251] STZ preferentially accumulates in pancreatic beta-cells owing to the presence of glucose moiety in its chemical structure allowing selective uptake *via* the GLUT-2 glucose transporter.[252] STZ then leads to DNA alkylation, fragmentation and damage by supposedly the nitric oxide donor effect of nitrosourea moiety which is cytotoxic thereby destroying beta-cells in pancreas.[253] Sudden weight loss due to diabetes is a common clinical manifestation owing to insufficient insulin production in the body preventing utilization of glucose for cellular energy production. The body then starts burning fat and muscle cells for energy that causes reduction in overall body weight. In all groups treated with STZ, drastic reduction in body weight was observed. However, a gradual recovery in body weight was observed following insulin therapy. Continuous reduction in body weight was observed in untreated (Group II) and insulin solution treated groups (Group III) up to 63 days (**Figure 29**). Thermosensitive copolymer formulation treated groups demonstrated significant increase in body weight compared

to untreated diabetic rats ($P < 0.01$) up to 16 weeks (112 days) post treatment. This can be attributed to the PD manifestation of administered insulin in glucose utilization, maintenance of overall health and energy balance.

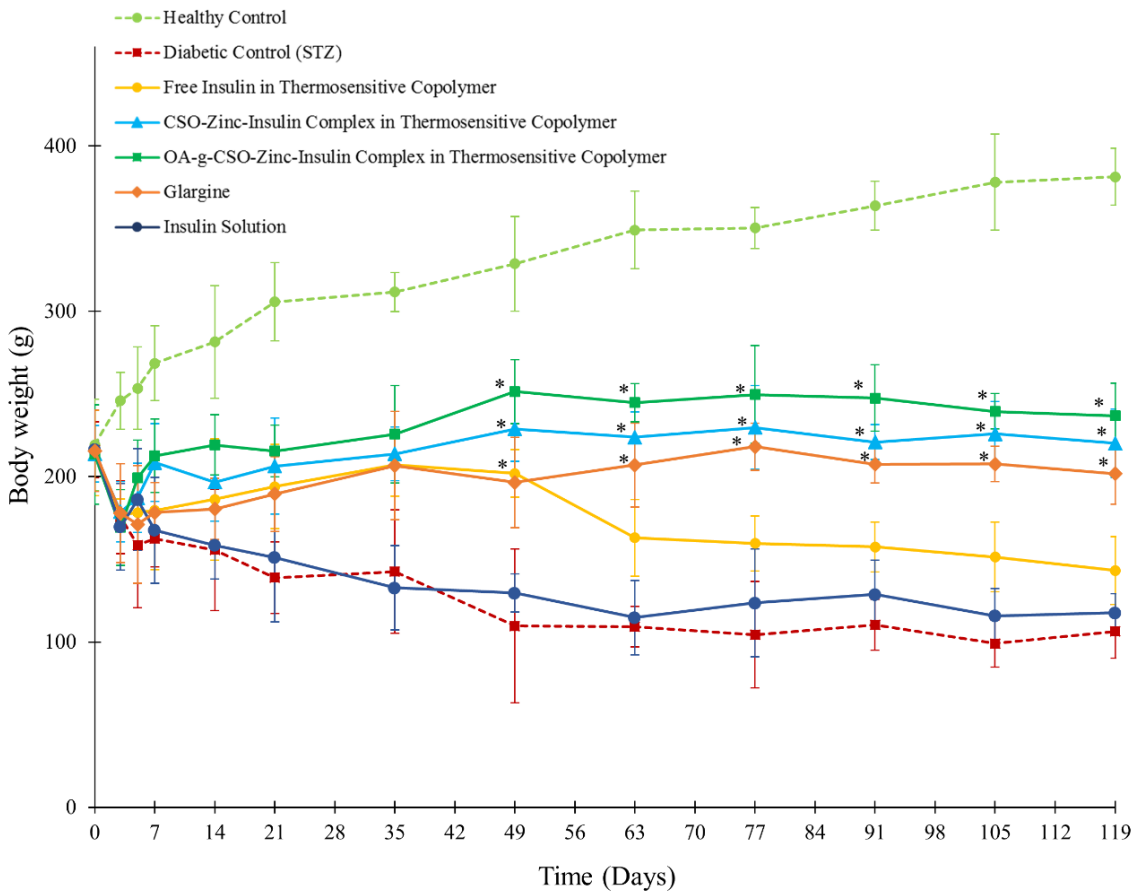

Figure 29. Body weight of rats following STZ and insulin treatment. Key: (●) healthy non-diabetic control; (■) untreated STZ-induced diabetic control; STZ-induced diabetic rats upon treatment with single administration of: (●) insulin solution, dose 0.5 IU/kg; (●) free insulin in thermosensitive copolymer, dose 45 IU/kg; (▲) CSO-zinc-insulin complex in thermosensitive copolymer, dose 45 IU/kg; and (■) oleic acid$_{(45\%)}$-grafted-CSO-zinc-insulin complex in thermosensitive copolymer, dose 45 IU/kg; or (◆) daily administration of glargine (Lantus® U-100), dose 0.5 IU/kg/day. [Data are expressed as mean ± S.D, n = 6; *: significantly higher compared to untreated STZ-induced diabetic control; at $p < 0.01$]

3.12. Detection of anti-insulin antibodies

Several protein-based therapeutics have an associated risk of eliciting undesirable immune response in patients that may often lead to reduction in therapeutic efficacy, serious anaphylaxis reaction, or life-threatening autoimmunity. Exogenous insulin preparations continue to be immunogenic to humans, and origin, storage condition, formulation, excipients, association state, aggregation and degradation products, have been found to be some of the contributing factors to enhanced immunogenicity.[254,255] In this study OA-g-CSO-zinc-insulin complexes were prepared and incorporated in thermosensitive copolymer solution for sustained release of basal level insulin. Hexameric association state of insulin was stabilized by electrostatic complex formation with OA-g-CSO polymer and maintained in the copolymeric micelles, which slowly diffused out through the copolymeric matrix and dissociated to zinc-insulin hexamers, insulin dimers, and ultimately monomeric insulin to be absorbed in the systemic circulation. To estimate immunogenic potential of insulin released from this formulation *in vivo*, presence of anti-insulin antibodies was determined in rat serum samples 1, 2, and 3-months post formulation administration (**Figure 28D**). Indirect sandwich ELISA technique was employed, and rat IgG antibody was used as positive control. No anti-insulin antibody formation was detected in any of the formulation groups initially as well as up to 90 days after formulation administration. The antibody response after insulin treatment was comparable to untreated control group (Group II). Therefore, it can be safely concluded that the thermosensitive copolymer-based formulations optimized in this study did not generate any undesirable immune response and the insulin released was non-immunogenic in nature.

3.13. Synthesis and characterization of oleic acid, mannose and adipose homing peptide grafted chitosan polymer

CS is a naturally derived biocompatible and biodegradable cationic polysaccharide. It is composed of chemically active primary amino and hydroxyl groups that can be modified into desirable derivatives. CS chain length and degree of deacetylation, both are known to contribute significantly to its transfection efficiency. CS chain length (CS 20 kDa) was optimized based on transfection efficiency of CS polymers of different chain lengths using pDNA encoding for enzyme β-galactosidase in *in vitro* inflammatory co-culture model (**Figure 30**). OA was conjugated on CS polymer (CS-OA) *via* carbodiimide-mediated coupling reaction, using ethyl-3-(3-dimethylaminopropyl) carbodiimide hydrochloride (EDC.HCl) and N-hydroxysuccinimide (NHS), forming an amide bond between amino group on CS backbone and carboxyl group of OA.[196] α-D-Mannopyranosylphenyl isothiocyanate (MAN) modified polymer (CS-MAN or CS-OA-MAN) were obtained by subsequent thiourea reaction between CS or CS-OA polymers and MAN *via* the formation of a phenylisothiocyanate bridge. AHP conjugation was performed similarly on CS or CS-OA polymer using EDC/NHS coupling reaction. Unreacted OA, MAN, AHP and coupling agents were completely removed by dialysis against deionized water followed by purification using ethanol. Chemical composition of synthesized polymers was confirmed using ^{1}H NMR and Fourier transform infrared (FT-IR) spectroscopy (**Figure 31 and 32**). Degree of substitution was determined using 2,4,6-trinitrobenzene sulfonic acid assay (TNBSA) for OA and MAN conjugation and bicinchoninic acid (BCA) assay for AHP conjugation and was determined to be ~ 20% for all the ligands (**Table 11)**. Ligand conjugation percentage of 20% was selected based on previous study from our group indicating maximum cell internalization and transfection efficiency at 15 – 20% conjugation.[195] Tight complex formation between CS and pDNA may

hinder its release leading to low transfection efficiency in physiological environment. Ligand conjugation on CS backbone reduces the overall cationic charge on CS backbone, which helps in maintaining a balance between endosomal escape capacity and nucleic acid release. Furthermore, ligand conjugation helps in targeting the therapeutic to selective cells/tissues while aiding cellular internalization by receptor/transporter mediated endocytosis. Fluorescence labelling of polymers was performed by reaction of synthesized polymers with fluorescein isothiocyanate (FITC) and was estimated to be 0.02 moles of dye per mole of glucosamine unit of CS for all the formulations.

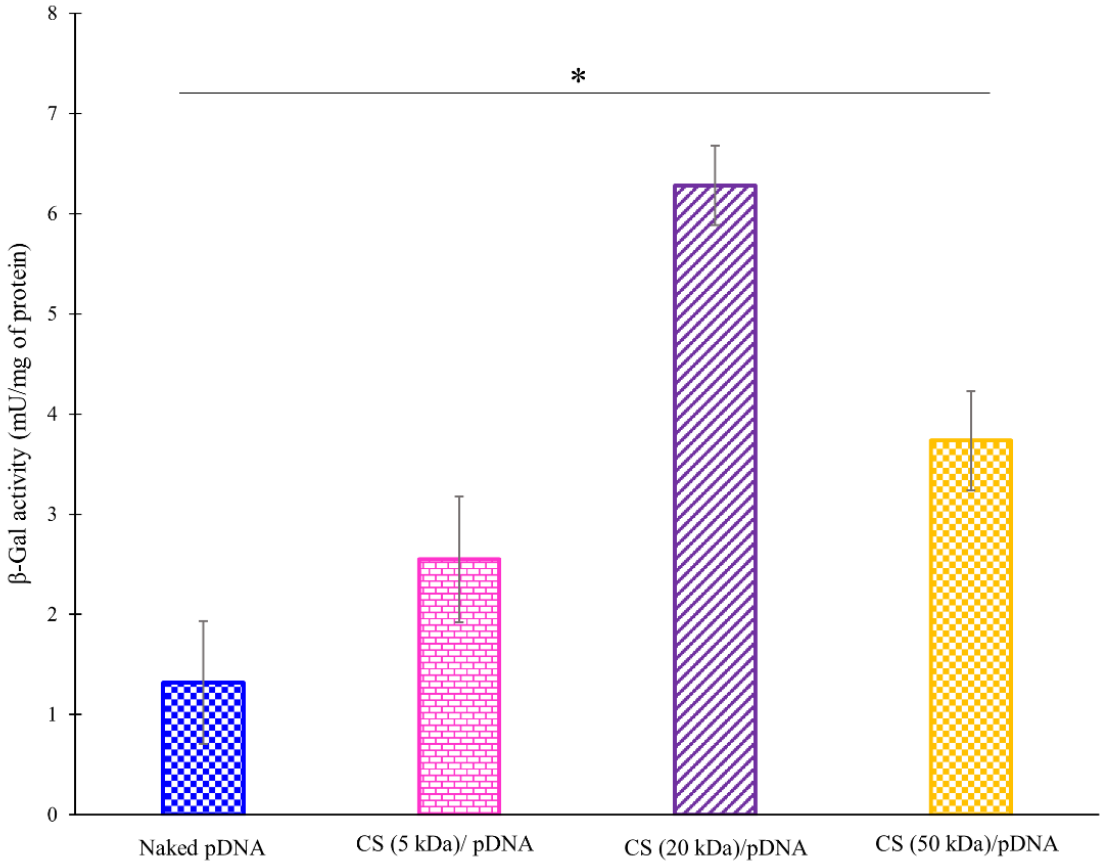

Figure 30. Effect of increasing chain lengths of chitosan on transfection efficiency of pDNA encoding for enzyme β-galactosidase in *in vitro* inflammatory contact co culture model of M1 polarized RAW 264.7 macrophages and differentiated 3T3-L1 adipocytes. [Data are expressed as mean ± S.D, n = 4; *: significantly different at $p < 0.05$]

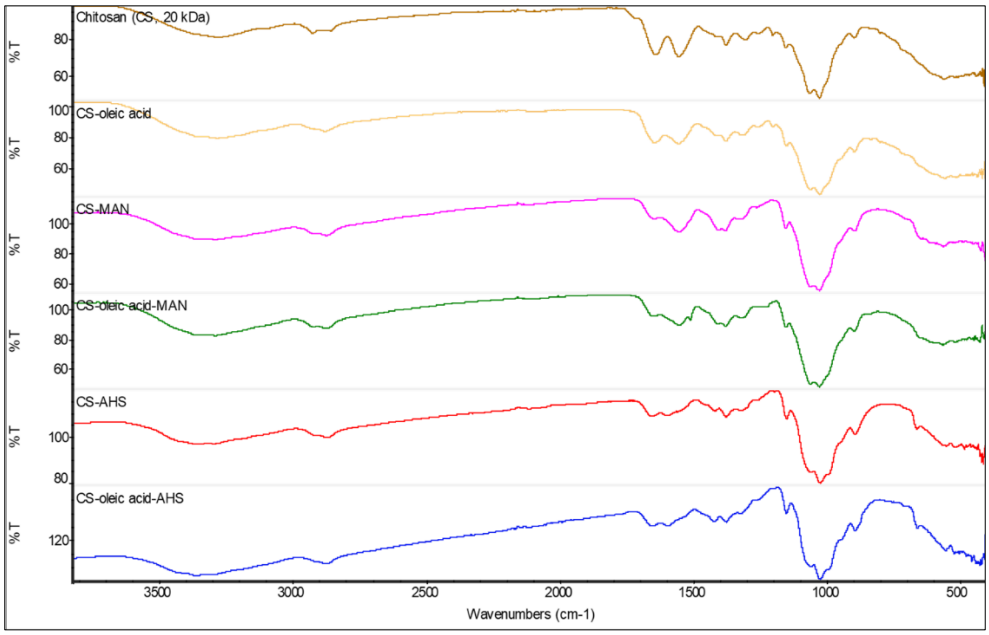

Figure 31. ^{1}H proton nuclear magnetic resonance (^{1}H NMR) spectra of chitosan, and/or oleic acid, α-D-mannopyranosylphenyl isothiocyanate (MAN), and adipose homing peptide (AHP) grafted chitosan polymers.

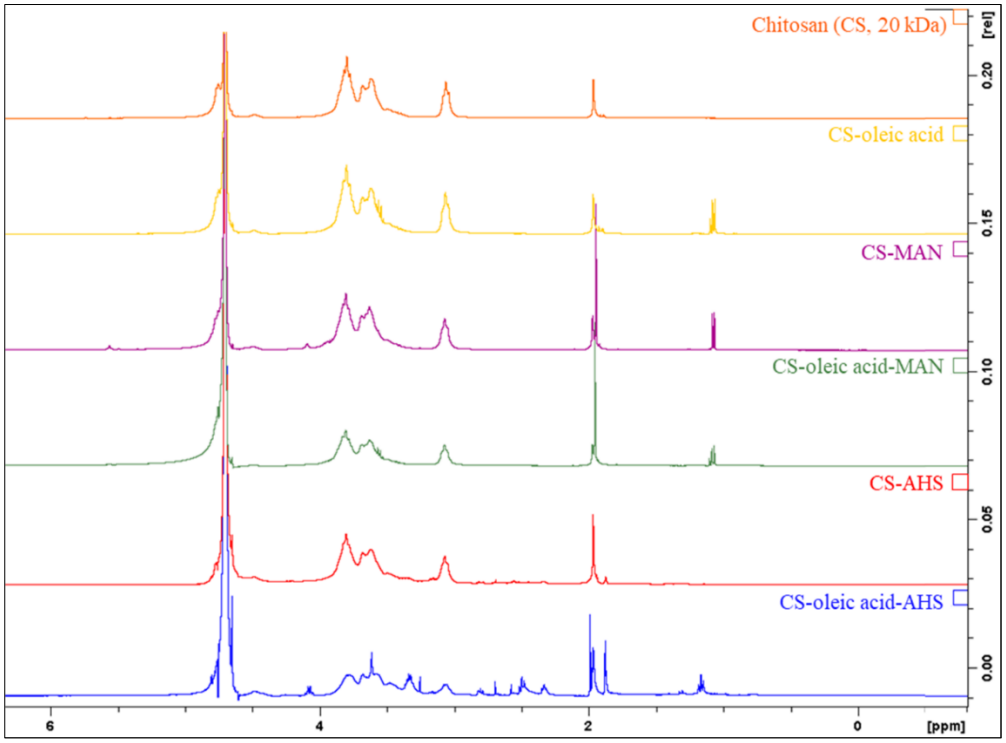

Figure 32. Fourier transform infrared (FT-IR) spectra of chitosan, and/or oleic acid, α-D-mannopyranosylphenyl isothiocyanate (MAN), and adipose homing peptide (AHP) grafted chitosan polymers.

Table 11. Degree of substitution of oleic acid, mannose and adipose homing peptide on chitosan polymer. Data represents mean ± SD, n = 4.

polymer sample	% Substitution
CS-**OA**	19.66 ± 1.25
CS-**MAN**	18.25 ± 3.16
CS-**AHP**	19.01 ± 2.83
CS-OA-**MAN**	17.89 ± 2.01
CS-OA-**AHP**	18.94 ± 1.87

3.14. Preparation and characterization of chitosan nanomicelles and pDNA polyplexes

OA conjugation onto CS polymer makes the CS-OA polymer amphiphilic and capable of forming nanomicelles above their critical micelle concentration (CMC). CMC of ligand-conjugated CS polymers was determined using pyrene as a hydrophobic probe. Fluorescence spectra of pyrene shows a sharp change as it is internalized into the hydrophobic core of micelles during micelle formation indicating the CMC. The CMC of CS-OA, CS-OA-MA, and CS-OA-AHP polymers was determined to be 62.7 ± 2.5, 88.3 ± 2.9 and 52.5 ± 3.5 µg/mL, respectively. Furthermore, particle size and their net surface charge are important determinants to cellular internalization and gene transfection. Presence of positively charged amino groups on CS polymer at physiological pH allows for electrostatic binding with negatively charged pDNA forming CS-pDNA polyplexes. Size and zeta potential of polyplexes prepared in this study is summarized in **table 12**. Overall, the particle size of the nanoparticles was lower than 200 nm, with positive net surface charge. Cationic nanoparticles with size < 200 nm show superior cell uptake *via* adsorption-mediated endocytosis owing to their interaction with negatively charged cell membrane.[86,139]

Table 12. Nanomicelle size and zeta potential determined using Malvern Zetasizer. Data represents mean ± SD, n = 4.

polymer sample	average hydrodynamic size (nm)	polydispersity index (PDI)	zeta potential (mV)
Chitosan (CS) (20kDa)	140.86 ± 7.41	0.29 ± 0.08	27.08 ± 1.46
CS-OA	166.53 ± 10.66	0.17 ± 0.05	20.7 ± 0.52
CS-MAN	138.56 ± 6.69	0.25 ± 0.03	16.5 ± 2.86
CS-AHP	164.60 ± 7.82	0.27 ± 0.06	17.23 ± 1.76
CS-OA-MAN	172.93 ± 5.03	0.18 ± 0.09	15.07 ± 1.51
CS-OA-AHP	173.15 ± 8.54	0.19 ± 0.06	19.27 ± 1.46

3.15. Determination of pDNA condensation, protection from nucleases and endosomal buffering capacity

Condensation of pDNA is essential for its encapsulation in the delivery system as well as to protect the nucleic matter from degradation.[256,257] Cationic polymers like CS form electrostatic complex with nucleic acids driving an orderly condensed state owing to reduced DNA-solvent interactions and overall improved stability of the DNA molecule in *in vitro* and *in vivo* environments.[256] Additionally, it protects the pDNA from nuclease degradation and reduces the volume occupied by the DNA molecule allowing effective translocation of nanoscale complexes through cellular openings. Nanomicelle polyplexes prepared in this study effectively condensed pDNA molecule as demonstrated by particle size range of 139 – 174 nm (**Table 12**). Efficiency of pDNA condensation by CS polymers was also investigated using agarose gel electrophoresis (**Figure 33a**). All CS polymer and pDNA formulations were prepared at polymer/pDNA (N/P) ratio of 20 which was successful in effectively condensing the pDNA molecule.[139] Furthermore, association efficiency of synthesized CS polymers and pDNA used in this study was found to be

around 96% and 97% for plasmid encoding for shRNA against TNFα (shTNFα) and plasmid encoding for shRNA against MCP-1 (shMCP1), respectively (**Figure 33b**).

Additionally, we investigated the ability of CS polymeric nanomicelles to protect the condensed pDNA from endonuclease degradation. Nuclease degradation is a major hindrance to activity and efficacy of the pDNA molecule. As shown in **figure 33d** naked pDNA when incubated with nucleases, shows absence of band after gel electrophoresis owing to complete digestion of pDNA by DNase I. On the other hand, complexation with CS polymeric nanomicelles efficiently condensed and protected the pDNA upon incubation with DNase I for 60 min, and following dissociation showed strong bands for stable nucleic acid as compared to control pDNA without incubation with nucleases. Quantitative evaluation of pDNA digestion over time upon incubation with DNase I also showed significant increase in absorbance of free pDNA owing to hyperchromic effect of DNA denaturation (**Figure 33e**).[258] The increase in absorbance was negligible in the CS/pDNA complex groups due to effective protection of pDNA molecule by CS polymeric nanomicelles.

Furthermore, effective gene delivery system requires preventing the nucleic acid from being trapped in the endosomes and degradation by lysosomal enzymes.[258] "Proton sponge action" of CS effectively facilitates endosomal escape of the pDNA owing to the buffering capability of its free amino groups.[196] The buffering action of CS polymers was determined by acid-base titration. As shown in **figure 33c**, all polymers show good buffering ability in the endosomal pH range 5 to 7. This characteristic of CS-based polymers is appreciable as it would help in osmotic swelling and disruption of the endocytic vesicles delivering pDNA into the cytosol, and preventing the nucleic cargo from lysosomal digestion.

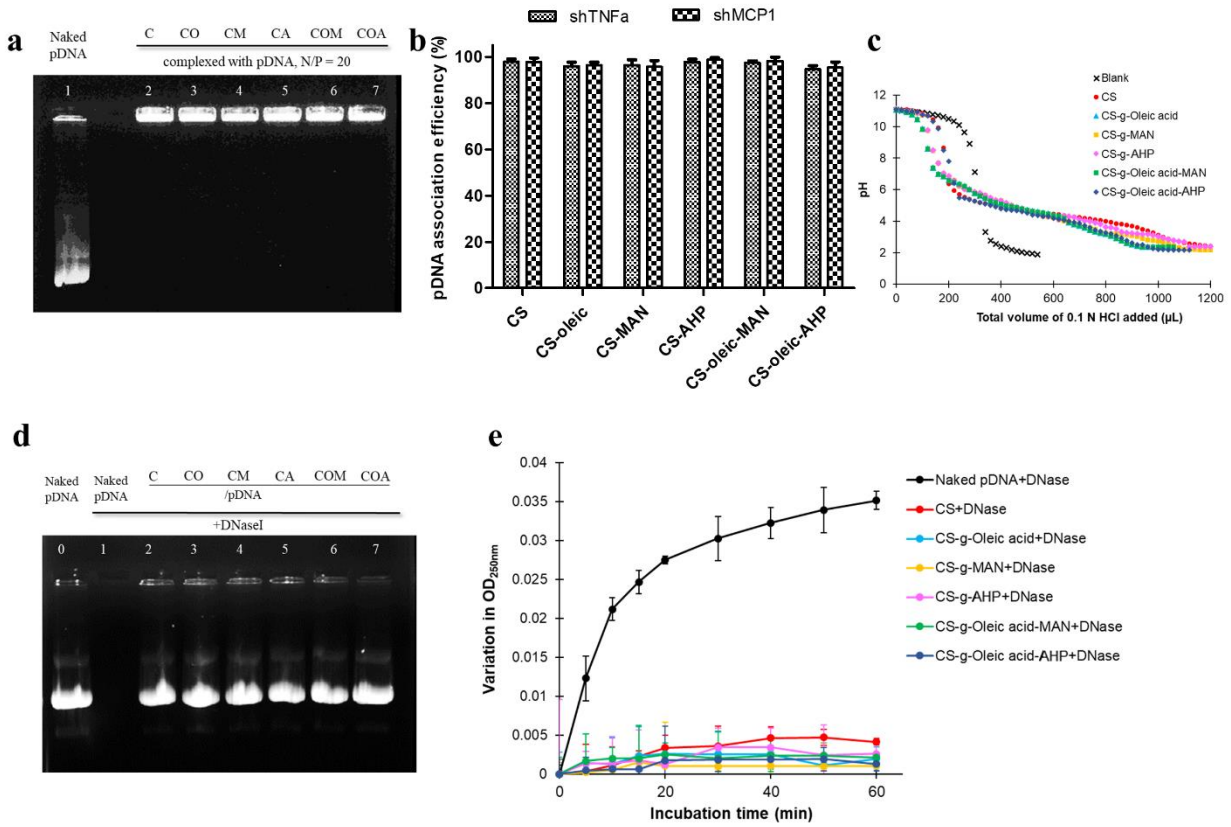

Figure 33. Characterization of chitosan-based nanomicelles and pDNA polyplexes. (a) Agarose gel retardation assay depicting condensation ability; (b) Association efficiency of pDNA encoding for shRNA against TNFα or MCP-1 (shTNFα or shMCP1); (c) Endosomal buffering capacity; (d) Protection of pDNA from nuclease degradation; and (e) Quantitative estimation of nuclease degradation of pDNA measured by variation in OD_{250nm}. [Key: Chitosan modified with: oleic acid (CO), mannose (CM), adipose homing peptide (CA), both oleic acid and mannose (COM), and both oleic acid and adipose homing peptide (COA); Data represents mean ± SD, n = 4.]

3.16. Preparation of *in vitro* cell culture model

Obesity changes the adipose tissue environment and leads to an increased release of pro-inflammatory cytokines and adipokines. As mentioned earlier, release of MCP-1 contributes to macrophage infiltration into the adipose tissue which in the inflammatory environment undergo polarization transition from an anti-inflammatory M2 phenotype to a pro-inflammatory M1 phenotype.[259] To mimic adipose tissue macrophages in obese-diabetic pathophysiology, RAW264.7 macrophages were activated with lipopolysaccharides (LPS) to induce polarization transition to M1 pro-inflammatory phenotype. Initially, cultured RAW 264.7 macrophages

appeared roundish with smaller cytoplasmic processes. Upon M1 polarization, the cells obtained amoeboid morphology with increased cell size and longer cytoplasmic extensions (**Figure 34a**).[260] M1 polarization was also confirmed by significantly increased levels of pro-inflammatory cytokines TNF-α, IL-1β, and IL-6, 24 h post LPS-induction (**Figure 35**).[261]

Furthermore, murine 3T3-L1 preadipocyte cell line was differentiated *in vitro* from fibroblast cell phenotype to mature adipocytes. Obesity and its associated metabolic syndrome occurs partially due to overabundance of fat cells. Fat cells in humans are of two main types: brown adipose tissue (BAT) and white adipose tissue (WAT). BAT is mainly responsible for thermoregulation *via* mitochondrial lipid oxidation. WAT is the predominant type in mammals which plays a major role in regulating metabolic functions. WAT serves as storage for lipids, as an endocrine organ for secreting essential adipokines, and for insulin-dependent disposal of glucose in the body.[262] Adipocyte cell culture was prepared by sequential induction of 3T3-L1 preadipocytes with differentiation promoting cues like glucocorticoids, 3-isobutyl-1-methylxanthine (IBMX) and insulin at specific concentrations.[263] First, preadipocytes are cultured to a growth arrest stage, followed by a combination-hormonal induction using insulin, dexamethasone, and IBMX for 48 h. Dexamethasone mediated stimulation of both glucocorticoid and mineralocorticoid receptors induces adipogenesis in a concentration-dependent manner. IBMX promotes adipogenesis in combination with glucocorticoids by nonselective, competitive inhibition of phosphodiesterase leading to increased cAMP and protein kinase A (PKA). PKA signaling promotes adipogenesis by transcriptional activation of PPARγ, thereby promoting adipogenic gene expression.[264] Insulin is an essential adipogenic hormone that promotes induction of several transcription factors essential in triggering adipocyte differentiation.[265] After 48 h, insulin alone is required to carry out the differentiation process. During the differentiation process,

3T3-L1 cells increase the synthesis of triglycerides which accumulate as lipid droplets embedded in the cytoplasm. Oil red staining of lipid deposits was performed to confirm differentiation (**Figure 34b**).

As mentioned earlier, in obesity there is infiltration and accumulation of macrophages in the adipose tissue. It has been estimated that the percentage of macrophages in obese adipose tissue is ~ 40%.[205] Therefore, an *in vitro* inflammatory cell culture model was prepared using a contact co-culture of 40% M1 polarized macrophages infiltrating differentiated mature adipocytes to mimic obese adipose tissue environment (**Figure 34c**).

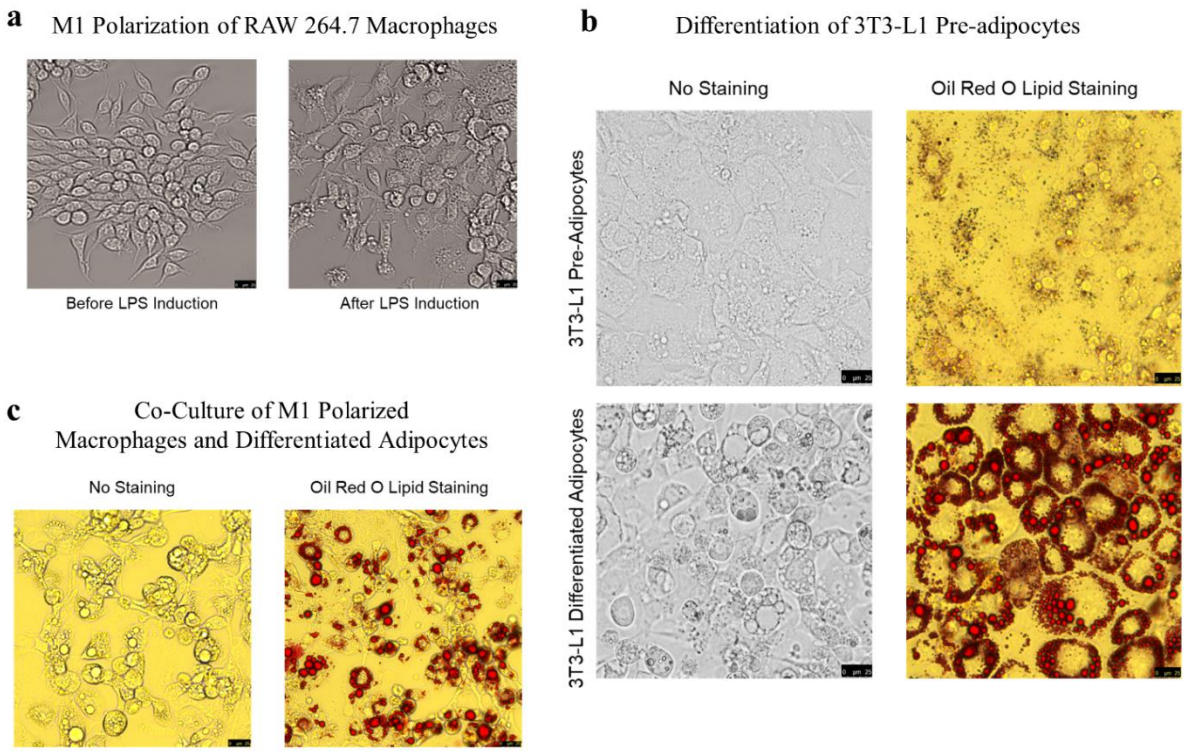

Figure 34. Preparation of *in vitro* cell culture models. (a) LPS-induced M1 polarization of RAW264.7 macrophages; (b) Differentiation of 3T3-L1 pre-adipocytes; (c) Co-culture of M1 polarized macrophages and differentiated adipocytes.

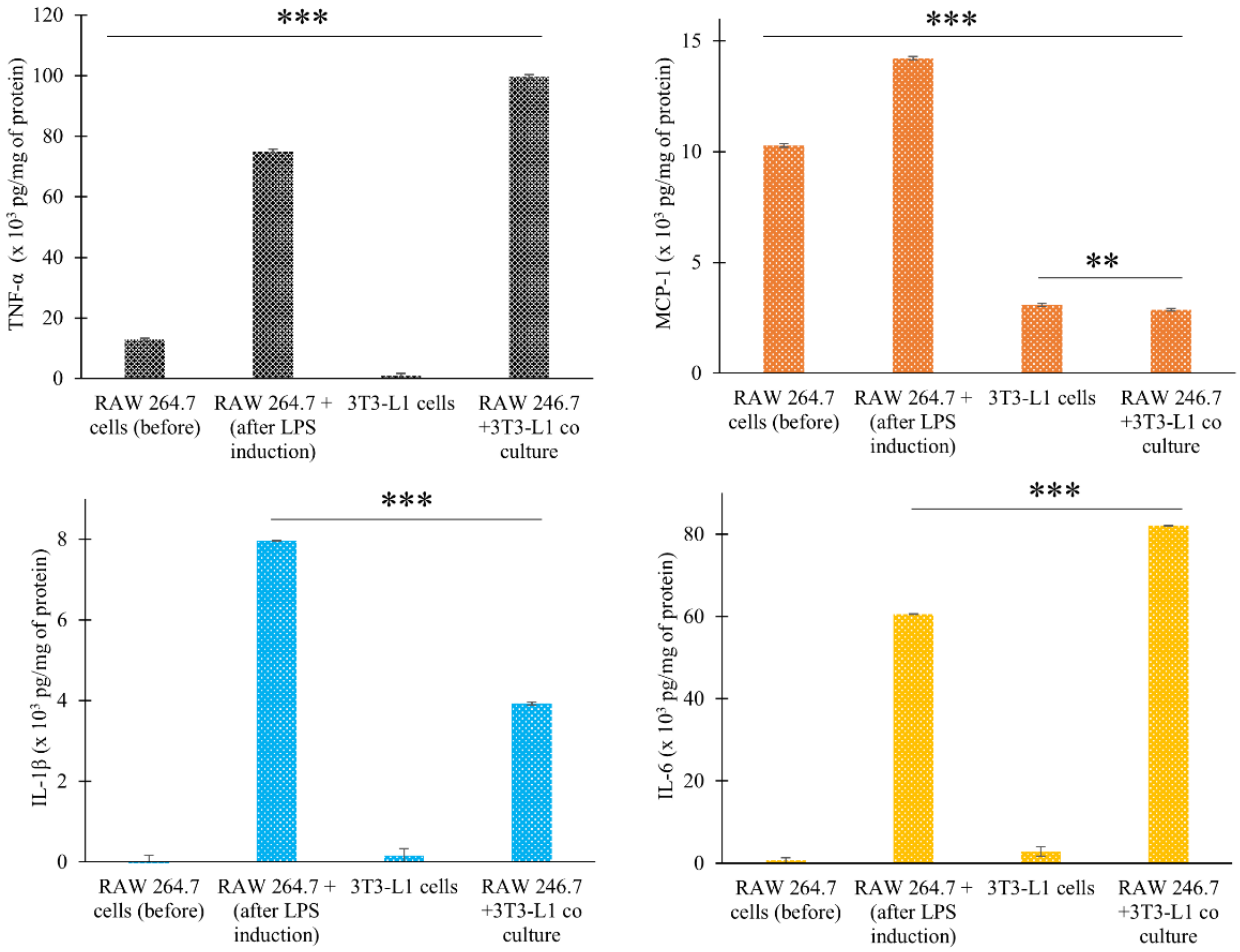

Figure 35. Quantitative estimation of cytokine levels in different *in vitro* cell culture models. [Data represents mean ± SD, n = 4. "**" and "***" depict significant difference at $p < 0.01$ and $p < 0.001$, respectively.]

3.17. *In vitro* cytocompatibility

Cationic polymeric delivery systems are known to be cytotoxic in nature which substantially limits their safety and applicability for *in vivo* gene transfection. Cyto-compatibility of CS-based polymers synthesized in this study was evaluated in M1 polarized macrophages, differentiated adipocytes and the *in vitro* inflammatory contact co-culture model. All formulations were found to be compatible in polymer concentration ranging from 0.1 to 1 mg/mL in all three cell culture models. Cell viability was found to be ≥ 85% relative to untreated control (**Figure 36a-**

c). Conjugation of fatty acid and other ligands reduces the overall cationic charge on CS polymeric micelles (**Table 11**). Moreover, CS aids cellular functions such as proliferation, attachment, and wound healing making it a safe and versatile delivery system with negligible cell toxicity.[197]

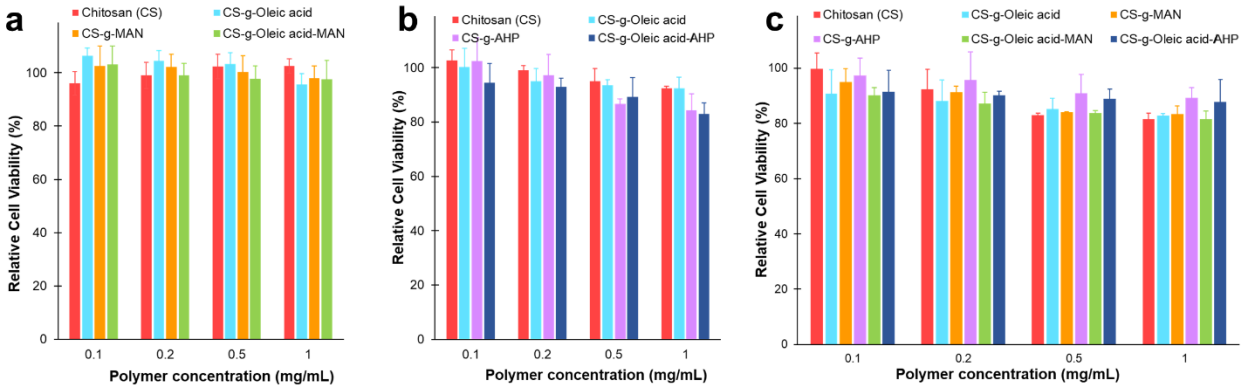

Figure 36. *In vitro* cyto-compatibility analysis of chitosan-based nanomicelles using MTT assay at increasing polymeric concentration analyzed in (a) M1 polarized RAW264.7 cells; (b) Differentiated adipocytes; and (c) *In vitro* inflammatory co-culture model; [Data represents mean ± SD, n = 4]

3.18. Cellular uptake and its mechanism

Efficiently delivering nucleic acid cargo inside the cell is a critical factor for allowing gene transfection. Cellular uptake can be mediated through several pathways and physiochemical characteristics of the delivery system play an essential role in uptake modulation. Parameters like particle size, charge, surface, and conjugation of cell-specific ligands can be manipulated to obtain desired cellular uptake characteristics. Effect of OA and MAN modification on cellular uptake of CS/pDNA FITC-labelled nanomicelles was investigated in M1 polarized RAW 264.7 macrophages. Quantitative estimation showed significantly higher uptake of nanomicelles modified with both OA and MAN compared to single modified and unmodified CS nanomicelles (**Figure 37a**). Fluorescence imaging of the cells following 2 h of incubation showed higher number of FITC-positive cells in the ligand-modified group (OA, MAN, and OA-MAN) compared to CS

nanomicelles without any surface modification (**Figure 37d**). OA modification on CS polymer helps increase interaction with cell membrane and increases cellular uptake efficiency. MAN conjugated nanomicelles were prepared to increase interaction with GLUT-1 transporter present on M1 polarized macrophages to enhance uptake by transporter-mediated endocytosis. Since, physiologically present sugars glucose and mannose are also a substrate for GLUT-1, competitive effect of physiological non-diabetic and diabetic levels of glucose and mannose on cellular uptake of OA and MAN modified nanomicelles was also determined. Nanomicelles containing just mannose as the targeting ligand showed significantly lower uptake at diabetic concentration of glucose and mannose, which was not observed with dual modified nanomicelles containing both OA and mannose (**Figure 38**). This suggests that the nanomicelles are targeting glucose transporters for uptake and that the competition with physiological sugars is somewhat overcome by using dual modification on the nanomicelles.

Similarly, cellular uptake was determined in differentiated adipocytes using OA and AHP modified FITC-labelled nanomicelles. Significantly higher uptake of dual modified (COA) nanomicelles was obtained compared to single modified and unmodified CS polymeric nanomicelles (**Figure 37b**). Fluorescence images also showed higher fluorescence of FITC in the dual modified group, followed by single modified and unmodified CS polymeric nanomicelles (**Figure 37e**). Furthermore, uptake in the *in vitro* inflammatory contact co-culture model was tested using all formulations modified with FITC as a fluorescent probe in diabetic concentration of glucose and mannose. Nanomicelles modified with OA and MAN or AHP were found to have a significantly higher uptake compared to single-modified and unmodified nanomicelles (**Figure 37c**). This can be attributed to additional contribution of GLUT-1 transporter-mediated and prohibitin receptor-mediated endocytosis of MAN and AHP modified nanomicelles, respectively.

Fluorescence images also showed much higher fluorescence of FITC in the dual modified group compared to other formulations (**Figure 37f**).

Since endocytosis is the most common mechanism of uptake of CS-polymeric nanomicelles, M1 polarized macrophages and differentiated adipocytes cells were incubated with sodium azide (10 mM) or at 4 °C to inhibit all energy-dependent endocytosis, amiloride (50 µg/mL) to prevent micropinocytosis, colchicine (100 µg/mL) to inhibit claveolae formation, and chlorpromazine (10 µg/mL) to prevent formation of clathrin vesicles. As depicted in **figure 39a-b**, pre-treatment at 4 °C resulted in significant reduction in cellular uptake ($p< 0.001$) in both M1 polarized macrophages and differentiated adipocytes. Decrease in cellular uptake following sodium azide treatment suggests that energy-dependent mechanisms contribute to 50 – 80% cellular internalization while the remaining uptake process could be due to passive diffusion or physical adsorption of the nanomicelles.[266] Chlorpromazine pre-treatment reduced the uptake of CS-MAN polyplexes by 70% and CS-OA polyplexes by 48%, compared to cells without any pre-treatment indicating clathrin-mediated endocytosis process in their internalization (**Figure 39a)**. Amiloride pre-treatment which prevents macropinocytosis by selectively inhibiting Na^+/H^+ exchange, and colchicine pre-treatment which is known to inhibit caveolae-mediated endocytosis were found to inhibit the uptake of CS-MAN nanomicelles by 65% and 62%, respectively. These studies suggest clathrin-mediated uptake as a major mechanism of internalization of CS-OA and CS-MAN nanomicelles in M1 polarized macrophages followed by macropinocytosis and caveolae-mediated (minor pathway) endocytosis mechanisms. However, as determined in differentiated adipocytes the internalization CS-AHP nanomicelles was most significantly reduced by 42.5% by colchicine pre-treatment, followed by 24% reduction due to chlorpromazine pre-treatment, indicating caveolae and clathrin-mediated endocytosis as major pathways of

internalization, respectively (**Figure 39b)**. Pre-treatment with amiloride did not significantly affect ($p > 0.05$) uptake of CS-AHP nanomicelles in differentiated adipocytes suggesting negligible association of macropinocytosis in cellular internalization of these nanomicelles. Overall, mechanism of uptake evaluation of CS/pDNA polyplexes suggest that the uptake is mediated *via* more than one endocytotic internalization pathways, which may be useful in achieving high efficiency of nucleic acid delivery *in vivo* and overcoming challenges associated with delivery of naked pDNA.

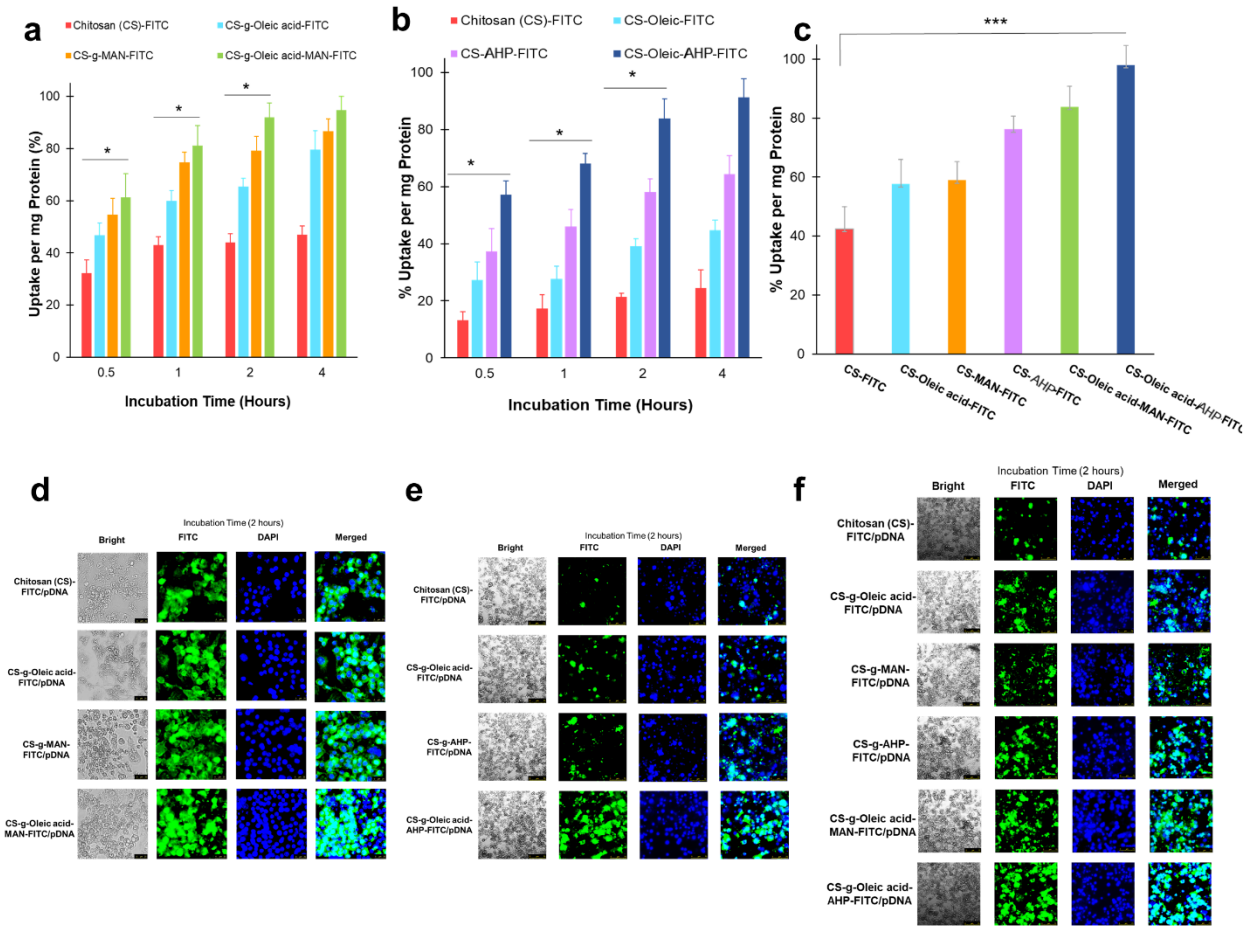

Figure 37. Quantitative and qualitative determination of cellular uptake of FITC labelled CS polymer/pDNA polyplexes analyzed in (a, d) M1 polarized RAW264.7 cells; (b, e) Differentiated 3T3-L1 adipocytes; (c, f) *In vitro* inflammatory co-culture model. [Data represents mean ± SD, n = 4; "*" and "***" depict significant difference at $p < 0.05$ and $p < 0.001$, respectively.]

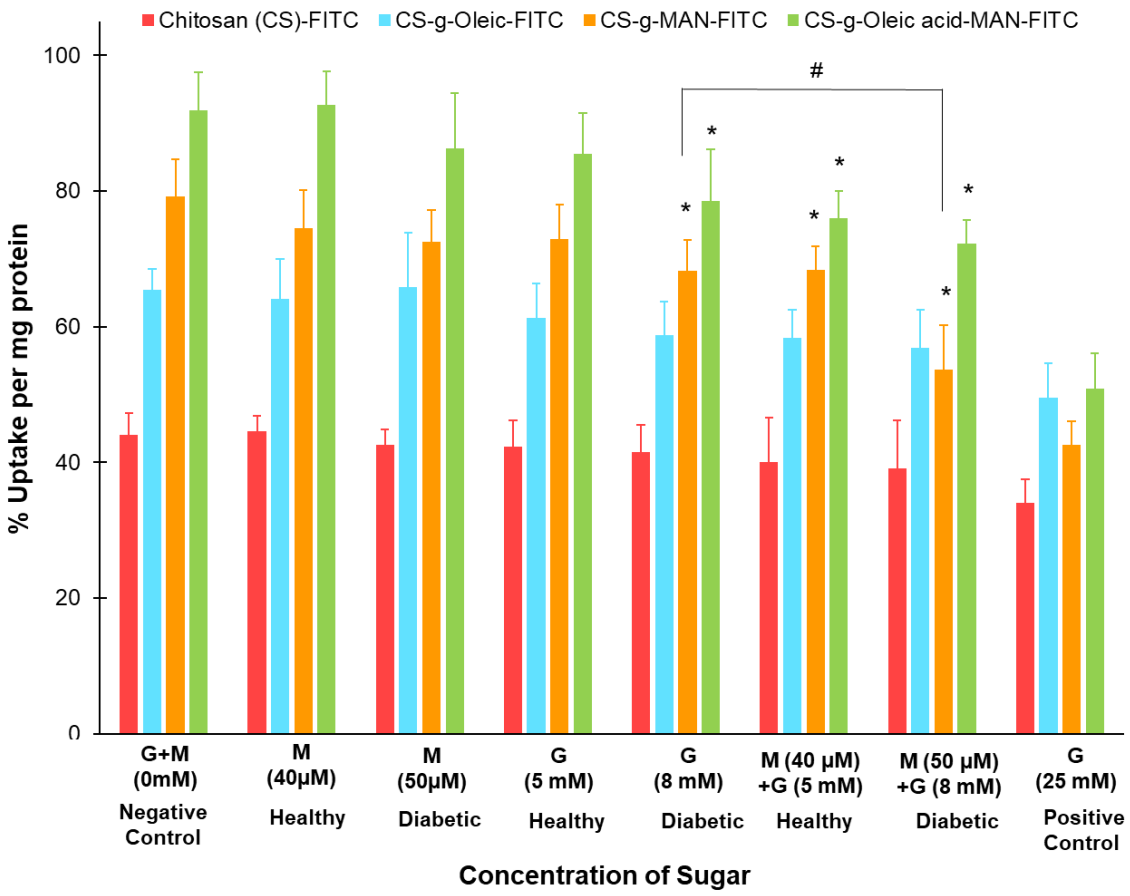

Figure 38. Competition assay of mannose conjugated nanomicelles with healthy and diabetic physiological concentration of glucose and mannose in M1 polarized RAW264.7 macrophages [Data represents mean ± SD, n = 4; "*" depicts significant difference from control at $p < 0.05$; "#" indicates significant difference at $p < 0.05$.]

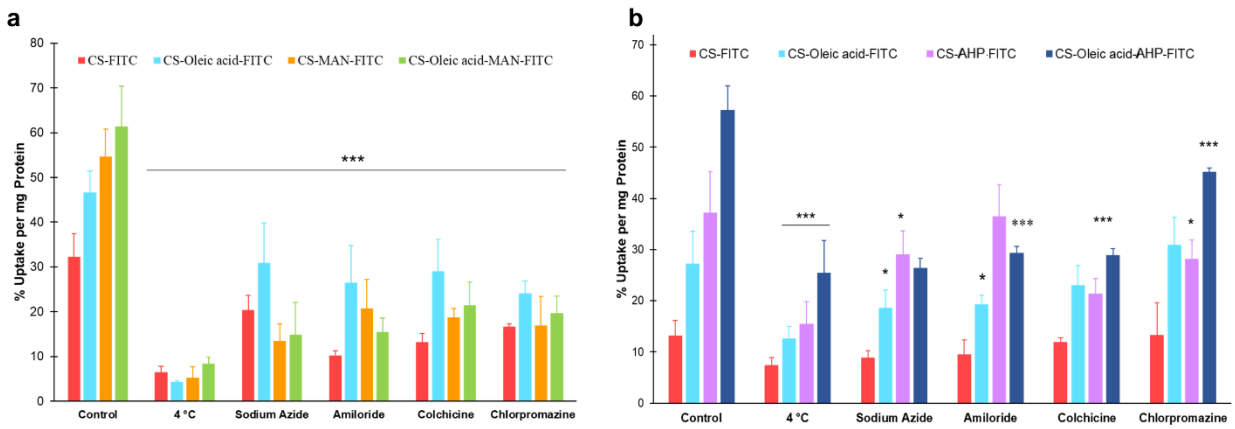

Figure 39. Determination of *in vitro* cellular uptake mechanism of FITC-labelled chitosan-based nanomicelles. Endocytic uptake pathway following 30 min pre-incubation with sodium azide (10 mM), at 4 °C, amiloride (50 µg/mL), colchicine (100 µg/mL), or chlorpromazine (10 µg/mL) in (a) M1 polarized RAW264.7 macrophages and (b) differentiated 3T3-L1 adipocytes. [Data represents mean ± SD, n = 4; "*", "**" "***" depict significant difference from control at $p < 0.05$, 0.01, and 0.001, respectively.]

3.19. *In vitro* gene transfection

Major limitation of non-viral gene delivery vectors is low gene transfection ability. However, since gene transfection is a critical aspect of developing a vector, we assessed if OA, MAN and AHP conjugation improved the gene transfection efficiency of CS-based polymeric nanomicelles. Two model pDNA were employed, encoding for enzyme β-galactosidase (pβgal) and green fluorescent protein (pGFP), to investigate gene transfection at protein and cellular level in M1 polarized macrophages, differentiated adipocytes, and *in vitro* inflammatory co-culture model. All experiments were performed in medium containing diabetic concentration of glucose (8 mM) and mannose (50 µM). CS-g-MAN and CS-OA-MAN polyplexes showed 2.4 and 3.3-fold higher β-galactosidase enzyme activity compared to naked pDNA (**Figure 40a**). Dual modified CS-OA-MAN polyplexes showed significantly higher ($p < 0.001$) transfection efficiency of β-galactosidase enzyme compared to marketed transfection reagent FuGENE® HD. On the other hand, conjugation to OA and AHP using CS-AHP and CS-OA-AHP polyplexes enhanced β-galactosidase enzyme activity by 3.5 and 6.6-fold, respectively, compared to naked pDNA in

differentiated 3T3-L1 adipocytes (**Figure 40b**). Both dual modified nanomicelles CS-OA-MAN (COM) and CS-OA-AHP (COA) showed significantly higher ($p < 0.001$) transfection efficiency of β-galactosidase enzyme compared to naked pDNA and marketed transfection reagent FuGENE® HD (**Figure 40c**).

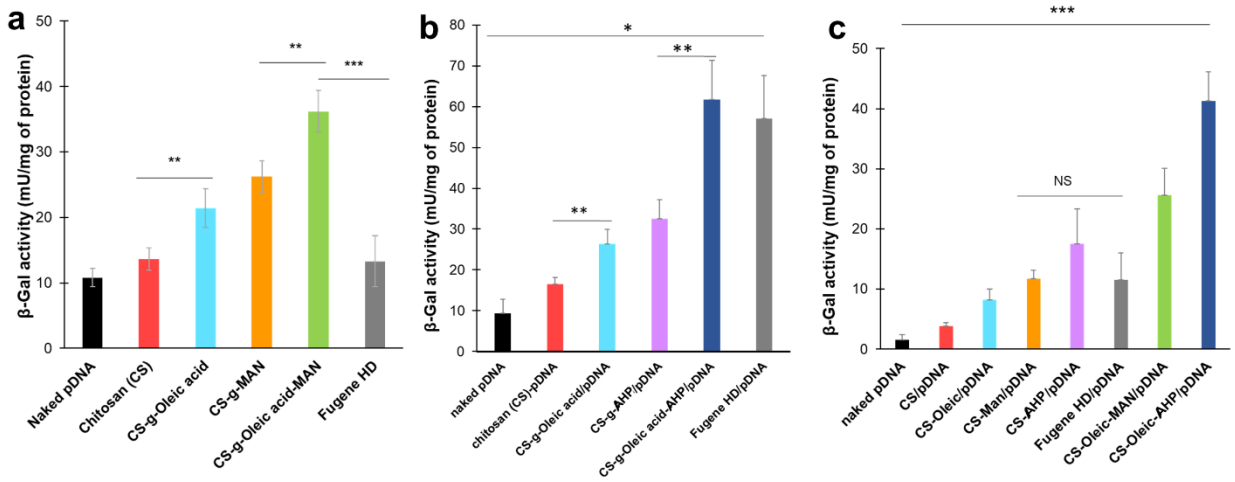

Figure 40. Determination of *in vitro* transfection efficiency of chitosan-based nanomicelles/pDNA polyplexes using model plasmid encoding for enzyme β-galactosidase. [Cell culture models: (a) M1 polarized RAW264.7 cells; (b) Differentiated adipocytes; (c) *In vitro* inflammatory co-culture model; Data represents mean ± SD, n = 4; "*", "**" "***" depict significant difference from control at $p < 0.05$, 0.01, and 0.001, respectively.]

Similar observations were noted with model pDNA for GFP. OA and MAN dual modified CS polyplexes exhibited significantly higher ($p < 0.001$) transfection efficiency with 41.1% GFP positive cells, compared to naked pDNA (2.8%) and FuGENE® HD/pDNA (8.9%) (**Figure 41a**). Fluorescence microscope examination also showed much higher fluorescence of GFP in the single modified and dual modified CS nanomicelles compared to naked pDNA, unmodified CS/pDNA nanomicelles and FuGENE® HD/pDNA (**Figure 41b**).

In vitro transfection analysis in differentiated adipocytes also showed improved transfection efficacy of pGFP using CS modified with OA (32.3%) and AHP (36.7%) (**Figure 42a**). Dual modified CS nanomicelles (CS-OA-AHP) showed significantly higher ($p < 0.001$)

percentage of GFP positive cells (58.1%) compared to free pGFP. Fluorescence imaging also showed higher fluorescence owing to transfected GFP using CS modified with OA and AHP (**Figure 42b**). GFP expression in *in vitro* inflammatory co-culture model showed significantly higher ($p < 0.001$) expression of GFP protein when transfected using COM and COA nanomicelles compared to naked pGFP and FuGENE® HD/pGFP (**Figure 43a,b**). Percentage of GFP positive cells using COM/pGFP were determined to be 8.5 and 1.8-fold higher than naked pGFP and FuGENE® HD/pGFP, respectively. GFP positive cells using COA/pGFP were found to be 10 and 2-fold higher than naked pGFP and FuGENE® HD/pGFP, respectively.

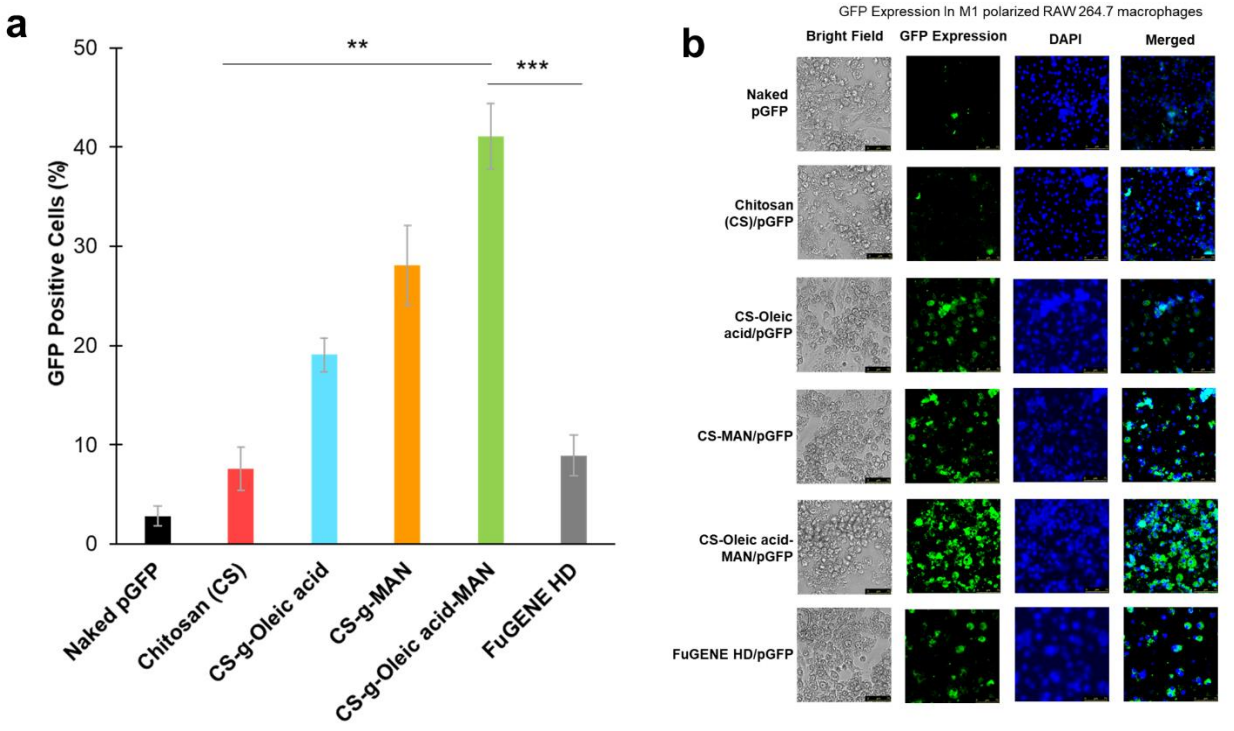

Figure 41. Determination of *in vitro* transfection efficiency of chitosan-based nanomicelles/pDNA polyplexes using model plasmid encoding green fluorescent protein (GFP) in M1 polarized RAW264.7 cells. (a) Quantitative estimation of percentage GFP transfected cells, (b) Qualitative fluorescence images of GFP transfected cells. [Data represents mean ± SD, n = 4; "*", "**" "***" depict significant difference from control at $p < 0.05$, 0.01, and 0.001, respectively.]

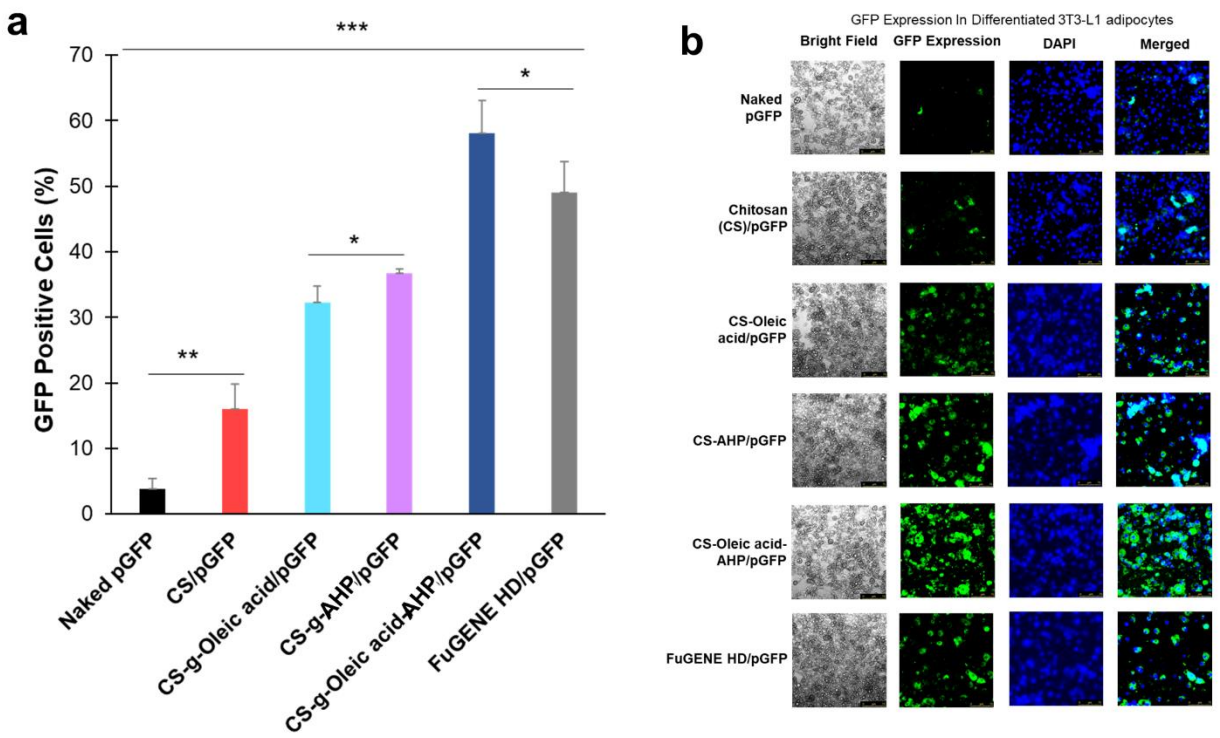

Figure 42. Determination of *in vitro* transfection efficiency of chitosan-based nanomicelles/pDNA polyplexes using model plasmid encoding green fluorescent protein (GFP) in differentiated 3T3-L1 adipocytes. (a) Quantitative estimation of percentage GFP transfected cells, (b) Qualitative fluorescence images of GFP transfected cells. [Data represents mean ± SD, n = 4; "*", "**" "***" depict significant difference from control at $p < 0.05$, 0.01, and 0.001, respectively.]

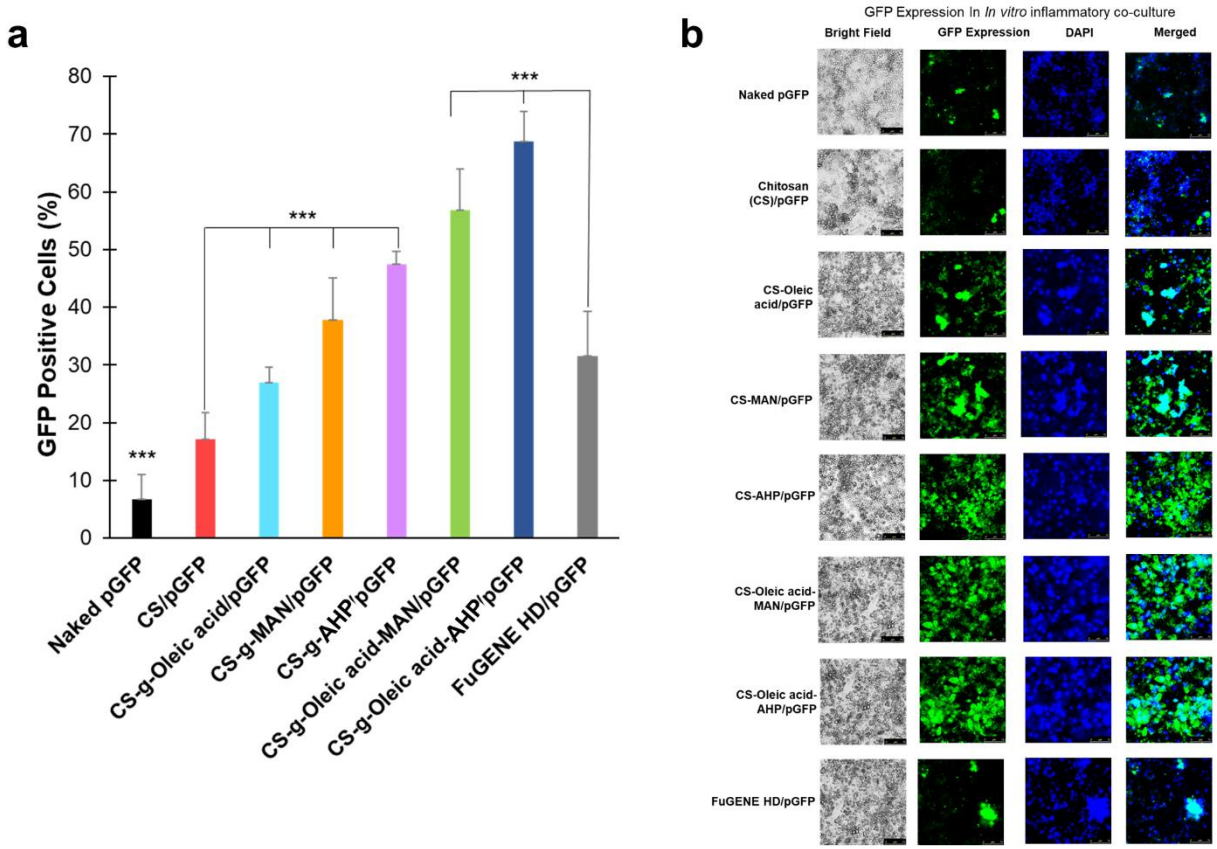

Figure 43. Determination of *in vitro* transfection efficiency of chitosan-based nanomicelles/pDNA polyplexes using model plasmid encoding green fluorescent protein (GFP) in inflammatory contact co culture of M1 polarized RAW 264.7 macrophages and differentiated 3T3-L1 adipocytes. (a) Quantitative estimation of percentage GFP transfected cells, (b) Qualitative fluorescence images of GFP transfected cells. [Data represents mean ± SD, n = 4; "*", "**" "***" depict significant difference from control at $p < 0.05$, 0.01, and 0.001, respectively.]

3.20. *In vitro* RNA interference efficacy of plasmid encoding shRNA against TNFα and MCP1

RNAi is a biological process where double stranded RNA (dsRNA) directs sequence-specific degradation of messenger RNA (mRNA).[267] Posttranscriptional gene silencing using RNAi is a powerful and efficient technique to downregulate expression of genes involved in the disease pathogenesis.[268] Initially, dsRNA is processed into small interfering RNA (siRNA) oligonucleotide fragments (~21 – 23 nucleotides) catalyzed by an enzyme 'Dicer'. In the second step, these siRNAs are integrated into multi-protein RNA-induced silencing complexes (RISC)

that facilitate unwinding of RNA duplex, followed by recognition of the target mRNA by the antisense RNA *via* base pairing, and finally cleavage and degradation of the specific mRNA.[269,270] However, since RNAi using siRNA is limited to cell cytosol leading to transient gene downregulation, small hairpin RNA (shRNA) were introduced which were capable of producing siRNA sequences *in situ* from plasmid DNA (pDNA) for a more sustained RNAi effect.[271] In this study, four unique plasmids encoding shRNA directed toward TNFα or MCP-1 were acquired from Origene Inc. and cytokine downregulation efficacy (TNFα or MCP-1) was evaluated in the *in vitro* inflammatory co-culture model. Two plasmid constructs showing maximum TNFα (TL515379-C lot#1215) or MCP-1 (TL501987-A lot#0116) downregulation were selected for all further analyses. CS polymer modified with OA and MAN (COM) was used to target the plasmid encoding shRNA against TNFα (shTNFα) to M1 polarized macrophages. CS polymer modified with OA and AHP (COA) was used to target the plasmid encoding shRNA against MCP-1 (shMCP1) to adipocytes. Polyplexes prepared using shTNFα and COM showed 61% knockdown of TNFα compared to cells without any treatment (untreated). TNFα concentration in cells treated with shTNFα/COM polyplexes was significantly lower compared to cells treated with naked shTNFα ($p < 0.001$) and untreated control ($p < 0.001$) demonstrating higher transfection efficiency of dual modified CS nanomicelles (**Figure 44a**). TNFα downregulation also resulted in reduction of MCP-1, IL-1β, and IL-6 by 68%, 56%, and 42% compared to untreated control, respectively (**Figure 44b-d**). Polyplexes prepared using shMCP1 and COA showed 66% knockdown of MCP-1 compared to cells without any treatment (untreated) (**Figure 44b**). MCP-1 concentration in cells treated with shMCP1/COA polyplexes was significantly lower compared to cells treated with naked shMCP1 ($p < 0.001$) and untreated control ($p < 0.001$) demonstrating higher transfection efficiency of dual modified CS nanomicelles. MCP-1 downregulation also resulted in reduction of

TNFα, IL-1β, and IL-6 by 40%, 54%, and 68% compared to untreated control, respectively (**Figure 44a,c,d)**. Pro-inflammatory cytokines are predominantly secreted by activated macrophages. Inflammatory stimuli like bacterial LPS leads to elevated levels of TNFα, IL-1β, and IL-6 production from activated/M1 polarized macrophages.[261,272] Cytokines are important stimulators or repressors of other cytokines in complex ways. In general, upregulation of pro-inflammatory cytokine decreases anti-inflammatory cytokines.[273] Moreover, production of inflammatory cytokines is often a cascade effect where action of cytokines on its target cells stimulates additional cytokine secretion.[274] TNFα secretion from activated macrophages induces upregulation of pro-inflammatory cytokine MCP-1 and downregulates anti-inflammatory adipokine adiponectin from differentiated 3T3-L1 adipocytes.[275] Moreover, free fatty acids released from differentiated adipocytes aggravate inflammation in macrophages.[275] *In vitro* downregulation of both TNFα and MCP-1 was shown to reduce concentration of other pro-inflammatory cytokines IL-1β and IL-6. TNFα knockdown resulted in marked downregulation of MCP-1 and IL-1 β suggesting it is a major cytokine-mediator of inflammation in adipocytes.[275] MCP-1 downregulation was shown to considerably affect concentration of IL-6, which may be due to the reduced stimulation of ERK1/2 by MCP-1, which in turn reduces IL-6 release.[276] Adiponectin, which is the most abundant adipokine secreted by adipocytes plays a critical role in lipid storage, adipogenesis, and enhances insulin sensitivity. Its levels are significantly lowered in obesity and obesity-induced insulin resistance in type-2 diabetes.[277–279] Increased levels of pro-inflammatory cytokines like TNFα in the chronic inflammatory environment in obese adipose tissue is known to play a role in reduced adiponectin levels.[280,281] However, no significant change in adiponectin concentration was observed with *in vitro* inflammatory co culture model preparation and 72 h post treatment with plasmids encoding shRNA against TNFα and MCP-1 (**Figure 44e**).

This is potentially due to longer incubation period and higher inhibitory concentration of pro-inflammatory cytokines required to observe changes in adiponectin concentration *in vitro*.[275,282] Finally, treatment using pDNA encoding scrambled shRNA control with and without polyplex formation with COM or COA showed TNFα, MCP-1, IL-1β and IL-6 concentration that was not significantly different from untreated control, serving as good negative control.

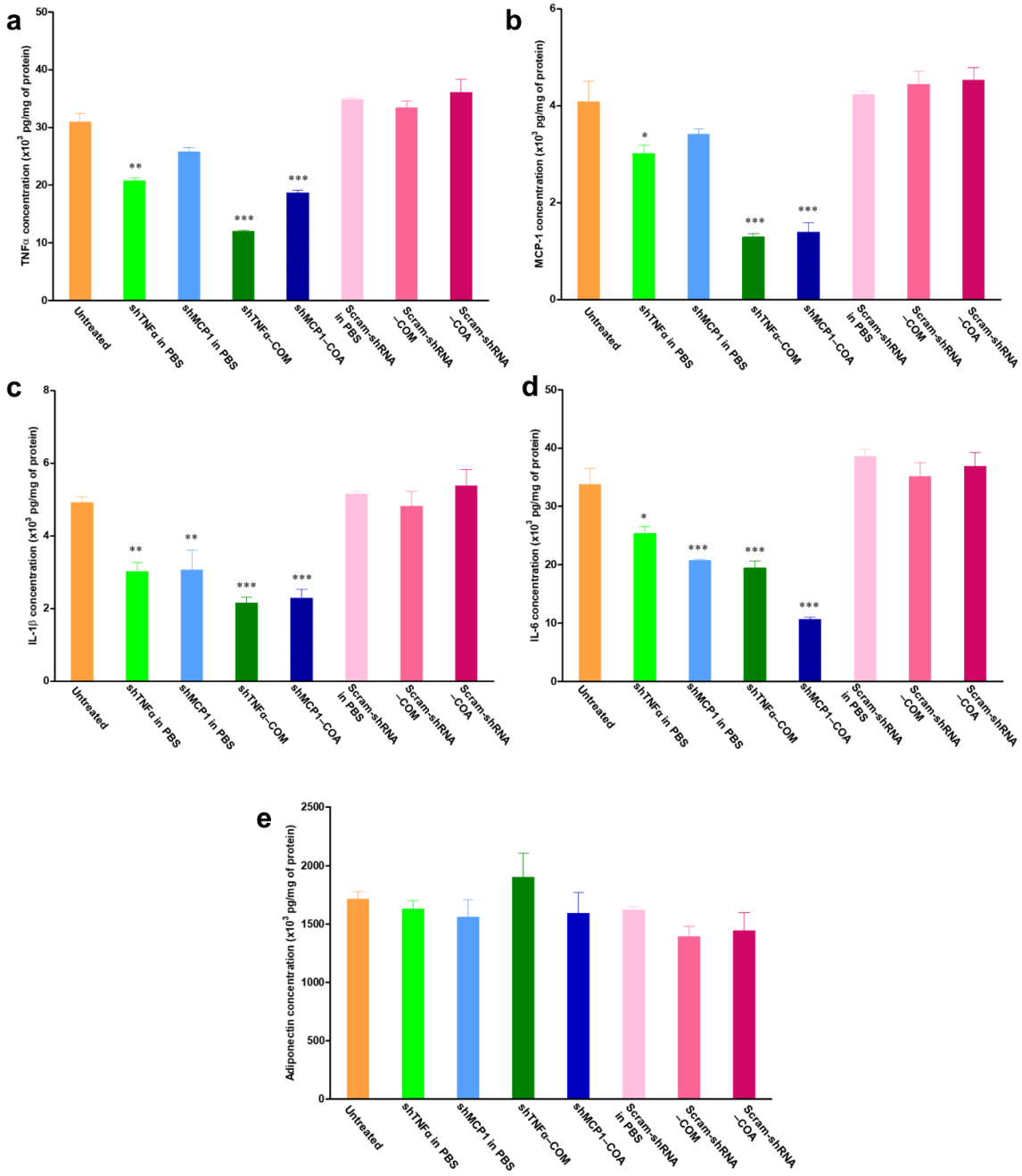

Figure 44. Determination of RNA interference efficacy of plasmid encoding shRNA against TNFα and MCP-1, in *in vitro* inflammatory co-culture model using macrophage or adipocytes targeted chitosan-based nanomicelles/pDNA polyplexes, respectively. Cytokine concentration was determined for (a) TNFα, (b) MCP-1, (c) IL-1β, (d) IL-6, and (e) Adiponectin, using respective high-sensitivity ELISA kits 72 h post transfection in cell culture supernatant and cell lysate. **[**Data represents mean ± SD, n = 6; "*", "**" "***" depict significant difference from untreated control at $p < 0.05$, 0.01, and 0.001, respectively.]

3.21. *In vivo* biodistribution and biocompatibility in obese diabetic mice model

Biodistribution of polyplexes prepared using pDNA and FITC-labelled CS polymeric nanomicelles was assessed in high-fat diet induced obese diabetic mice model. Subcutaneous route of administration was chosen to locally target activated macrophages and adipocytes. Subcutaneous route is also of considerable benefit owing to relatively slow distribution, longer residence time, and ease of self-administration for long-term treatment. After injection, the therapeutic is transported through the interstitium to reach blood or lymph capillaries which is majorly dependent on the size and charge of the therapeutic.[283] In this study, CS nanomicelles were surface modified with MAN and AHP to specifically target GLUT-1 transporter on M1 polarized macrophages and prohibitin receptor on adipose tissue vasculature, respectively. Dual modified nanomicelles (COM and COA) demonstrated significantly higher accumulation in the subcutaneous tissue near injection site (~2.2 – 2.8% ID/g of tissue) as well as a remote site (~2.2% ID/g of tissue) away from injection site (**Figure 45a**). The accumulation was ~2-fold higher and significantly ($p < 0.05$) improved compared to unmodified CS-FITC/pDNA and CS-OA-FITC/pDNA nanomicelles. Owing to the cationic nature of CS polymer, it also exhibits interaction with various cells and proteins in the body which are anionic in nature.[284] Interaction with highly negatively charged glycosaminoglycans (GAGs), an important component of the extracellular matrix, could be responsible for slow diffusion or convection mediated transport *via* interstitium to reach lymph and blood capillaries.[283,285] As expected, high accumulation was seen in spleen and liver owing to uptake by the macrophages in the reticuloendothelial system (RES).[286,287] Other studies have also reported high distribution in liver for higher molecular weight CS with high (> 50%) degree of deacetylation.[284,287] Moreover, high density of prohibitin receptors on spleen, liver, lungs and kidney are potentially responsible for higher accumulation of AHP modified

nanomicelles in these tissues.[288] Obesity-induced inflammatory cytokines produced by adipocytes and macrophages in obesity are critical mediators of hepatic inflammation. Portal venous system carries these cytokines to 'Kupffer' cells and hepatocytes, which are stimulated to produce more cytokines eventuating an inflammatory cascade in the liver and leading to hepatic insulin resistance.[289] High distribution in liver may be beneficial in RNAi of pro-inflammatory cytokines by transfecting liver macrophages thereby improving overall insulin sensitivity in obesity-induced type-2 diabetes. Fluorescence analysis in serum was non-detectable for all CS polymeric formulations which can be attributed to lysosomal degradation followed by elimination. Biodegradation and elimination of CS-based polymers are closely associated with its degree of deacetylation and molecular weight. High degree of deacetylation reduces rate of degradation.[287] High molecular weight CS mandates biodegradation (chemical or enzymatic) prior to elimination of CS polymer fragments (oligosaccharides) by renal clearance.[284]

CS is extensively regarded as a biocompatible polymer with wide applications as a dietary constituent and wound dressings.[287,290] However, modifications on CS polymer may affect its toxicity and compatibility *in vivo*. Biocompatibility of CS/pDNA nanomicelles prepared in this study was evaluated by histological examination of tissues using hematoxylin-eosin staining (H&E) (**Figure 45b**). Tissue sections from mice administered with sterile PBS were used as negative control. There was no evident change in morphological appearance tissues treated with CS polymeric formulations compared to control. Tissue sections derived from liver, spleen, lungs, heart and kidney were carefully examined for histological changes. Presence of inflammatory cells in the tissues was expected owing to the chronic inflammatory condition induced by high-fat diet treatment. However, inflammation in the tissues was comparable to tissues derived from mice injected with saline, implying no additional inflammation induced due to the delivery system.

There was no sign of tissue necrosis, nuclei enlargement, change in morphology of the hepatocytes or spleen cells, with no evidence of ballooning (**Figure 45b**). Histological examination of the lungs did not show any abnormal thickening of the alveolar septae or fibrotic deposition. Cardiac tissues did not demonstrate any myofibrillar loss or diffuse fibrosis of myocardium in any of the treatment groups. Moreover, histological evaluation of kidney tissues did not show any abnormal vasculature, interstitial congestions, lesion, hemorrhage or pigmentation in the glomeruli and collecting tubules. Biocompatibility was also evaluated 7 days' post-treatment with delivery system for RNAi of pro-inflammatory cytokines. Inflammatory cell concentration was observed to be markedly reduced in tissue sections (**Figure 45b**). Histological examination showed no sign of necrosis, lesion, and/or irregular morphological changes. Moreover, no sign of pain, behavioral alterations, changes in food/water intake, or loss of physical activity was observed in mice between different treatment groups. Overall, it can be safely concluded that the different polymeric CS/pDNA nanomicelles used in this study are non-toxic, and biocompatible in nature with no significant evidence of toxicity in major tissues and organs.

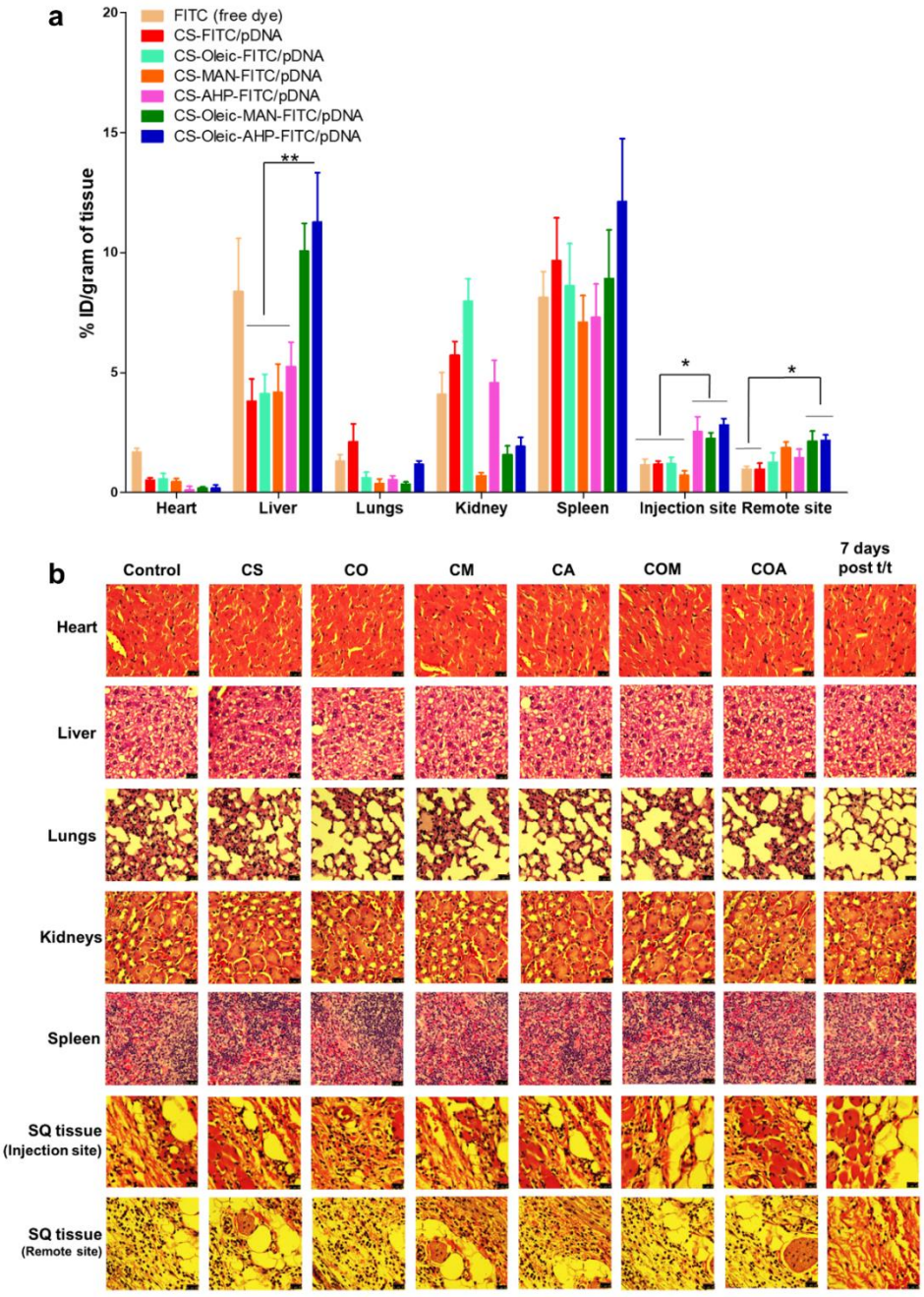

Figure 45. *In vivo* biodistribution and biocompatibility chitosan-based nanomicelles/pDNA polyplexes. (a) Biodistribution of FITC-labelled nanomicelles/pDNA (b) Histological examination of different tissues at 20X magnification 24 h after treatment with different formulations, and 7 days' post treatment with single dose of dual treatment with plasmid encoding shRNA against TNFα and MCP-1, in high-fat diet-induced obese-diabetic C57BL/6 mice using macrophage (COM) or adipocytes (COA) targeted chitosan-based nanomicelles/pDNA polyplexes, respectively. **[**Data represents mean ± SD, n = 6; "*" and "**" depict significant difference at $p < 0.05$ and 0.01, respectively.]

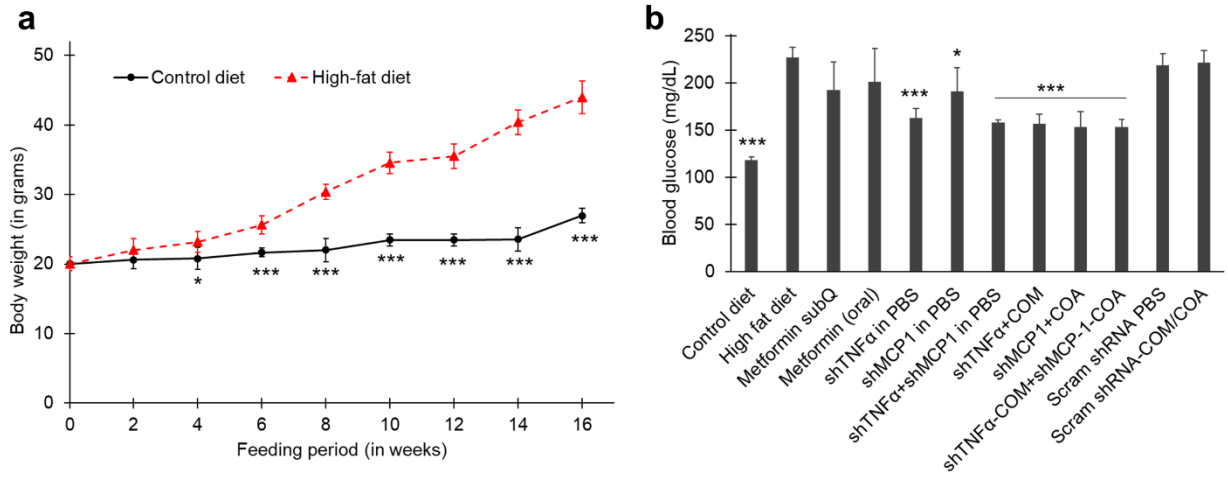

Figure 46. Comparison of (a) body weight following control diet and high-fat diet treatment, (b) Fasting blood glucose of untreated mice following control diet or high fat diet treatment, and of obese diabetic mice on high fat diet one week following single administration of respective treatments. [Data represents mean ± SD, n = 6; "***" depicts significant difference from untreated obese control at $p < 0.001$.]

3.22. *In vivo* tissue and serum cytokine estimation and efficacy in obese diabetic mice model

Obesity is a complex phenomenon associated with over-nutrition that elicits stress and stimulates inflammatory *milieu* in metabolically active sites such as white adipose tissue, liver and immune cells. Obesity induced inflammation, insulin resistance and type 2 diabetes is a complex metabolic syndrome that needs to be studied in close correlation of all parameters. High-fat diet treatment in rodent model closely mimics gradual weight gain and body fat accumulation over a relatively long duration that resembles clinically relevant obesity-induced insulin resistance development in human population.[291] Western diet with a high percentage of fat (42 % energy by fat) and sugar (34 % w/w) content simulates the nature of popular processed foods responsible for positive energy balance, exceeding energy expenditure. High-fat diet fed C57BL/6 mice demonstrate the phenotypic weight gain, fat accumulation, hyperglycemia, inflammation, insulin resistance and associated metabolic syndrome resulting in a reliable model to study obesity-induced insulin resistance and type-2 diabetes.[291–294] Mice fed with high-fat diet for 16 weeks

depicted significantly higher weight gain, hyperglycemia as depicted in **figure 46** along with reduced insulin sensitivity and low glucose tolerance compared to mice fed with normal diet (**Figures 49, 50**). It is suggested that obesity-induced inflammatory mechanisms produce chronic low-grade inflammation in visceral and subcutaneous adipose tissues.[295,296] In this study, cytokine concentration was determined both at serum (systemic) and tissue (local) level. Visceral and subcutaneous adipose tissues are two most abundant depots producing unique profile of cytokines and adipokines.[274] Cytokine concentration at tissue level was therefore determined in subcutaneous adipose tissue (SAT), perirenal visceral adipose tissue (PVAT) and epididymal visceral adipose tissue (EVAT) (**Figure 47**). Cytokine levels in age-matched animals fed with healthy diet had significantly lower TNFα, MCP-1, IL-1β and IL-6 concentrations compared to obese-diabetic animals after 16-weeks of high fat diet treatment (**Figure 48a-h**). Treatment with metformin (marketed control) was performed by administering a single dose (35 mg/kg) given orally or subcutaneously. In addition to glucose lowering and insulin sensitizing effects of metformin, it also known to attenuate inflammation by inhibition of nuclear factor κB (NFκB) *via* AMP-activated protein kinase (AMPK)-dependent and independent pathways.[297,298] Slight attenuation in serum and tissue TNFα, MCP-1, IL-1β and IL-6 concentration was observed 7-days post treatment (**Figure 48a-h**). Metformin administered using oral gavage showed improved efficacy compared to subcutaneously injected metformin, which is expected due to its possible mechanism of action in the gut.[299,300] Significant improvement ($p < 0.05$) in insulin sensitivity and glucose tolerance was observed compared to untreated obese diabetic mice (**Figure 48d,f**). However, there was no significant change in fasting blood glucose level one-week post metformin treatment (**Figure 48b**). On average, there was ~2.4 and 4-fold reduction in TNFα concentration in SAT, EVAT and PVAT one-week post treatment with shTNFα in PBS and shTNFα/COM polyplexes,

respectively, compared to untreated obese control (**Figure 48a**), which was significantly lower than ($p < 0.001$) untreated obese diabetic mice. Serum TNFα levels were also attenuated by 1.5 and 2.5-fold one-week post treatment with shTNFα in PBS and shTNFα/COM polyplexes, respectively, compared to untreated obese control (**Figure 48b**). Treatment using shTNFα/COM polyplexes produced significantly higher ($p < 0.05$) attenuation in cytokine concentration alongside improved efficacy compared to naked pDNA, which may be attributed to protection from nuclease degradation, improved cellular uptake, and higher transfection efficiency using COM nanomicelles. Furthermore, electrostatic complex formation with COM polymer also helps in endosomal escape which supports increased bioavailability and efficacy of pDNA. As observed *in vitro*, downregulation of TNFα using shTNFα/COM polyplexes significantly ($p < 0.001$) reduced tissue and serum levels of MCP-1, IL-1β and IL-6 (**Figure 48c-h**). On the other hand, tissue and serum adiponectin levels were found to be significantly increased ($p < 0.001$) compared to untreated obese diabetic mice and were comparable to healthy tissue and serum adiponectin concentration (**Figure 48i-j**). MCP-1 knockdown using shMCP1 in PBS and shMCP1/COA polyplexes resulted in on average 6 and 10-fold reduction in MCP-1 concentration in SAT, EVAT and PVAT one-week post treatment, respectively, compared to untreated obese diabetic mice, which was significantly lower than ($p < 0.001$) concentration in tissue lysate and serum (**Figure 48c-d**). Naked pDNA in PBS encoding shRNA against MCP-1 also showed appreciable reduction in cytokine levels, however, it was significantly lower ($p < 0.05$) compared to shMCP1/COA polyplexes. MCP-1 knockdown of MCP-1 using shMCP1/COA polyplexes also significantly ($p < 0.001$) attenuated tissue and serum levels of TNFα, IL-1β and IL-6 (**Figure 48a,b,e-h**). MCP-1 downregulation markedly affected IL-6 concentration and showed little to no effect on tissue adiponectin levels. Conversely IL-1β and adiponectin concentration were strikingly altered in

response to TNFα downregulation. This emphasizes close relationship between specific cytokines and their codependent upregulation and downregulation in response to pathological or therapeutic factors.[276,301–303] Dual treatment with both shTNFα/COM and shMCP1/COA polyplexes resulted in superior downregulation of TNFα, MCP-1, IL-1β and IL-6 levels both at tissue and serum level, which was remarkably lower compared obese tissue and serum cytokine concentrations (**Figure 48**). Adiponectin levels in tissue lysate and serum were also seen to be appreciably increased in response to dual treatment targeting RNAi of both TNFα and MCP-1 (**Figure 48i-j**). Treatment with scrambled shRNA with and without polyplex formation using COM/COA did not result in significant changes in the tissue and serum concentration of TNFα, MCP-1, IL-1β, IL-6 and adiponectin.

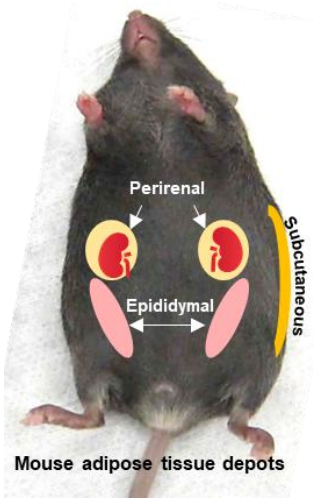

Figure 47. Schematic showing location of adipose tissue depots analyzed in this study.

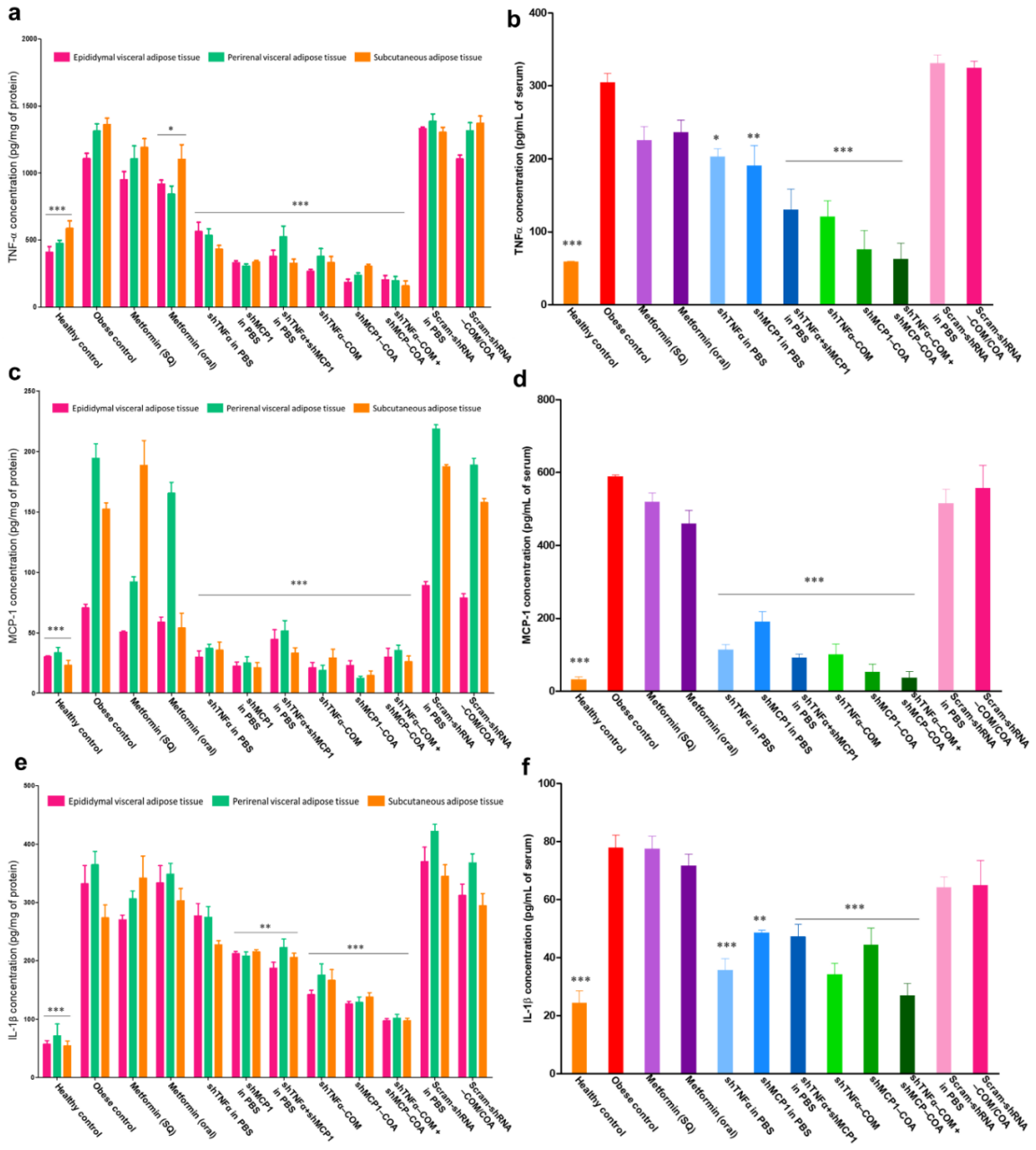

Figure 48. Evaluation of RNA interference efficacy of plasmid encoding shRNA against TNFα and MCP-1, in high-fat diet-induced obese-diabetic C57BL/6 mice using macrophage (COM) or adipocytes (COA) targeted chitosan-based nanomicelles/pDNA polyplexes, respectively. Concentration of (a-b) TNFα, (c-d) MCP-1, (e-f) IL-1β, (g-h) IL-6, and (i-j) Adiponectin, were determined in pg/mg of protein of epididymal visceral adipose tissue, perirenal visceral adipose tissue, and subcutaneous adipose tissue, and in pg/mL of serum using respective high-sensitivity ELISA kits one week post single subcutaneous administration of optimized formulations. Healthy and obese control represent untreated non-obese non-diabetic mice on control diet, and obese diabetic mice on high-fat diet, respectively. [Data represents mean ± SD, n = 6; "*", "**" "***" depict significant difference from untreated obese control at $p < 0.05$, 0.01, and 0.001, respectively.]

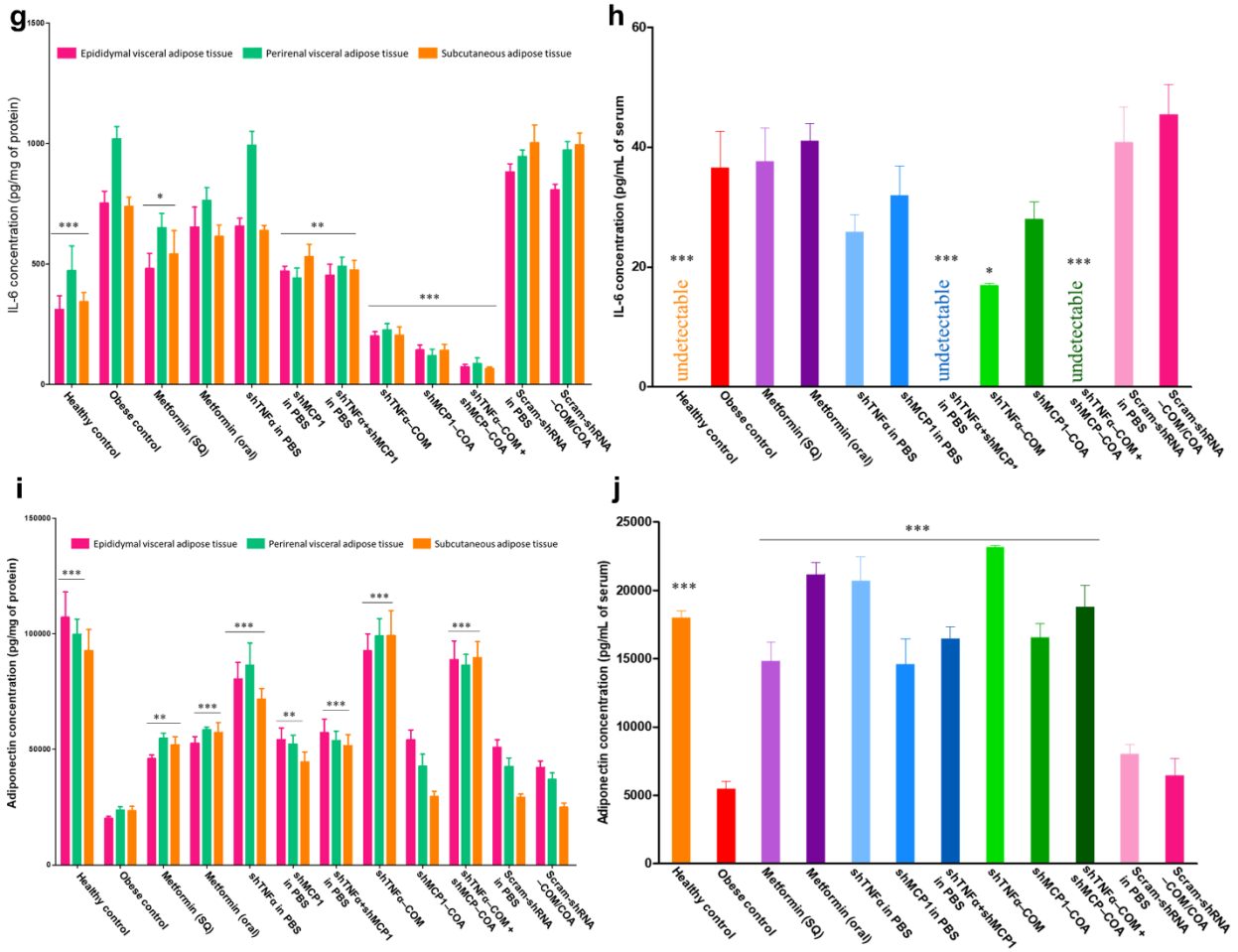

Figure 48. Evaluation of RNA interference efficacy of plasmid encoding shRNA against TNFα and MCP-1, in high-fat diet-induced obese-diabetic C57BL/6 mice using macrophage (COM) or adipocytes (COA) targeted chitosan-based nanomicelles/pDNA polyplexes, respectively. Concentration of (a-b) TNFα, (c-d) MCP-1, (e-f) IL-1β, (g-h) IL-6, and (i-j) Adiponectin, were determined in pg/mg of protein of epididymal visceral adipose tissue, perirenal visceral adipose tissue, and subcutaneous adipose tissue, and in pg/mL of serum using respective high-sensitivity ELISA kits one week post single subcutaneous administration of optimized formulations. Healthy and obese control represent untreated non-obese non-diabetic mice on control diet, and obese diabetic mice on high-fat diet, respectively. [Data represents mean ± SD, n = 6; "*", "**" "***" depict significant difference from untreated obese control at $p < 0.05$, 0.01, and 0.001, respectively.] (continued).

Insulin sensitivity test was performed, before and after treatment with different formulations, to determine their efficacy in attenuating insulin resistance. Percentage change from baseline blood glucose levels were calculated with respect to respective initial blood glucose level at 0 min. Maximum efficacy in insulin sensitivity was observed when TNFα and MCP-1 were

downregulated using shTNFα/COM and shMCP1/COA polyplexes (**Figure 49**). This may be correlated to reduced action of pro-inflammatory cytokines on negative regulators of insulin signaling. Pro-inflammatory cytokines like TNFα activate IκB kinaseβ in the NFκB pathway and C-Jun N-terminal kinase 1 (Jnk1) in the JNK/Activator protein-1 pathway which catalyze serine phosphorylation of insulin receptor substrate proteins (IRS).[304] Additionally, inflammation induced activity of suppressor of cytokine signaling (SOCS1) promotes ubiquitylation and subsequent degradation of IRS proteins.[305,306] Serine phosphorylation and ubiquitination of IRS1 prevent tyrosine phosphorylation and insulin signal transduction, thus resulting in insulin resistance in insulin sensitive tissues. RNAi mediated downregulation of pro-inflammatory cytokines helps in decreasing their inhibitory effect on insulin signaling thereby improving insulin sensitivity.

Glucose tolerance and fasting blood glucose level were also observed to be significantly improved upon TNFα and MCP-1 downregulation using shTNFα/COM and shMCP1/COA polyplexes (**Figure 50**). Downregulation in pro-inflammatory cytokines also results in improved levels of adiponectin, which is a crucial insulin sensitizing adipokine. Adiponectin facilitates glucose uptake and utilization by multiple actions in adipose tissue, liver and skeletal muscles including activating adenosine monophosphate activated protein kinase (AMPK) and increasing the expression and activity of protein phosphorylation activator receptor-α (PPAR-α). AMPK phosphorylates acetyl coenzyme-A carboxylase (ACC), stimulates β-oxidation, increases fatty-acid combustion, upregulates insulin-stimulated AKT signaling, as well as reduces hepatic gluconeogenesis to improve glucose homeostasis.[307,308] PPAR-α activation leads to increased fatty-acid and energy combustion *via* upregulation of acetyl CoA oxidase (ACO) and uncoupling

proteins (UCPs).[309] In addition to this, adiponectin also suppresses inflammatory response and promotes macrophage polarization to anti-inflammatory M2 phenotype.[307,309]

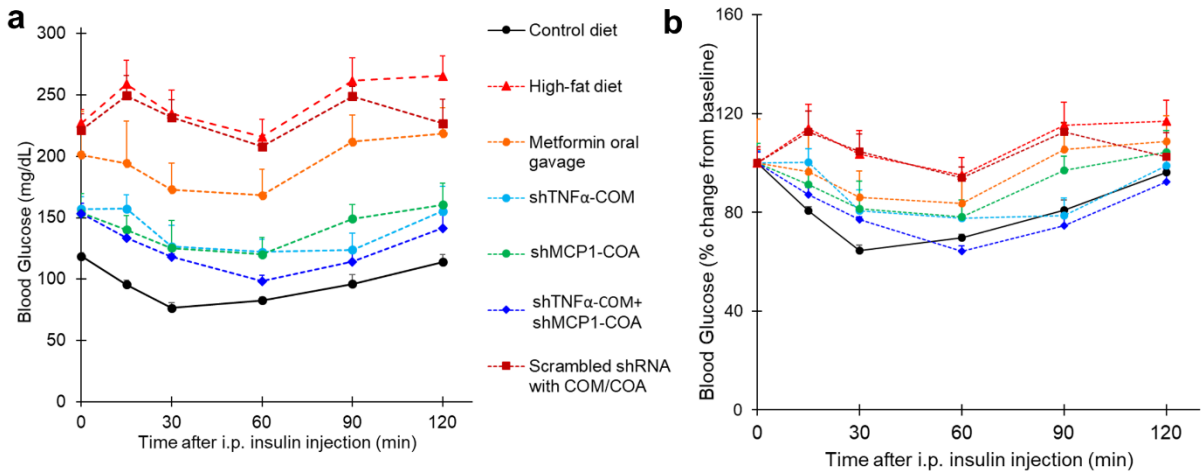

Figure 49. Insulin sensitivity assay depicting (a) blood glucose concentration, (b) percentage change from baseline blood glucose concentration, one-week post administration of different treatments. Control and high-fat diet represent untreated non-obese non-diabetic mice as healthy control, and obese diabetic mice as obese control, respectively. Legend refers to both graphs a and b. [Data represents mean ± SD, n = 6]

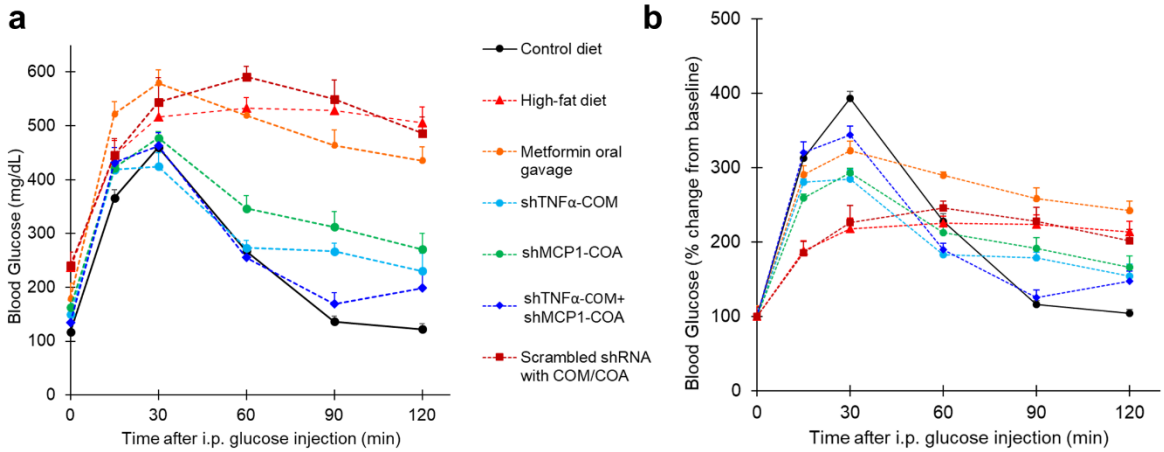

Figure 50. Glucose tolerance assay depicting (a) blood glucose concentration, (b) percentage change from baseline blood glucose concentration, one-week post administration of different treatments. Control and high-fat diet represent untreated non-obese non-diabetic mice as healthy control, and obese diabetic mice as obese control, respectively. Legend refers to both graphs a and b. [Data represents mean ± SD, n = 6]

In order to assess duration of efficacy of anti-inflammatory treatment by RNAi of pro-inflammatory cytokines TNFα and MCP-1, mice were treated with shTNFα/COM and shMCP1/COA polyplexes and sacrificed at 1, 2, 4 and 6 weeks after administration. Tissue and serum cytokines were quantified using specific ELISA kits. Fasting blood glucose, IST and GT were performed to determine efficacy of the treatment. Tissue and serum cytokine levels showed gradual increase with time (**Figure 51**). Serum TNFα concentration 2 weeks post treatment was significantly higher ($p < 0.001$) than healthy control but tissue levels were significantly ($p < 0.01$) lower than untreated obese control up to 6 weeks post treatment (**Figure 51f**). As mentioned earlier, MCP-1 is a chemokine secreted majorly by adipocytes and ATMs driving the recruitment of monocytes from systemic circulation to the damaged or inflamed tissues.[304] Interestingly, serum MCP-1 concentration were significantly lower ($p < 0.001$) than untreated obese-diabetic control which is extremely beneficial in intercepting one of the primary steps in adipose tissue inflammation in obesity and obesity induced-insulin resistance in diabetes (**Figure 51g**). IL-1β and IL-6 concentration in tissues and serum were also determined to be lower than obese control for up to 2 – 4 weeks post treatment, steadily increasing to baseline level (**Figure 51c,d,h,i**). Furthermore, serum and tissue adiponectin concentration were maintained at a significantly higher level compared to obese control group up to 6 weeks which can be attributed to the low inflammatory environment after COM/COA nanomicelles mediated RNAi of pro-inflammatory cytokines TNFα and MCP-1 (**Figure 51e,j**).

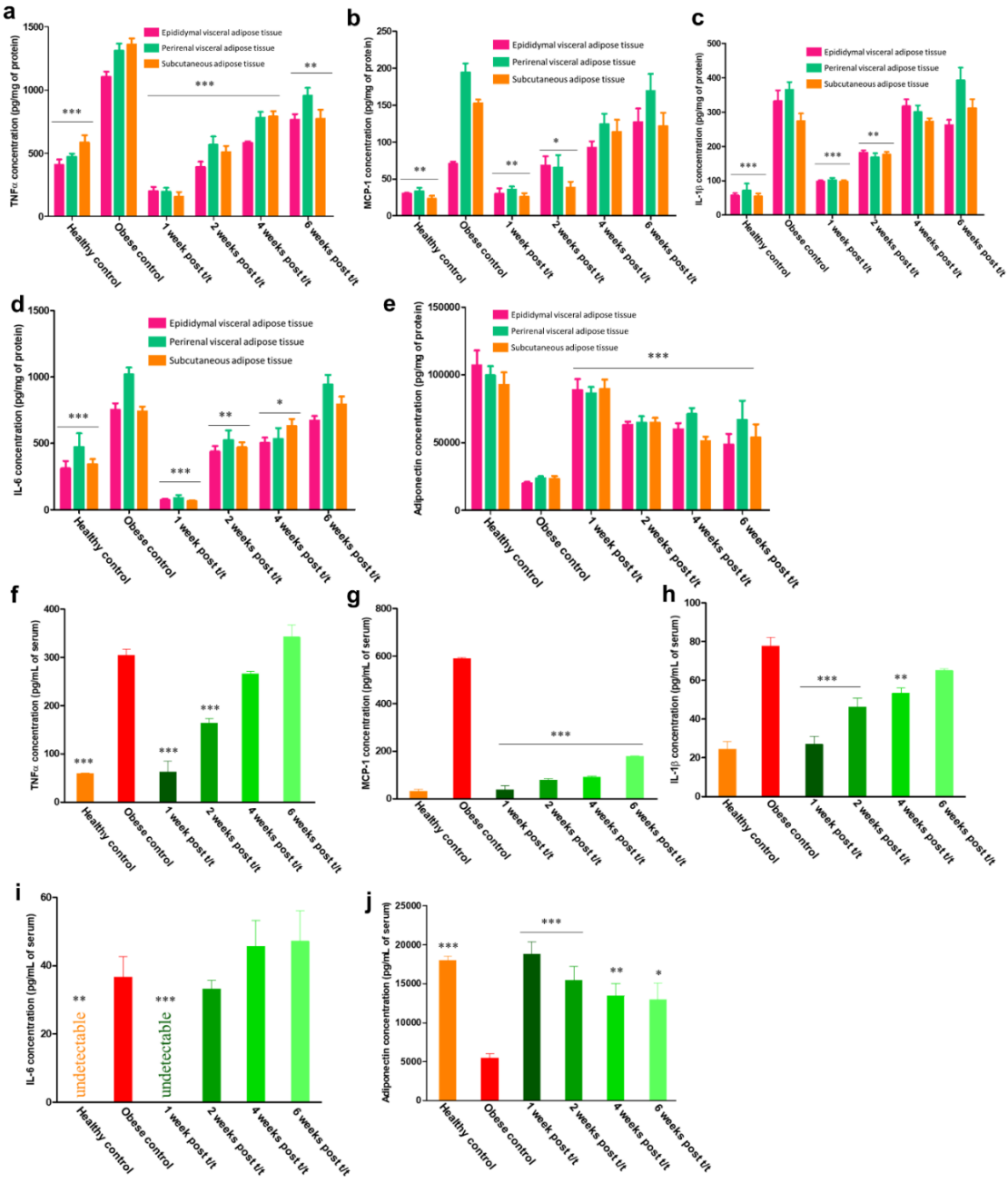

Figure 51. Estimation of (a-e) tissue and (f-j) serum, cytokine levels post treatment with single dose of dose of optimized formulation (shTNFα-COM + shMCP1-COA). Concentration of (a, f) TNFα, (b, g) MCP-1, (c, h) IL-1β, (d, i) IL-6, and (e, j) Adiponectin, were determined in pg/mg of protein of epididymal visceral adipose tissue, perirenal visceral adipose tissue, and subcutaneous adipose tissue, and in pg/mL of serum using respective high-sensitivity ELISA kits. [Data represents mean ± SD, n = 6; "*", "**" "***" depict significant difference from untreated obese control at $p < 0.05$, 0.01, and 0.001, respectively.]

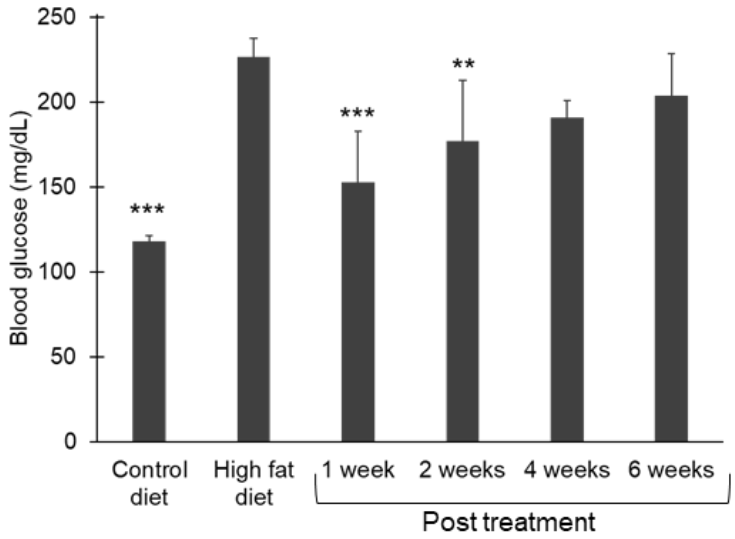

Figure 52. Fasting blood glucose concentration 1, 2, 4, and 6-weeks following treatment with optimized formulation, shTNFα-COM + shMCP-1-COA. Control and high-fat diet represent untreated non-obese non-diabetic mice as healthy control, and obese diabetic mice as obese control, respectively. Legend refers to both graphs a and b. [Data represents mean ± SD, n = 6; "**" and "***" depict significant difference from untreated obese control at $p < 0.01$ and 0.001, respectively.]

This also reflected in IST and GT determined at 1, 2, 4, and 6 weeks post treatment with shTNFα/COM and shMCP1/COA polyplexes, showing gradual increase in fasting blood glucose concentration (**Figure 52**), and steady decline in insulin sensitivity and glucose tolerance over time. However, following treatment with optimized formulation insulin treatment and glucose tolerance were significantly improved up to 4 and 6 weeks respectively, compared to untreated obese diabetic mice **(Figures 53, 54**). Overall these results strongly suggest efficacy of locally targeting and downregulating pro-inflammatory cytokines in adipocytes and adipose tissue macrophages in improving insulin sensitivity and glucose tolerance in obesity-induced type 2 diabetes preclinical model. Moreover, targeted COM/COA nanomicelles are potentially a safe, effective and superior method of mediating localized RNAi to downregulate pro-inflammatory cytokines that are inherently elevated in obese adipose tissue environment.

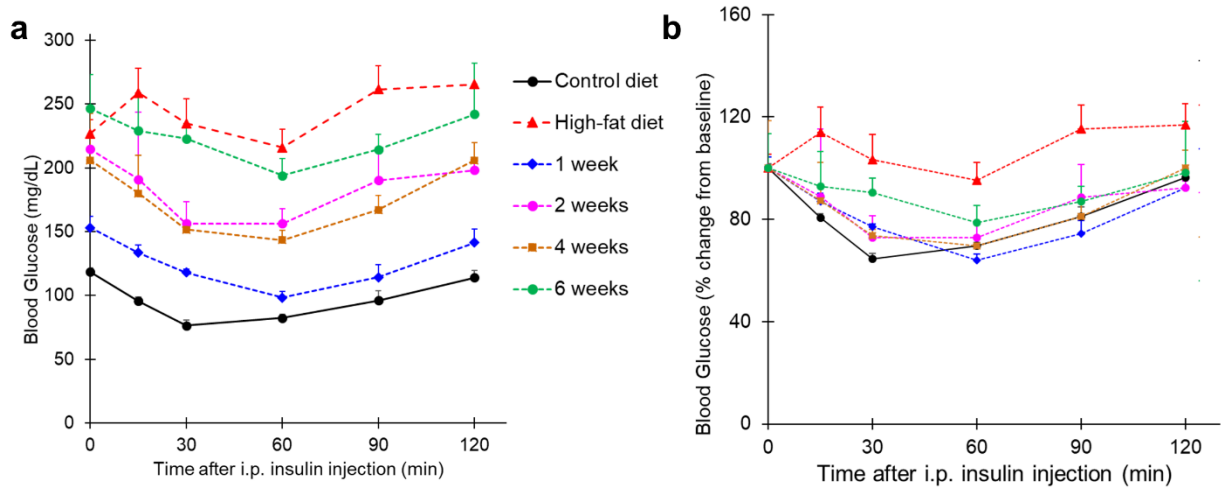

Figure 53. Insulin sensitivity assay depicting (a) blood glucose concentration, (b) percentage change from baseline blood glucose concentration, 1, 2, 4, and 6-weeks following treatment with optimized formulation, shTNFα-COM and shMCP-1-COA Control and high-fat diet represent untreated non-obese non-diabetic mice as healthy control, and obese diabetic mice as obese control, respectively. Legend refers to both graphs a and b. [Data represents mean ± SD, n = 6]

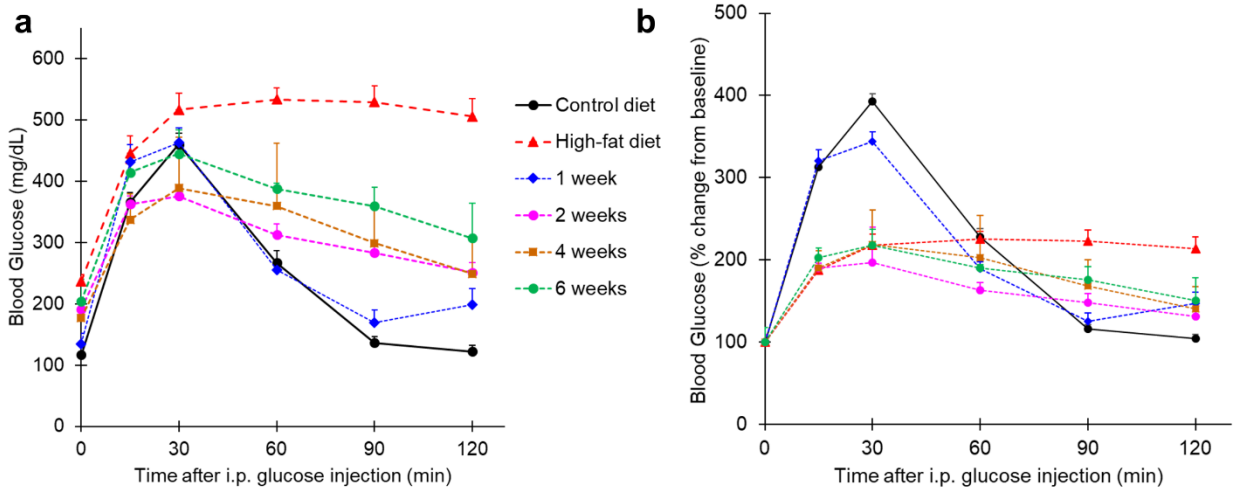

Figure 54. Glucose tolerance assay depicting (a) blood glucose concentration, (b) percentage change from baseline blood glucose concentration, 1, 2, 4, and 6-weeks following treatment with optimized formulation, shTNFα-COM and shMCP-1-COA Control and high-fat diet represent untreated non-obese non-diabetic mice as healthy control, and obese diabetic mice as obese control, respectively. Legend refers to both graphs a and b. [Data represents mean ± SD, n = 6]

4. SUMMARY AND CONCLUSION

Daily long-acting insulin administration or multiple bolus doses through an insulin pump every few hours are the only treatments available for basal insulin delivery in type 1 diabetic patients. In this study, we successfully optimized an *in situ* gel forming delivery system that provides basal level insulin with relatively peak-free pharmacokinetic profile for up to 90 days in type-1 diabetic rat model. Thermosensitive copolymer PLA_{1500}-PEG_{1500}-PLA_{1500} was synthesized using ring opening polymerization of D, L-lactide using PEG as an initiator and stannous octoate as the catalyst. Structural composition and molecular weight of the synthesized copolymer was confirmed using ^{1}H and ^{13}C NMR and GPC, respectively. Aqueous copolymer concentration of 35% w/v was found to be easily injectable from a 25 G syringe with a thermal gelation temperature of 26 °C, allowing it to instantaneously form a gel depot following subcutaneous administration. In order to improve stability and release characteristics of insulin, it was modified using zinc and CS. Addition of zinc ions allows association of three insulin dimers to form zinc-insulin hexamer with improved thermal stability indicated by a higher Tm value of 72.5 °C, determined using nano DSC. Electrostatic complex formation between negatively charged zinc-insulin hexamers and positively charged CS resulted in a much higher Tm (86 – 89 °C) indicating increased thermostability of insulin when complexed with CS. Electrostatic complex formation and high thermal stability of insulin was maintained upon complex formation using different chain length of CS and CS modified using oleic acid (OA-g-CSO).

It has been widely established that release through PLA-PEG-PLA copolymer can be affected by size and nature of the incorporated therapeutic. Addition of zinc and CS to free insulin significantly reduced initial burst release owing to the incorporation of less soluble zinc-insulin hexamers and CS-zinc-insulin complexes and restricted diffusion of larger hexamers and

complexes through the copolymer matrix. Additionally, formulation containing CS showed low secondary burst release owing to the buffering action of free amino groups on CS backbone. CS chain length significantly affected the rate of insulin release with largest (200 kDa) and smallest chain length (5 kDa) releasing insulin at the fastest and slowest rate, respectively. Comparing degradation profile of the copolymer between different formulations suggested that thermosensitive copolymer incorporating CS-zinc-insulin complexes of higher chain length CS (200 kDa, large hydrophilic polymer) resulted in rapid degradation of copolymer, while CS-zinc-insulin complexes containing lower molecular weight CS (5 kDa) demonstrated slower degradation profile, which can be related to the larger or smaller size of the pores formed during initial release followed by entry of water molecules to cause rapid or slow degradation of copolymer for longer and shorter chain length CS, respectively. Hydrophobically modified OA-g-CSO-zinc-insulin complexes further extended the rate of insulin release *in vitro* which was potentially due to their partition into the hydrophobic core of copolymer micelles resulting in slow diffusion of complexes over time.

Structural and conformational stability of insulin is pertinent to its biological activity. OA-g-CSO-zinc-insulin complexes also helped protect structural, conformational and chemical stability of insulin released *in vitro* analyzed using Nano DSC, CD spectroscopy, and RP-HPLC, respectively. Storage stability of OA-g-CSO-zinc-insulin complexes incorporated in PLA-PEG-PLA copolymer at 4 °C also showed lack of insulin aggregation, and preservation of its structural, conformational and chemical stability up to 9 months.

Furthermore, controlled release of insulin *in vivo* was assessed in STZ-induced type diabetic SD rats and compared with different formulation controls and daily administration of marketed long-acting insulin, glargine. Insulin glargine showed a relatively sustained profile of

insulin release reaching peak serum concentration between 2 – 4 h and blood glucose lowering effect lasting between 18 – 20 h. Formulation incorporating OA-g-CSO-zinc-insulin complexes demonstrated relatively stable serum insulin levels of 21.8 mU/L for up to 91 days. Daily 24 h administration of glargine resulted in fluctuating blood glucose levels between 91 – 443 mg/dL. On the other hand, OA-g-CSO-zinc-insulin complexes incorporating formulation resulted in blood glucose levels 102 ± 9 mg/dL for 91 days. There was no significant difference ($P < 0.05$) between the blood glucose levels of OA-g-CSO-zinc-insulin complexes formulation group between consecutive time intervals, which can be attributed to the slow release of insulin diffusing from the depot inside the hydrophobic depot of the copolymer micelles. Additionally, owing to the sustained maintenance of basal insulin levels from OA-g-CSO-zinc-insulin complexes incorporated in thermosensitive copolymer formulation, there was negligible build-up of ketone bodies and absence of cataract formation in diabetic rats, suggesting much lower risk of diabetes complications. Moreover, this formulation was found to be biocompatible *in vitro* and *in vivo*, determined using MTT cell viability assay of copolymer degradation products and H&E staining of injection site, respectively. Absence of cytotoxicity, inflammation, tissue damage, necrosis, and collagen deposition suggest that his formulation is safe and compatible for repeated use.

Overall, single administration of our controlled release formulation will help replace 90 – 180 long-acting insulin injections over a period of three months. This will be beneficial in achieving improved patient compliance owing to low frequency of administration and reduced injection site pain, inflammation and damage. The results indicate that our delivery system closely mimics physiological basal insulin secretion required to maintain normal glycemic control in type-1 diabetes patients. Moreover, as demonstrated in this study, long-term controlled release of basal

level insulin may help improve patient outcomes while reducing overall economic cost of diabetes by preventing development of diabetes complications.

Additionally, OA conjugation onto CS polymer makes the CS-OA polymer amphiphilic and capable of forming nanomicelles in aqueous environment. Cationic nature of CS nanomicelles at physiological pH enables electrostatic interaction with negatively charged pDNA forming CS/pDNA polyplexes which have been studied to improve cell internalization and transfection efficiency of pDNA involved. In this study, CS modified with OA and targeting ligands (mannose, AHP) was investigated as a non-viral vector for transfection of plasmid encoding shRNA against pro-inflammatory cytokines. Obesity, a state of chronic low-level inflammation, has been established as the leading risk factor in the development of insulin resistance and progression of type-2 DM. This is primarily due to excess secretion of pro-inflammatory cytokines like TNFα, MCP-1, IL1β, and IL6 by ATMs and adipocytes. Increased level of pro-inflammatory cytokines interferes with insulin signaling in insulin sensitive tissues such as liver, skeletal muscles, and adipose tissues making them insulin resistant. In this study, we explored targeted knockdown of pro-inflammatory cytokines TNFα and MCP-1 in ATMs and adipocytes as a treatment strategy to improve insulin sensitivity and glucose tolerance in obesity-induced type 2 DM.

In order to preferentially target ATMs, CS-OA polymers were conjugated to mannose to enhance internalization by GLUT-1 transporter mediated endocytosis. Conjugation with AHP was performed to promote prohibitin receptor mediated endocytosis in WAT vasculature. Synthesized polymers were characterized using ^{1}H NMR and FT-IR spectroscopy. Percent conjugation was determined using TNBSA and BCA kit for mannose and AHP, respectively, and was found to be around 20%. CMC of ligand-conjugated CS polymers was determined using pyrene as a hydrophobic probe. The CMC of CS-OA, CS-OA-MA, and CS-OA-AHP polymers was

determined to be about 62.7, 88.3 and 52.5 µg/mL, respectively. CS polymer and pDNA poplyplexes were prepared by adding CS polymer solution dropwise to pDNA solution (N to P ratio of 20) followed by vortexing for 5 min. Particle size of the nanoparticles was lower than 200 nm, with positive net surface charge. Association efficiency of synthesized CS polymers and pDNA used in this study was found to be around 96% and 97% for plasmid encoding for shRNA against TNFα (shTNFα) and plasmid encoding for shRNA against MCP-1 (shMCP1), respectively. Moreover, pDNA polyplex formation with CS polymers assisted in its condensation and protection from nucleases, as observed using agarose gel electrophoresis. CS nanoparticles prepared in this study also showed buffering capacity in endosomal pH range, which facilitates endosomal escape of the pDNA and prevents degradation by lysosomal enzymes.

In order to investigate and optimize cytocompatibility, cellular uptake and transfection efficiency of synthesized CS polymers, three different *in vitro* cell culture models were utilized. To mimic ATMs in obese-diabetic pathophysiology, RAW264.7 macrophages were activated with LPS to induce polarization transition to M1 pro-inflammatory phenotype. Murine 3T3-L1 preadipocyte cell line was differentiated *in vitro* from fibroblast cell phenotype to mature adipocytes. Furthermore, to replicate infiltration and accumulation of macrophages in obese adipose tissue, a contact co-culture of M1 polarized macrophages infiltrating differentiated mature adipocytes was prepared. Concentration of pro-inflammatory cytokines (TNFα, MCP-1, IL1β, IL6) in the cell culture models was determined using cytokine specific ELISA kits, and was found to be significantly upregulated in M1 polarized macrophages and inflammatory co-culture model. All formulations were found to be compatible in polymer concentration ranging from 0.1 to 1 mg/mL in all three cell culture models. Dual modified CS nanomicelles (COM, and COA) demonstrated significantly improved cellular internalization in presence of diabetic physiological

concentration of glucose and mannose. Furthermore, CS modified with MAN and AHP showed superior transfection in *in vitro* cell culture models for both model plasmids encoding for β-galactosidase and GFP, compared to naked pDNA and marketed transfection reagent FuGENE® HD.

Subsequently, RNAi efficacy was tested using dual modified nanomicelles complexed with shTNFα (COM-shTNFα) and shMCP1 (COA-shMCP1) in *in vitro* inflammatory co-culture model to preferentially downregulate TNFα and MCP-1 in ATMs and adipocytes, respectively. COM-shTNFα and COA-shMCP1 showed 61% and 66% knockdown of respective pro-inflammatory cytokines TNFα and MCP-1, compared to untreated control. This also resulted in significant downregulation of other inflammatory cytokines (IL-1β, and IL-6) in co-culture. In the next step, the efficacy of the formulation was assessed *in vivo* in high fat diet-induced obese diabetic mouse model. Mice fed with high-fat diet for 16 weeks depicted significantly higher weight gain, hyperglycemia, reduced insulin sensitivity and low glucose tolerance compared to mice fed with normal diet. Marketed anti-hyperglycemic drug metformin showed only slight attenuation in serum and tissue TNFα, MCP-1, IL-1β and IL-6 concentration, 7-days post treatment. However, treatment with COM-shTNFα and COA-shMCP1 demonstrated significant downregulation of pro-inflammatory cytokines (TNFα, MCP-1, IL-1β and IL-6) and upregulation of insulin sensitizing adipokine, adiponectin. Treatment with both COM-shTNFα and COA-shMCP1 administered at separate injection sites, showed the best outcome in pro-inflammatory cytokine attenuation. Low levels of pro-inflammatory cytokines were closely related with improved insulin sensitivity and glucose tolerance in obese diabetic mice. This may be attributed to reduced action of pro-inflammatory cytokines on negative regulators of insulin signaling. Efficacy of dual treatment with both COM-shTNFα and COA-shMCP1 was seen to gradually decrease over a period of 6 weeks.

However, significantly improved glycemic control was maintained up to 6 weeks following single administration of the optimized formulation (COM-shTNFα + COA-shMCP1). Histological examination of major organs and injection site tissue showed no sign of necrosis, lesion, and/or irregular morphological changes. Moreover, no sign of pain, behavioral alterations, changes in food/water intake, or loss of physical activity was observed in mice between different treatment groups.

In conclusion, CS modified with OA in combination with MAN (COM) or AHP (COA) demonstrated superior cellular uptake and transfection efficiency *in vitro* and significantly enhanced downregulation of pro-inflammatory cytokines *in vivo* in high-fat diet induced obese-diabetic preclinical mouse model. Formulation prepared and optimized in this study were non-toxic and exhibited good biocompatibility *in vitro* and *in vivo* which is beneficial for treatment of a chronic disease like diabetes. Reduction in pro-inflammatory cytokine level correlated with improved insulin sensitivity, glucose tolerance and fasting blood glucose levels. Most importantly, the response resulting from CS nanomicelles mediated RNAi was prolonged and reflected in improved insulin response and glucose tolerance up to 6 weeks after single treatment. The results from this study demonstrate that CS nanomicelles mediated gene therapy is a promising strategy for attenuating insulin resistance, chief underlying factor in progression of diabetes. This is a safe and efficient therapy to potentially reverse the progression of disease and lower risk of associated-complications concomitant to the disease.

4.1. Future directions

Type 1 diabetes mellitus occurs due to selective autoimmune destruction of pancreatic β-cells, leading to absolute deficiency of insulin production. According to current knowledge it cannot be prevented, however, tight glycemic control with efficient exogenous insulin therapy can delay the onset and progression of associated complications. In this study, we optimized a thermosensitive copolymer-based *in situ* depot forming system capable of releasing insulin at basal level for up to three months. Moving forward, it would be necessary to study the effect of such delivery systems in non-rodent animal models such as pigs, dogs and primates.[310]

Additionally, long-term basal insulin therapy (> 1 year) over a period of multiple administrations should be studied while closely monitoring food intake, bolus insulin doses, weight gain and frequency of hyper/hypoglycemic episodes. This will be essential in rationalizing clinical outcomes in type-1 diabetes patients more effectively. Besides, improved thermal stability of insulin upon modification with zinc and chitosan can also be exploited for oral delivery of insulin prior to encapsulation in biocompatible polymeric delivery systems such as PLGA microspheres. Moreover, the PLA-PEG-PLA based thermosensitive copolymeric delivery system can further be used for sustained delivery of various other therapeutic proteins and peptides (salmon calcitonin, erythropoietin, monoclonal antibodies, *etc.*) which require frequent administration over prolonged duration.[311]

On the other hand, the incidence and prevalence of obesity and diabetes is growing at a rapid pace, affecting all age and socioeconomic groups in the world. Obesity has been recognized as a global epidemic that negatively affects our body and has been linked to multiple disorders including hypertension, coronary artery disease, gallbladder disease, osteoarthritis, breathing problems, cancer, cognitive dysfunction, insulin resistance, and type-2 diabetes.[312]

Results from our study show promising improvement in insulin sensitivity and glucose tolerance of high fat diet-induced obese diabetic mice following chitosan nanomicelles mediated downregulation of pro-inflammatory cytokines. More studies need to be performed for dose optimization and to study long-term effect of this treatment in obesity, insulin resistance and type-2 disease pathophysiology as suggested in **figure 55**. Studying other immunological as well as non-immunological parameters such as leptin, adiponectin, peroxisome proliferator–activated receptor (PPAR)-γ, smoking, alcohol consumption, lifestyle factors *etc.* alongside targeting inflammatory cytokines may also be of particular interest.[313–315] Adiponectin, a major insulin sensitizing adipokine secreted by adipocytes plays an important role in glucose and lipid metabolism. Adiponectin levels have been found to be significantly reduced in obesity and type-2 diabetes.[279] Gene therapy to increase adiponectin concentration in insulin sensitive tissues may also potentially help improve insulin sensitivity. Additionally, combination of gene therapy with anti-hyperglycemic (e.g. metformin) and/or anti-obesity (e.g. orlistat) drugs may also be useful in simultaneous management of insulin resistance and the underlying pathological mechanisms in obesity to reverse the disease trend and obtain better patient outcomes.

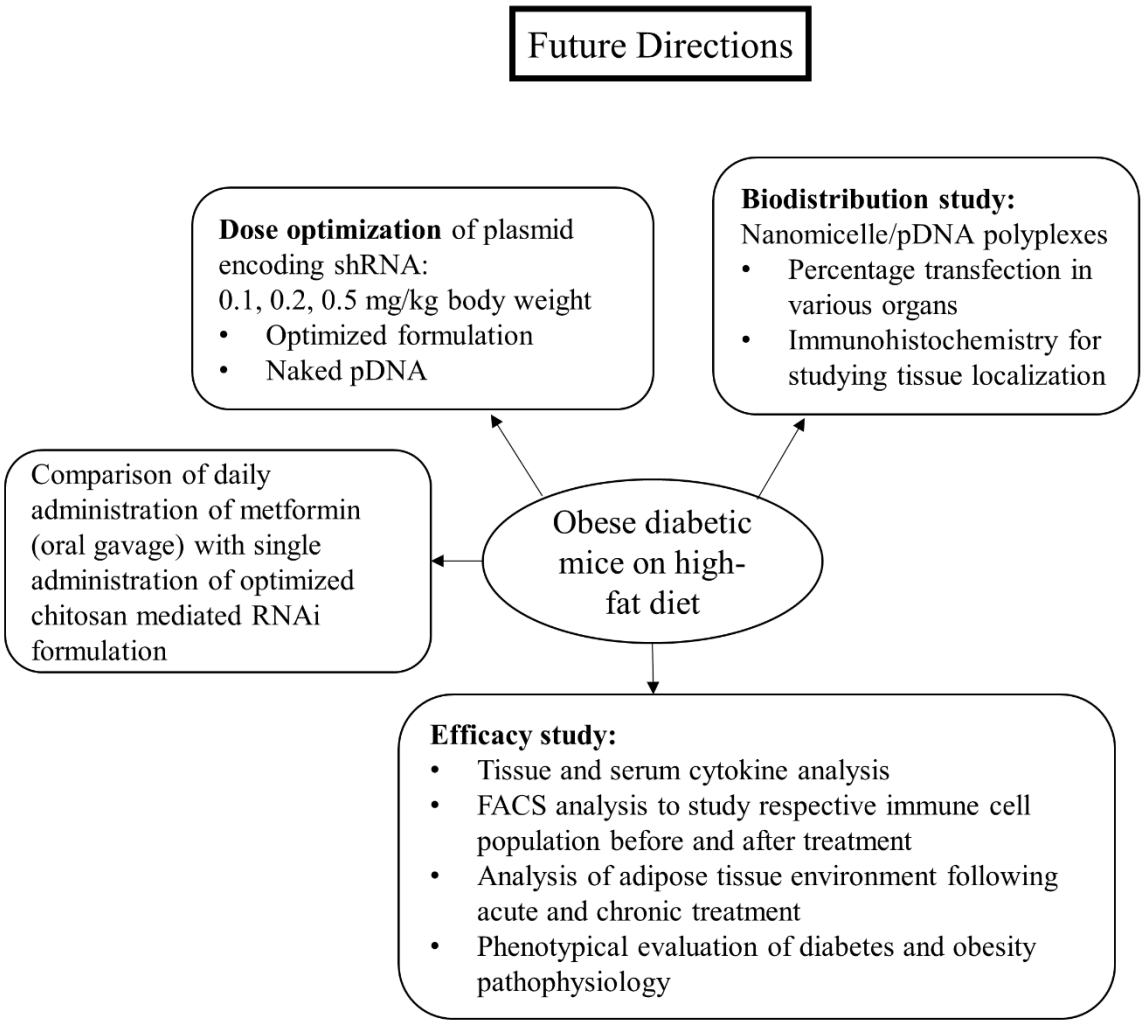

Figure 55. Suggested future studies for studying chitosan nanomicelles mediated downregulation of pro-inflammatory cytokines in high fat diet induced obese diabetic mice for the treatment of insulin resistance.

REFERENCES

1. Cataloguing, W. L. *Global Report on Diabetes*. *ISBN* **978**, (2016).
2. Centers for Disease Control and Prevention. *National Diabetes Statistics Report*. (2017).
3. Diabetes Control and Complications Trial Research. The Effect of Intensive Treatment of Diabetes on the Development and Progression of Long-Term Complications in Insulin-Dependent Diabetes Mellitus. *N. Engl. J. Med.* **329**, 977–986 (1993).
4. World Health Organization. *The top 10 causes of death*. (2018).
5. Mayo Clinic. *Diabetes - Symptoms and causes*. (2018).
6. Yang, W. *et al.* Economic costs of diabetes in the U.S. *Diabetes Care* **41**, 917–928 (2017).
7. Herman, W. H. The economic costs of diabetes: Is it time for a new treatment paradigm? *Diabetes Care* **36**, 775–776 (2013).
8. Randall, L. *et al.* Recurrent diabetic ketoacidosis in inner-city minority patients: Behavioral, socioeconomic, and psychosocial factors. *Diabetes Care* **34**, 1891–1896 (2011).
9. Sari Harrar. *Insulin Prices Skyrocketing: Diabetics Paying the Price in More Ways Than One*. (2018).
10. Juvenile Diabetes Research Foundation. Type 1 Diabetes Facts. **56**, (2011).
11. Polonsky, W. H. & Henry, R. R. Poor medication adherence in type 2 diabetes: Recognizing the scope of the problem and its key contributors. *Patient Prefer. Adherence* **10**, 1299–1306 (2016).
12. Wajngot, A. *et al.* Quantitative contributions of gluconeogenesis to glucose production during fasting in type 2 diabetes mellitus. *Metabolism.* **50**, 47–52 (2001).
13. Coelho, J. F. J., Ferreira, P. & Gil, M. H. New Approaches in Drug Delivery Systems: Application Treatment. *Infect. Disord. - Drug Targets* **2**, 119–128 (2008).
14. Porcellati, F., Lucidi, P., Bolli, G. B. & Fanelli, C. G. Thirty years of research on the dawn phenomenon: Lessons to optimize blood glucose control in diabetes. *Diabetes Care* **36**, 3860–3862 (2013).
15. Hu, X. *et al.* H2O2-Responsive Vesicles Integrated with Transcutaneous Patches for Glucose-Mediated Insulin Delivery. *ACS Nano* **11**, 613–620 (2017).
16. Gupta, R. & Mohanty, S. Controlled release of insulin from folic acid-insulin complex nanoparticles. *Colloids Surfaces B Biointerfaces* **154**, 48–54 (2017).
17. Choi, S. & Kim, S. W. Injectable Biodegradable Triblock Copolymer Depot in ZDF Rats. **20**, 2008–2010 (2008).
18. Barnes, A. S. The Epidemic of Obesity and Diabetes. **38**, (2011).
19. Verma, S. & Hussain, M. E. Obesity and diabetes: An update. *Diabetes Metab. Syndr. Clin. Res. Rev.* **11**, 73–79 (2017).
20. Fuster, J. J., Ouchi, N., Gokce, N. & Walsh, K. Obesity-induced Changes in Adipose Tissue Microenvironment and Their Impact on Cardiovascular Disease. *Circ. Res.* **118**, 1786–1807 (2016).
21. Castoldi, A., De Souza, C. N., Saraiva Câmara, N. O. & Moraes-Vieira, P. M. The macrophage switch in obesity development. *Front. Immunol.* **6**, 1–11 (2016).
22. Stern, J. H., Rutkowski, J. M. & Scherer, P. E. Adiponectin, Leptin, and Fatty Acids in the Maintenance of Metabolic Homeostasis through Adipose Tissue Crosstalk. *Cell Metab.* **23**, 770–784 (2016).

23. Codoñer-Franch, P. & Alonso-Iglesias, E. Resistin: Insulin resistance to malignancy. *Clin. Chim. Acta* **438**, 46–54 (2015).
24. Zentner, M. & Shih, C. Biodegradable block copolymeric compositions for drug delivery. **1**, (2004).
25. Jeong, B., Bae, Y. H. & Kim, S. W. Drug release from biodegradable injectable thermosensitive hydrogel of PEG – PLGA – PEG triblock copolymers. *J. Control. Release* **63**, 155–163 (2000).
26. Oak, M. Controlled delivery of basal level of insulin. 180 (2012).
27. Rathi, R. C. & Zentener, G. M. Biodegradable low molecular weight triblock poly(lactide-co-glycolide) polyethylene glycol copolymers having reverse thermal gelation properties. *Thin Films* **111111**, (2009).
28. Pratten, M. K., Lloyd, J. B., Hörpel, G. & Ringsdorf, H. Micelle-forming block copolymers : Pinocytosis by macrophages and interaction with model membranes. *Die Makromol. Chemie* **186**, 725–733 (1985).
29. Chen, S. & Singh, J. Controlled delivery of testosterone from smart polymer solution based systems: In vitro evaluation. *Int. J. Pharm.* **295**, 183–190 (2005).
30. Chen, S., Pieper, R., Webster, D. C. & Singh, J. Triblock copolymers: Synthesis, characterization, and delivery of a model protein. *Int. J. Pharm.* **288**, 207–218 (2005).
31. Tang, Y. & Singh, J. Biodegradable and biocompatible thermosensitive polymer based injectable implant for controlled release of protein. *Int. J. Pharm.* **365**, 34–43 (2009).
32. Tang, Y. & Singh, J. Thermosensitive drug delivery system of salmon calcitonin: In vitro release, in vivo absorption, bioactivity and therapeutic efficacies. *Pharm. Res.* **27**, 272–284 (2010).
33. Lu, L. *et al.* Complete regression of xenograft tumors using biodegradable mPEG-PLA-SN38 block copolymer micelles. *Colloids Surfaces B Biointerfaces* **142**, 417–423 (2016).
34. Gao, Y., Sun, Y., Ren, F. & Gao, S. PLGA-PEG-PLGA hydrogel for ocular drug delivery of dexamethasone acetate. *Drug Dev Ind Pharm* **36**, 1131–1138 (2010).
35. Li, K. *et al.* A long-acting formulation of a polypeptide drug exenatide in treatment of diabetes using an injectable block copolymer hydrogel. *Biomaterials* **34**, 2834–2842 (2013).
36. Kim, Y. J. *et al.* Controlled release of insulin from biodegradable triblock copolymer. *Pharm. Res.* **18**, 548–550 (2001).
37. Zentner, G. M. *et al.* Biodegradable block copolymers for delivery of proteins and water-insoluble drugs. *J. Control. Release* **72**, 203–215 (2001).
38. Chen, S., Pederson, D., Oak, M. & Singh, J. In Vivo Absorption of Steroidal Hormones from Smart Polymer Based Delivery Systems. *J. Pharm. Sci.* **99**, 3381–3388 (2010).
39. Ma, H. *et al.* PLK1shRNA and doxorubicin co-loaded thermosensitive PLGA-PEG-PLGA hydrogels for osteosarcoma treatment. *Biomaterials* **35**, 8723–8734 (2014).
40. Lipp, L., Sharma, D., Banerjee, A. & Singh, J. Controlled Delivery of Salmon Calcitonin Using Thermosensitive Triblock Copolymer Depot for Treatment of Osteoporosis. *ACS omega* **4**, 1157–1166 (2019).
41. Singh, S., Webster, D. C. & Singh, J. Thermosensitive polymers: Synthesis, characterization, and delivery of proteins. *Int. J. Pharm.* **341**, 68–77 (2007).
42. Al-Tahami, K., Oak, M., Mandke, R. & Singh, J. Basal level insulin delivery: In vitro release, stability, biocompatibility, and in vivo absorption from thermosensitive triblock copolymers. *J. Pharm. Sci.* **100**, 4790–4803 (2011).

43. Oak, M. & Singh, J. Controlled delivery of basal level of insulin from chitosan-zinc-insulin-complex-loaded thermosensitive copolymer. *J. Pharm. Sci.* **101**, 1079–96 (2012).
44. Oak, M. & Singh, J. Chitosan-zinc-insulin complex incorporated thermosensitive polymer for controlled delivery of basal insulin in vivo. *J. Control. Release* **163**, 145–153 (2012).
45. Motiei, M., Kashanian, S., Lucia, L. A. & Khazaei, M. Intrinsic parameters for the synthesis and tuned properties of amphiphilic chitosan drug delivery nanocarriers. *Journal of Controlled Release* (2017). doi:10.1016/j.jconrel.2017.06.010
46. Tharanathan, R. N. & Kittur, F. S. Chitin - The Undisputed Biomolecule of Great Potential. *Critical Reviews in Food Science and Nutrition* (2003). doi:10.1080/10408690390826455
47. VOLLENWEIDER, R. A. Concerning calculation methods and limitations of proxy-estimates of Proteins, Carbohydrates and Lipids in crustacean zooplankton from CHN analyses. *J. Limnol.* (2000). doi:10.4081/jlimnol.2000.170
48. Cauchie, H. M. Chitin production by arthropods in the hydrosphere. *Hydrobiologia* (2002). doi:10.1023/A:1015615819301
49. Lee, M. K. *et al.* The use of chitosan as a condensing agent to enhance emulsion-mediated gene transfer. *Biomaterials* (2005). doi:10.1016/j.biomaterials.2004.07.008
50. Shu, X. Z. & Zhu, K. J. The influence of multivalent phosphate structure on the properties of ionically cross-linked chitosan films for controlled drug release. *Eur. J. Pharm. Biopharm.* (2002). doi:10.1016/S0939-6411(02)00052-8
51. Rao, S. B. & Sharma, C. P. Use of chitosan as a biomaterial: Studies on its safety and hemostatic potential. *J. Biomed. Mater. Res.* (1997). doi:10.1002/(SICI)1097-4636(199701)34:1<21::AID-JBM4>3.0.CO;2-P
52. Aspden, T. J. *et al.* Chitosan as a nasal delivery system: The effect of chitosan solutions on in vitro and in vivo mucociliary transport rates in human turbinates and volunteers. in *Journal of Pharmaceutical Sciences* (1997). doi:10.1021/js960182o
53. Struszczyk, M. H. Chitin and Chitosan: Part I. Properties and production. *Polimery/Polymers* (2002).
54. Diebold, Y. *et al.* Ocular drug delivery by liposome-chitosan nanoparticle complexes (LCS-NP). *Biomaterials* (2007). doi:10.1016/j.biomaterials.2006.11.028
55. Kean, T. & Thanou, M. Biodegradation, biodistribution and toxicity of chitosan. *Advanced Drug Delivery Reviews* (2010). doi:10.1016/j.addr.2009.09.004
56. Lai, W. F. & Lin, M. C. M. Nucleic acid delivery with chitosan and its derivatives. *Journal of Controlled Release* (2009). doi:10.1016/j.jconrel.2008.11.021
57. Kato, Y., Onishi, H. & Machida, Y. Application of Chitin and Chitosan Derivatives in the Pharmaceutical Field. *Curr. Pharm. Biotechnol.* (2003). doi:10.2174/1389201033489748
58. Onishi, H. & Machida, Y. Biodegradation and distribution of water-soluble chitosan in mice. *Biomaterials* **20**, 175–182 (1999).
59. Lizardi-Mendoza, J., Argüelles Monal, W. M. & Goycoolea Valencia, F. M. Chemical Characteristics and Functional Properties of Chitosan. in *Chitosan in the Preservation of Agricultural Commodities* (2016). doi:10.1016/B978-0-12-802735-6.00001-X
60. Okuyama, K. *et al.* Structural diversity of chitosan and its complexes. *Carbohydr. Polym.* (2000). doi:10.1016/S0144-8617(99)00142-3
61. Ogawa, K., Yui, T. & Okuyama, K. Three D structures of chitosan. *International Journal of Biological Macromolecules* (2004). doi:10.1016/j.ijbiomac.2003.11.002

62. Wu, L. Q. *et al.* Voltage-dependent assembly of the polysaccharide chitosan onto an electrode surface. *Langmuir* (2002). doi:10.1021/la020381p
63. Mao, S., Sun, W. & Kissel, T. Chitosan-based formulations for delivery of DNA and siRNA. *Advanced Drug Delivery Reviews* (2010). doi:10.1016/j.addr.2009.08.004
64. Skorik, A. S. K. and S. A. and Y. A. Chitosan and its derivatives: vectors in gene therapy. *Russ. Chem. Rev.* **86**, 231 (2017).
65. Nilsen-Nygaard, J. *et al.* Chitosan: Gels and Interfacial Properties. *Polymers (Basel).* **7**, 552–579 (2015).
66. El-Hefian, E. A., Elgannoudi, E. S., Mainal, A. & Yahaya, A. H. Characterization of chitosan in acetic acid: Rheological and thermal studies. *Turkish J. Chem.* **34**, 47–56 (2010).
67. Zheng, L.-Y. & Zhu, J.-F. Study on antimicrobial activity of chitosan with different molecular weights. *Carbohydr. Polym.* **54**, 527–530 (2003).
68. Muzzarelli, R. *et al.* Antimicrobial properties of N-carboxybutyl chitosan. *Antimicrob. Agents Chemother.* **34**, 2019–23 (1990).
69. Messai, I. *et al.* Poly(D,L-lactic acid) and chitosan complexes: Interactions with plasmid DNA. *Colloids Surfaces A Physicochem. Eng. Asp.* (2005). doi:10.1016/j.colsurfa.2004.12.023
70. Köping-Höggård, M. *et al.* Chitosan as a nonviral gene delivery system. Structure-property relationships and characteristics compared with polyethylenimine in vitro and after lung administration in vivo. *Gene Ther.* **8**, 1108–1121 (2001).
71. Kiang, T., Wen, J., Lim, H. W. & Leong, K. W. The effect of the degree of chitosan deacetylation on the efficiency of gene transfection. *Biomaterials* (2004). doi:10.1016/j.biomaterials.2003.12.036
72. Romøren, K., Pedersen, S., Smistad, G., Evensen, Ø. & Thu, B. J. The influence of formulation variables on in vitro transfection efficiency and physicochemical properties of chitosan-based polyplexes. *Int. J. Pharm.* (2003). doi:10.1016/S0378-5173(03)00301-6
73. Lavertu, M., Méthot, S., Tran-Khanh, N. & Buschmann, M. D. High efficiency gene transfer using chitosan/DNA nanoparticles with specific combinations of molecular weight and degree of deacetylation. *Biomaterials* **27**, 4815–4824 (2006).
74. Xu, T., Xin, M., Li, M., Huang, H. & Zhou, S. Synthesis, characteristic and antibacterial activity of N,N,N-trimethyl chitosan and its carboxymethyl derivatives. *Carbohydr. Polym.* **81**, 931–936 (2010).
75. Park, J. H., Saravanakumar, G., Kim, K. & Kwon, I. C. Targeted delivery of low molecular drugs using chitosan and its derivatives. *Advanced Drug Delivery Reviews* (2010). doi:10.1016/j.addr.2009.10.003
76. Issa, M. M. *et al.* Targeted gene delivery with trisaccharide-substituted chitosan oligomers in vitro and after lung administration in vivo. *J. Control. Release* (2006). doi:10.1016/j.jconrel.2006.06.029
77. Kadiyala, I., Loo, Y., Roy, K., Rice, J. & Leong, K. W. Transport of chitosan-DNA nanoparticles in human intestinal M-cell model versus normal intestinal enterocytes. *Eur. J. Pharm. Sci.* (2010). doi:10.1016/j.ejps.2009.11.002
78. Gao, S. *et al.* Galactosylated low molecular weight chitosan as DNA carrier for hepatocyte-targeting. *Int. J. Pharm.* (2003). doi:10.1016/S0378-5173(03)00082-6

79. Jiang, H. L. *et al.* Galactosylated poly(ethylene glycol)-chitosan-graft-polyethylenimine as a gene carrier for hepatocyte-targeting. *J. Control. Release* (2008). doi:10.1016/j.jconrel.2008.07.029
80. Corbet, C. *et al.* Delivery of siRNA targeting tumor metabolism using non-covalent PEGylated chitosan nanoparticles: Identification of an optimal combination of ligand structure, linker and grafting method. *J. Control. Release* (2016). doi:10.1016/j.jconrel.2015.12.020
81. Jin, H. *et al.* Folate-Chitosan Nanoparticles Loaded with Ursolic Acid Confer Anti-Breast Cancer Activities in vitro and in vivo. *Sci. Rep.* (2016). doi:10.1038/srep30782
82. Breunig, M. *et al.* Mechanistic investigation of poly(ethylene imine)-based siRNA delivery: Disulfide bonds boost intracellular release of the cargo. *J. Control. Release* (2008). doi:10.1016/j.jconrel.2008.05.016
83. Varkouhi, A. K. *et al.* Gene silencing activity of siRNA polyplexes based on thiolated N, N, N -trimethylated chitosan. *Bioconjug. Chem.* (2010). doi:10.1021/bc1003789
84. Martien, R., Loretz, B., Thaler, M., Majzoob, S. & Bernkop-Schnürch, A. Chitosan-thioglycolic acid conjugate: An alternative carrier for oral nonviral gene delivery? *J. Biomed. Mater. Res. - Part A* (2007). doi:10.1002/jbm.a.31135
85. Lee, D. *et al.* Thiolated chitosan/DNA nanocomplexes exhibit enhanced and sustained gene delivery. *Pharm. Res.* (2007). doi:10.1007/s11095-006-9136-9
86. Layek, B., Lipp, L. & Singh, J. Cell penetrating peptide conjugated chitosan for enhanced delivery of nucleic acid. *Int. J. Mol. Sci.* **16**, 28912–28930 (2015).
87. Sharma, G. *et al.* Cell penetrating peptide tethered bi-ligand liposomes for delivery to brain in vivo: Biodistribution and transfection. *J. Control. Release* **167**, 1–10 (2013).
88. Gao, Y. *et al.* Arginine-chitosan/DNA self-assemble nanoparticles for gene delivery: In vitro characteristics and transfection efficiency. *Int. J. Pharm.* (2008). doi:10.1016/j.ijpharm.2008.03.037
89. Malhotra, M., Tomaro-Duchesneau, C. & Prakash, S. Synthesis of TAT peptide-tagged PEGylated chitosan nanoparticles for siRNA delivery targeting neurodegenerative diseases. *Biomaterials* (2013). doi:10.1016/j.biomaterials.2012.10.013
90. Pichon, C., Billiet, L. & Midoux, P. Chemical vectors for gene delivery: Uptake and intracellular trafficking. *Current Opinion in Biotechnology* (2010). doi:10.1016/j.copbio.2010.07.003
91. Mumper, R. J. *et al.* Polyvinyl derivatives as novel interactive polymers for controlled gene delivery to muscle. *Pharm. Res.* (1996). doi:10.1023/A:1016039330870
92. Glasspool-Malone, J. & Malone, R. W. Marked Enhancement of Direct Respiratory Tissue Transfection by Aurintricarboxylic Acid. *Hum. Gene Ther.* (1999). doi:10.1089/10430349950017707
93. Kawabata, K., Takakura, Y. & Hashida, M. The Fate of Plasmid DNA After Intravenous Injection in Mice: Involvement of Scavenger Receptors in Its Hepatic Uptake. *Pharm. Res. An Off. J. Am. Assoc. Pharm. Sci.* (1995). doi:10.1023/A:1016248701505
94. Thibault, M., Nimesh, S., Lavertu, M. & Buschmann, M. D. Intracellular trafficking and decondensation kinetics of chitosan-pDNA polyplexes. *Mol. Ther.* (2010). doi:10.1038/mt.2010.143
95. Corsi, K., Chellat, F., Yahia, L. & Fernandes, J. C. Mesenchymal stem cells, MG63 and HEK293 transfection using chitosan-DNA nanoparticles. *Biomaterials* (2003). doi:10.1016/S0142-9612(02)00507-0

96. Peng, S. F. *et al.* Mechanisms of cellular uptake and intracellular trafficking with chitosan/DNA/poly(γ-glutamic acid) complexes as a gene delivery vector. *Biomaterials* (2011). doi:10.1016/j.biomaterials.2010.08.081
97. Sahay, G., Alakhova, D. Y. & Kabanov, A. V. Endocytosis of nanomedicines. *Journal of Controlled Release* (2010). doi:10.1016/j.jconrel.2010.01.036
98. Mao, H. Q. *et al.* Chitosan-DNA nanoparticles as gene carriers: Synthesis, characterization and transfection efficiency. *J. Control. Release* (2001). doi:10.1016/S0168-3659(00)00361-8
99. Fang, N., Chan, V., Mao, H. Q. & Leong, K. W. Interactions of phospholipid bilayer with chitosan: Effect of molecular weight and pH. *Biomacromolecules* (2001). doi:10.1021/bm015548s
100. JONES, R. A. *et al.* Poly(2-alkylacrylic acid) polymers deliver molecules to the cytosol by pH-sensitive disruption of endosomal vesicles. *Biochem. J.* (2003). doi:10.1042/bj20021945
101. Tae, H. K., Su, I. K., Akaike, T. & Chong, S. C. Synergistic effect of poly(ethylenimine) on the transfection efficiency of galactosylated chitosan/DNA complexes. *J. Control. Release* (2005). doi:10.1016/j.jconrel.2005.03.024
102. Kim, T. H., Ihm, J. E., Choi, Y. J., Nah, J. W. & Cho, C. S. Efficient gene delivery by urocanic acid-modified chitosan. *J. Control. Release* (2003). doi:10.1016/j.jconrel.2003.08.017
103. Regnström, K., Ragnarsson, E. G. E., Fryknäs, M., Köping-Höggård, M. & Artursson, P. Gene expression profiles in mouse lung tissue after administration of two cationic polymers used for nonviral gene delivery. *Pharm. Res.* (2006). doi:10.1007/s11095-006-9563-7
104. Raftery, R., O'Brien, F. J. & Cryan, S. A. Chitosan for gene delivery and orthopedic tissue engineering applications. *Molecules* (2013). doi:10.3390/molecules18055611
105. Badding, M. A., Lapek, J. D., Friedman, A. E. & Dean, D. A. Proteomic and functional analyses of protein-DNA complexes during gene transfer. *Mol. Ther.* (2013). doi:10.1038/mt.2012.231
106. Badding, M. A., Vaughan, E. E. & Dean, D. A. Transcription factor plasmid binding modulates microtubule interactions and intracellular trafficking during gene transfer. *Gene Ther.* (2012). doi:10.1038/gt.2011.96
107. Dean, D. A. Import of plasmid DNA into the nucleus is sequence specific. *Exp. Cell Res.* (1997). doi:10.1006/excr.1996.3427
108. Dowty, M. E., Williams, P., Zhang, G., Hagstrom, J. E. & Wolff, J. A. Plasmid DNA entry into postmitotic nuclei of primary rat myotubes. *PNAS* (1995). doi:10.1073/pnas.92.10.4572
109. Illum, L. Chitosan and its use as a pharmaceutical excipient. *Pharmaceutical Research* (1998). doi:10.1023/A:1011929016601
110. Roller, S. & Covill, N. The antifungal properties of chitosan in laboratory media and apple juice. *Int. J. Food Microbiol.* (1999). doi:10.1016/S0168-1605(99)00006-9
111. Coma, V., Deschamps, A. & Martial-Gros, A. Bioactive Packaging Materials from Edible Chitosan Polymer - Antimicrobial Activity Assessment on Dairy-Related Contaminants. *J. Food Sci.* (2003). doi:10.1111/j.1365-2621.2003.tb05806.x

112. Wedmore, I., McManus, J. G., Pusateri, A. E. & Holcomb, J. B. A special report on the chitosan-based hemostatic dressing: Experience in current combat operations. *J. Trauma - Inj. Infect. Crit. Care* **60**, 655–658 (2006).
113. Chung, M. J., Park, J. K. & Park, Y. Il. Anti-inflammatory effects of low-molecular weight chitosan oligosaccharides in IgE–antigen complex-stimulated RBL-2H3 cells and asthma model mice. *Int. Immunopharmacol.* **12**, 453–459 (2012).
114. Chatelet, C., Damour, O. & Domard, A. Influence of the degree of acetylation on some biological properties of chitosan films. *Biomaterials* **22**, 261–268 (2001).
115. Cao, W. *et al.* Effects of the degree of deacetylation on the physicochemical properties and Schwann cell affinity of chitosan films. *J. Biomater. Appl.* **20**, 157–177 (2005).
116. Revi, D., Paul, W., Anilkumar, T. V. & Sharma, C. P. Chitosan scaffold co-cultured with keratinocyte and fibroblast heals full thickness skin wounds in rabbit. *J. Biomed. Mater. Res. - Part A* **102**, 3273–3281 (2014).
117. Funkhouser, J. D. & Aronson, N. N. Chitinase family GH18: Evolutionary insights from the genomic history of a diverse protein family. *BMC Evol. Biol.* **7**, 1–16 (2007).
118. Kean, T. & Thanou, M. Chitin and chitosan - Sources, production and medical applications. in *Renewable Resources for Functional Polymers and Biomaterials: Polysaccharides, Proteins and Polyesters* 327–361 (2011). doi:10.1039/9781849733519-00292
119. Xu, J., McCarthy, S. P., Gross, R. A. & Kaplan, D. L. Chitosan film acylation and effects on biodegradability. *Macromolecules* (1996). doi:10.1021/ma951638b
120. Yang, Y. M., Hu, W., Wang, X. D. & Gu, X. S. The controlling biodegradation of chitosan fibers by N-acetylation in vitro and in vivo. *J. Mater. Sci. Mater. Med.* **18**, 2117–2121 (2007).
121. Hirano, S. *et al.* Enhancement of serum lysozyme activity by injecting a mixture of chitosan oligosaccharides intravenously in rabbits. *Agric. Biol. Chem.* **55**, 2623–2625 (1991).
122. Harding, S. E. Some observations on the effects of bioprocessing on biopolymer stability. *J. Drug Target.* **18**, 732–740 (2010).
123. Jones, C., Crane, D., Lemercinier, X., Bolgiano, B. & Yost, S. Physicochemical studies of the structure and stability of poly-saccharide-protein conjugate vaccines. *Dev. Biol. Stand.* **87**, 143–151 (1996).
124. Kam, H. M., Khor, E. & Lim, L. Y. Storage of partially deacetylated chitosan films. *J. Biomed. Mater. Res.* **48**, 881–888 (1999).
125. Knapczyk, J. Antimycotic buccal and vaginal tablets with chitosan. *Int. J. Pharm.* **88**, 9–14 (1992).
126. Patel, B. J., Vignesh, N. K. & Hortelano, G. Chitosan DNA nanoparticles for oral gene delivery. *World J. Med. Genet.* **6**, 22 (2016).
127. Jayakumar, R. *et al.* Chitosan conjugated DNA nanoparticles in gene therapy. *Carbohydr. Polym.* **79**, 1–8 (2010).
128. Leong, K. W. *et al.* DNA-polycation nanospheres as non-viral gene delivery vehicles. in *Journal of Controlled Release* (1998). doi:10.1016/S0168-3659(97)00252-6
129. Mucha, M. & Pawlak, A. Complex study on chitosan degradability. *Polimery/Polymers* **47**, 509–516 (2002).

130. M Buys, G., Plessis, L., Marais, A., Kotzé, A. & Hamman, J. *Direct Compression Of Chitosan: Process And Formulation Factors To Improve Powder Flow And Tablet Performance. Current drug delivery* **10**, (2013).
131. Wanjun, T., Cunxin, W. & Donghua, C. Kinetic studies on the pyrolysis of chitin and chitosan. *Polym. Degrad. Stab.* **87**, 389–394 (2005).
132. López, F. A., Mercê, A. L. R., Alguacil, F. J. & López-Delgado, A. A kinetic study on the thermal behaviour of chitosan. *J. Therm. Anal. Calorim.* **91**, 633–639 (2008).
133. Varum, K. M., Ottoy, M. H. & Smidsrod, O. Acid hydrolysis of chitosans. *Carbohydr. Polym.* **46**, 89–98 (2001).
134. Nguyen, T. T. B., Hein, S., Ng, C. H. & Stevens, W. F. Molecular stability of chitosan in acid solutions stored at various conditions. *J. Appl. Polym. Sci.* **107**, 2588–2593 (2008).
135. Hafner, A., Dürrigl, M., Pepić, I. & Filipović-Grčić, J. Short- and long-term stability of lyophilised melatonin-loaded lecithin/chitosan nanoparticles. *Chem. Pharm. Bull. (Tokyo).* **59**, 1117–1123 (2011).
136. Schuetz, Y. B., Gurny, R. & Jordan, O. A novel thermoresponsive hydrogel based on chitosan. *Eur. J. Pharm. Biopharm.* **68**, 19–25 (2008).
137. Yang, F. *et al.* Anti-tumor effects in mice induced by survivin-targeted siRNA delivered through polysaccharide nanoparticles. *Biomaterials* **34**, 5689–5699 (2013).
138. Tahamtan, A. *et al.* Antitumor effect of therapeutic HPV DNA vaccines with chitosan-based nanodelivery systems. *J. Biomed. Sci.* **21**, 69 (2014).
139. Layek, B., Lipp, L. & Singh, J. APC targeted micelle for enhanced intradermal delivery of hepatitis B DNA vaccine. *J. Control. Release* **207**, 143–153 (2015).
140. Guliyeva, U., Oner, F., Ozsoy, S. & Haziroglu, R. Chitosan microparticles containing plasmid DNA as potential oral gene delivery system. *Eur. J. Pharm. Biopharm.* **62**, 17–25 (2006).
141. Noh, S. M. *et al.* Pegylated poly-l-arginine derivatives of chitosan for effective delivery of siRNA. *J. Control. Release* **145**, 159–164 (2010).
142. Mandke, R. & Singh, J. Cationic Nanomicelles for Delivery of Plasmids Encoding Interleukin-4 and Interleukin-10 for Prevention of Autoimmune Diabetes in Mice. *Pharm. Res.* **29**, 883–897 (2012).
143. Zhao, K. *et al.* Preparation and immunological effectiveness of a swine influenza DNA vaccine encapsulated in chitosan nanoparticles. *Vaccine* **29**, 8549–8556 (2011).
144. Sawaengsak, C. *et al.* Intranasal chitosan-DNA vaccines that protect across influenza virus subtypes. *Int. J. Pharm.* **473**, 113–125 (2014).
145. Jean, M. *et al.* Chitosan-plasmid nanoparticle formulations for IM and SC delivery of recombinant FGF-2 and PDGF-BB or generation of antibodies. *Gene Ther.* **16**, 1097–1110 (2009).
146. Lee, S. J. *et al.* TNF-alpha gene silencing using polymerized siRNA/thiolated glycol chitosan nanoparticles for rheumatoid arthritis. *Mol. Ther.* **22**, 397–408 (2014).
147. Zhang, Y., Satterlee, A. & Huang, L. In vivo gene delivery by nonviral vectors: Overcoming hurdles. *Mol. Ther.* **20**, 1298–1304 (2012).
148. Nayerossadat, N., Ali, P. & Maedeh, T. Viral and nonviral delivery systems for gene delivery. *Adv. Biomed. Res.* **1**, 27 (2012).
149. Al-dosari, M. S. & Gao, X. Nonviral gene delivery: principle, limitations, and recent progress. *AAPS J.* **11**, 671–81 (2009).

150. Mansouri, S. *et al.* Chitosan-DNA nanoparticles as non-viral vectors in gene therapy: Strategies to improve transfection efficacy. *European Journal of Pharmaceutics and Biopharmaceutics* (2004). doi:10.1016/S0939-6411(03)00155-3
151. Ragelle, H., Vandermeulen, G. & Préat, V. Chitosan-based siRNA delivery systems. *J. Control. Release* **172**, 207–218 (2013).
152. Buschmann, M. D. *et al.* Chitosans for delivery of nucleic acids. *Adv. Drug Deliv. Rev.* (2013). doi:10.1016/j.addr.2013.07.005
153. Ji, J. *et al.* Chemical Modifications of Chitosan and Its Applications. *Polym. Plast. Technol. Eng.* **53**, 1494–1505 (2014).
154. Jiang, H.-L., Cui, P.-F., Xie, R.-L. & Cho, C.-S. *Chapter Six - Chemical Modification of Chitosan for Efficient Gene Therapy*. *Marine Carbohydrates: Fundamentals and Applications, Part B* **73**, (Elsevier Inc., 2014).
155. Sashiwa, H. & Aiba, S. I. Chemically modified chitin and chitosan as biomaterials. *Prog. Polym. Sci.* **29**, 887–908 (2004).
156. Zhang, J. *et al.* Chitosan modification and pharmaceutical/biomedical applications. *Mar. Drugs* **8**, 1962–1987 (2010).
157. Cheung, R. C. F., Ng, T. B., Wong, J. H. & Chan, W. Y. *Chitosan: An update on potential biomedical and pharmaceutical applications*. *Marine Drugs* **13**, (2015).
158. Whinnery, C. & Kirsch, W. M. Recent Advances in Chitosan- Based Gene Carrier Application and Design. **3**, (2016).
159. Rudzinski, W. E., Palacios, A., Ahmed, A., Lane, M. A. & Aminabhavi, T. M. Targeted delivery of small interfering RNA to colon cancer cells using chitosan and PEGylated chitosan nanoparticles. *Carbohydr. Polym.* **147**, 323–332 (2016).
160. Kwon, O. J., Kang, E., Choi, J. W., Kim, S. W. & Yun, C. O. Therapeutic targeting of chitosan-PEG-folate-complexed oncolytic adenovirus for active and systemic cancer gene therapy. *J. Control. Release* **169**, 257–265 (2013).
161. Yhee, J. Y. *et al.* Cancer-targeted MDR-1 siRNA delivery using self-cross-linked glycol chitosan nanoparticles to overcome drug resistance. *J. Control. Release* **198**, 1–9 (2015).
162. Ragelle, H. *et al.* Intracellular siRNA delivery dynamics of integrin-targeted, PEGylated chitosan-poly(ethylene imine) hybrid nanoparticles: A mechanistic insight. *J. Control. Release* **211**, 1–9 (2015).
163. Van Woensel, M. *et al.* Development of siRNA-loaded chitosan nanoparticles targeting Galectin-1 for the treatment of glioblastoma multiforme via intranasal administration. *J. Control. Release* **10**, 71–81 (2016).
164. Rodríguez, P. *et al.* Redefining the Facilitated Transport of Mannose in Human Cells: Absence of a Glucose-Insensitive, High-Affinity Facilitated Mannose Transport System †. *Biochemistry* **44**, 313–320 (2005).
165. Freemerman, A. J. *et al.* Metabolic Reprogramming of Macrophages. *J. Biol. Chem.* **289**, 7884–7896 (2014).
166. Godoy, A. *et al.* Differential subcellular distribution of glucose transporters GLUT1–6 and GLUT9 in human cancer: Ultrastructural localization of GLUT1 and GLUT5 in breast tumor tissues. *J. Cell. Physiol.* **207**, 614–627 (2006).
167. Barnhart, K. F. *et al.* A peptidomimetic targeting white fat causes weight loss and improved insulin resistance in obese monkeys. *Sci. Transl. Med.* **3**, (2011).
168. Kolonin, M. G., Saha, P. K., Chan, L., Pasqualini, R. & Arap, W. Reversal of obesity by targeted ablation of adipose tissue. *Nat. Med.* **10**, 625–632 (2004).

169. Kolonin, M. G., Saha, P. K., Chan, L., Pasqualini, R. & Arap, W. Reversal of obesity by targeted ablation of adipose tissue. *Nat. Med.* **10**, 625–632 (2004).
170. Barnhart, K. F. *et al.* A Peptidomimetic Targeting White Fat Causes Weight Loss and Improved Insulin Resistance in Obese Monkeys. *Sci. Transl. Med.* **3**, 108ra112-108ra112 (2011).
171. Kim, D.-H., Woods, S. C. & Seeley, R. J. Peptide Designed to Elicit Apoptosis in Adipose Tissue Endothelium Reduces Food Intake and Body Weight. *Diabetes* **59**, 907–915 (2010).
172. Karges, B. *et al.* Association of Insulin Pump Therapy vs Insulin Injection Therapy With Severe Hypoglycemia, Ketoacidosis, and Glycemic Control Among Children, Adolescents, and Young Adults With Type 1 Diabetes. *JAMA* **318**, 1358–1366 (2017).
173. Pickup, J. C. & Renard, E. Long-Acting Insulin Analogs Versus Insulin Pump Therapy for the Treatment of Type 1 and Type 2 Diabetes. *Diabetes Care* **31**, S140–S145 (2008).
174. Laimer, M. *et al.* Variability of basal rate profiles in insulin pump therapy and association with complications in type 1 diabetes mellitus. *PLoS One* **11**, 1–10 (2016).
175. Sandor, M., Enscore, D., Weston, P. & Mathiowitz, E. Effect of protein molecular weight on release from micron-sized PLGA microspheres. *J. Control. Release* **76**, 297–311 (2001).
176. Oak, M., Mandke, R., Lakkadwala, S., Lipp, L. & Singh, J. Effect of molar mass and water solubility of incorporated molecules on the degradation profile of the triblock copolymer delivery system. *Polymers (Basel).* **7**, 1510–1521 (2015).
177. Horvath, K. *et al.* Long-acting insulin analogues versus NPH insulin (human isophane insulin) for type 2 diabetes mellitus. in *Cochrane Database of Systematic Reviews* (ed. Horvath, K.) (John Wiley & Sons, Ltd, 2007). doi:10.1002/14651858.CD005613.pub3
178. Haahr, H. & Heise, T. A review of the pharmacological properties of insulin degludec and their clinical relevance. *Clin. Pharmacokinet.* **53**, 787–800 (2014).
179. Gliemann, J. & Gammeltoft, S. The Biological Activity and the Binding Affinity of Modified Insulins Determined on Isolated Rat Fat Cells. *Diabetologia* **10**, 105–113 (1974).
180. Fleischman, A., Shoelson, S. E., Bernier, R. & Goldfine, A. B. Salsalate Improves Glycemia and Inflammatory Parameters in Obese Young Adults. *Diabetes Care* **31**, 289–294 (2008).
181. Goldfine, A. B. *et al.* Use of Salsalate to Target Inflammation in the Treatment of Insulin Resistance and Type 2 Diabetes. *Clin. Transl. Sci.* **1**, 36–43 (2008).
182. Goldfine, A. B. *et al.* Salicylate (Salsalate) in Patients With Type 2 Diabetes. *Ann. Intern. Med.* **159**, 1 (2013).
183. Van De Laar, M. *et al.* Pain Treatment in Arthritis-Related Pain: Beyond NSAIDs. *Open Rheumatol. J.* **6**, 320–330 (2012).
184. Gupta-Ganguli, M., Cox, K., Means, B., Gerling, I. & Solomon, S. S. Does therapy with anti-TNF-α improve glucose tolerance and control in patients with type 2 diabetes? *Diabetes Care* **34**, 2011 (2011).
185. Stanley, T. L. *et al.* TNF-alpha antagonism with etanercept decreases glucose and increases the proportion of high molecular weight adiponectin in obese subjects with features of the metabolic syndrome. *J. Clin. Endocrinol. Metab.* **96**, E146-50 (2011).
186. Report, C. Effects of infliximab treatment on insulin resistance in patients with rheumatoid arthritis and ankylosing spondylitis. *Ann Rheum Dis* **64**, 765–766 (2005).

187. Larsen, C. M. *et al.* Interleukin-1-receptor antagonist in type 2 diabetes mellitus. *N. Engl. J. Med.* **357**, 302–303; author reply 303 (2007).
188. Hensen, J., Howard, C. P., Walter, V. & Thuren, T. Impact of interleukin-1β antibody (canakinumab) on glycaemic indicators in patients with type 2 diabetes mellitus: Results of secondary endpoints from a randomized, placebo-controlled trial. *Diabetes Metab.* **39**, 524–531 (2013).
189. Ogawa, N. *et al.* Gene Therapy for Neuropathic Pain by Silencing of TNF-a Expression with Lentiviral Vectors Targeting the Dorsal Root Ganglion in Mice. *PLoS One* **9**, 1–13 (2014).
190. Ma, X. & Xu, S. TNF inhibitor therapy for rheumatoid arthritis. *Biomed. REPORTS* **1**, 177–184 (2013).
191. Tłustochowicz, M., Dębowska, G., Spytek, J. & Tłustochowicz, W. Rheumatoid arthritis treatment with TNF inhibitors and alternative procedures in case of its failure – results of the Polish survey in the context of EULAR recommendations. *Reumatol. Reumatol. Reumatol.* **53**, 200–206 (2015).
192. Donath, M. Y. & Shoelson, S. E. Type 2 diabetes as an inflammatory disease. *Nat. Rev. Immunol.* **11**, 98–107 (2011).
193. Di Rocco, P., Manco, M., Rosa, G., Greco, A. V. & Mingrone, G. Lowered tumor necrosis factor receptors, but not increased insulin sensitivity, with infliximab. *Obes. Res.* **12**, (2004).
194. Layek, B. & Singh, J. N-hexanoyl, N-octanoyl and N-decanoyl chitosans: Binding affinity, cell uptake, and transfection. *Carbohydr. Polym.* **89**, 403–410 (2012).
195. Layek, B. & Singh, J. Caproic acid grafted chitosan cationic nanocomplexes for enhanced gene delivery: Effect of degree of substitution. *Int. J. Pharm.* **447**, 182–191 (2013).
196. Sharma, D. & Singh, J. Synthesis and Characterization of Fatty Acid Grafted Chitosan Polymer and Their Nanomicelles for Nonviral Gene Delivery Applications. *Bioconjug. Chem.* **28**, 2772–2783 (2017).
197. Sharma, D., Arora, S. & Singh, J. Smart thermosensitive copolymer incorporating chitosan–zinc–insulin electrostatic complexes for controlled delivery of insulin: effect of chitosan chain length. *Int. J. Polym. Mater. Polym. Biomater.* 1–15 (2019). doi:10.1080/00914037.2019.1655750
198. Hayton, W. L. & Chen, T. Correction of Perfusate Concentration for Sample Removal. *J. Pharm. Sci.* **71**, 820–821 (1982).
199. Vital, P., Larrieta, E. & Hiriart, M. Sexual dimorphism in insulin sensitivity and susceptibility to develop diabetes in rats. *J. Endocrinol.* **190**, 425–432 (2006).
200. Aung, M. H., Kim, M. K., Olson, D. E., Thule, P. M. & Pardue, M. T. Early visual deficits in streptozotocin-induced diabetic long evans rats. *Investig. Ophthalmol. Vis. Sci.* **54**, 1370–1377 (2013).
201. Muranov, K. *et al.* Protection by iodide of lens from selenite-induced cataract. *Graefe's Arch. Clin. Exp. Ophthalmol.* **242**, 146–151 (2004).
202. Layek, B. & Singh, J. Amino acid grafted chitosan for high performance gene delivery: Comparison of amino acid hydrophobicity on vector and polyplex characteristics. *Biomacromolecules* **14**, 485–494 (2013).
203. Vishwanath, D. *et al.* Novel method to differentiate 3T3 L1 cells in vitro to produce highly sensitive adipocytes for a GLUT4 mediated glucose uptake using fluorescent glucose analog. *J. Cell Commun. Signal.* **7**, 129–140 (2013).

204. Kim, M.-Y., Kim, D.-H. & Do, M.-S. B-cell-activating factor is a regulator of adipokines and a possible mediator between adipocytes and macrophages. *Exp. Mol. Med.* **45**, e4 (2013).
205. Weisberg, S. P. *et al.* Obesity is associated with macrophage accumulation in adipose tissue. *J. Clin. Invest.* **112**, 1796–1808 (2003).
206. Hong, J., Stubbins, R. E., Smith, R. R., Harvey, A. E. & Nǔez, N. P. Differential susceptibility to obesity between male, female and ovariectomized female mice. *Nutr. J.* **8**, (2009).
207. Bowe, J. E. *et al.* Assessing glucose homeostasis in rodent models. *J. Endocrinol.* **222**, 13–25 (2014).
208. Mashat, M., Chrystyn, H., Clark, B. J. & Assi, K. H. Development and validation of HPLC method for the determination of tobramycin in urine samples post-inhalation using pre-column derivatisation with fluorescein isothiocyanate. *J. Chromatogr. B. Analyt. Technol. Biomed. Life Sci.* **869**, 59–66 (2008).
209. Layek, B. Evaluation of hydrophobically modified low molecular weight chitosan as a potential nonviral vector for DNA vaccine delivery. (North Dakota State University of Agriculture and Applied Science, 2014).
210. Ulery, B. D., Nair, L. S. & Laurencin, C. T. Biomedical applications of biodegradable polymers. *J. Polym. Sci. Part B Polym. Phys.* **49**, 832–864 (2011).
211. Jeong, B., Han Bae, Y. & Wan Kim, S. Biodegradable thermosensitive micelles of PEG-PLGA-PEG triblock copolymers. *Colloids Surfaces B Biointerfaces* **16**, 185–193 (1999).
212. Gyarmati, B., Hegyesi, N., Pukánszky, B. & Szilágyi, A. A colourimetric method for the determination of the degree of chemical cross-linking in aspartic acid-based polymer gels. *Express Polym. Lett.* **9**, 154–164 (2015).
213. Cayot, P. & Tainturier, G. The quantification of protein amino groups by the trinitrobenzenesulfonic acid method: A reexamination. *Anal. Biochem.* **249**, 184–200 (1997).
214. Iwai, W. *et al.* A neutron crystallographic analysis of T6 porcine insulin at 2.1 A resolution. *Acta Crystallogr. D. Biol. Crystallogr.* **65**, 1042–50 (2009).
215. Wang, Q. Z. *et al.* Protonation constants of chitosan with different molecular weight and degree of deacetylation. *Carbohydr. Polym.* **65**, 194–201 (2006).
216. Azevedo, J. R. *et al.* Physical and chemical characterization insulin-loaded chitosan-TPP nanoparticles. *J. Therm. Anal. Calorim.* **106**, 685–689 (2011).
217. Li, Y. V. Zinc and insulin in pancreatic beta-cells. *Endocrine* **45**, 178–189 (2014).
218. Jeong, B., Bae, Y. H. & Kim, S. W. Drug release from biodegradable injectable thermosensitive hydrogel of PEG–PLGA–PEG triblock copolymers. *J. Control. Release* **63**, 155–163 (2000).
219. Brange, J., Andersen, L., Laursen, E. D., Meyn, G. & Rasmussen, E. Toward Understanding Insulin Fibrillation. *J. Pharm. Sci.* **86**, 517–525 (1997).
220. Hua, Q. X., Jia, W. & Weiss, M. A. Conformational dynamics of insulin. *Front. Endocrinol. (Lausanne).* **2**, 1–11 (2011).
221. Brange, J. & Langkjoer, L. Insulin structure and stability. *Pharm. Biotechnol.* **5**, 315–50 (1993).
222. Xu, Y., Yan, Y., Seeman, D., Sun, L. & Dubin, P. L. Multimerization and aggregation of native-state insulin: Effect of zinc. *Langmuir* **28**, 579–586 (2012).

223. Kelly, S. M. & Price, N. C. The Use of Circular Dichroism in the Investigation of Protein Structure and Function. *Curr. Protein Pept. Sci.* **1**, 349–384 (2000).
224. Oak, M. & Singh, J. Chitosan–zinc–insulin complex incorporated thermosensitive polymer for controlled delivery of basal insulin in vivo. *J. Control. Release* **163**, 145–153 (2012).
225. Ellis, M. J., Darby, S. C., Jones, R. H. & Sonksen, P. H. In Vitro Bioactivity of Insulin Analogues: Lipogenic and Anti-Lipolytic Potency and Their Interaction with the Effect of Native Insulin. *Diabetologia* **15**, 403–410 (1978).
226. Al-Tahami, K., Oak, M., Mandke, R. & Singh, J. Basal level insulin delivery: In vitro release, stability, biocompatibility, and in vivo absorption from thermosensitive triblock copolymers. *J. Pharm. Sci.* **100**, 4790–4803 (2011).
227. Makadia, H. K. & Siegel, S. J. Poly Lactic-co-Glycolic Acid (PLGA) as biodegradable controlled drug delivery carrier. *Polymers (Basel).* **3**, 1377–1397 (2011).
228. Kucharczyk, P., Pavelková, A., Stloukal, P. & Sedlarík, V. Degradation behaviour of PLA-based polyesterurethanes under abiotic and biotic environments. *Polym. Degrad. Stab.* **129**, 222–230 (2016).
229. Mei, T. *et al.* Synthesis, characterization, and biocompatibility of alternating block polyurethanes based on PLA and PEG. *J. Biomed. Mater. Res. - Part A* **102**, 3243–3254 (2014).
230. Elsawy, M. A., Kim, K. H., Park, J. W. & Deep, A. Hydrolytic degradation of polylactic acid (PLA) and its composites. *Renew. Sustain. Energy Rev.* **79**, 1346–1352 (2017).
231. Straus, D. S. Effects of insulin on cellular growth and proliferation. *Life Sci.* **29**, 2131–2139 (1981).
232. Li, Y. V. Zinc and insulin in pancreatic beta-cells. *Endocrine* **45**, 178–189 (2014).
233. Teng, D. From Chitin to Chitosan. in *Chitosan-Based Hydrogels: Functions and Applications* (eds. Yao, K., Li, J., Yao, F. & Yin, Y.) 521 (CRC Press, 2017).
234. Ignatius, A. A. A. & Claes, L. E. E. In vitro biocompatibility of bioresorbable polymers: poly(L, DL-lactide) and poly(L-lactide-co-glycolide). *Biomaterials* **17**, 831–839 (1996).
235. Onuki, Y., Bhardwaj, U., Papadimitrakopoulos, F. & Burgess, D. J. A review of the biocompatibility of implantable devices: current challenges to overcome foreign body response. *J. Diabetes Sci. Technol.* **2**, 1003–15 (2008).
236. Veronese, F. M. & Pasut, G. PEGylation, successful approach. **10**, 1451–1458 (2005).
237. Wake, M. C., Gupta, P. K. & Mikos, A. G. Fabrication of pliable biodegradable polymer foams to engineer soft tissues. *Cell Transplant.* **5**, 465–73 (1996).
238. Bonacucina, G., Cespi, M., Mencarelli, G., Giorgioni, G. & Palmieri, G. F. Thermosensitive self-assembling block copolymers as drug delivery systems. *Polymers (Basel).* **3**, 779–811 (2011).
239. Chamberlain, J. J. *et al.* Treatment of Type 1 Diabetes: Synopsis of the 2017 American Diabetes Association Standards of Medical Care in Diabetes. *Ann. Intern. Med.* **167**, 493 (2017).
240. Matejko, B. *et al.* Basal Insulin Dose in Adults with Type 1 Diabetes Mellitus on Insulin Pumps in Real-Life Clinical Practice: A Single-Center Experience. *Adv. Med.* **2018**, 1473160 (2018).
241. Melmed, S., Polonsky, K. S., Larsen, P. R. & Kronenberg, H. *Williams textbook of endocrinology*. (2015).

242. (UK), N. C. G. C. *Type 1 Diabetes in Adults: Diagnosis and Management*. *Type 1 Diabetes in Adults: Diagnosis and Management* (National Institute for Health and Care Excellence (UK), 2015).
243. Xun, P. *et al.* Fasting Insulin Level Is Positively Associated With Incidence of Hypertension Among American Young Adults: A 20-year follow-up study. *Diabetes Care* **35**, 1532–1537 (2012).
244. Heise, T. & Pieber, T. R. Towards peakless, reproducible and long-acting insulins. An assessment of the basal analogues based on isoglycaemic clamp studies. *Diabetes, Obes. Metab.* **9**, 648–659 (2007).
245. Eliaschewitz, F. G. & Barreto, T. Concepts and clinical use of ultra-long basal insulin. *Diabetol. Metab. Syndr.* **8**, 1–8 (2016).
246. Jeong, B., Bae, Y. H. & Kim, S. W. Drug release from biodegradable injectable thermosensitive hydrogel of PEG-PLGA-PEG triblock copolymers. *J. Control. Release* **63**, 155–63 (2000).
247. Hildebrandt, P. Subcutaneous absorption of insulin in insulin-dependent diabetic patients. Influence of species, physico-chemical properties of insulin and physiological factors. *Dan. Med. Bull.* **38**, 337–46 (1991).
248. Kang, S., Brange, J., Burch, A., Volund, A. & Owens, D. R. Subcutaneous Insulin Absorption Explained by Insulin's Physicochemical Properties: Evidence From Absorption Studies of Soluble Human Insulin and Insulin Analogues in Humans. *Diabetes Care* **14**, 942–948 (1991).
249. Lodhi, G. *et al.* Chitooligosaccharide and its derivatives: preparation and biological applications. *Biomed Res. Int.* **2014**, 654913 (2014).
250. Mukherjee, S., Mondal, S., Deshmukh, A. A., Gopal, B. & Bagchi, B. What Gives an Insulin Hexamer Its Unique Shape and Stability? Role of Ten Confined Water Molecules. *J. Phys. Chem. B* **122**, 1631–1637 (2018).
251. Dhatariya, K. Blood Ketones: Measurement, Interpretation, Limitations, and Utility in the Management of Diabetic Ketoacidosis. *Rev. Diabet. Stud.* **13**, 217–225 (2016).
252. Elsner, M., Guldbakke, B., Tiedge, M., Munday, R. & Lenzen, S. Relative importance of transport and alkylation for pancreatic beta-cell toxicity of streptozotocin. *Diabetologia* **43**, 1528–1533 (2000).
253. Szkudelski, T. The mechanism of alloxan and streptozotocin action in B cells of the rat pancreas. *Physiol. Res.* **50**, 537–46 (2001).
254. Fineberg, S. E. *et al.* Immunological Responses to Exogenous Insulin. *Endocr. Rev.* **28**, 625–652 (2007).
255. Baker, M., Reynolds, H. M., Lumicisi, B. & Bryson, C. J. Immunogenicity of protein therapeutics: The key causes, consequences and challenges. *Self. Nonself.* **1**, 314–322 (2010).
256. Bloomfield, V. A. DNA condensation. *Curr. Opin. Struct. Biol.* **6**, 334–341 (1996).
257. Tsoi, M. *et al.* Characterization of condensed plasmid DNA models for studying the direct effect of ionizing radiation. *Biophys. Chem.* **147**, 104–10 (2010).
258. D'Abramo, M., Castellazzi, C. L., Orozco, M. & Amadei, A. On the Nature of DNA Hyperchromic Effect. *J. Phys. Chem. B* **117**, 8697–8704 (2013).
259. Kanda, H. *et al.* MCP-1 contributes to macrophage infiltration into adipose tissue, insulin resistance, and hepatic steatosis in obesity. *J. Clin. Invest.* **116**, 1494–1505 (2006).

260. Heinrich, F. *et al.* Morphologic, phenotypic, and transcriptomic characterization of classically and alternatively activated canine blood-derived macrophages in vitro. *PLoS One* **12**, e0183572 (2017).
261. Bartosh, T. J. & Ylostalo, J. H. Macrophage Inflammatory Assay. *Bio-protocol* **4**, (2014).
262. Armani, A. *et al.* Cellular models for understanding adipogenesis, adipose dysfunction, and obesity. *J. Cell. Biochem.* **110**, 564–572 (2010).
263. Zebisch, K., Voigt, V., Wabitsch, M. & Brandsch, M. Protocol for effective differentiation of 3T3-L1 cells to adipocytes. *Anal. Biochem.* **425**, 88–90 (2012).
264. Scott, M. A., Nguyen, V. T., Levi, B. & James, A. W. Current Methods of Adipogenic Differentiation of Mesenchymal Stem Cells. *Stem Cells Dev.* **20**, 1793 (2011).
265. Klemm, D. J. *et al.* Insulin-induced adipocyte differentiation. Activation of CREB rescues adipogenesis from the arrest caused by inhibition of prenylation. *J. Biol. Chem.* **276**, 28430–5 (2001).
266. Wang, B., He, C., Tang, C. & Yin, C. Effects of hydrophobic and hydrophilic modifications on gene delivery of amphiphilic chitosan based nanocarriers. *Biomaterials* **32**, 4630–4638 (2011).
267. Zamore, P. D., Tuschl, T., Sharp, P. A. & Bartel, D. P. RNAi: Double-stranded RNA directs the ATP-dependent cleavage of mRNA at 21 to 23 nucleotide intervals. *Cell* **101**, 25–33 (2000).
268. Singh, D. *et al.* RNA Interference Technology — Applications and Limitations. in *RNA Interference* (InTech, 2016). doi:10.5772/61760
269. Zeng, Y. & Cullen, B. R. RNA interference in human cells is restricted to the cytoplasm. *RNA* **8**, 855–860 (2002).
270. Elbashir, S. M., Lendeckel, W. & Tuschl, T. RNA interference is mediated by 21- and 22-nucleotide RNAs. *Genes Dev.* **15**, 188–200 (2001).
271. Tsujiuchi, T., Miller, A. D., Wakabayashi, T. & Natsume, A. RNA Interference Therapeutics for Tumor Therapy: Promising Work in Progress. in *Gene Therapy of Cancer: Translational Approaches from Preclinical Studies to Clinical Implementation: Third Edition* 393–408 (Elsevier Inc., 2013). doi:10.1016/B978-0-12-394295-1.00027-5
272. Rider, P., Carmi, Y. & Cohen, I. Biologics for Targeting Inflammatory Cytokines, Clinical Uses, and Limitations. *International Journal of Cell Biology* 1–11 (2016). doi:10.1155/2016/9259646
273. Zhang, J. M. & An, J. Cytokines, inflammation, and pain. *International Anesthesiology Clinics* **45**, 27–37 (2007).
274. Samaras, K., Botelho, N. K., Chisholm, D. J. & Lord, R. V. Subcutaneous and visceral adipose tissue gene expression of serum adipokines that predict type 2 diabetes. *Obesity (Silver Spring).* **18**, 884–9 (2010).
275. Suganami, T., Nishida, J. & Ogawa, Y. A paracrine loop between adipocytes and macrophages aggravates inflammatory changes: role of free fatty acids and tumor necrosis factor alpha. *Arterioscler. Thromb. Vasc. Biol.* **25**, 2062–8 (2005).
276. Liu, X. *et al.* The CC chemokine ligand 2 (CCL2) mediates fibroblast survival through IL-6. *Am. J. Respir. Cell Mol. Biol.* **37**, 121–128 (2007).
277. Stern, J. H., Rutkowski, J. M. & Scherer, P. E. Adiponectin, Leptin, and Fatty Acids in the Maintenance of Metabolic Homeostasis through Adipose Tissue Crosstalk. *Cell Metab.* **23**, 770–784 (2016).

278. Xie, L., O'Reilly, C. P., Chapes, S. K. & Mora, S. Adiponectin and leptin are secreted through distinct trafficking pathways in adipocytes. *Biochim. Biophys. Acta - Mol. Basis Dis.* **1782**, 99–108 (2008).
279. Achari, A. E. & Jain, S. K. Adiponectin, a therapeutic target for obesity, diabetes, and endothelial dysfunction. *International Journal of Molecular Sciences* **18**, (2017).
280. He, Y. *et al.* The multimerization and secretion of adiponectin are regulated by TNF-alpha. *Endocrine* **51**, 456–68 (2016).
281. Kern, P. A., Di Gregorio, G. B., Lu, T., Rassouli, N. & Ranganathan, G. Adiponectin expression from human adipose tissue: Relation to obesity, insulin resistance, and tumor necrosis factor-α expression. *Diabetes* **52**, 1779–1785 (2003).
282. Xie, L., Ortega, ‡ M Teresa, Mora, S. & Chapes, S. K. Interactive Changes between Macrophages and Adipocytes. *Clin. VACCINE Immunol.* **17**, 651–659 (2010).
283. Richter, W. F. & Jacobsen, B. Subcutaneous absorption of biotherapeutics: Knowns and unknowns. *Drug Metabolism and Disposition* **42**, 1881–1889 (2014).
284. Onishi, H. & Machida, Y. Biodegradation and distribution of water-soluble chitosan in mice. *Biomaterials* **20**, 175–182 (1999).
285. Seyrek, E. & Dubin, P. Glycosaminoglycans as polyelectrolytes. *Advances in Colloid and Interface Science* **158**, 119–129 (2010).
286. Li, S. D. & Huang, L. Nanoparticles evading the reticuloendothelial system: Role of the supported bilayer. *Biochim. Biophys. Acta - Biomembr.* **1788**, 2259–2266 (2009).
287. Kean, T. & Thanou, M. Biodegradation, biodistribution and toxicity of chitosan. *Advanced Drug Delivery Reviews* **62**, 3–11 (2010).
288. Signorile, A., Sgaramella, G., Bellomo, F. & De Rasmo, D. Prohibitins: A Critical Role in Mitochondrial Functions and Implication in Diseases. *Cells* **8**, 71 (2019).
289. Sun, B. & Karin, M. Obesity, inflammation, and liver cancer. *Journal of Hepatology* **56**, 704–713 (2012).
290. Thanou, M., Verhoef, J. C. & Junginger, H. E. Oral drug absorption enhancement by chitosan and its derivatives. *Advanced Drug Delivery Reviews* **52**, 117–126 (2001).
291. Barrett, P., Mercer, J. G. & Morgan, P. J. Preclinical models for obesity research. *DMM Disease Models and Mechanisms* **9**, 1245–1255 (2016).
292. Speakman, J. R. Use of high-fat diets to study rodent obesity as a model of human obesity. *International Journal of Obesity* (2019). doi:10.1038/s41366-019-0363-7
293. Wang, C. Y. & Liao, J. K. A mouse model of diet-induced obesity and insulin resistance. *Methods Mol. Biol.* **821**, 421–433 (2012).
294. Williams, L. M. *et al.* The development of diet-induced obesity and glucose intolerance in C57Bl/6 mice on a high-fat diet consists of distinct phases. *PLoS One* **9**, (2014).
295. Castro, A. M., Macedo-de la Concha, L. E. & Pantoja-Meléndez, C. A. Low-grade inflammation and its relation to obesity and chronic degenerative diseases. *Rev. Médica del Hosp. Gen. México* **80**, 101–105 (2017).
296. Di Rocco, P., Manco, M., Rosa, G., Greco, A. V. & Mingrone, G. Lowered Tumor Necrosis Factor Receptors, but Not Increased Insulin Sensitivity, with Infliximab. *Obes. Res.* **12**, 734–739 (2004).
297. Cameron, A. R. *et al.* Anti-Inflammatory Effects of Metformin Irrespective of Diabetes Status. *Circ. Res.* **119**, 652–665 (2016).
298. Saisho, Y. Metformin and Inflammation: Its Potential Beyond Glucose-lowering Effect. *Endocrine, Metab. Immune Disord. Targets* **15**, 196–205 (2015).

299. Buse, J. B. *et al.* The Primary Glucose-Lowering Effect of Metformin Resides in the Gut, Not the Circulation: Results From Short-term Pharmacokinetic and 12-Week Dose-Ranging Studies. *Diabetes Care* **39**, 198–205 (2016).
300. Pentikäinen, P. J., Neuvonen, P. J. & Penttilä, A. Pharmacokinetics of metformin after intravenous and oral administration to man. *Eur. J. Clin. Pharmacol.* **16**, 195–202 (1979).
301. Stanley, T. L. *et al.* TNF-α Antagonism with Etanercept Decreases Glucose and Increases the Proportion of High Molecular Weight Adiponectin in Obese Subjects with Features of the Metabolic Syndrome. *J. Clin. Endocrinol. Metab.* **96**, E146–E150 (2011).
302. Hensen, J., Howard, C. P., Walter, V. & Thuren, T. Impact of interleukin-1β antibody (canakinumab) on glycaemic indicators in patients with type 2 diabetes mellitus: Results of secondary endpoints from a randomized, placebo-controlled trial. *Diabetes Metab.* **39**, 524–531 (2013).
303. Huh, J. Y., Park, Y. J., Ham, M. & Kim, J. B. Crosstalk between Adipocytes and Immune Cells in Adipose Tissue Inflammation and Metabolic Dysregulation in Obesity. *Mol. Cells* **37**, 365–371 (2014).
304. de Luca, C. & Olefsky, J. M. Inflammation and Insulin Resistance. *FEBS Lett.* **582**, 97–105 (2008).
305. Esser, N., Legrand-Poels, S., Piette, J., Scheen, A. J. & Paquot, N. Inflammation as a link between obesity, metabolic syndrome and type 2 diabetes. *Diabetes Research and Clinical Practice* **105**, 141–150 (2014).
306. Ueki, K., Kondo, T. & Kahn, C. R. Suppressor of Cytokine Signaling 1 (SOCS-1) and SOCS-3 Cause Insulin Resistance through Inhibition of Tyrosine Phosphorylation of Insulin Receptor Substrate Proteins by Discrete Mechanisms. *Mol. Cell. Biol.* **25**, 8762–8762 (2005).
307. Yadav, A., Kataria, M. A., Saini, V. & Yadav, A. Role of leptin and adiponectin in insulin resistance. *Clin. Chim. Acta.* **417**, 80–4 (2013).
308. Lihn, A. S., Pedersen, S. B. & Richelsen, B. Adiponectin: action, regulation and association to insulin sensitivity. *Obes. Rev.* **6**, 13–21 (2005).
309. Ruan, H. & Dong, L. Q. Adiponectin signaling and function in insulin target tissues. *Journal of Molecular Cell Biology* **8**, 101–109 (2016).
310. King, A. J. F. The use of animal models in diabetes research. *British Journal of Pharmacology* **166**, 877–894 (2012).
311. Cicero, A. F. G., Fogacci, F. & Colletti, A. Potential role of bioactive peptides in prevention and treatment of chronic diseases: a narrative review. *British Journal of Pharmacology* **174**, 1378–1394 (2017).
312. Bentham, J. *et al.* Worldwide trends in body-mass index, underweight, overweight, and obesity from 1975 to 2016: a pooled analysis of 2416 population-based measurement studies in 128·9 million children, adolescents, and adults. *Lancet* **390**, 2627–2642 (2017).
313. Shu, C. J., Benoist, C. & Mathis, D. The immune system's involvement in obesity-driven type 2 diabetes. *Seminars in Immunology* **24**, 436–442 (2012).
314. Herder, C. *et al.* Immunological and Cardiometabolic Risk Factors in the Prediction of Type 2 Diabetes and Coronary Events: MONICA/KORA Augsburg Case-Cohort Study. *PLoS One* **6**, e19852 (2011).
315. Kolb, H. & Martin, S. Environmental/lifestyle factors in the pathogenesis and prevention of type 2 diabetes. *BMC Medicine* **15**, (2017).

APPENDIX A. MAPS OF PLASMIDS USED IN THIS STUDY

A.1. Images retrieved from respective plasmid suppliers' website.

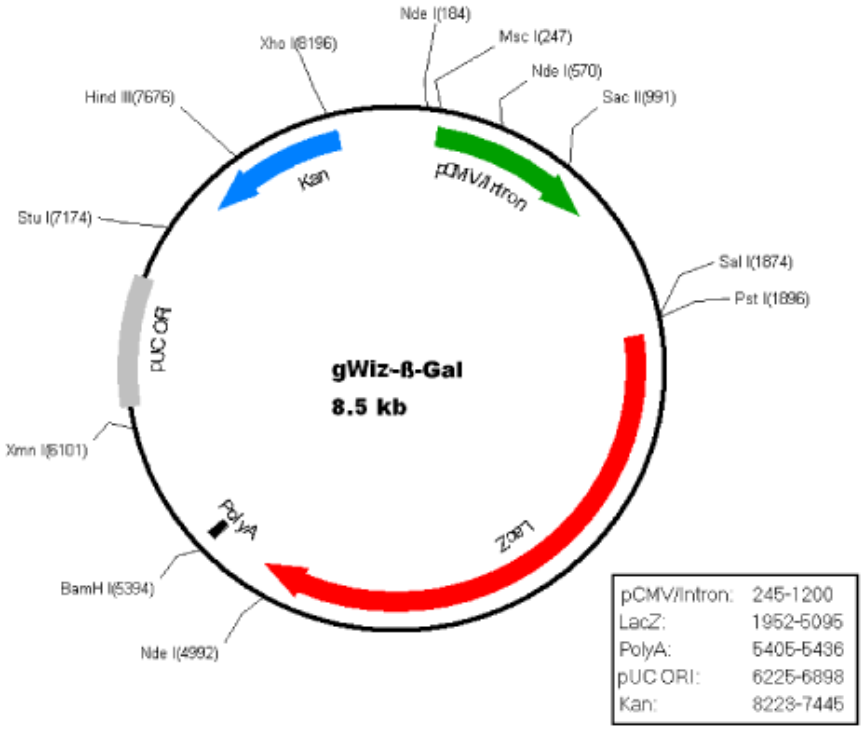

Figure A1. Map of gWiz beta-galactosidase encoding plasmid DNA.

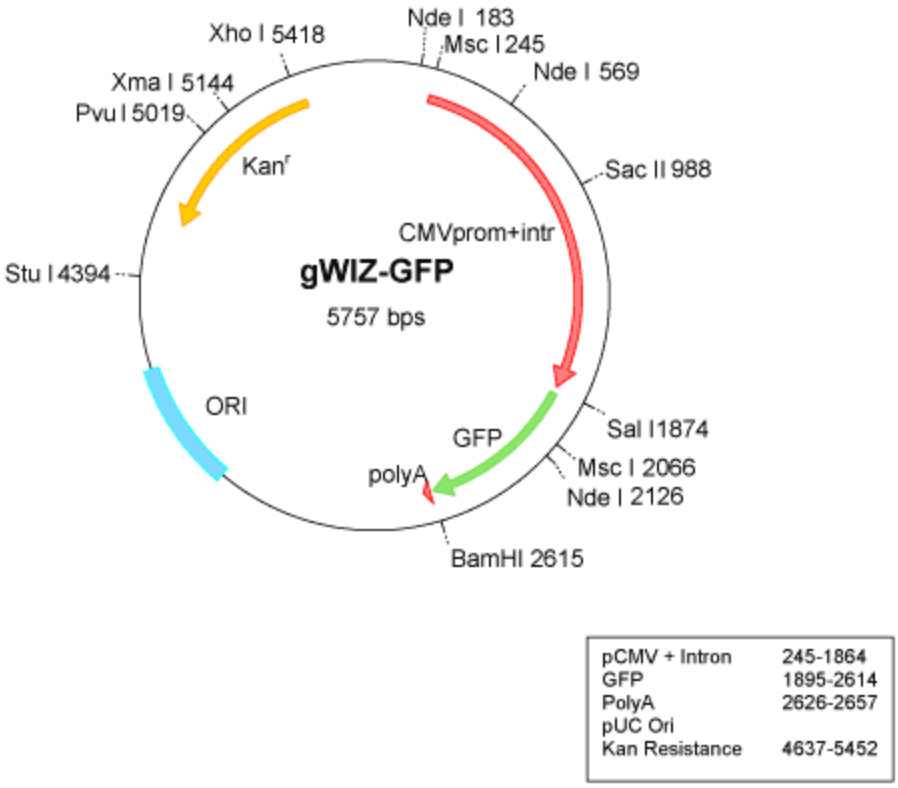

Figure A2. Map of gWiz green fluorescent protein encoding plasmid DNA.

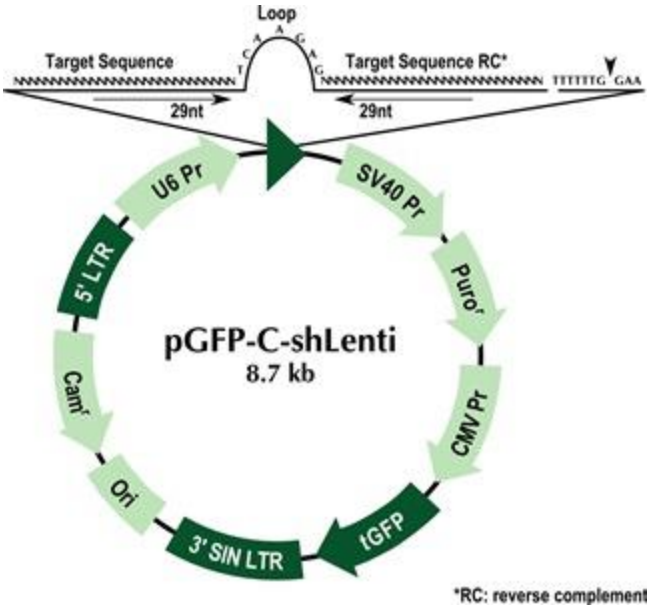

Figure A3. Map of plasmid DNA encoding shRNA against TNFα/ MCP-1.

APPENDIX B. NUCLEOTIDE SEQUENCES

B.1. Nucleotide sequence for OriGene's pGFP-C-shLenti shRNA-29 expression vector

GTCGACGGATCGGGAGATCTCCCGATCCCCTATGGTGCACTCTCAGTACAATCTGCTCTGAT
GCCGCATAGTTAAGCCAGTATCTGCTCCCTGCTTGTGTGTTGGAGGTCGCTGAGTAGTGCGC
GAGCAAAATTTAAGCTACAACAAGGCAAGGCTTGACCGACAATTGCATGAAGAATCTGCTT
AGGGTTAGGCGTTTTGCGCTGCTTCGCGATGTACGGGCCAGATATCGCGTTGACATTGATTA
TTGACTAGTTATTAATAGTAATCAATTACGGGGTCATTAGTTCATAGCCCATATATGGAGTTC
CGCGTTACATAACTTACGGTAAATGGCCCGCCTGGCTGACCGCCCAACGACCCCCGCCCATT
GACGTCAATAATGACGTATGTTCCCATAGTAACGCCAATAGGGACTTTCCATTGACGTCAAT
GGGTGGAGTATTTACGGTAAACTGCCCACTTGGCAGTACATCAAGTGTATCATATGCCAAGT
ACGCCCCCTATTGACGTCAATGACGGTAAATGGCCCGCCTGGCATTATGCCCAGTACATGAC
CTTATGGGACTTTCCTACTTGGCAGTACATCTACGTATTAGTCATCGCTATTACCATGGTGAT
GCGGTTTTGGCAGTACATCAATGGGCGTGGATAGCGGTTTGACTCACGGGGATTTCCAAGTC
TCCACCCCATTGACGTCAATGGGAGTTTGTTTTGGCACCAAAATCAACGGGACTTTCCAAAA
TGTCGTAACAACTCCGCCCCATTGACGCAAATGGGCGGTAGGCGTGTACGGTGGGAGGTCTA
TATAAGCAGCGCGTTTTGCCTGTACTGGGTCTCTCTGGTTAGACCAGATCTGAGCCTGGGAG
CTCTCTGGCTAACTAGGGAACCCACTGCTTAAGCCTCAATAAAGCTTGCCTTGAGTGCTTCA
AGTAGTGTGTGCCCGTCTGTTGTGTGACTCTGGTAACTAGAGATCCCTCAGACCCTTTTAGTC
AGTGTGGAAAATCTCTAGCAGTGGCGCCCGAACAGGGACTTGAAAGCGAAAGGGAAACCAG
AGGAGCTCTCTCGACGCAGGACTCGGCTTGCTGAAGCGCGCACGGCAAGAGGCGAGGGGCG
GCGACTGGTGAGTACGCCAAAAATTTTGACTAGCGGAGGCTAGAAGGAGAGAGATGGGTGC
GAGAGCGTCAGTATTAAGCGGGGGAGAATTAGATCGCGATGGGAAAAAATTCGGTTAAGGC
CAGGGGGAAAGAAAAAATATAAATTAAAACATATAGTATGGGCAAGCAGGGAGCTAGAAC
GATTCGCAGTTAATCCTGGCCTGTTAGAAACATCAGAAGGCTGTAGACAAATACTGGGACA
GCTACAACCATCCCTTCAGACAGGATCAGAAGAACTTAGATCATTATATAATACAGTAGCAA
CCCTCTATTGTGTGCATCAAAGGATAGAGATAAAAGACACCAAGGAAGCTTTAGACAAGAT
AGAGGAAGAGCAAAACAAAAGTAAGACCACCGCACAGCAAGCGGCCGGCCGCTGATCTTC
AGACCTGGAGGAGGAGATATGAGGGACAATTGGAGAAGTGAATTATATAAATATAAAGTAG
TAAAAATTGAACCATTAGGAGTAGCACCCACCAAGGCAAAGAGAAGAGTGGTGCAGAGAG
AAAAAAGAGCAGTGGGAATAGGAGCTTTGTTCCTTGGGTTCTTGGGAGCAGCAGGAAGCAC
TATGGGCGCAGCGTCAATGACGCTGACGGTACAGGCCAGACAATTATTGTCTGGTATAGTGC
AGCAGCAGAACAATTTGCTGAGGGCTATTGAGGCGCAACAGCATCTGTTGCAACTCACAGTC
TGGGGCATCAAGCAGCTCCAGGCAAGAATCCTGGCTGTGGAAAGATACCTAAAGGATCAAC
AGCTCCTGGGGATTTGGGGTTGCTCTGGAAAACTCATTTGCACCACTGCTGTGCCTTGGAAT
GCTAGTTGGAGTAATAAATCTCTGGAACAGATTTGGAATCACACGACCTGGATGGAGTGGG
ACAGAGAAATTAACAATTACACAAGCTTAATACACTCCTTAATTGAAGAATCGCAAAACCA
GCAAGAAAAGAATGAACAAGAATTATTGGAATTAGATAAATGGGCAAGTTTGTGGAATTGG
TTTAACATAACAAATTGGCTGTGGTATATAAAATTATTCATAATGATAGTAGGAGGCTTGGT
AGGTTTAAGAATAGTTTTTGCTGTACTTTCTATAGTGAATAGAGTTAGGCAGGGATATTCAC
CATTATCGTTTCAGACCCACCTCCCAACCCCGAGGGGACCCGACAGGCCCGAAGGAATAGA
AGAAGAAGGTGGAGAGAGAGACAGAGACAGATCCATTCGATTAGTGAACGGATCGGCACT
GCGTGCGCCAATTCTGCAGACAAATGGCAGTATTCATCCACAATTTTAAAAGAAAAGGGGG
GATTGGGGGGTACAGTGCAGGGGAAAGAATAGTAGACATAATAGCAACAGACATACAAACT
AAAGAATTACAAAAACAAATTACAAAAATTCAAAATTTTCGGGTTTATTACAGGGACAGCA
GAGATCCAGTTTGGTTAGTACCGGGCCCGCTCTAGGAATTCCCCAGTGGAAAGACGCGCAG
GCAAAACGCACCACGTGACGGAGCGTGACCGCGCGCCGAGCGCGCGCCAAGGTCGGGCAG
GAAGAGGGCCTATTTCCCATGATTCCTTCATATTTGCATATACGATACAAGGCTGTTAGAGA
GATAATTAGAATTAATTTGACTGTAAACACAAAGATATTAGTACAAAATACGTGACGTAGA

AAGTAATAATTTCTTGGGTAGTTTGCAGTTTTAAAATTATGTTTTAAAATGGACTATCATATG
CTTACCGTAACTTGAAAGTATTTCGATTTCTTGGGTTTATATATCTTGTGGAAAGGACGCGGG
ATCCACTGGACCAGGCAGCAGCGTCAGAAGACTTTTTTTTGGAACGTCTCAAGCTTGTCGAC
CCTGTGGAATGTGTGTCAGTTAGGGTGTGGAAAGTCCCCAGGCTCCCCAGCAGGCAGAAGT
ATGCAAAGCATGCATCTCAATTAGTCAGCAACCATAGTCCCGCCCCTAACTCCGCCCATCCC
GCCCCTAACTCCGCCCAGTTCCGCCCATTCTCCGCCCCATGGCTGACTAATTTTTTTTATTTAT
GCAGAGGCCGAGGCCGCCTCGGCCTCTGAGCTATTCCAGAAGTAGTGAGGAGGCTTTTTTGG
AGGCCTAGGCTTTTGCAAAAAGCTAGCTTACCATGACCGAGTACAAGCCCACGGTGCGCCTC
GCCACCCGCGACGACGTCCCCAGGGCCGTACGCACCCTCGCCGCCGCGTTCGCCGACTACCC
CGCCACGCGCCACACCGTCGATCCGGACCGCCACATCGAGCGGGTCACCGAGCTGCAAGAA
CTCTTCCTCACGCGCGTCGGGCTCGACATCGGCAAGGTGTGGGTCGCGGACGACGGCGCCGC
GGTGGCGGTCTGGACCACGCCGGAGAGCGTCGAAGCGGGGGCGGTGTTCGCCGAGATCGGC
CCGCGCATGGCCGAGTTGAGCGGTTCCCGGCTGGCCGCGCAGCAACAGATGGAAGGCCTCC
TGGCGCCGCACCGGCCCAAGGAGCCCGCGTGGTTCCTGGCCACCGTCGGCGTGTCGCCCGAC
CACCAGGGCAAGGGTCTGGGCAGCGCCGTCGTGCTCCCCGGAGTGGAGGCGGCCGAGCGCG
CCGGGGTGCCCGCCTTCCTGGAGACCTCCGCGCCCCGCAACCTCCCCTTCTACGAGCGGCTC
GGCTTCACCGTCACCGCCGACGTCGAGGTGCCCGAAGGACCGCGCACCTGGTGCATGACCC
GCAAGCCCGGTGCCTGAGTTTGTTTGAATGAGGCTTCAGTACTTTACAGAATCGATAAAATA
AAAGATTTTATTTAGTCTCCAGAAAAAGGGGGGAATGAAAGACCCCACCTGTAGGTTTGGC
AAGCTAGCTTAAGTAACGCCATTTTGCAAGGCATGGAAAAATACATAACTGAGAATAGAGA
AGTTCAGATCAAGGTCAGGAACAGATGGAACAGCTGAATATGGGCCAAACAGGATATCTGT
GGTAAGCAGTTCCTGCCCCGGCTCAGGGCCAAGAACAGATGGAACAGCTGAATATGGGCCA
AACAGGATATCTGTGGTAAGCAGTTCCTGCCCCGGCTCAGGGCCAAGAACAGATGGTCCCC
AGATGCGGTCCAGCCCTCAGCAGTTTCTAGACATGTCCAATATGACCGCCATGTTGACATTG
ATTATTGACTAGTTATTAATAGTAATCAATTACGGGGTCATTAGTTCATAGCCCATATATGGA
GTTCCGCGTTACATAACTTACGGTAAATGGCCCGCCTGGCTGACCGCCCAACGACCCCCGCC
CATTGACGTCAATAATGACGTATGTTCCCATAGTAACGCCAATAGGGACTTTCCATTGACGT
CAATGGGTGGAGTATTTACGGTAAACTGCCCACTTGGCAGTACATCAAGTGTATCATATGCC
AAGTCCGCCCCCTATTGACGTCAATGACGGTAAATGGCCCGCCTGGCATTATGCCCAGTACA
TGACCTTACGGGACTTTCCTACTTGGCAGTACATCTACGTATTAGTCATCGCTATTACCATGG
TGATGCGGTTTTGGCAGTACACCAATGGGCGTGGATAGCGGTTTGACTCACGGGGATTTCCA
AGTCTCCACCCCATTGACGTCAATGGGAGTTTGTTTTGGCACCAAAATCAACGGGACTTTCC
AAAATGTCGTAATAACCCCGCCCCGTTGACGCAAATGGGCGGTAGGCGTGTACGGTGGGAG
GTCTATATAAGCAGAGCTCGTTTAGTGAACCGTCAGAATTTTGTAATACGACTCACTATAGG
GCGGCCGGGAATTGATCCGGTACCGAGGAGACTGCCGCCGCGATCGCCGGCGCGCCAGATC
TCAAGCTTAACTAGTTAGCGGACCGACGCGTACGCGGCCGCTCGAGATGGAGAGCGACGAG
AGCGGCCTGCCCGCCATGGAGATCGAGTGCCGCATCACCGGCACCCTGAACGGCGTGGAGT
TCGAGCTGGTGGGCGGCGGAGAGGGCACCCCCGAGCAGGGCCGCATGACCAACAAGATGA
AGAGCACCAAAGGCGCCCTGACCTTCAGCCCCTACCTGCTGAGCCACGTGATGGGCTACGGC
TTCTACCACTTCGGCACCTACCCCAGCGGCTACGAGAACCCCTTCCTGCACGCCATCAACAA
CGGCGGCTACACCAACACCCGCATCGAGAAGTACGAGGACGGCGGCGTGCTGCACGTGAGC
TTCAGCTACCGCTACGAGGCCGGCCGCGTGATCGGCGACTTCAAGGTGATGGGCACCGGCTT
CCCCGAGGACAGCGTGATCTTCACCGACAAGATCATCCGCAGCAACGCCACCGTGGAGCAC
CTGCACCCCATGGGCGATAACGATCTGGATGGCAGCTTCACCCGCACCTTCAGCCTGCGCGA
CGGCGGCTACTACAGCTCCGTGGTGGACAGCCACATGCACTTCAAGAGCGCCATCCACCCCA
GCATCCTGCAGAACGGGGGCCCCATGTTCGCCTTCCGCCGCGTGGAGGAGGATCACAGCAA
CACCGAGCTGGGCATCGTGGAGTACCAGCACGCCTTCAAGACCCCGGATGCAGATGCCGGT
GAAGAAAGAGTTTAAACGGCCGGCCGCGGTCTGTACAAGTAGGATTCGTCGAGGGACCTAA
TAACTTCGTATAGCATACATTATACGAAGTTATACATGTTTAAGGGTTCCGGTTCCACTAGGT
ACAATTCGATATCAAGCTTATCGATAATCAACCTCTGGATTACAAAATTTGTGAAAGATTGA
CTGGTATTCTTAACTATGTTGCTCCTTTTACGCTATGTGGATACGCTGCTTTAATGCCTTTGTA

TCATGCTATTGCTTCCCGTATGGCTTTCATTTTCTCCTCCTTGTATAAATCCTGGTTGCTGTCT
CTTTATGAGGAGTTGTGGCCCGTTGTCAGGCAACGTGGCGTGGTGTGCACTGTGTTTGCTGA
CGCAACCCCCACTGGTTGGGGCATTGCCACCACCTGTCAGCTCCTTTCCGGGACTTTCGCTTT
CCCCCTCCCTATTGCCACGGCGGAACTCATCGCCGCCTGCCTTGCCCGCTGCTGGACAGGGG
CTCGGCTGTTGGGCACTGACAATTCCGTGGTGTTGTCGGGGAAATCATCGTCCTTTCCTTGGC
TGCTCGCCTGTGTTGCCACCTGGATTCTGCGCGGGACGTCCTTCTGCTACGTCCCTTCGGCCC
TCAATCCAGCGGACCTTCCTTCCCGCGGCCTGCTGCCGGCTCTGCGGCCTCTTCCGCGTCTTC
GCCTTCGCCCTCAGACGAGTCGGATCTCCCTTTGGGCCGCCTCCCCGCATCGATACCGTCGA
CCTCGATCGAGACCTAGAAAAACATGGAGCAATCACAAGTAGCAATACAGCAGCTACCAAT
GCTGATTGTGCCTGGCTAGAAGCACAAGAGGAGGAGGAGGTGGGTTTTCCAGTCACACCTC
AGGTACCTTTAAGACCAATGACTTACAAGGCAGCTGTAGATCTTAGCCACTTTTTAAAAGAA
AAGGGGGGACTGGAAGGGCTAATTCACTCCCAACGAAGACAAGATATCCTTGATCTGTGGA
TCTACCACACACAAGGCTACTTCCCTGATTGGCAGAACTACACACCAGGGCCAGGGATCAG
ATATCCACTGACCTTTGGATGGTGCTACAAGCTAGTACCAGTTGAGCAAGAGAAGGTAGAA
GAAGCCAATGAAGGAGAGAACACCCGCTTGTTACACCCTGTGAGCCTGCATGGGATGGATG
ACCCGGAGAGAGAAGTATTAGAGTGGAGGTTTGACAGCCGCCTAGCATTTCATCACATGGC
CCGAGAGCTGCATCCGGACTGTACTGGGTCTCTCTGGTTAGACCAGATCTGAGCCTGGGAGC
TCTCTGGCTAACTAGGGAACCCACTGCTTAAGCCTCAATAAAGCTTGCCTTGAGTGCTTCAA
GTAGTGTGTGCCCGTCTGTTGTGTGACTCTGGTAACTAGAGATCCCTCAGACCCTTTTAGTCA
GTGTGGAAAATCTCTAGCAGCATGTGAGCAAAAGGCCAGCAAAAGGCCAGGAACCGTAAAA
AGGCCGCGTTGCTGGCGTTTTTCCATAGGCTCCGCCCCCCTGACGAGCATCACAAAAATCGA
CGCTCAAGTCAGAGGTGGCGAAACCCGACAGGACTATAAAGATACCAGGCGTTTCCCCCTG
GAAGCTCCCTCGTGCGCTCTCCTGTTCCGACCCTGCCGCTTACCGGATACCTGTCCGCCTTTC
TCCCTTCGGGAAGCGTGGCGCTTTCTCATAGCTCACGCTGTAGGTATCTCAGTTCGGTGTAGG
TCGTTCGCTCCAAGCTGGGCTGTGTGCACGAACCCCCCGTTCAGCCCGACCGCTGCGCCTTA
TCCGGTAACTATCGTCTTGAGTCCAACCCGGTAAGACACGACTTATCGCCACTGGCAGCAGC
CACTGGTAACAGGATTAGCAGAGCGAGGTATGTAGGCGGTGCTACAGAGTTCTTGAAGTGG
TGGCCTAACTACGGCTACACTAGAAGAACAGTATTTGGTATCTGCGCTCTGCTGAAGCCAGT
TACCTTCGGAAAAAGAGTTGGTAGCTCTTGATCCGGCAAACAAACCACCGCTGGTAGCGGTG
GTTTTTTTGTTTGCAAGCAGCAGATTACGCGCAGAAAAAAAGGATCTCAAGAAGATCCTTTG
ATCTTTTCTACGGGGTCTGACGCTCAGTGGAACGAAAACTCACGTTAAGGGATTTTGGTCAT
GATTACGCCCCGCCCTGCCACTCATCGCAGTACTGTTGTAATTCATTAAGCATTCTGCCGACA
TGGAAGCCATCACAAACGGCATGATGAACCTGAATCGCCAGCGGCATCAGCACCTTGTCGC
CTTGCGTATAATATTTGCCCATGGTGAAAACGGGGGCGAAGAAGTTGTCCATATTGGCCACG
TTTAAATCAAAACTGGTGAAACTCACCCAGGGATTGGCTGAAACGAAAAACATATTCTCAAT
AAACCCTTTAGGGAAATAGGCCAGGTTTTCACCGTAACACGCCACATCTTGCGAATATATGT
GTAGAAACTGCCGGAAATCGTCGTGGTATTCACTCCAGAGCGATGAAAACGTTTCAGTTTGC
TCATGGAAAACGGTGTAACAAGGGTGAACACTATCCCATATCACCAGCTCACCGTCTTTCAT
TGCCATACGGAACTCCGGATGAGCATTCATCAGGCGGGCAAGAATGTGAATAAAGGCCGGA
TAAAACTTGTGCTTATTTTTCTTTACGGTCTTTAAAAAGGCCGTAATATCCAGCTGAACGGTC
TGGTTATAGGTACATTGAGCAACTGACTGAAATGCCTCAAAATGTTCTTTACGATGCCATTG
GGATATATCAACGGTGGTATATCCAGTGATTTTTTTCTCCATACTCTTCCTTTTTCAATATTAT
TGAAGCATTTATCAGGGTTATTGTCTCATGAGCGGATACATATTTGAATGTATTTAGAAAAA
TAAACAAATAGGGGTTCCGCGCACATTTCCCCGAAAAGTGCCACCTGAC

B.2. Features for pGFP-C-shLenti vector:

Start	End	Description
835	1015	5LTR
2618	2624	EcoR1
2693	2949	U6 promoter
3039	3230	SV40 promoter
3294	3893	Puromycin-N-acetyl transferase
4269	4275	Xba1
4280	4985	CMV promoter
5034	5738	tGFP
7070	7250	sinLTR
7217	7836	pBR322 origin replication
7896	8555	CAM^r for Chloramphenicol resistance

B.3. Sequences used in this research

TL501987A MCP-1 (CCL2) shRNA: TGTTGGCTCAGCCAGATGCAGTTAACGCC

TL515379C TNFα shRNA: GCAGGTCTACTTTGGAGTCATTGCTCTGT

TR30021 scrambled control shRNA: GCACTACCAGAGCTAACTCAGATAGTACT

APPENDIX C. LIST OF PUBLICATIONS

C.1. Peer-reviewed research articles

- **Divya Sharma**, Sanjay Arora, and Jagdish Singh. “Smart Thermosensitive Copolymer Incorporating Chitosan-Zinc-Insulin Electrostatic Complexes for Controlled Delivery of Insulin: Effect of Chitosan Chain Length.” International Journal of Polymeric Materials and Polymeric Biomaterials (2019). (DOI: 10.1080/00914037.2019.1655750)
- Lindsey Lipp, **Divya Sharma**, Amrita Banerjee, and Jagdish Singh. "Controlled Delivery of Salmon Calcitonin Using Thermosensitive Triblock Copolymer Depot for Treatment of Osteoporosis.” ACS Omega 4 (2019): 1157-1166.
- **Divya Sharma** and Jagdish Singh. "Synthesis and Characterization of Fatty Acid Grafted Chitosan Polymer and their Nanomicelles for Nonviral Gene Delivery Applications." Bioconjugate Chemistry 28.11 (2017): 2772-2783.
- **Divya Sharma** and Jagdish Singh. "Synthesis and Characterization of Fatty Acid Grafted Chitosan Polymer and their Nanomicelles for Nonviral Gene Delivery Applications." Bioconjugate Chemistry 28.11 (2017): 2772-2783.
- **Divya Sharma** and Jagdish Singh. " Nanomicelles of Fatty Acid Grafted Chitosan Polymer for Drug and Gene Delivery." Annals of Pharmacology and Pharmaceutics (Short Communication) 2.10 (2017): 1101.
- Lindsey Lipp, **Divya Sharma**, Amrita Banerjee, and Jagdish Singh. "*In Vitro* and *In Vivo* Optimization of Phase Sensitive Smart Polymer for Controlled Delivery of Rivastigmine for Treatment of Alzheimer’s Disease.” Pharmaceutical Research (under review).

- **Divya Sharma** and Jagdish Singh. "Long-term glycemic control and prevention of diabetes complications *in vivo* using oleic acid-grafted-chitosan-zinc-insulin complexes incorporated in thermosensitive copolymer." (under submission).
- **Divya Sharma**, Sanjay Arora, Amrita Banerjee and Jagdish Singh. "Chitosan Nanomicelles Mediated Targeted Downregulation of Proinflammatory Cytokines in Adipose Tissue for Treatment of Insulin Resistance in High-Fat Diet-induced Diabetic Mouse Model." (under submission).
- Amrita Banerjee, **Divya Sharma**, Riddhi Trivedi, and Jagdish Singh. "Treatment of insulin resistance in obesity associated type 2 diabetes mellitus through adiponectin gene therapy." (under submission).

C.2. Book chapters

- **Divya Sharma**, Lindsey Lipp, Sanjay Arora, Jagdish Singh. "Diblock and Triblock Copolymers of Polylactide and Polyglycolide." Composites in Biomedical Engineering: Matrices (Series A). Elsevier; Chapter 13 (2018): 449-478.
- Bruna Rodrigues, Sushant Lakkadwala, **Divya Sharma**, Jagdish Singh. Chitosan for Gene, DNA Vaccine and Drug Delivery." Composites in Biomedical Engineering: Particles (Series C). Elsevier; Chapter 15 (2018): 515-550.
- **Divya Sharma**, Sanjay Arora, Bruna dos Santos Rodrigues, Sushant Lakkadwala, Amrita Banerjee, and Jagdish Singh. Chitosan-based Systems for Gene Delivery. Springer Nature Publisher (2019) (under publishing).

C.3. Conference presentations

- **Divya Sharma**, Jagdish Singh. Long-term glycemic control and prevention of diabetes complications *in vivo* using oleic acid-grafted-chitosan-zinc-insulin complexes incorporated in thermosensitive copolymer. Presented at AAPS PharmSci 360, November 3-6, 2019, San Antonio, TX.
- **(Best abstract award) Divya Sharma**, Amrita Banerjee, and Jagdish Singh. Targeted knockdown of pro-inflammatory cytokines in adipose tissue macrophages and adipocytes for the treatment of insulin resistance. Presented at AAPS PharmSci 360, November 3-6, 2019, San Antonio, TX.
- **(Best poster award) Divya Sharma**, Amrita Banerjee, Jagdish Singh. Targeted knockdown of pro-inflammatory cytokines in adipose tissue macrophages and adipocytes for the treatment of insulin resistance. Presented at 6th Annual AAPS –NDSU Pharmaceutical Research Symposium, September 26, 2019, Fargo, ND.
- **Divya Sharma**, Jagdish Singh. (Oral Presentation) Controlled Delivery of Insulin using Smart Polymer Provides Long-term Glucose Control and Prevention of Diabetes Complications. Presented at Pharmaceutics Graduate Student Research Meeting, June 13-15, 2019, Madison, WI.
- **Divya Sharma**, Jagdish Singh. Oleic Acid-Grafted-Chitosan and Thermosensitive Copolymer Based Depot-in-Depot System for Controlled Delivery of Basal Insulin: Effect of Degree of Oleic Acid Substitution. Presented at AAPS PharmSci 360, November 4-7, 2018, Washington, DC.

- **Divya Sharma**, Jagdish Singh. Effect of Copolymer Concentration and Drug Loading on Release Profile of Insulin Incorporated in Thermosensitive Copolymer Based Delivery System. Presented at AAPS PharmSci 360, November 4-7, 2018, Washington, DC.
- **Divya Sharma**, Amrita Banerjee, Jagdish Singh. Dual Functionalized Chitosan Nanomicelles Mediated Gene Delivery for Targeting Pro-Inflammatory Macrophages for the Treatment of Insulin Resistance. Presented at AAPS PharmSci 360, November 4-7, 2018, Washington, DC.
- **Divya Sharma**, Amrita Banerjee, and Jagdish Singh. Pro-Inflammatory Macrophages and Adipocytes Targeted Gene Delivery for the Treatment of Insulin Resistance. Presented at 5th Annual AAPS –NDSU Pharmaceutical Research Symposium, October 25, 2018, Fargo, ND.
- **Divya Sharma**, Jagdish Singh. Long-Term Glycemic Control *In Vivo* using Thermosensitive Copolymeric Depot-based System incorporating Oleic acid-grafted-chitosan-zinc-insulin Complexes. Presented at 5th Annual AAPS –NDSU Pharmaceutical Research Symposium, October 25, 2018, Fargo, ND.
- **(Best oral presentation award)** Divya Sharma, Jagdish Singh. (Oral Presentation) Controlled Delivery of Basal Insulin from Thermosensitive Polymeric Depot Based System. Presented at Pharmaceutics Graduate Student Research Meeting, June 7-9, 2018, Minneapolis, MN.
- **Divya Sharma**, Jagdish Singh. Effect of Chitosan Chain Length on the *In Vitro* Release and Stability of Insulin from Chitosan-Zinc-Insulin Complex Incorporated into Thermosensitive Copolymer. Presented at AAPS Annual Meeting and Exposition, November 12-15, 2017, San Diego, CA.

- **Divya Sharma**, Jagdish Singh. Effect of Fatty Acid Modification of Chitosan on the Stability and *In Vitro* Release of Insulin from Chitosan-Zinc-Insulin Complex Incorporated into Thermosensitive Copolymer. Presented at AAPS Annual Meeting and Exposition, November 12-15, 2017, San Diego, CA.
- **(Best poster award) Divya Sharma**, Jagdish Singh. Effect of Increasing Chitosan Chain Length on the *In Vitro* Release and Stability of Insulin from Chitosan-Zinc-Insulin Complex Incorporated into Thermosensitive Copolymer. Presented at 4th Annual AAPS – NDSU Pharmaceutical Research Symposium, September 12, 2017, Fargo, ND.
- **Divya Sharma**, Jagdish Singh. Effect of Chitosan Chain Length on the *In Vitro* Release and Stability of Insulin from Chitosan-Zinc-Insulin Complex Incorporated into Thermosensitive Copolymer. Presented at Pharmaceutics Graduate Student Research Meeting, June 15-17, 2017, Ann Arbor, MI.
- **Divya Sharma**, Jagdish Singh. Controlled Delivery of Basal Insulin from Thermosensitive Polymeric Systems. Presented at AAPS Annual Meeting and Exposition, November 13-17, 2016, Denver, CO.
- **(Best poster award) Divya Sharma**, Jagdish Singh. Thermosensitive Polymer for Controlled Delivery of Basal Level Insulin. Presented at 3rd Annual AAPS – NDSU Pharmaceutical Research Symposium, September 8, 2016, Fargo, ND.
- **Divya Sharma**, Jagdish Singh. Thermosensitive Polymers for Controlled Delivery of Insulin. Presented at Pharmaceutics Graduate Student Research Meeting, June 16-18, 2016, Kansas City, MO. pertaining to how your appendix material should be presented.